Lancaster Environment Centre
Faculty of Science and Technology
Lancaster University

Investigating the occurrence and accumulation of perfluoroalkylated substances and other persistent organic pollutants in snow and ice of the Earth's Polar regions

Jack Garnett MChem (Hons)

This thesis is submitted in partial fulfilment of the requirements
for the degree of Doctor of Philosophy

August 2020

"I hereby declare that this thesis is my original work and the work has not been submitted elsewhere, in whole or in part, to qualify for any other academic award of a higher degree. All sections of this thesis with joint research/collaborators have been appropriately acknowledged and referenced."

Candidate: .....  *.....Date:.....22-Jul-21.....*

Mr Jack R. Garnett

Abstract

Persistent organic pollutants (POPs) are a highly diverse group of synthetic chemicals that are released into the environment from human activities and display a host of adverse effects in wildlife and humans. Perfluoroalkylated substances (PFASs) are one major group of industrial chemicals that are globally produced in vast quantities and are subject to various global regulations. However, PFASs are present in the Earth's Polar Regions and yet little is known about their environmental fate and behaviour, particularly their accumulation and fate in snow and ice and the wider cryosphere. Moreover, climate change is altering the cryosphere, affecting sea ice and its properties for example, which in turn may affect the biogeochemical cycling of these pollutants and could lead to altered or enhanced biological exposure and uptake. This thesis examines the accumulation of PFASs in snow and firn as a useful recorder of environmental contamination in Antarctica, a region which lacks a multi-decadal time series of air monitoring data. The thesis also investigates in detail the processes that result in the uptake, distribution and accumulation of persistent organic pollutants in sea ice, particularly in the context of a warmer Arctic, where sea ice is now dominated by brine-rich single season ice.

There is a lack of monitoring data on the levels of PFASs in Antarctica, and so a snow core was taken from Kohnen Station (East Antarctica plateau) to determine the historical deposition rates in the region. Results revealed low or non-detectable levels of perfluorosulfonic acids (PFSAs) but showed increasing trends of perfluorocarboxylates (PFCAs) between 1958 – 2017. Deposition rates for PFCAs in snow varied depending on chain length, with PFBA (C_4) showing up to 2-orders of magnitude higher (1.3 and 280 ng m^{-2} yr^{-1}) than PFOA (C_8) (1.6 and 12.6 ng m^{-2} yr^{-1}). Furthermore, correlations between PFCAs of varying chain length were strong ($r^2 > 0.7$, $p < 0.01$). This information suggests that PFASs in the remote polar region, dominated in the main by the PFCAs, share similar transport pathways which can be largely attributed to the long-range atmospheric transport of volatile chemical precursors, which includes fluorotelomer alcohols (FTOHs) and other new CFC-replacement compounds. Together, this shows that global emissions of this group of chemicals is ongoing and have continued to rise following regulatory measures and also demonstrates the usefulness of a snow/firn core as a proxy for past atmospheric levels. In lieu of air monitoring infrastructure across Antarctica, then analysis of dated snow/ice cores provide a useful 'barometer' for global pollution and allow the effectiveness of international regulations in curbing the use of certain chemicals to be realized.

Given the marked alterations to the cryosphere through climate change, there is a need to assess how the biogeochemical cycling of chemical contaminants may also be affected, particularly with respect to changing sea ice and altered pathways of exposure to organisms at the base of the marine food web. Hence, a series of laboratory experiments (in a dedicated sea ice chamber) were conducted in order to understand the chemical fate and behaviour of various 'legacy' and 'emerging' POPs in artificial sea ice. Results showed that POPs are incorporated into sea ice during its formation and growth with their distribution strongly

influenced by salt (brine) dynamics. Enrichment factors (i.e. relative concentration) also demonstrate that some POPs (e.g., long-chain PFASs) behave differently with respect to other homologues, leading to their enrichment in bulk sea ice by up to 3-fold more (with respect to salt). This suggests that additional factors which are independent of physical processes also play a role in their environmental behaviour and chemical uptake during ice growth. Further results gathered from a controlled melt experiment indicates that this behaviour is related to the physicochemical properties of POPs, which alters the chemical partitioning between solid (i.e. ice) and liquid (i.e. brine) phases within sea ice. Importantly, concentrations of POPs were calculated for the *in-situ* brine environment, which show that POPs are present at significantly higher concentrations (e.g. up to 1-order of magnitude higher for PFOA) than in the initial underlying seawater and indicates the importance of brine for controlling chemical fate and biological exposure in young/single season sea ice, the dominant ice type in a warming Arctic.

The presence of PFASs in the polar marine environment raises particular concern during summer when periods of high biological activity may be accompanied by intense chemical uptake and subsequent transfer through the marine food web. Moreover, the occurrence of ice-rafted snowpack along with the thinning of sea ice observed in recent decades risks the formation of more snow-ice, an ice type that is particularly susceptible to rapid melting through surface temperature fluctuations, which in turn could release its chemical burden into the underlying ocean. Various samples of sea ice, snow and under-ice seawater were collected during late summer in the Arctic. Based on previously determined differences in partitioning and environmental tendencies of PFASs with varying chain length, chemicals were grouped into short-chain (C_4 – C_7) and long-chain (C_8 –C_{14}) PFASs. Concentrations of $\Sigma PFAS_{\text{short-chain}}$ (around 3.0 ng L^{-1}) were significantly higher in comparison to $\Sigma PFAS_{\text{long-chain}}$ (around 0.1 ng L^{-1}) in snow. While in seawater, concentrations of $\Sigma PFAS_{\text{long-chain}}$ (around 1.0 ng L^{-1}) were higher than $\Sigma PFAS_{\text{short-chain}}$ (around 0.4 ng L^{-1}). This demonstrates that snow is still a major atmospheric pathway of contemporary PFASs (predominantly short-chain PFASs) to the Arctic marine environment and also shows seawater holds a large chemical burden of PFAS (historical and current) emissions. PFASs were also measured in sea ice and the levels and composition reflected inputs from snow and seawater. In particular, some surface layers (i.e. snow-ice) displayed especially high concentrations of $\Sigma PFAS_{\text{short-chain}}$ (up to 32 ng L^{-1}) and $\Sigma PFAS_{\text{long-chain}}$ (up to 2.6 ng L^{-1}). Furthermore, results showed that PFAS concentrations in the under-ice seawater were over 2-fold higher at one site which is suspected to have endured an early season melting episode. These results demonstrate that snow and sea ice are important dynamic reservoirs of these chemicals, and that rapid melting can dramatically influence the transfer and hence concentrations in adjacent compartments like surface seawater.

In summary, the main findings from this thesis indicate that atmospheric transport of POPs and their chemical precursors from industrial regions to very remote regions like Antarctica (and well removed from local anthropogenic activities) is ongoing and continuing to rise. Secondly, the incorporation, distribution and enrichment of POPs in sea ice is strongly influenced by the presence and dynamics of ice brine; a major feature in fresh, single season ice which now dominates ice cover across the Arctic Ocean. Thirdly, snow-ice and hence the ice-rafted snowpack contains relatively high concentrations of PFAS. These findings in

combination with changes to the physical aspects of the ice environment such as the transition from thicker multi-year sea ice a much thinner first-year sea ice, extreme temperature fluctuations and hence earlier and more intense seasonal ice melting, are all likely to influence the biogeochemistry and cycling of POPs in the Polar marine environment. In particular, sympagic organisms of the lower marine food web (e.g. ice algae, copepods, amphipods etc) whose niche includes brine channels on the underside of sea-ice may be subject to increased contaminant exposure in a warming Arctic

Acknowledgements

I would like to thank the teams of people behind organisations such as NERC and my ENVISION doctorate training programme who funded my research. I would like to thank my supervisors Crispin Halsall, Peter Wynn and Amber Leeson. In particular, Crispin was there to support me from the onset to the end, put a great deal of trust in me and was always positive and reassuring. He created several opportunities through which I was able to meet many special people and share some incredible experiences – ones that I feel very lucky and privileged to have been a part of! I'd especially like to thank key people at HZG (Ralf Ebinghaus), BAS (Robert Mulvaney), UEA (Jan Kaiser), and the Nansen Legacy (Marit Reigstad) for inviting me as a guest to work with them at their institutions. I'd then like to also send my appreciation to each and every person working within their groups for their efforts, and for making me feel so welcome during all of my visits - all of this made for an exciting learning experience which undoubtedly contributed to the overall success of this thesis. I would also like to thank Cris, Gustaf, Jon and Brittany and everyone else in LEC for being good friends, and my good mate, Dan, for lending me an escape from PhD life during the weekends. Finally, I would also like to thank my family. They all provided me with, in one way or another, the motivation to knuckle down, suffer the long hours and follow my dreams.

"Through endurance we conquer." - Ernest Shackleton

Abbreviations

AFFF	aqueous film forming foam
AMAP	arctic monitoring and assessment programme
BAF	bioaccumulation factor
BCF	bioconcentration factor
DDT	dichlorodiphenyltrichloroethane
ESI	electrospray ionization
FOSAs	Perfluoroalkane sulfonamides
FOSEs	Perfluoroalkane sulfonamido ethanols
FTIs	fluorotelomer iodides
FTOHs	fluorotelomer alcohols
HCHs	hexachlorocyclohexanes
HRMS	high resolution mass spectrometry
HZG	Helmholtz-Zentrum Geesthacht
IDL	instrumental detection limit
K_H	Henrys Law constant
km	kilometre
LC	liquid chromatography
log K_{OW}	log octanol-water partition coefficient
LRTP	long-range transport potential
MDL	method detection limit
MQL	method quantification limit
MRM	multiple reaction monitoring
MS	mass spectrometry
MS/MS	tandem mass spectrometry
OP	organochlorine pesticides
p^0	vapour pressure
PBDEs	polybrominated diphenylethers
PASF	perfluoroalkane sulfonyl fluoride
PCBs	polychlorinated biphenyls
PFAAs	perfluoroalkyl acids
PFASs	per- and polyfluoroalkyl substances
PFCAs	perfluoroalkyl carboxylic acids
PFSAs	perfluoroalkane sulfonic acids
POPs	persistent organic pollutants
PTFE	polytetrafluoroethylene
PVDF	polyvinylidene fluoride
QqQ	triple quadrupole
QToF	quadrupole time-of-flight
SD	standard deviation
SO_2	Sulphur dioxide
SPE	solid phase extraction
UNEP	united nations environment program
WAX	weak anion exchange

Chapter 1

An introduction to Persistent Organic Pollutants in the Polar Regions.

This chapter provides a brief introduction to Persistent Organic Pollutants (POPs) and their environmental properties. It details our current understanding of the biogeochemical cycling and fate in the environment. Particular attention is given to PFASs and includes a review of previous research undertaken.

1.1. POPs characteristics

Persistent organic pollutants (POPs) are becoming an increasingly diverse group of chemicals that display a wide range of physicochemical properties and pose a high risk to human health and the environment. The term POPs first originated around the 1970s following the publication of Rachel Carsen's book *Silent Spring* which highlighted that many of the chemicals that were being manufactured to help improve human society in fact were also harmful to wildlife even at ultra-low levels (Carson, 2002). Classification of POPs was first established as part of the Stockholm Convention in 2004 (https://www.env.go.jp/chemi/pops/treaty/treaty_en2009.pdf) which bases its assessment on four main criteria. These include a chemicals resistance to degradation (i.e. persistence; P), bioaccumulation potential (B), and toxicity (T), as specified in Annex D of the Stockholm Convention. In addition, a chemical must also display long-range transport potential (See Table 1).

Table 1: Hazard criteria used by the UNEP Stockholm Convention on POPs to designate candidate chemicals as persistent organic pollutants (POPs).

Chemical property or criteria	Criteria
Persistence (P)	$t_{1/2}$ >2 months [water] $t_{1/2}$ > 6 months [soil, sediment]
Bioaccumulation (B)	log K_{OW} >5, or Bioconcentration factor (BCFs) in aquatic species >5000
Toxicity (T)	Evidence (or *potential)* of adverse effects to human health or to the environment
Long-range transport potential (LRTP)	$t_{1/2}$ >2 days [air]

POPs are often halogenated compounds, meaning that they contain one or more bromine, chlorine or fluorine atoms bonded to a carbon atom within their chemical structure. The high stability of these bonds gives chemicals the capacity to resist biotic and abiotic degradation in the environment, resulting in long environmental half-lives ($t_{1/2}$) of over up to several decades. As such, POPs are not easily metabolised in the body of organisms and instead accumulate in

biological tissues over time. Their accumulation in tissues is related to their high solubility in fatty tissues (lipophilic) or ability to bind to proteins (proteinophillic) such as tissues in the liver. A chemical substance's bioaccumulation potential is usually evaluated in a regulatory context by two quantitative criteria. The first screening criterion is based on the logarithm of K_{OW} (log K_{OW}). The log K_{OW} is a partition coefficient for the two-phase system consisting of *n*-octanol and water (at equilibrium), where n-octanol is used as a chemical surrogate to fat (see Table 2). Compounds with log K_{OW} values of 5 are considered to be bioaccumulative. While K_{OW}-based criteria is appropriate for predicting the partitioning of some lipophilic substances, for many contaminants of emerging concern (CECs) which display surfactant-like properties, such as PFAS, its use is not suitable due to their tendency to accumulate at medium interfaces. Instead, a second criterion which is applicable to both organic lipophilic and CEC contaminants is based on empirical bioaccumulation data, expressed as either bioconcentration factor (BCF) or bioaccumulation factor (BAF) values. Values for BCFs can be measured in the laboratory using standardized protocols with aquatic organisms using a water-borne exposure procedure e.g. (OECD, 2012). However, while BCF values estimate chemical uptake into a biological matrix only from its surrounding medium (i.e. water) under controlled laboratory conditions, BAF values express the uptake of chemical from multiple exposure routes such as water and food and can be estimated from laboratory experiments or data collected in the field. Ratios of BAF/BCF can then be used as an alternative method for classifying a chemical as having bioaccumulative potential. POPs elicit a number of serious toxicological effects and neurotoxicity, carcinogenicity and endocrine disrupting (hormone) effects have all commonly been reported in different. Hence, even at low doses they pose a high risk to the environment. As many POPs are semi-volatile chemicals, they are able to undergo long-range transport potential (LRTP) across the globe with prevailing oceanic and air currents. Assessing the LRTP of a substance in either air or water is generally performed by taking a modelling approach which consider physicochemical properties and reversible transport to other environmental media. (Beyer et al., 2000)

1.2. Sources of POPs

Many POPs were, and still are intentionally manufactured for uses in a variety of agricultural and industrial applications, consumer goods, and some formed as by-products of combustion processes. As such, POPs are released into the environment from a range of point (i.e. industrial chimney stacks and waste water effluent) and diffuse (i.e. consumer use) sources throughout their production, usage and disposal (Dinglasan-Panlilio and Mabury, 2006, Barber et al., 2007, Wang et al., 2014a, Wang et al., 2014b). Organochlorine pesticides (OCPs) were developed for large-scale use around the 1940s and used extensively as agricultural insecticides (e.g., HCH; hexachlorocyclohexane) and spread in the environment (DDT; dichlorodiphenyltrichloroethane) in order to increase food productivity and prevent the spread of insect-borne human diseases, such as malaria. Others were developed for use in electrical, heat transfer and hydraulic equipment along with plasticizers in paints, plastics and rubber products (e.g. polychlorinated biphenyls; PCBs). While others were incorporated within furniture items and electrical goods as flame retardants (e.g. polybrominated diphenyl ethers; PBDEs) to improve fire safety records. Many sources of these now so-called 'legacy' POPs have been subject to global policy, leading to the reduction in use and, in many cases, eliminating their use altogether (See Section 1.4).

However, there are an increasing number of 'emerging' chemicals that fulfil the criteria of being a POP. Consisting of several thousand individual members and structural isomers, per- and polyfluoroalkyl substances (PFASs) have been used in wide array of industrial processes and consumer goods since the 1950s as high-performance surface acting chemicals (i.e. surfactants) such as aqueous film forming foam (AFFF) in firefighting foams or during the manufacture of fluoropolymers like Teflon. The chemicals structure of PFASs consist of a carbon chain of varying length (usually C_4 – C_{14}) that is either fully (per) or partly (poly) fluorinated and connected to different functional groups. Based on these features, PFASs can be categorised into many sub-groups in order to differentiate their distinct functional and environmental behaviours (See Figure 1).

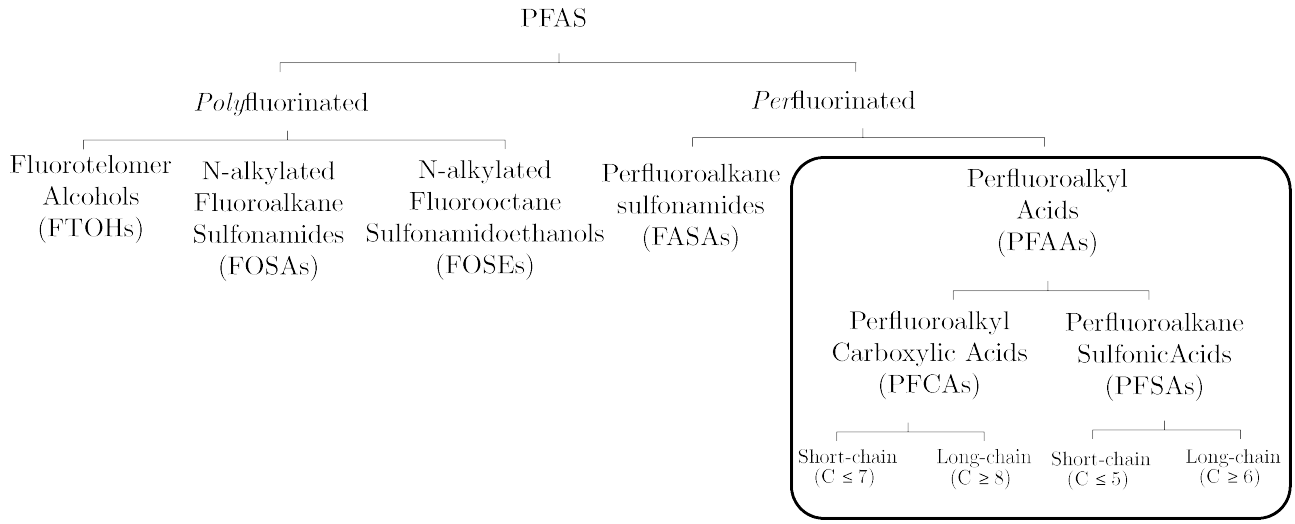

Figure 1: Boxed group indicates key PFASs discussed in this thesis.

Perfluoroalkyl acids (PFAAs) are a key group of PFASs that show significant adverse impacts on the environment. PFAAs are comprised of perfluoroalkyl carboxylic acids (PFCAs) and perfluoroalkane sulfonic acids (PFSAs). Key members of each respective group include PFOA (C8) and PFOS (C8) (See Figure 2), and both have been used widely throughout industry leading to their direct release into the environment. However, in addition to their direct emissions, PFAAs are also formed indirectly in the environment from a range of volatile chemical precursors (Butt et al., 2009, Sulbaek Andersen et al., 2005, D'Eon J et al., 2006) for example) which are also broadly encompassed in Figure 1. These compounds are often used as chemical intermediates for end-products and contained as residual impurities in some polymeric products used to provide stain and water repellency to textiles and paper packaging (Paul et al., 2009). Recently, Pickard et al., (2020) determined that a number of CFC-replacement compounds (e.g. heat exchange fluids) also probably served as large sources of ultra-short-chain PFCAs (e.g. Trifluoroacetic acid; TFA) to the polar environment.

Perflurocarboxylates

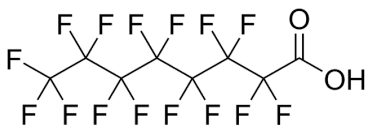

Perfluorosulfonic acids

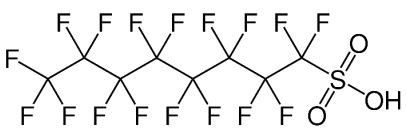

Figure 1: Examples of chemical structures of perflurocarboxylates (PFOA, C_8) [left] and perfluorosulfonic acids (PFOS, C_8) [right].

1.3. Pathways of POPs to polar regions

A comprehensive discussion regarding the processes involved in the global cycling of POPs is provided in a review (Wania, 1996) and illustrated in Figure 2. Briefly, POPs are transported by a combination of oceanic and atmospheric currents, or a global "distillation process", through which chemicals undergo repeated cycling of evaporation and deposition. Chemicals that partitions to air will more readily be transported from source regions to polar regions than those that partition to water due to the large difference in transport timescales of air (days) compared with ocean (years) currents. A substance's physicochemical properties (Table 1) is therefore one of the major factors driving the long-range transport. Many POPs are semi-volatile nature (i.e. vapour pressures of logP -1 to -7), which enables them to partition to air at ambient temperatures and hence sensitive to ambient temperature fluctuations. This property facilitates their migration from lower latitudes to remote regions at higher latitudes through repeated cycles of volatilisation (T = 'high') and partitioning/sorption to surfaces (T = 'cold'), a process commonly referred to as the 'grasshopper effect'.

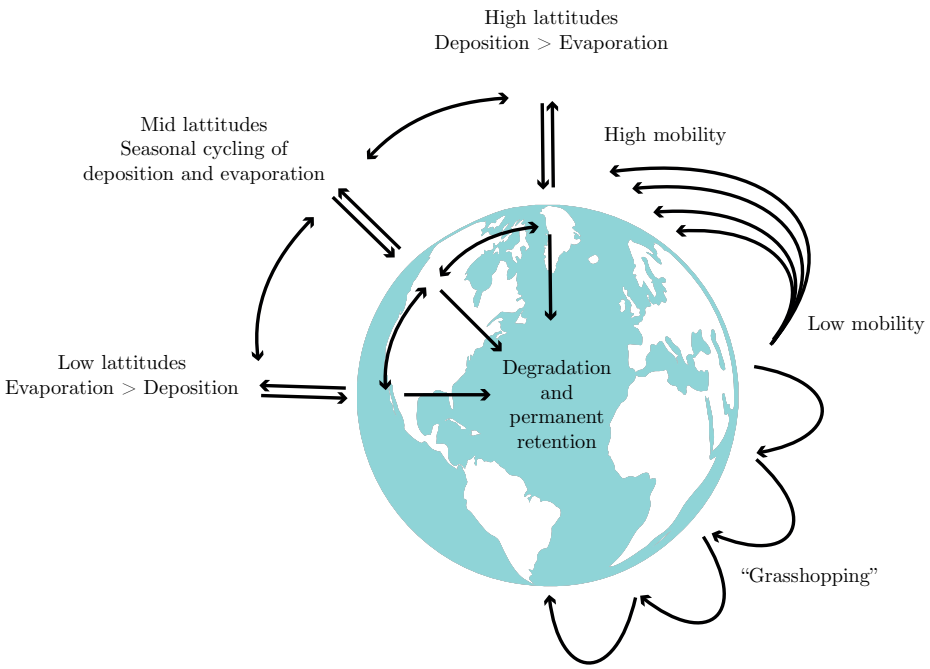

Figure 3: Major processes driving the long-range transport of POPs in the environment (adapted from Wania, 1996)

Another key physicochemical property that closely influences the long-range transport potential of a substance is its aqueous solubility. Its affect is best illustrated through the Henry's Law constant (K_H, Equation 1), which describes the relationship between the amount of a gaseous substance in air and in water (at equilibrium) representing the propensity of a chemical to remain in the gas-phase at a given temperature. It is therefore an important environmental parameter for pollutant characterisation and determining their environmental fate. Chemicals that display higher K_H values are more likely to partition to the gaseous-phase and be carried to the poles through air currents, while those that exhibit lower K_H values tend to partition to the dissolved-phase and transported by ocean currents. As a result, even semi-volatile POPs which display relatively low volatilities may be inclined to partition to air if their aqueous solubility is suitably low (i.e. high K_H values). Given that vapour pressure (p^0) decreases and the aqueous solubility of gases increases with lower temperatures, it is clear to see that under the colder climates K_H values decrease for many chemicals and thus partition from air towards cold polar waters.

Table 2: Description of key physicochemical properties used to determine the long-range transport potential of chemicals in the environment.

Physicochemical property	Description
Vapour pressure [Pa]	Vapour pressure (p^0) is a measure of the tendency of a material to change into the gaseous or vapour state, and it increases with temperature (Schwarzenbach, 1993).
Aqueous solubility [mol/m^3]	The aqueous solubility (Paul et al.) is the maximum amount of a chemical substance (the solute) that can dissolve in a given volume of water, and it usually increases with decreased water temperature (Schwarzenbach, 1993) . Note: Organic compounds tend to become less soluble with added salts
Henry's Law Constant [Pa m^3/mol]	The Henry's law constant (K_H) (also called the air–water partition coefficient) is the ratio of a compound's partial pressure in air to the concentration of the compound in water at a given temperature at equilibrium. $K_H = p/C_W$ Equation 1 where p = partial pressure of gas with a solution (Pa) C_W =molar concentration of gas in liquid solution (mol/m^3)
Octanol-water partition coefficient (K_{OW}) [dimensionless]	The octanol-water partition coefficient (K_{OW}) is widely used to represent the equilibrium distribution of organic contaminants between lipid phases and water. It can be defined as a ratio of chemical solubility in octanol and water, and it varies weakly with temperature. $K_{OW} = C_O/C_W$ Equation 2 where C_O = molar concentration in octanol (mol/m^3) C_W =molar concentration in water (mol/m^3) * n-octanol is C_8 aliphatic organic compounds used as a surrogate for fat

Importantly, some precursor compounds (See Table 1) exhibit extraordinarily high K_H values (>7-orders-of magnitude higher than corresponding POPs) and display sufficiently long atmospheric lifetimes (i.e. $t_{1/2}$ > 2 days). that prevailing air currents proceed as a highly

efficient transport mechanism for these compounds into the polar regions These include, for example, fluorotelomer alcohols, n-alkyl perfluoroalkane sulphonamides and n-alkyl perfluoroalkane sulphonamide ethanols (Butt et al., 2009, D'Eon J et al., 2006, Ellis et al., 2004, Sulbaek Andersen et al., 2005, Wallington et al., 2006). Their subsequent photochemical oxidation in the atmosphere has been shown to yield PFAAs, such as PFOS and PFOA, and demonstrates an important indirect transport pathway for POPs to enter into the remote polar regions (Yeung et al., 2017, Benskin et al., 2011, Casal et al., 2017).

Table 3: Physicochemical properties of key POPs and chemical precursors. Values for physicochemical properties represent the range reported for that particular chemical group. K_H values were calculated using vapour pressures and aqueous solubility. PFAA-precursors include fluorotelomer alcohols, n-alkylated perfluoroalkane sulfonamidoethanols and n-alkylated perfluoroalkane sulphonamides and perfluoro methacrylate. PFAAs include PFOA and PFOS. HCH include both alpha and gamma isomers. PCBs include tri to deca-PCBs. PBDEs include tri- to hepta-BDEs. n/a indicates values that were not applicable.

Chemical	Log K_{OW}	Vp (Pa)	S_W (mol/m^3)	K_H (Pa m^3/mol)
PFAA-Precursors (Xie et al., 2013) (Concawe, 2016)	3.2 – 6.7	5.0×10^{-3} – 3.4×10^{2}	5.3×10^{-8} – 1.6×10^{-1}	3.2×10^{2} – 5.8×10^{7}
PFAAs (Kaiser et al., 2005) (Kauck and Diesslin, 1951) (Concawe, 2016)	2.8 – 7.7	2.7×10^{-1} – 4.2×10^{0}	1.4×10^{0} – 2.3×10^{1}	2.0×10^{-1} – 3.1×10^{1}
HCHs (Xiao et al., 2004)	3.8	7.6×10^{-2} – 2.5×10^{-1}	2.5×10^{-1} – 3.3×10^{-1}	3.1×10^{-1} – 7.4×10^{-1}
PCBs (Mackay, 2006)	5.0 – 8.2	3.0×10^{-5} – 2.2×10^{-1}	1.4×10^{-6} – 2.4×10^{-3}	2.1×10^{0} – 9.2×10^{0}
PBDEs (Wania and Dugani, 2003)	5.7 – 8.3	1.1×10^{-6} – 1.6×10^{-3}	8.7×10^{-6} – 8.2×10^{-4}	1.3×10^{-1} – 2.0×10^{0}

It should be noted that Kow values for most PFAS are difficult to measure as they do not follow the typical lipid partition dynamics, due to their unique surfactant-like properties.

The transport of POPs to remote regions is complicated and involves partitioning between environmental matrices, such as water, vegetation and soil/organic matter. Chemical parameters such as the octanol-water partition coefficient (K_{OW}) (See Equation 2) is frequently used to describe such partitioning between different phases. Similarly, although advection with surface ocean currents is predicted to operate on much longer timescales, relative to transport

in the atmosphere, model simulations show that deep Arctic seawater holds a large chemical burden and concentrations are still increasing for some POPs, such as PFOS, thus may be important in the future ocean (Yeung et al., 2017). Equally, in Antarctica, the Antarctic Circumpolar Current (ACC) is thought to play a unique role in the Southern Ocean which helps to prevent the exchange of surface waters originating from temperate, relatively contaminated regions with more pristine coastal waters around the continent (Bengtson Nash et al., 2010). Nevertheless, the generation of marine aerosols at the ocean surface (Johansson et al., 2019, McMurdo et al., 2008, Reth et al., 2011) may play a role in water-to-air transfer of some pollutants, complicating the pathways by which POPs enter the polar regions. Similarly, semi-volatile POPs tend to partition strongly to organic phases in the environment, such as organic matter (airborne particle matter, soil, sediment) and lipids in biota. For example, the movement of biomass (e.g. associated with large scale seasonal migrations of certain species) from relatively polluted oceans to polar seas can provide a localised source of contaminants to the polar regions (Blais, 2005).

1.4. Key biogeochemical processes affecting POPs in the marine polar environment

Once present in remote cold environments, the environmental half-life (i.e. persistence) of POPs is anticipated to be enhanced compared with temperate regions due to low temperatures and low sunlight, both of which reduce the rate of abiotic (photolytic) and biotic (microbial) degradation processes and which are reported to offer some influence on the seasonality in Arctic air levels of some substances (Wong et al., 2021). While the presence of POPs has been reported in environmental compartments (e.g. air, seawater, snow, ice, soil, biota) within both the Arctic and Antarctic regions (See Table 2 for studies investigating PFASs), the fate of these chemicals and their transfer processes between different matrices or environmental compartments is not well understood (AMAP, 2010). It is predicted that their spatiotemporal distribution is dependent on a highly dynamic system of interlinked processes, for example, the coastal marine system of the Arctic (illustrated in Figure 2). Importantly, some abiotic processes may be closely coupled with biotic systems, meaning that natural processes (e.g. ice growth, snow deposition) could significantly raise chemical concentrations (e.g. through snow

accumulation), thereby enhancing biological exposure in nearby matrices. Given that most of the primary productivity in the Arctic occurs within the surface oceans, this region seems most likely to host a major role in the uptake of POPs into the marine food web.

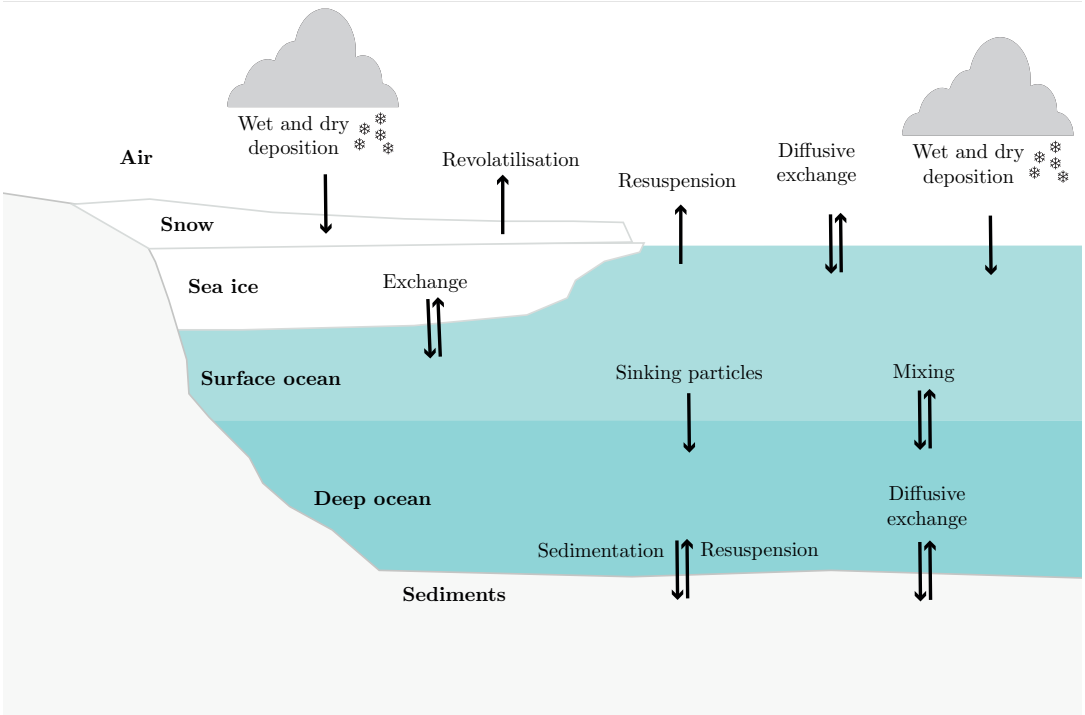

Figure 4: A qualitative illustration of key biogeochemical processes affecting the distribution of persistent organic pollutants in the Polar marine environment

The mechanisms involved in atmospheric transport of POPs and their subsequent exchange between adjacent compartments can be complex and depends on specific physicochemical properties. Diffusive processes at the air-ocean interface are believed to play an important seasonal role through the so-called 'biological pump', which occurs through the uptake of POPs into marine phytoplankton in surface waters (bioaccumulation), thereby enhancing the diffusive drawdown or flux of POPs from the atmosphere into the oceans. While this may be important for some semi-volatile POPs (e.g. HCH) (Jantunen et al., 2015, Wong et al., 2011, Jantunen et al., 2008, Jantunen and Bidleman, 2006), for others that are characterised by low vapour pressures and high water solubilities (e.g. PFAAs), this process is predicted to be relatively less important. Instead, wet and dry deposition are likely to be the major mechanisms of removal of PFAS from the atmosphere, which can occur from the scavenging of particle-bound PFAS (Wong et al.) or partitioning of gaseous PFAS to water (wet) droplets (Dreyer

et al., 2010, Barton et al., 2007). Due to the lower temperatures in polar regions, gaseous POPs present in the atmosphere partition more from a vapour-phase towards solid or condensed phases. As such, snow has been shown to be a highly efficient scavenger of many airborne POPs (Halsall, 2004, Xie et al., 2015, Burniston et al., 2007) and shown to play a crucial role in the biogeochemistry of many POPs in polar regions.

Snow is deposited directly onto ocean surfaces and on sea ice surfaces throughout the year in the Polar regions, serving as a source and temporary reservoir of POPs (Casal et al., 2019) to the polar environment. Melting and changes in snow properties, particularly increases in snow density during snow aging after a snow deposition event, leads to a reduction in its storage capacity of POPs (Herbert et al., 2006). While this can result in a large fraction and the net transfer of many semi-volatile POPs back into to air (Casal et al., 2019), there is less information regarding the environmental fate those chemical that remain dissolved within snowmelt, which may be particularly pertinent for other less volatile POPs, such as PFAAs. Given that PFASs have been widely detected in the remote polar environment (See Table 3), questions still remain regarding whether these chemicals are subsequently incorporated into sea ice or transferred to the underlying ocean.

Table 4: Studies that investigated PFASs in the remote polar environment.

Matrix	Reference	Concentrations of select PFAAs
Air	(Wong et al., 2018) (Xie et al., 2015) †(Wang et al., 2015) †(Dreyer et al., 2009) †(Vento et al., 2012)	PFBA = <0.01 – 29 pg m^{-3} (Wong et al., 2018) PFBS = <0.01 – 1.5 pg m^{-3} (Wong et al., 2018) PFOA = <0.01 – 4.0 pg m^{-3} (Wong et al., 2018) PFOS = <0.04 – 2.8 pg m^{-3} (Wong et al., 2018)
Snow	(Kwok et al., 2013) (Pickard et al., 2020) (Pickard et al., 2018) (Codling et al., 2014) (Macinnis et al., 2017) (MacInnis et al., 2019) (Cai et al., 2012b) †(Xie et al., 2020) † (Cai et al., 2012a) †(Casal et al., 2019)	PFBA = <130 – 1000 pg L^{-1} (Cai et al., 2012b) PFBS = <17 – 170 pg L^{-1} (Cai et al., 2012b) PFOA = 39 – 82 pg L^{-1} (Cai et al., 2012b) PFOS = <21 pg L^{-1} (Cai et al., 2012b)
Sea ice	(Cai et al., 2012b) (Bertrand et al, unpublished) *There are currently no studies investigasting the levels of PFAS in sea ice in the Southern Ocean and Antarctica*	PFBA = <130 – 430 pg L^{-1} (Cai et al., 2012b) PFBS = <17 – 1500 pg L^{-1} (Cai et al., 2012b) PFOA = 57 – 710 pg L^{-1} (Cai et al., 2012b) PFOS = <21 – 73 pg L^{-1} (Cai et al., 2012b)
Seawater	(Joerss et al., 2020) (Yeung et al., 2017) (Cai et al., 2012b) (Li et al., 2018, Benskin et al., 2012, Rosenberg, 2008) (Bertrand et al, unpublished; see (Muir, 2019 #167)· †(Zhao et al., 2012)	PFBA = <130 – 360 pg L^{-1} (Cai et al., 2012b) PFBS = <17 – 78 pg L^{-1} (Cai et al., 2012b) PFOA = <20 – 67 pg L^{-1} (Cai et al., 2012b) PFOS = <21 – 53 pg L^{-1} (Cai et al., 2012b)

Studies investigating air mostly include volatile precursor compounds but also show PFAAs (e.g. Wong et al., 2018) †Denotes those studies that are based in Antarctica and the Southern Ocean. Examples of concentrations data are shown for select short-chain (PFBA and PFBS) and long-chain (PFOA and PFOS) PFAAs in remote Arctic region.

Currently, there is a limited number of studies that have investigated the occurrence and accumulation of POPs in sea ice (Pućko et al., 2011, Lacorte et al., 2009, Douglas et al., 2012, Gustafsson et al., 2005, Hargrave et al., 1988, Hargrave et al., 1992, Melnikov et al., 2003, Dickhut et al., 2005, Dickhut et al., 2012, Chiuchiolo et al., 2004, Tanabe et al., 1983). Recently though, Pućko *et al.* (Pućko et al., 2010a, Pućko et al., 2010b, Pućko et al., 2012, Pućko et al., 2015) provided several field based studies focussing around the Beaufort Sea that investigated the behaviour of α-hexacyclohexane (α-HCH), which provided a much more comprehensive understanding of the processes involved during sea ice formation, ageing and processes associated with melt-ponds (See Figure 5). Their key findings implied that brine, a salt-rich liquid that forms during the freezing of seawater within sea ice, was a major

component of sea ice and strongly influenced the concentrations and distribution of α-HCH during sea ice formation and melt. Moreover, the fluid transport of brine was strongly affected by atmospheric conditions (i.e. temperature) and α-HCH concentrations were also affected by the overlying snowpack and melt ponds.

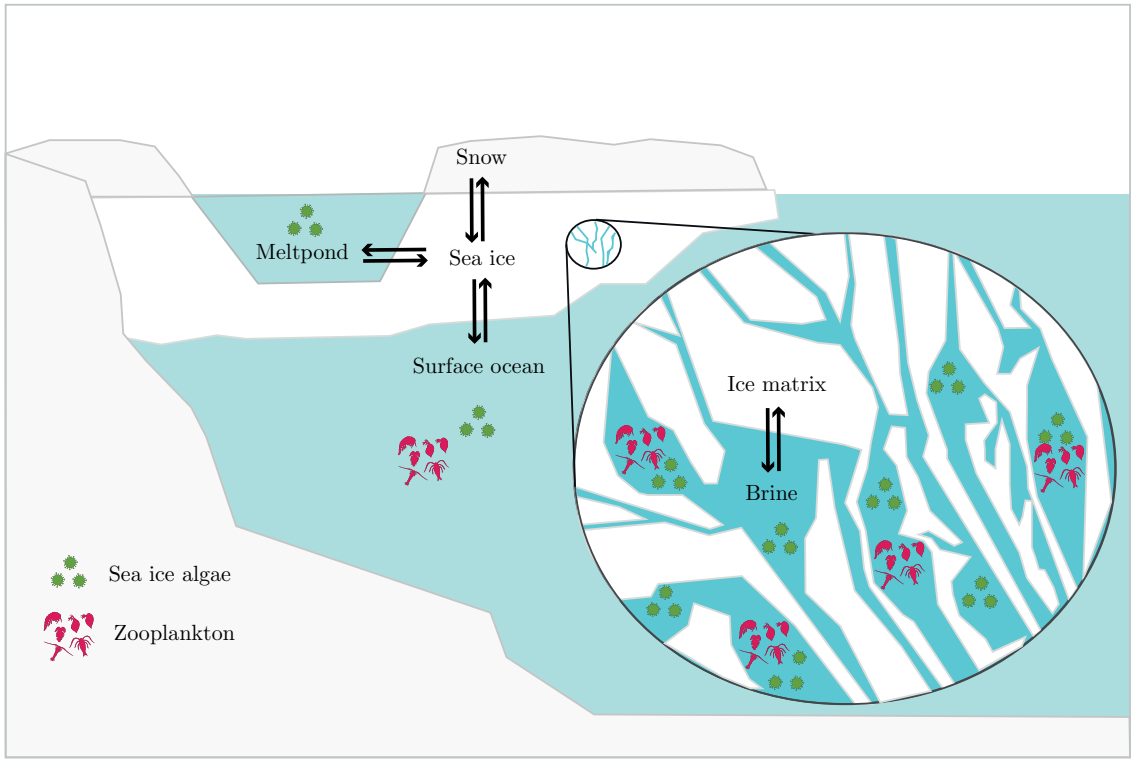

Figure 5: Transfer processes of POPs associated with sea ice

Sea ice is a major component of the polar environment that is formed from the ocean and in Winter covers a vast area in the Arctic (approx.15 million km^2) and Antarctic (approx. 20 million km^2). Until recently, sea ice has been regarded as an inert barrier that limited the exchange of materials between adjacent compartments. Yet, its influence on the uptake, storage and release of cycling of inorganic (e.g. nutrients) and organic matter and chemicals during its lifecycle has been realised for a long time. Sea ice is a major habitat for a rich and diverse community of micro-organisms (sympagic organisms) that can be responsible for up to 60% of the total marine primary productivity in polar oceans at certain time of the year (Fernández-Méndez et al., 2015). Moreover, sea ice serves as a refuge and feeding ground for invertebrates and other biological organisms further up the food web. Hence, it is possible that

sea ice influences the spatiotemporal distribution of POPs in the polar environment and crucially provides a pathway for contaminants to enter into the marine food web (Chiuchiolo et al., 2004, Zhang et al., 2019).

1.5. Overview to international legislative controls of POPs

The 1979 Geneva Convention on Long-range Transboundary Air Pollution was the first legally binding policy that aimed to promote intergovernmental cooperation for the protection of the environment. It was developed after the disastrous effects of acid rain on Scandinavian lakes were shown to have originated from the emissions of sulphur dioxide (SO_2) and other compounds (Grennfelt et al., 2020) thousands of kilometres away in Europe. In 1991, the Arctic Monitoring and Assessment Programme (AMAP) was established to monitor a number of priority 'pollution issues of concern', which revealed unexpectedly high levels of some pollutants in the region. Following data collected under AMAP, important negotiations led to the Aarhus Protocol on POPs in 1998, one of eight additional protocols that was adopted into the Geneva Convention, each one focussing on a key groups of air pollutants. Later supported by UNEP, the Stockholm Convention on POPs in 2004 included an initial list of 12 groups of chemicals and aims to eliminate or restrict the production and use of persistent organic pollutants.

Presently, only a small number of PFASs have been officially regulated through the Stockholm Convention despite signs that many of these chemicals share similar properties and demonstrate a similar risk profile to humans and wildlife. One recent addition is perfluorooctane sulfonic acid (PFOS) and perfluorooctane sulfonyl fluoride (POSF), which is permitted for "restricted use" (Annex B) in 2009. Additionally, perfluorooctane carboxylic acid (PFOA), its salts and PFOA-related compounds was banned (Annex A) of the Stockholm List in 2017. Several major fluorochemical companies aided by the Unites States Environmental Protection Agency (US EPA) adopted a voluntary regulatory program in 2000. The goal of this global PFOA Stewardship Program was to reduce chemical production and environmental releases of PFOA, its precursors and other long-chain PFAAs by 2015 (US_EPA, 2018).

The effect of phasing out long-chain per- and polyfluoroalkyl substances on the concentrations of perfluoroalkyl acids and their precursors in the global environment; however, remains in question. Land et al. (2018) recently published a systematic review which highlighted that while the levels of some PFSA- and PFCA- precursors in the global atmosphere have seen a significant reduction, others appear to be stable or even increased in remote air (e.g. FTOHs). Moreover, there are currently no clear patterns of declining levels of perfluoroalkyl acids in the environment (Land et al., 2018). Hence, continued monitoring of PFASs in the environment is essential to evaluate the global impact of policies.

1.6. Climate change

The polar regions are reported to be currently undergoing unprecedented climate-related changes, affecting several key environmental properties such as atmospheric and ocean temperature. So far, trends indicate that the Arctic is warming at more than twice the rate of the global average, which is having a substantial impact on sea ice. Scientists have already observed a strong declining trend in the areal extent of Arctic sea ice cover during winter and summer, which currently ranges between 4 and 16 million km^2, respectively. This has also been tied with a reduction in the volume.

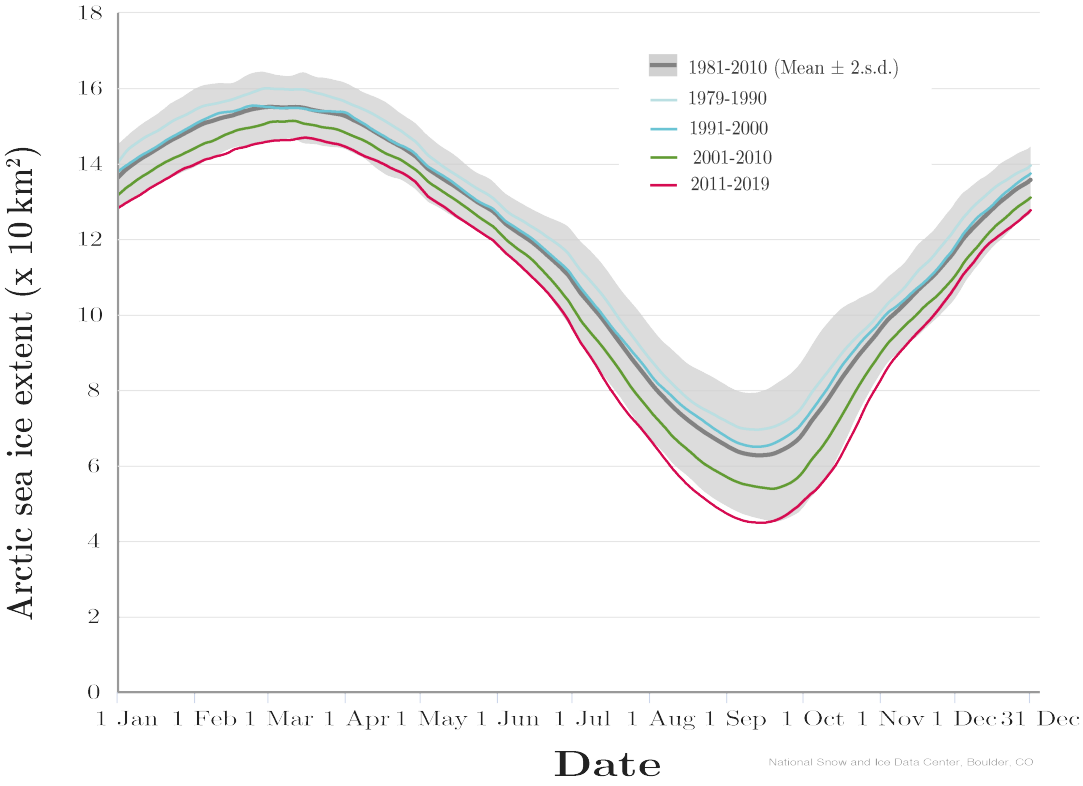

Figure 6: Seasonal variation in Arctic sea ice extent determined from satellite sensing data (Area of ocean with at least 15% sea ice)(NSIDC, 2020a)

Furthermore, the nature of sea ice is also changing, with over 70% of the sea ice in the Arctic Ocean now belonging to first-year sea ice (FYI). The transition of sea ice from an older multi-year ice (MYI) to a predominantly FYI sea ice brings with it an elevated chance of containing a higher brine content, being significantly thinner ice pack and possibly relatively more snow. The onset of spring melt has also been shown to occur earlier in the annual cycle and it has been reported in some regions of the Arctic that melting is occurring more intensely. Collectively, these processes are likely to have a dramatic impact on the biogeochemical cycling of POPs in the future, possibly through the increase in brine increasing their amount during winter and suddenly releasing chemicals during spring/summer when biological activity in the oceans and sea ice is high. Together these processes could exacerbate bioaccumulation and biomagnification, resulting in entire ecosystems being subject to additional stressors and increasing risk to human health through diet.

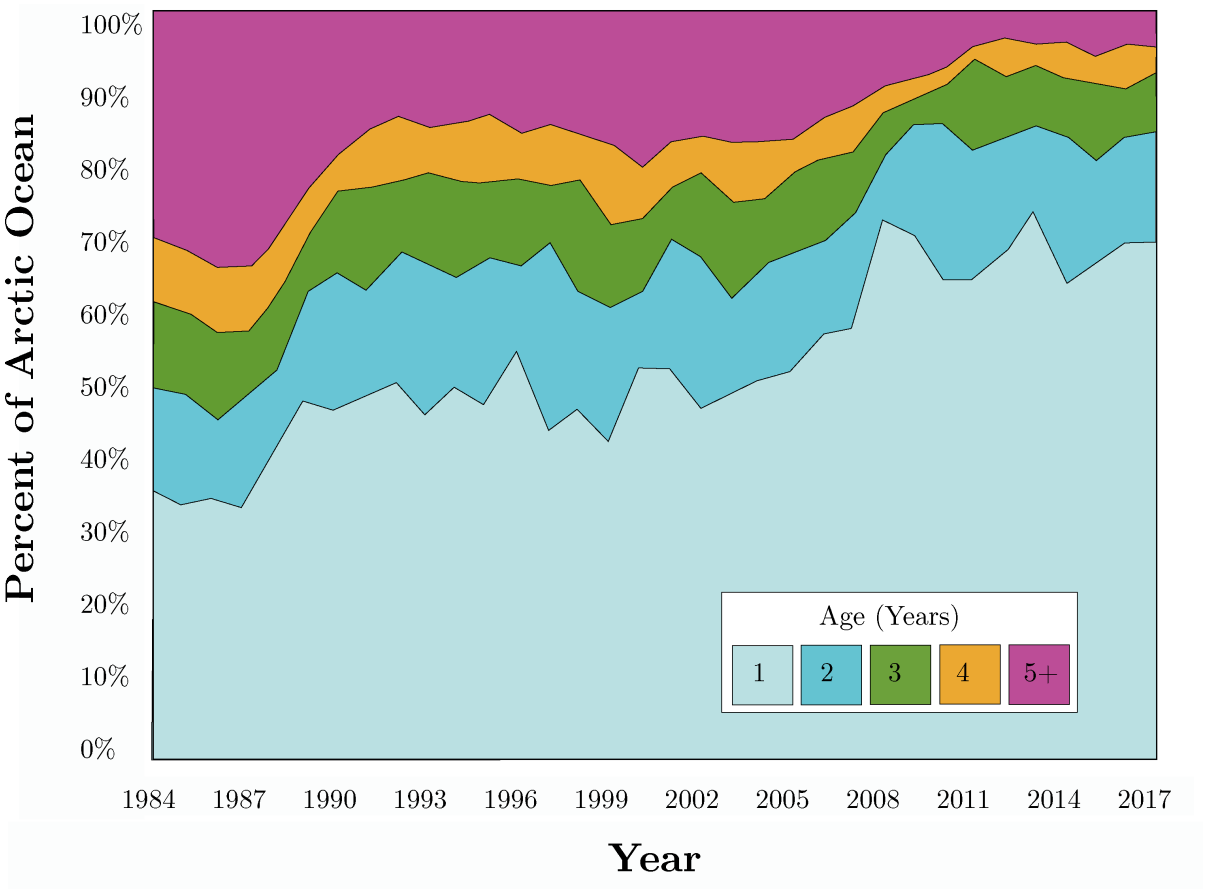

Figure 2: Timeseries of sea ice age percent coverage of the Arctic Ocean determined using satellite sensing data (NSIDC, 2020b)

1.7. Knowledge gap and thesis aims

POPs display widely different environmental characteristics, present a range of chemical sources and follow various long-range transport pathways into the polar regions. Despite being heavily regulated throughout the world, many POPs and their precursors are still expected to be in use around the world and a large proportion of historical global emissions are expected to continue adding to the existing chemical burden in polar regions. Currently, there is a lack of long-term monitoring data in polar regions and an absence of data regarding their spatial distribution. Moreover, there is little knowledge on how different POPs interact with their surroundings and are transferred between different compartments (i.e. snow, sea ice and seawater), in particular at times of the year that undergo large seasonal changes in temperature. Given the scale of change that is currently being observed in those regions, an urgent effort to understand how fundamental physical and chemical processes govern the fate and behaviour of POPs in these sensitive ecosystems is needed. Hence, the overall aim of this PhD thesis is to investigate the occurrence and accumulation of POPs in snow and ice of the Earths Polar regions. The specific objectives are:

a) To establish a decadal time series of PFAS contamination in a dated remote Antarctic snowpack and determine chemical sources as a proxy for global emission patterns (Chapter 2)

b) To obtain empirical evidence in a controlled laboratory setting which enables a mechanistic insight into the uptake and fate of persistent organic pollutants in sea ice during ice growth and melt (Chapter 3)

c) To further investigate the uptake and enrichment of POPs using poly- and perfluoroalkylated substances (PFASs) in artificial sea ice (Chapter 4)

d) To evaluate the distribution of PFASs in the Arctic marine environment and determine possible chemical pathways into the Arctic marine food web (Chapter 5)

e) To consolidate the information throughout the previous chapters to provide a broad overview of the importance of biogeochemical cycling of POPs in a future warming polar climate (Chapter 6)

1.8. References

AMAP 2010. AMAP Assessment 2009: Persistent Organic Pollutants (POPs) in the Arctic. *Science of the Total Environment.*

BARBER, J. L., BERGER, U., CHAEMFA, C., HUBER, S., JAHNKE, A., TEMME, C. & JONES, K. C. 2007. Analysis of per- and polyfluorinated alkyl substances in air samples from Northwest Europe. *Journal of Environmental Monitoring,* 9**,** 530-541.

BARTON, C. A., KAISER, M. A. & RUSSELL, M. H. 2007. Partitioning and removal of perfluorooctanoate during rain events: the importance of physical-chemical properties. *Journal of Environmental Monitoring,* 9**,** 839-846.

BENGTSON NASH, S., RINTOUL, S. R., KAWAGUCHI, S., STANILAND, I., HOFF, J. V. D., TIERNEY, M. & BOSSI, R. 2010. Perfluorinated compounds in the Antarctic region: Ocean circulation provides prolonged protection from distant sources. *Environmental Pollution,* 158**,** 2985-2991.

BENSKIN, J. P., MUIR, D. C. G., SCOTT, B. F., SPENCER, C., DE SILVA, A. O., KYLIN, H., MARTIN, J. W., MORRIS, A., LOHMANN, R., TOMY, G., ROSENBERG, B., TANIYASU, S. & YAMASHITA, N. 2012. Perfluoroalkyl Acids in the Atlantic and Canadian Arctic Oceans. *Environmental Science & Technology,* 46**,** 5815-5823.

BENSKIN, J. P., PHILLIPS, V., ST. LOUIS, V. L. & MARTIN, J. W. 2011. Source Elucidation of Perfluorinated Carboxylic Acids in Remote Alpine Lake Sediment Cores. *Environmental Science & Technology,* 45**,** 7188-7194.

BEYER, A., MACKAY, D., MATTHIES, M., WANIA, F. & WEBSTER, E. 2000. Assessing Long-Range Transport Potential of Persistent Organic Pollutants. *Environmental Science & Technology,* 34**,** 699-703.

BLAIS, J. M. 2005. Arctic Seabirds Transport Marine-Derived Contaminants. *Science,* 309**,** 445-445.

BURNISTON, D. A., STRACHAN, W. J. M., HOFF, J. T. & WANIA, F. 2007. Changes in Surface Area and Concentrations of Semivolatile Organic Contaminants in Aging Snow. *Environmental Science & Technology,* 41**,** 4932-4937.

BUTT, C. M., YOUNG, C. J., MABURY, S. A., HURLEY, M. D. & WALLINGTON, T. J. 2009. Atmospheric chemistry of 4:2 fluorotelomer acrylate [C4F9CH2CH2OC(O)CH=CH2]: kinetics, mechanisms, and products of

chlorine-atom- and OH-radical-initiated oxidation. *J Phys Chem A,* 113**,** 3155-61.

CAI, M., YANG, H., XIE, Z., ZHAO, Z., WANG, F., LU, Z., STURM, R. & EBINGHAUS, R. 2012a. Per- and polyfluoroalkyl substances in snow, lake, surface runoff water and coastal seawater in Fildes Peninsula, King George Island, Antarctica. *Journal of Hazardous Materials,* 209-210**,** 335-342.

CAI, M., ZHAO, Z., YIN, Z., AHRENS, L., HUANG, P., CAI, M., YANG, H., HE, J., STURM, R., EBINGHAUS, R. & XIE, Z. 2012b. Occurrence of Perfluoroalkyl Compounds in Surface Waters from the North Pacific to the Arctic Ocean. *Environmental Science & Technology,* 46**,** 661-668.

CARSON, R. 2002. *Silent spring*, 40th anniversary edition. Boston : Houghton Mifflin, 2002. ©1962.

CASAL, P., CASAS, G., VILA-COSTA, M., CABRERIZO, A., PIZARRO, M., JIMÉNEZ, B. & DACHS, J. 2019. Snow Amplification of Persistent Organic Pollutants at Coastal Antarctica. *Environmental Science & Technology,* 53**,** 8872-8882.

CASAL, P., ZHANG, Y., MARTIN, J. W., PIZARRO, M., JIMÉNEZ, B. & DACHS, J. 2017. Role of Snow Deposition of Perfluoroalkylated Substances at Coastal Livingston Island (Maritime Antarctica). *Environ Sci Technol,* 51**,** 8460-8470.

CHIUCHIOLO, A., DICKHUT, R., COCHRAN, M. & DUCKLOW, H. 2004. Persistent organic pollutants at the base of the Antarctic marine food web. *Environmental Science & Technology,* 38**,** 3551-3557.

CODLING, G., HALSALL, C., AHRENS, L., DEL VENTO, S., WIBERG, K., BERGKNUT, M., LAUDON, H. & EBINGHAUS, R. 2014. The fate of per- and polyfluoroalkyl substances within a melting snowpack of a boreal forest. *Environmental Pollution,* 191**,** 190-198.

CONCAWE 2016. Environmental fate and effects of poly- and perfluoroalkyl substances (PFAS).

D'EON J, C., HURLEY, M. D., WALLINGTON, T. J. & MABURY, S. A. 2006. Atmospheric chemistry of N-methyl perfluorobutane sulfonamidoethanol, C4F9SO2N(CH3)CH2CH2OH: kinetics and mechanism of reaction with OH. *Environ Sci Technol,* 40**,** 1862-8.

DICKHUT, R. M., CINCINELLI, A., COCHRAN, M. & DUCKLOW, H. W. 2005. Atmospheric concentrations and air-water flux of organochlorine pesticides along the Western Antarctic Peninsula. *Environmental science & technology,* 39**,** 465.

DICKHUT, R. M., CINCINELLI, A., COCHRAN, M. & KYLIN, H. 2012. Aerosol-Mediated Transport and Deposition of Brominated Diphenyl Ethers to Antarctica. *Environmental Science & Technology,* 46**,** 3135-3140.

DINGLASAN-PANLILIO, M. J. A. & MABURY, S. A. 2006. Significant residual fluorinated alcohols present in various fluorinated materials. *Environmental science & technology,* 40**,** 1447.

DOUGLAS, T. A., DOMINE, F., BARRET, M., ANASTASIO, C., BEINE, H. J., BOTTENHEIM, J., GRANNAS, A., HOUDIER, S., NETCHEVA, S., ROWLAND, G., STAEBLER, R. & STEFFEN, A. 2012. Frost flowers growing in the Arctic ocean-atmosphere–sea ice–snow interface: 1. Chemical composition. *Journal of Geophysical Research: Atmospheres,* 117**,** n/a-n/a.

DREYER, A., MATTHIAS, V., WEINBERG, I. & EBINGHAUS, R. 2010. Wet deposition of poly- and perfluorinated compounds in Northern Germany. *Environmental Pollution,* 158**,** 1221-1227.

DREYER, A., WEINBERG, I., TEMME, C. & EBINGHAUS, R. 2009. Polyfluorinated Compounds in the Atmosphere of the Atlantic and Southern Oceans: Evidence for a Global Distribution. *Environmental Science & Technology,* 43**,** 6507-6514.

ELLIS, D., MARTIN, J., DE SILVA, A. & MABURY, S. 2004. Degradation of fluorotelomer alcohols: A likely atmospheric source of perfluorinated carboxylic acids. *Environmental Science & Technology,* 38**,** 3316-3321.

FERNÁNDEZ-MÉNDEZ, M., KATLEIN, C., RABE, B., NICOLAUS, M., PEEKEN, I., BAKKER, K., FLORES, H. & BOETIUS, A. 2015. Photosynthetic production in the central Arctic Ocean during the record sea-ice minimum in 2012. *Biogeosciences,* 12**,** 3525-3549.

GRENNFELT, P., ENGLERYD, A., FORSIUS, M., HOV, Ø., RODHE, H. & COWLING, E. 2020. Acid rain and air pollution: 50 years of progress in environmental science and policy. *Ambio,* 49**,** 849-864.

GUSTAFSSON, Ö., ANDERSSON, P., AXELMAN, J., BUCHELI, T. D., KÖMP, P., MCLACHLAN, M. S., SOBEK, A. & THÖRNGREN, J. O. 2005. Observations of the PCB distribution within and in-between ice, snow, ice-rafted debris, ice-interstitial water, and seawater in the Barents Sea marginal ice zone and the North Pole area. *Science of the Total Environment,* 342**,** 261-279.

HALSALL, C. J. 2004. Investigating the occurrence of persistent organic pollutants (POPs) in the arctic: their atmospheric behaviour and interaction with the seasonal snow pack. *Environ Pollut,* 128**,** 163-75.

HARGRAVE, B., HARDING, G., VASS, W., ERICKSON, P., FOWLER, B. & SCOTT, V. 1992. Organochlorine pesticides and polychlorinated biphenyls in the Arctic Ocean food web. *Archives of Environmental Contamination and Toxicology,* 22**,** 41-54.

HARGRAVE, B. T., VASS, W. P., ERICKSON, P. E. & FOWLER, B. R. 1988. Atmospheric transport of organochlorines to the Arctic Ocean. *Tellus B: Chemical and Physical Meteorology,* 40**,** 480-493.

HERBERT, B. M. J., VILLA, S. & HALSALL, C. J. 2006. Chemical interactions with snow: Understanding the behavior and fate of semi-volatile organic compounds in snow. *Ecotoxicology and Environmental Safety,* 63**,** 3-16.

JANTUNEN, L. M. & BIDLEMAN, T. F. 2006. Henry's law constants for hexachlorobenzene, p, p′-DDE and components of technical chlordane and estimates of gas exchange for Lake Ontario. *Chemosphere,* 62**,** 1689-1696.

JANTUNEN, L. M., HELM, P. A., RIDAL, J. J. & BIDLEMAN, T. F. 2008. Air-water gas exchange of chiral and achiral organochlorine pesticides in the Great Lakes.(Report). *Atmospheric Environment,* 42**,** 8533.

JANTUNEN, L. M., WONG, F., GAWOR, A., KYLIN, H., HELM, P. A., STERN, G. A., STRACHAN, W. M. J., BURNISTON, D. A. & BIDLEMAN, T. F. 2015. 20 Years of Air-Water Gas Exchange Observations for Pesticides in the Western Arctic Ocean. *Environmental science & technology,* 49**,** 13844.

JOERSS, H., XIE, Z., WAGNER, C. C., VON APPEN, W.-J., SUNDERLAND, E. M. & EBINGHAUS, R. 2020. Transport of Legacy Perfluoroalkyl Substances and the Replacement Compound HFPO-DA through the Atlantic Gateway to the Arctic Ocean—Is the Arctic a Sink or a Source? *Environmental Science & Technology.*

JOHANSSON, J. H., SALTER, M. E., ACOSTA NAVARRO, J. C., LECK, C., NILSSON, E. D. & COUSINS, I. T. 2019. Global transport of perfluoroalkyl acids via sea spray aerosol. *Environmental science. Processes & impacts,* 21**,** 635.

KAISER, M. A., LARSEN, B. S., KAO, C.-P. C. & BUCK, R. C. 2005. Vapor Pressures of Perfluorooctanoic, -nonanoic, -decanoic, -undecanoic, and -dodecanoic Acids. *Journal of Chemical & Engineering Data,* 50**,** 1841-1843.

KAUCK, E. A. & DIESSLIN, A. R. 1951. Some Properties of Perfluorocarboxylic Acids. *Industrial & Engineering Chemistry,* 43**,** 2332-2334.

KWOK, K. Y., YAMAZAKI, E., YAMASHITA, N., TANIYASU, S., MURPHY, M. B., HORII, Y., PETRICK, G., KALLERBORN, R., KANNAN, K., MURANO, K. & LAM, P. K. S. 2013. Transport of Perfluoroalkyl substances (PFAS) from an arctic glacier to downstream locations: Implications for sources. *Science of the Total Environment,* 447**,** 46-55.

LACORTE, S., QUINTANA, J., TAULER, R., VENTURA, F., TOVAR-SÁNCHEZ, A. & DUARTE, C. M. 2009. Ultra-trace determination of Persistent Organic Pollutants in Arctic ice using stir bar sorptive extraction and gas chromatography coupled to mass spectrometry. *Journal of Chromatography A,* 1216**,** 8581-8589.

LAND, M., DE WIT, C. A., BIGNERT, A., COUSINS, I. T., HERZKE, D., JOHANSSON, J. H. & MARTIN, J. W. 2018. What is the effect of phasing out long-chain per- and polyfluoroalkyl substances on the concentrations of

perfluoroalkyl acids and their precursors in the environment? A systematic review. *Environmental Evidence,* 7**,** 4.

LI, L., ZHENG, H., WANG, T., CAI, M. & WANG, P. 2018. Perfluoroalkyl acids in surface seawater from the North Pacific to the Arctic Ocean: Contamination, distribution and transportation. *Environmental Pollution,* 238**,** 168-176.

MACINNIS, J. J., FRENCH, K., MUIR, D. C. G., SPENCER, C., CRISCITIELLO, A., DE SILVA, A. O. & YOUNG, C. J. 2017. Emerging investigator series: a 14-year depositional ice record of perfluoroalkyl substances in the High Arctic. *Environ. Sci.: Processes Impacts,* 19**,** 22-30.

MACINNIS, J. J., LEHNHERR, I., MUIR, D. C. G., ST. PIERRE, K. A., ST. LOUIS, V. L., SPENCER, C. & DE SILVA, A. O. 2019. Fate and Transport of Perfluoroalkyl Substances from Snowpacks into a Lake in the High Arctic of Canada. *Environmental Science & Technology,* 53**,** 10753-10762.

MACKAY, D. S., W. Y.; MA, K. C.; LEE, S. C 2006. *Handbook of physical-chemical properties and environmental fate for organic chemicals. Volume II. Halogenated hydrocarbons,* Boca Raton, CRC Press, Taylor & Francis.

MCMURDO, C. J., ELLIS, D. A., WEBSTER, E., BUTLER, J., CHRISTENSEN, R. D. & REID, L. K. 2008. Aerosol Enrichment of the Surfactant PFO and Mediation of the Water−Air Transport of Gaseous PFOA. *Environmental Science & Technology,* 42**,** 3969-3974.

MELNIKOV, S., CARROLL, J., GORSHKOV, A., VLASOV, S. & DAHLE, S. 2003. Snow and ice concentrations of selected persistent pollutants in the Ob–Yenisey River watershed. *Science of the Total Environment,* 306**,** 27-37.

NSIDC. 2020a. *charctic-interactive-sea-ice-graph* [Online]. University of Colorado. Available: https://nsidc.org/arcticseaicenews/charctic-interactive-sea-ice-graph/ [Accessed 21/08 2020].

NSIDC. 2020b. *Timeseries of sea ice age percent coverage for the Arctic Ocean* [Online]. National Snow and Ice Data Center-M. Tschudi, C. Fowler, J. Maslanik, R. Stewart/University of Colorado Boulder; W. Meier/NASA Cryospheric Sciences. Available: http://nsidc.org/arcticseaicenews/2017/05/warm-arctic-cool-continents/ [Accessed 21/08 2020].

OECD 2012. *Test No. 305: Bioaccumulation in Fish: Aqueous and Dietary Exposure.*

PAUL, A. G., JONES, K. C. & SWEETMAN, A. J. 2009. A First Global Production, Emission, And Environmental Inventory For Perfluorooctane Sulfonate. *Environmental Science & Technology,* 43**,** 386-392.

PICKARD, H. M., CRISCITIELLO, A. S., PERSAUD, D., SPENCER, C., MUIR, D. C. G., LEHNHERR, I., SHARP, M. J., DE SILVA, A. O. & YOUNG, C. J. 2020. Ice Core Record of Persistent Short-Chain Fluorinated Alkyl Acids: Evidence of the Impact From Global Environmental Regulations. *Geophysical Research Letters,* 47**,** e2020GL087535.

PICKARD, H. M., CRISCITIELLO, A. S., SPENCER, C., SHARP, M. J., MUIR, D. C. G., DE SILVA, A. O. & YOUNG, C. J. 2018. Continuous non-marine inputs of per- and polyfluoroalkyl substances to the High Arctic: a multi-decadal temporal record. *Atmos. Chem. Phys.,* 18**,** 5045-5058.

PUĆKO, M., STERN, G., MACDONALD, R. W. & BARBER, D. G. 2010a. alpha- and gamma-Hexachlorocyclohexane Measurements in the Brine Fraction of Sea Ice in the Canadian High Arctic Using a Sump-Hole Technique. *Environmental Science & Technology,* 44**,** 9258-9264.

PUĆKO, M., STERN, G. A., BARBER, D. G., MACDONALD, R. W. & ROSENBERG, B. 2010b. The international polar year (IPY) circumpolar flaw lead (CFL) system study: The importance of brine processes for α- and γ-hexachlorocyclohexane (HCH) accumulation or rejection in sea ice. *Atmosphere-Ocean,* 48**,** 244-262.

PUĆKO, M., STERN, G. A., BARBER, D. G., MACDONALD, R. W., WARNER, K. A. & FUCHS, C. 2012. Mechanisms and implications of α-HCH enrichment in melt pond water on Arctic sea ice. *Environmental Science & Technology,* 46**,** 11862.

PUĆKO, M., STERN, G. A., MACDONALD, R. W., JANTUNEN, L. M., BIDLEMAN, T. F., WONG, F., BARBER, D. G. & RYSGAARD, S. 2015. The delivery of organic contaminants to the Arctic food web: Why sea ice matters. *Science of the Total Environment,* 506-507**,** 444-452.

PUĆKO, M., STERN, G. A., MACDONALD, R. W., ROSENBERG, B. & BARBER, D. G. 2011. The influence of the atmosphere-snow-ice-ocean interactions on the levels of hexachlorocyclohexanes in the Arctic cryosphere. *Journal of Geophysical Research: Oceans,* 116**,** n/a-n/a.

RETH, M., BERGER, U., BROMAN, D., COUSINS, I. T., NILSSON, E. D. & MCLACHLAN, M. S. 2011. Water-to-air transfer of perfluorinated carboxylates and sulfonates in a sea spray simulator. *Environmental Chemistry,* 8**,** 381-388.

ROSENBERG, B. D., J.; MACHUTCHON, A.; STERN, G.; SPENCER, C.; SCOTT, B.; LOPEZ, E.; MUIR, D.; TOMY, G. 2008. Spatial and Vertical Distribution of Perfluorinated Compounds in Canadian Arctic and Sub-Arctic Ocean Water. *Organohalogen Compounds***,** 386-390.

SCHWARZENBACH, R. P. G., PHILLIP M; IMBODEN, DIETER M 1993. *Environmental Organic Chemistry,* New York, Wiley.

SULBAEK ANDERSEN, M. P., NIELSEN, O. J., HURLEY, M. D., BALL, J. C., WALLINGTON, T. J., ELLIS, D. A., MARTIN, J. W. & MABURY, S. A. 2005. Atmospheric chemistry of 4:2 fluorotelomer alcohol (n-C4F9CH2CH2OH): products and mechanism of Cl atom initiated oxidation in the presence of NOx. *J Phys Chem A,* 109**,** 1849-56.

TANABE, S., HIDAKA, H. & TATSUKAWA, R. 1983. PCBs and chlorinated hydrocarbon pesticides in Antarctic atmosphere and hydrosphere. *Chemosphere,* 12**,** 277-288.

US_EPA. 2018. *Fact Sheet: 2010/2015 PFOA Stewardship Program* [Online]. United States Environmental Protection Agency. Available: https://www.epa.gov/assessing-and-managing-chemicals-under-tsca/fact-sheet-20102015-pfoa-stewardship-program [Accessed 06-Aug 2020].

VENTO, S. D., HALSALL, C., GIOIA, R., JONES, K. & DACHS, J. 2012. Volatile per- and polyfluoroalkyl compounds in the remote atmosphere of the western Antarctic Peninsula: an indirect source of perfluoroalkyl acids to Antarctic waters? *Atmospheric Pollution Research,* 3**,** 450-455.

WALLINGTON, T. J., HURLEY, M. D., XIA, J., WUEBBLES, D. J., SILLMAN, S., ITO, A., PENNER, J. E., ELLIS, D. A., MARTIN, J., MABURY, S. A., NIELSEN, O. J. & SULBAEK ANDERSEN, M. P. 2006. Formation of C7F15COOH (PFOA) and other perfluorocarboxylic acids during the atmospheric oxidation of 8:2 fluorotelomer alcohol. *Environmental science & technology,* 40**,** 924.

WANG, Z., COUSINS, I. T., SCHERINGER, M., BUCK, R. C. & HUNGERBÜHLER, K. 2014a. Global emission inventories for C4-C14 perfluoroalkyl carboxylic acid (PFCA) homologues from 1951 to 2030, Part I: production and emissions from quantifiable sources. *Environ Int,* 70**,** 62-75.

WANG, Z., COUSINS, I. T., SCHERINGER, M., BUCK, R. C. & HUNGERBÜHLER, K. 2014b. Global emission inventories for C4-C14 perfluoroalkyl carboxylic acid (PFCA) homologues from 1951 to 2030, part II: the remaining pieces of the puzzle. *Environ Int,* 69**,** 166-76.

WANG, Z., XIE, Z., MI, W., MÖLLER, A., WOLSCHKE, H. & EBINGHAUS, R. 2015. Neutral Poly/Per-Fluoroalkyl Substances in Air from the Atlantic to the Southern Ocean and in Antarctic Snow. *Environmental science & technology,* 49**,** 7770.

WANIA, F. & DUGANI, C. 2003. Assessing the long-range transport potential of polybrominated diphenyl ethers: A comparison of four multimedia models. *Environmental Toxicology and Chemistry,* 22**,** 1252-1261.

WANIA, F. M., D 1996. Peer Reviewed: Tracking the Distribution of Persistent Organic Pollutants. *Environmental Science & Technology,* 30**,** 390A-396A.

WONG, F., HUNG, H., DRYFHOUT-CLARK, H., AAS, W., BOHLIN-NIZZETTO, P., BREIVIK, K., MASTROMONACO, M. N., LUNDÉN, E. B., ÓLAFSDÓTTIR, K., SIGURÐSSON, Á., VORKAMP, K., BOSSI, R., SKOV, H., HAKOLA, H., BARRESI, E., SVERKO, E., FELLIN, P., LI, H., VLASENKO, A., ZAPEVALOV, M., SAMSONOV, D. & WILSON, S. 2021. Time trends of persistent organic pollutants (POPs) and Chemicals of Emerging

Arctic Concern (CEAC) in Arctic air from 25 years of monitoring. *Science of The Total Environment,* 775**,** 145109.

WONG, F., JANTUNEN, L. M., PUĆKO, M., PAPAKYRIAKOU, T., STAEBLER, R. M., STERN, G. A. & BIDLEMAN, T. F. 2011. Air-water exchange of anthropogenic and natural organohalogens on International Polar Year (IPY) expeditions in the Canadian Arctic. *Environmental science & technology,* 45**,** 876.

WONG, F., SHOEIB, M., KATSOYIANNIS, A., ECKHARDT, S., STOHL, A., BOHLIN-NIZZETTO, P., LI, H., FELLIN, P., SU, Y. & HUNG, H. 2018. Assessing temporal trends and source regions of per- and polyfluoroalkyl substances (PFASs) in air under the Arctic Monitoring and Assessment Programme (AMAP). *Atmospheric Environment,* 172**,** 65-73.

XIAO, H., LI, N. & WANIA, F. 2004. Compilation, evaluation, and selection of physical-chemical property data for alpha-, beta-, and gamma-hexachlorocyclohexane. *Journal of Chemical and Engineering Data.*

XIE, Z., WANG, Z., MAGAND, O., THOLLOT, A., EBINGHAUS, R., MI, W. & DOMMERGUE, A. 2020. Occurrence of legacy and emerging organic contaminants in snow at Dome C in the Antarctic. *The Science of the total environment,* 741.

XIE, Z., WANG, Z., MI, W., MÖLLER, A., WOLSCHKE, H. & EBINGHAUS, R. 2015. Neutral Poly-/perfluoroalkyl Substances in Air and Snow from the Arctic. *Scientific Reports,* 5**,** 8912.

XIE, Z., ZHAO, Z., MÖLLER, A., WOLSCHKE, H., AHRENS, L., STURM, R. & EBINGHAUS, R. 2013. Neutral poly- and perfluoroalkyl substances in air and seawater of the North Sea. *Environmental Science and Pollution Research,* 20**,** 7988-8000.

YEUNG, L. W. Y., DASSUNCAO, C., MABURY, S., SUNDERLAND, E. M., ZHANG, X. & LOHMANN, R. 2017. Vertical Profiles, Sources, and Transport of PFASs in the Arctic Ocean. *Environmental Science & Technology,* 51**,** 6735-6744.

ZHANG, X., LOHMANN, R. & SUNDERLAND, E. M. 2019. Poly- and Perfluoroalkyl Substances in Seawater and Plankton from the Northwestern Atlantic Margin. *Environmental science & technology,* 53**,** 12348.

ZHAO, Z., XIE, Z., MÖLLER, A., STURM, R., TANG, J., ZHANG, G. & EBINGHAUS, R. 2012. Distribution and long-range transport of polyfluoroalkyl substances in the Arctic, Atlantic Ocean and Antarctic coast. *Environmental Pollution,* 170**,** 71-77.

Overview to the thesis

To address some of the major research gaps in the biogeochemistry of POPs in the polar regions, PFASs were selected as the focus of most studies. PFASs are a large class of chemicals undergoing scrutiny by various regulatory agencies across the globe and a range of excellent analytical methods (e.g. low sample volumes) for their detection in environmental samples at ultra-low levels (pg/L – ng/L) are available with colleagues at Helmholtz Zentrum Geesthacht (HZG). Where possible, a number of organochlorine (OC) chemicals were also selected as model compounds to assess the behaviour of 'legacy' POPs and the chemical analysis was performed at Lancaster Environment Centre. Given the lack of long-term air monitoring in Antarctica, then a proxy for atmospheric emissions of PFASs over the last few decades was sought, and an undisturbed snowpack from East Antarctic Plateau where low accumulation rates prevail was investigated. **Paper I** arose through a collaboration with British Antarctic Survey and involved shallow snow/firn core drilling as part of the *Isotopic constraints on past ozone layer in polar ice* (ISOL-ICE) campaign. **Paper II** and **Paper III** followed the development a state-of-the-art facility that was built for the purpose of studying environmental processes in Polar regions. The Roland von Glasow air-sea-ice chamber, named in honour of its late founder, allows users to simulate sea ice growth and decay in a controlled environment. The increasing prevalence of thinner and younger sea ice (<1yr old) in the Arctic made this facility ideal to study the chemical dynamics of POPs in sea ice while in the absence of additional chemical inputs such as snow. **Paper IV** arose through a unique collaboration with various institutes across the globe as part of the Norwegian led *Nansen Legacy* project. In terms of sea ice, the Barents Sea area is one of the most rapidly changing regions in the Arctic and a fortunate opportunity to join a scientific expedition on an icebreaker to collect samples in the region took place during late summer 2019. This provided an excellent platform to obtain a holistic view of the Arctic marine environment in order to understand how PFASs are transferred between snow, sea ice and the surrounding environment during summer, a period when biological activity in the polar region is high.

Chapter 2

Increasing accumulation of perfluorocarboxylate contaminants revealed in an Antarctic snow core (1958-2017)

This chapter presents the first study of historical deposition of PFASs in a firn core taken at a site located on the Antarctic continental shelf. It evaluates probable source compounds and environmental transport pathways to this remote region. It also provides information regarding the efficacy of regulatory measures.

This chapter was prepared as a scientific research article for the journal *Nature Communications* and will be submitted in 2021

The candidate's contribution was analysing the field samples; structuring own and co-authors' ideas as a manuscript; writing the manuscript for supervisor review; co-ordinating co-author feedback; submission of manuscript.

Candidate: ..... J.garnett. *.....Date:.....22-Jul-21.....*

Mr Jack R. Garnett

Supervisor: .....

.....Date:...26-Jul-21.....

Prof. Crispin J. Halsall.

Increasing accumulation of perfluorocarboxylate contaminants revealed in an Antarctic snow core (1958-2017)

Jack Garnett[1], Crispin Halsall[1*], Robert Mulvaney[2], Anna Jones[2], Holly Winton[2], Hanna Joerss[3], Ralf Ebinghaus[3], Amber Leeson[1], Peter Wynn[1]

1 Lancaster Environment Centre, Lancaster University, Lancaster, LA1 4YQ, UK

2 British Antarctic Survey, Cambridge, High Cross, Madingley Road, Cambridge, CB3 0ET, UK

3 Helmholtz-Zentrum Hereon, Max-Planck-Straße 1, 21502 Geesthacht, Germany

Email: c.halsall@lancaster.ac.uk

Abstract

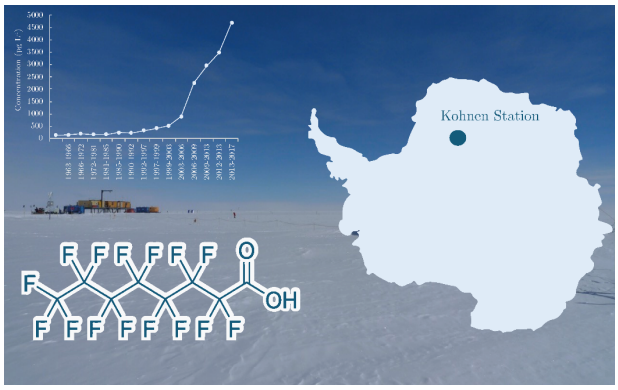

Poly- and perfluoroalkylated substances (PFAS) are synthetic chemicals that are widely present in the global environment. Included in this group of chemicals are perfluoroalkyl acids that are persistent, bioaccumulative and present in Antarctica through a combination of atmospheric and oceanic transport pathways. Here we use a dated-snow core from Kohnen Station (East Antarctic Plateau) to construct an accumulation time-series of atmospheric deposition and as a proxy for global use patterns over the last 60 years. Using older ice as field blanks that pre-dated the onset of PFAS production, we observed increasing accumulation of perfluorocarboxylates (PFCA; C_4, $C_6 - C_9$) from 1958 to 2017 with no evidence of a reduction of perfluorooctanoic acid (PFOA; C_8) despite international restrictions on the production and use of this chemical. A pronounced increase in the accumulation flux of perfluorobutanoic acid (PFBA; C_4) was apparent from the year 2000 onwards, which corresponds to the shift to the use of short-chain chemicals by industry but is also likely from a large unaccounted source of PFBA in the global environment. Strong correlations between concentrations of PFHxA (C_6) and PFHpA (C_7) ($r_s = 0.8$, $p<0.001$; $n=10$) and PFOA (C_8) and PFNA (C_9) ($r_s > 0.9$, $p<0.01$; $n=11$) support evidence that their occurrence is due to the industrial emission and long-range atmospheric transport of volatile precursors such as fluorotelomer alcohols (FTOH). Perfluoroalkylated sulfonic acids were below detection limits in the snow layers suggesting that the atmospheric transport of these chemicals to the interior of the Antarctic continent is not as efficient as the corresponding carboxylates, with preferential removal in the coastal margins.

1. Introduction

Poly- and per-fluorinated alkylated substances (PFAS) are a large group of synthetic chemicals that have been manufactured since the 1950s; they do not occur naturally in the environment. Their chemical structure often combines a fully fluorinated carbon chain (typically C_3 – C_{15}) that is hydrophobic (i.e. water hating) and a terminal functional group (e.g. COOH, SOOH etc) that is hydrophilic (i.e. water loving), providing high resistance to environmental degradation and ability to function as surface active agents. As such, PFAS are widely used as stain repellents in consumer products (e.g. Scotchgard®) and used as processing additives in the manufacture of fluoropolymers (e.g. Teflon®).

Perfluoroalkyl acids (PFAA) are a key group of PFAS that consist of perfluorocarboxylates (PFCA) and perfluorosulphonic acids (PFSA). In 2000, the largest fluorochemical producer, 3M Co., phased out the production of perfluorooctane sulphonic acid (PFOS) after concerns that human exposure is associated with a variety of adverse health effects, including prenatal development, liver toxicity and kidney and testicular cancer (Vieira et al., 2013,Barry, 2013 #170). PFAA are released into the environment directly from various industrial sites (Hu et al., 2016) and also formed indirectly in the atmosphere from the oxidation of volatile precursor compounds (Benskin et al., 2011, Dreyer et al., 2009b, Pickard et al., 2020, Pickard et al., 2018, Vento et al., 2012, Xie et al., 2020, Xie et al., 2015). As a result, PFAA are global contaminants and have been subject to various regulatory measures.

To meet ongoing and increasing global demand for high performance surfactants, one approach has been to substitute long-chain PFAS with short-chain analogues, which appear to be less bioaccumulative and therefore pose a reduced risk to the environment (Wang et al., 2015). While many of these chemicals show similar industrial functions, their somewhat inferior technical performance is often compensated by higher usages (Poulsen, 2005) despite relatively little being known about their environmental fate (Lau, et al., 2006). Similarly, global PFAS production has shifted from the US and Europe to the Far East and China which is likely to affect the global environmental distribution of these chemicals. The impact of regulations,

changing chemical sources and geographical locations highlight the need for global monitoring (Brendel et al., 2018).

Recent measurements at several polar sites in Antarctica demonstrate that PFAS are transported to this region through atmospheric currents (Casal et al., 2019, Casal et al., 2017, Xie et al., 2020). Once deposited within snow, PFAA are expected to remain there due to their high environmental persistence and low volatility. Subsequent accumulation of snow layers can therefore serve as a natural archive and *proxy* for past global emissions. A number of studies have followed similar methods in the Arctic (Pickard et al., 2020, Pickard et al., 2018) and Tibetan Plateau (Wang et al., 2014a). However, their proximity to pollution sources and influence from distinct air masses provide only an indication of temporal trends at the regional level (Wang et al., 2014a). Sampling sites located in the southern hemisphere, such as on the East Antarctic Plateau, are even further from large industrial sources and are affected by air masses derived from various regions thus are better equipped to inform us of mechanisms of global atmospheric processes and emissions (Stauffer et al., 2004). The aim of this study is therefore to obtain time trends of PFAS deposition using a snow core collected from continental Antarctica to evaluate global trends and evaluate the efficacy of regulatory measures.

2. Methods

2.1 Sample site and collection

A 9.8m firn core was taken during the "Isotopic Constraints on Past Ozone Layer in Polar Ice" (ISOL-ICE) project in January 2017 at Kohnen Research Station, Dronning Maud land, Antarctica (75°00'S, 00°04'O, 2892m a.s.l) (Figure 1). Samples were collected using a stainless-steel hand drill (100mm I.D.) and actions were taken to avoid contact with materials potentially containing fluoropolymers (e.g. Goretex^{TM}). Samples were wrapped in aluminium foil, placed in polyethylene (PE) bags, shipped to the United Kingdom and stored at -35°C in polyethylene bags until further handling.

Figure 3: Antarctic map with Kohnen station (BAS, 2020)

2.2. Dating and ancillary measurements

Snow core dating was achieved via the annual layer counting that is made from the continuous concentration profiles of seasonally varying $\delta^{18}O_{H20}$. A time-depth scale was transposed directly using depth measurements from an adjacent firn core (See Table S1) that was mechanically drilled during the ISOL-ICE field campaign (BAS, 2020) at the same time (2017) and location as the core used in this study. The $\delta^{18}O_{H20}$ isotopic ratio displayed a seasonal trend, marked by higher values in summer precipitation and lower values in winter.

2.3. Sample handling and extraction

In order to obtain sufficient meltwater for PFAS analysis (> 0.5 L), snow core samples were sectioned into layers which represented multiple years ($\overline{x}$ = 4 years; See Table S2). All samples were placed into sterile PE bags, melted at room temperature and then transferred to pre-cleaned 2 L PE containers. Each sample was spiked with 400 pg of a mass-labelled internal standard (IS) solution (50 µL of a 8 pg μL^{-1} methanol solution) containing 9 isotopically labelled surrogate standards ($^{13}C_4$-PFBA, $^{13}C_2$-PFHxA, $^{13}C_4$-PFOA, $^{13}C_5$-PFNA, $^{13}C_2$-PFDA, $^{13}C_2$-PFUnDA, $^{13}C_2$-PFDoDA, $^{18}O_2$-PFHxS, $^{13}C_4$-PFOS) to assess analytical recovery (%). Detailed information on the target analytes as well as on the standards' purity and concentration is presented in Table S3.

Samples were extracted for PFAS using a 12-port vacuum manifold system equipped with weak anion exchange cartridges (OASIS® WAX, 6 cc, 150 mg sorbent, 30 µm particle size, Waters, USA) that had been preconditioned with 3 mL formic acid (0.1 % v/v), followed by 3 mL methanol and then 3 mL water. Samples were loaded at a flow rate of 2 - 3 drops s^{-1} and a washing step was implemented using 6 mL SPE-cleaned MilliQ water. Cartridges were mounted with an additional cartridge before being air-dried under vacuum for 40 minutes to avoid air-borne contamination and remove residual water, respectively. Cartridges were stored at -20 °C until further analysis. The target analytes were eluted using 5 mL methanol followed by 5 mL ammonium hydroxide in methanol (0.1 % v/v). Finally, the eluates were reduced to 150 µL under nitrogen and 400 pg of the injection standard $^{13}C_8$-PFOA (10 µL of a 40 pg μL^{-1} 80:20 (v/v) methanol:water) was added.

2.4. Instrumental analysis

Instrumental analysis was performed by HPLC-MS/MS, using an HP 1100 LC system (Agilent Technologies, USA) coupled to an API 4000 triple quadrupole mass spectrometer (AB Sciex, USA). It was equipped with a Turbo V Ion Source (AB Sciex, USA) operating in negative electrospray ionization mode. The injection volume was 10 µL for all test solutions. For chromatographic separation, a polar embedded reversed phase C_{18} separation column (Synergi Fusion-RP C18, 150 mm x 2 mm, particle size 4 µm, pore size 80 Å, Phenomenex, USA) was combined with a reversed phase guard column (4 mm x 2 mm, Phenomenex, USA). A flow of 0.2 mL min^{-1} was set using a gradient elution with 2 mM ammonium acetate aqueous solution (A) and 0.05 % acetic acid in methanol (B).

2.5. Quality assurance and quality control (QA/QC)

Sample processing was undertaken in a class 1000 clean room facility (British Antarctic Survey, Cambridge) and analysed in a dedicated PFAS-free laboratory (Helmholtz Zentrum Geesthacht, Germany). A novel approach to obtain field blanks (n=3; 1.5 L; with IS) that would assess potential PFAS contamination arising from handling/transport/storage was performed in a side-study which involved analysing a dated snow core section (around 1920s) that had been acquired in a historical sampling campaign in Antarctica and which pre-dated the onset of PFAS production in the 1950s (See Table S4). A number of laboratory blanks (n=4; with IS; & n=3; without IS) consisting of pre-extracted MilliQ grade water (n=4; 1.5

L; with IS) were also prepared to ascertain background PFAS levels associated with laboratory consumables and solutions. All procedural blanks were processed in an identical manner as field samples. Repeatability measurements were obtained for some field samples where sufficient meltwater was obtained for duplicate (n=2) analyses.

A 14-point mixed calibration standard was prepared for quantification (80:20 (v/v) methanol:water) in the range from 0 to 25 pg μL^{-1}. A linear regression model was utilized and resulted in all analyte calibration curves $R^2 > 0.99$. Curves were weighted applying a factor of 1/x to improve accuracy for low concentration levels. All target analytes in samples were recovery-corrected using either an mass-labelled or structurally similar chemical surrogate (e.g. $CF_3(CF_2)_{n\pm1}COOH$). Laboratory blanks (n=4) were used to calculate method detection limits ($MDL = \overline{x}_{\text{laboratory blank}} + 3 \cdot s.d_{\text{laboratory blank}}$). In cases where analyte concentrations were less than limit of detection (LOD) in laboratory blanks, average field blanks (n=2; $\overline{x}_{\text{field blank}}$) were used to establish method detection limits for each chemical (See Table S5).

2.6. Data analysis

Sample concentrations in this study were not blank-corrected but samples <MDL are clearly highlighted in all Figures and Tables. Estimates for total concentration uncertainty were acquired from both laboratory and field replicates (See Equation S1). Dated-snow density measurements (See Table S6) were used to calculate average snow accumulation rates and annual deposition fluxes of chemicals (ng m^{-2} a^{-1}) (See Equation S1 and Figure S1). Statistical analyses were performed using concentration data (pg L^{-1}) in RStudio (Version 1.1.453; RStudio Team, 2015) using a significance level of $\alpha = 0.05$. Normality was tested using the Shapiro-Wilks test before further statistical testing followed. Spearmans rank correlation analysis was subsequently used to assess relationships between PFAS homologs.

3. Results

3.1. Snow accumulation at the Kohnen station

Kohnen station is situated on the East Antarctic Plateau approximately 500 km from the coast (See Figure 1 for map) and is characterized by having low annual average air temperature of -46 °C (typically ranging between −15 and −70 °C) and relatively low net snow accumulation

rates (Oerter et al., 1999). According to the snow core dating, the average accumulation rates of snow (snow water equivalent) during the time period was 68 ± 18 kg m^{-2} yr^{-1}, which is in excellent agreement with 71 ± 21 kg m^{-2} yr^{-1} determined by others at the same site (Oerter et al., 1999). The presence of chemical and particle constituents in the snow will be influenced by the prevailing meteorology (i.e. wind direction), and relative proximity of sources such as scientific bases and marine influences. (Weller and Wagenbach, 2007). Time-series data can be affected by various post-depositional processes (Pinglot et al., 2003, Codling et al., 2014, Meyer et al., 2009b, Meyer et al., 2009a) which can alter the chronology of chemical contaminants in the snowpack and therefore result in temporal trends that possibly reflect local sources (Wild et al., 2015) rather than synoptic or even global influences.

The occurrence of PFAA in the remote polar environment has been associated with direct transport through ocean currents (Joerss et al., 2020) and air together with volatile precursor compounds with subsequent photochemical oxidation and deposition. It has been proposed that in Antarctica, pollutant advection via ocean currents is minor due to the Antarctic circumpolar current (ACC) which limits the exchange of relatively polluted waters with the pristine waters of the Southern Ocean (Bengtson Nash et al., 2010). Nevertheless, (Casal et al., 2017) did show evidence that oceanic transport of PFAS can occur and, as a result, this may result in the transport of PFAA directly to remote continental sites, such as Kohnen, bound to marine sea salt aerosols (Johansson et al., 2019).

3.2. PFAA concentrations in snow

PFAA were detected in all the snow core samples and the complete data set can be found in Table S7. Concentrations of ΣPFAA (C_4 -C_{14}) ranged between 137 – 4711 pg L^{-1} (melt water equivalent). Perfluorocarboxylates (PFCA) were the only PFAS that were detected at quantifiable levels with PFBA (C_4) concentrations over 2-orders of magnitude higher compared to other PFCA (>95% ΣPFAA). Perfluorosulphonic acids (PFSA), such as PFBS (C_4), was not detected in any of the snow samples, and PFOS (C_8), was below the method detection limits (in the SI?) The concentrations in the present study were compared with other Polar and remote locations. In general, the concentrations of PFAA (C_6 – C_{14}) at Kohnen Station were akin, albeit lower, to other studies during similar time periods. For example, the

concentration of PFOA (C_8) was ~120 pg L^{-1} (between 1997 - 1999), compared to about 150 pg L^{-1} and 181 pg L^{-1} in snow from the Tibetan Plateau (Wang et al., 2014a) and Canadian Devon ice Cap (Pickard et al., 2018), respectively. Similarly, the concentration of PFOA (C_8) and other long-chain PFAA in fresh surface snow from coastal Antarctica (Casal et al., 2017) in 2015 were much higher (PFOA = 210 pg L^{-1}) compared to Kohnen Station (PFOA = 100 pg L^{-1}). Concentrations of PFBA (C_4) (about 4.4 ng L^{-1} around 2014) were also akin to other studies in remote regions, (Pickard et al., 2020) recently reported levels of 1.9 ng L^{-1} on the Mt Oxford icefield in Canada, in 2014. The finding of concentrations of PFAA in snow which are similar to other remote regions highlights the remoteness of Kohnen Station with lower levels reflecting the global remoteness of this site. Higher concentrations of some chemicals, such as PFBA, may reflect more efficient transport pathways to the continental site.

3.3. Time-series and depositional fluxes of PFAA

Figure 1 displays concentration time-series of PFAA (C_4 – C_9) with the corresponding annual depositional fluxes (ng m^{-2} yr^{-1}), calculated based on the annual SWE accumulation summarised in Table S8. It should be noted that the level of all PFAA in snow at Kohnen station were well above background levels measured in our earliest snow sample dated around late-1950s, which illustrates that these chemicals originate from long-range transport processes and not contamination from the nearby research station (Xie et al., 2020) which opened in 2001 (AWI, 2018). For PFBA (C_4), the concentrations increased continuously during the studied time period (1958 – 2017) and showed a rapid increase following the years 1999 – 2003. It should also be noted that temporal trends for individual PFAA in abiotic and biotic media vary widely in the literature (Land et al., 2018, Muir, 2019 #70). However, the observed trends in the Kohnen snow core closely matches the trend observed for PFBA and other short-chain PFCA ($<C_3$) observed by (Pickard et al., 2020) in remote high alpine regions of Canada.

In contrast to PFBA, the concentrations of other PFAA were more variable and showed marked changes at various timepoints during the time-series. In particular, PFOA (C_8) showed a sharp increase between 1997 and 1999, followed by a decline in 1999 – 2003 and then a gradual increase up to 2013 until it reduced again in 2015. The sharp increase in PFOA levels occurred prior to the announcement in 2000 by 3M (a major producer of PFOS) that it would

phase-out production of PFOS. As a result, many industrial sources located in the US, Europe and Japan are reported to have also stopped production and therefore may be responsible for the observed decline over the 1999 – 2003 period.

However, our results suggest that rather than continuing to decline post-2002, the levels of PFOA and other PFCA in Antarctica began to increase again, which is contrast to statements given by the chemical industry and contradicts modelled estimates of global emissions (Wang et al., 2014b). Following a general trend in the closure of several major industrial sites of PFAS production (long-chain PFCA, fluoropolymers and other PFAS products) across the US, Western Europe and Japan, geographical production shifted to emerging economies in continental Asia, such as China and India (OECD, 2015). As such, increasing fluorochemical production in these regions are likely to offset any emission reductions across North America and Europe and account for the for the higher concentrations observed in the later years of the snow core.

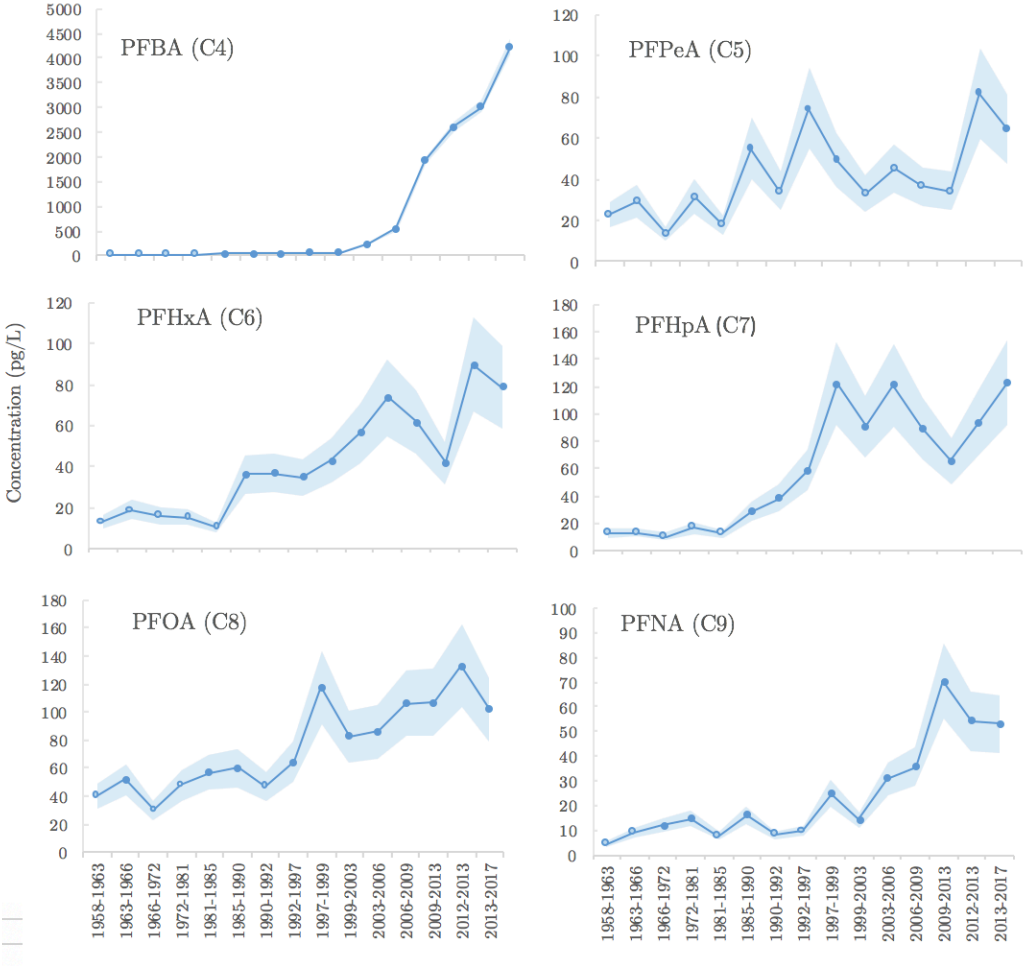

Figure 1: Concentration time-series of PFCA (C_4 – C_9) between 1958 - 2017. Open symbols represent those samples that were below method detection limits. Shading indicates uncertainty (±1.s.d.) derived from analytical and field sample replicates.

Perfluoroalkyl acids (PFAA) are highly persistent and non-volatile, making chemical-losses from the snowpack through volatilisation (Grannas et al., 2013) or degradation of minor significance. Nonetheless, PFAA are affected by other post-depositional processes such as snowpack aging, precipitation and/or episodes of meltwater percolation (Meyer et al., 2009b, Meyer et al., 2009a) from the surface during periods of higher temperatures. However, low temperatures at the site (annual mean = –46 °C) (Laepple et al., 2016) and well-preserved isotopic profiles with few visible 'ice lenses' (indicative of freeze-thaw activity) provide confidence that the occurrence of such processes during the studied time period were negligible. Furthermore, short-chain PFAA, such as PFBA (C_4), which display relatively high aqueous

solubilities do not show any evidence of post-depositional migration in the snow column due to percolating meltwater with PFBA temporal profile illustrated in Figure 1.

3.4. Sources of PFAA

While PFAA at remote sites like Kohnen Station are expected to have derived primarily from the atmospheric oxidation of gas-phase volatiles followed by wet deposition, PFAA could have also arisen from the direct transport of gas-phase and/or particulate-bound PFAA from processes such as the resuspension from the sea surface micro layer (Johansson et al., 2019). However, transport of marine aerosols in prevailing air masses affecting Kohnen station is considered to be relatively small (Weller and Wagenbach, 2017) and parallel studies to this one demonstrated very low levels of particulate matter in the snow (Winton et al). Moreover, Johansson et al., (2019) showed that aerosol fractions were significantly enriched in only the long-chain PFCA (mainly those with $>C_9$), which comprised only small component in the snow samples collected in this study. Xie et al (2020) suggested that research stations were a source of PFAS contamination, particularly within the locality of the station itself. The snow coring site in this study was located away from the Kohnen buildings and there is no evidence of local contamination affecting our sample site, such as erratic or high levels of a variety of PFAS (See Table S4).

It is currently unclear whether the atmospheric photochemical transformation process of precursor compounds occurs in the gas phase with subsequent scavenging of the PFAA by snowfall, or a heterogeneous reaction occurring on ice-crystal surfaces or some combination of the two. Concentrations of PFAA in the snow samples were not correlated with annual snow accumulation (Snow water equivalent; kg m^{-2} yr^{-1}), which suggests that snow plays a minor role in the chemical transformation of PFAA-precursors. Nevertheless, snow is an effective scavenger of airborne pollutants (Grannas et al., 2013) including PFAA due to its large surface area and low temperatures which promote surface sorption. As a result, snow has been shown to play an important role in air-water transfer of gas-phase PFCA and PFSA in the atmosphere to remote marine (Cai et al., 2012), alpine (Benskin et al., 2011, Macinnis et al., 2017, Pickard et al., 2020, Pickard et al., 2018), and coastal regions of Antarctica (Casal et al., 2019, Casal et al., 2017). An array of volatile fluorinated precursors (Prevedouros et al., 2006) are known

to give rise to short- and long-chain PFCA during atmospheric transport (Young et al., 2008, Wallington et al., 2006, Nakayama et al., 2007, Butt et al., 2009, Ellis et al., 2003,Martin, 2006 #193) and display sufficient atmospheric lifetimes (i.e. >2 days) to undergo long-range atmospheric transport to continental Antarctica (See Table S9-S10). A major class of volatile precursor compounds include fluorotelomer alcohols (FTOH) (Hurley et al., 2004) with atmospheric oxidation of n:2FTOH by hydroxyl radicals resulting in roughly equal proportions of even and odd carbon chain length homologs consisting of 'n' and 'n + 1' carbons (Wallington et al., 2006). For example, 6:2FTOH is expected to produce similar molar yields of PFHxA (C_6) and PFHpA (C_7). Strong correlations for PFHxA:PFHpA (r_s=0.78, $p<0.001$; n=10) and PFOA:PFNA (r_s =0.85, $p<0.01$; n=11) (See Table S11) present in the snow core suggests that these pairs share a common source and may have originated from 6:2FTOH and 8:2FTOH, respectively. In addition, a depositional even-odd flux ratio of 0.9 ± 0.3 (mean ± 1.s.d.) for PFHxA:PFHpA averaged for the entire time-series (see Figure 2; data shown in Table S12) provides further evidence that that the dominant process responsible for the presence of PFHxA (C_6) and PFHpA (C_7) in the accumulated snow pack is the photochemical oxidation of 6:2FTOH.

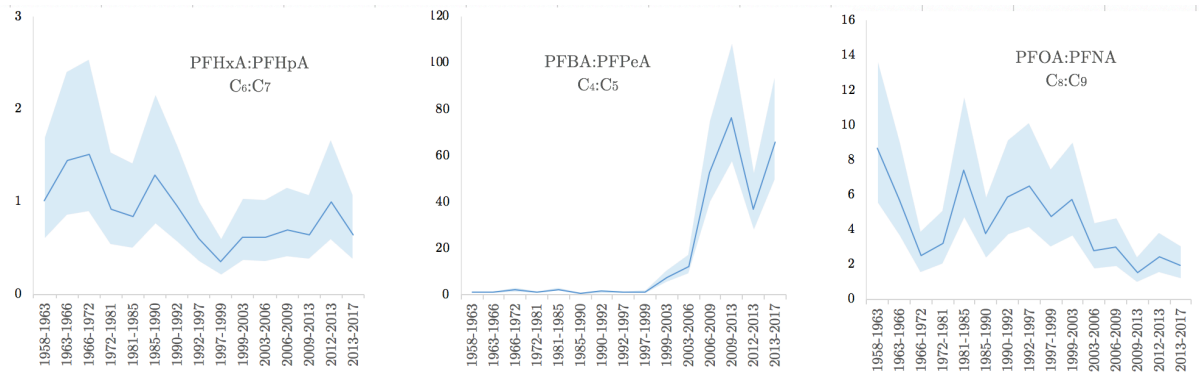

Figure 2: Time-series of depositional flux ratios for even-odd PFCA. Shading indicates combined uncertainty (±1.s.d.) derived from analytical and field sample replicates.

The high concentrations of PFBA, may be attributed to the shift in manufacturing around the year 2000 toward short-chain products such as the volatile fluorotelomer alcohol, 4:2FTOH, recently measured in ambient air across Asia (Li et al., 2011). Whilst some variation in the photochemical product yield from FTOH in the environment is expected (Thackray and Selin,

2017), depositional flux ratios >1 for PFBA:PFPeA (18 ± 27) suggest that FTOH are actually a minor source of PFCA to Kohnen and hence additional precursors are likely to account for the observed increase in PFBA. Increased production of short-chain perfluoroalkane sulfonyl fluoride (PFASF)-based substances has been reported in the early 2000s, with measurements of n-MeFBSA and n-MeFBSE (D'Eon J et al., 2006) in the coastal atmosphere off the Antarctic continent (Dreyer et al., 2009a, Vento et al., 2012). However, given the remarkably high concentrations of PFBA in the snow with high depositional flux-ratios, and the absence of PFBS (C_4) in snow (a known degradant of PFBSF-based compounds), it is unlikely that either 4:2FTOH or PFBSF-based chemicals can account for the marked increases in the concentrations of PFBA in recent years. It is plausible that chemicals associated with the direct manufacture of PFBA for unknown uses may also be a source, although one major producer (US) ceased production in 1998 before concentrations at Kohnen began to rise (Wang et al., 2014c). Using the average concentration (pg L^{-1}) observed in the uppermost part of the Kohnen snow core (specifically between the years 2013 - 2017) and scaling up to account for the snow accumulation on the entire Antarctic continent (2100 Gt) modelled by Rignot, 2019 #202) results in the annual accumulation of 8892 ± 353 kg of PFBA. (See Table S13). This indicates that a significant contemporary global source of PFBA exists, most likely through precursor chemicals which are subsequently transformed to PFBA in the environment. Many CFC (chlorofluorocarbon) replacement compounds have been identified as potential precursors to PFBA. One particular group is the hydrofluoroethers (HFE), which are used as specialized electronic cleaning solvents, heat transfer fluids and in cosmetic applications (NICNAS, 2006), which include HFE-7100 ($C_4F_9OCH_3$) and HFE-7200 ($C_4F_9OC_2H_5$). Both of these are reported to be widely used chemicals (Tsai, 2005) and can lead to the formation of PFBA (Wang et al., 2014) and other PFAA (Bravo et al., 2010) through photochemical oxidation processes in the environment. In 2000, this class of compounds were submitted to the US EPA for production (GPO, 2000), coinciding with the observed upward trend of PFBA in the snow core from 2000, and possibly accounting for the trends observed for the other short-chain PFAA (Pickard et al., 2020). It is plausible that CFC replacement compounds remain likely candidates for the observed increase in short-chain PFAA.

The depositional flux-ratio was also >1 (4.4 ± 2.2) for PFOA:PFNA, which indicates that in addition to 8:2FTOH, other chemical precursors contribute to the presence of PFCA. Various PFASF-based (perfluoroalkane sulfonyl fluoride) compounds such as n-alkane perfluorooctane sulphonamides (n-FOSA) and n-alkane perfluorooctane sulphonamide ethanols (n-FOSE) represent possible degradation products of PFCA and have previously been measured in the remote Southern Ocean atmosphere. However, the atmospheric oxidation of these compounds are also major sources of PFOS (C_8) in the remote environment, which we detected low levels (with no discernible temporal trend) in snow samples obtained at Kohnen Station. This could suggest that PFOSF-based substances yield PFCA as preferred degradation products under certain environment conditions (Martin et al., 2006). Although having sufficient atmospheric lifetimes, the long-range atmospheric transport potential (See Figure 3) of PFOSF-based precursors is considerably lower compared to FTOH due to their stronger sorption to snow surfaces (Xie et al., 2015). This interaction with snow could reduce the transport distance in cold polar environments and may explain why PFSA were not detected at appreciable levels at our continental sampling site. It is also noteworthy that the occasional detection of long-chain PFCA (e.g. PFCA >C_9) may also be due to lower mobility of long-chain precursors, such as 10:2FTOH, and the reason Casal et al., (2017) observed higher proportions of long-chain PFCA in fresh snow deposited in Antarctic coastal snow. Nevertheless, the atmospheric oxidation of many chemical precursors is a multi-step process in which chemical intermediates (e.g. perfluoroalkyl aldehydes; PFAL) are formed are also susceptible to long-range transport (Sulbaek Andersen et al., 2005). Time-series data for PFOA (Figure 1) shows a decrease in concentrations following the introduction of US and European environmental regulations of PFOS and PSOSF-based precursors around the year 2000, which implies that Kohnen Station is influenced by emissions of such precursors, albeit through a more indistinct chemical pathway. Nevertheless, a downward trend in depositional flux time-series for PFOA-PFNA (See Figure 2) shows that levels of PFNA (C_9) in recent years have increased considerably, relative to PFOA (C_8). Thus, it can be inferred that there are rising global emissions of other long-chain PFAA-precursors, specifically leading to the formation of PFNA (C_9). These may have developed as impurities of other FT-based compounds or formed intentionally (e.g. fluorotelomer olefins; FTO) as intermediates for processing aids in fluoropolymer manufacture,

notably polyvinylidene fluoride which has seen an increase in production (Prevedouros et al., 2006).

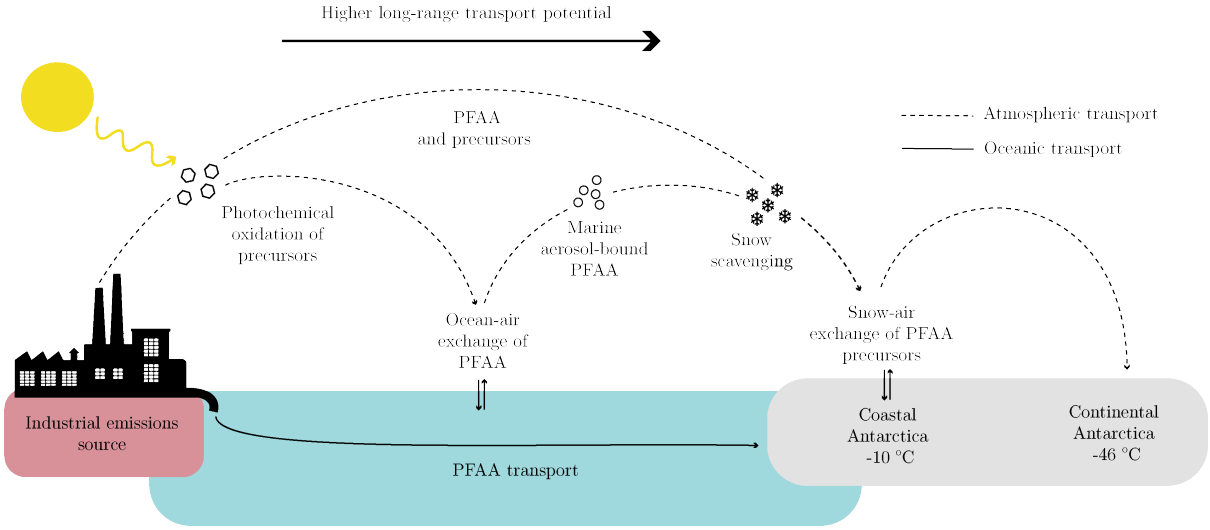

Figure 3: Schematic of long-range transport in the polar environment. Note that chemicals with a higher long-range transport potential will be transferred further and therefore more likely to be deposited in snow at remote inland sites such as Kohnen Station, Antarctica.

3.5. Global emissions and policy implications

The accumulation of PFAA in snow at Kohnen Station, Antarctica, over the period 1958-2017 appears to be primarily driven from the transport of volatile precursors. The dated firn core is the longest record of PFAS deposition in the remote snowpack and is the first to examine a PFAA time-series within the Southern Hemisphere. Although we show that there are differences in PFAA concentrations and composition compared with other remote sites around the world, temporal trends and homologue ratios enabled us to determine with a high degree of certainty several broad groups of chemicals that contribute PFAA to Antarctica, and thus affect the global environment. Crucially, we established that a major source of PFBA is likely from a high production volume chemical and possibly used to replace CFCs or related compounds. We also identified various fluorotelomer-derived chemicals as major sources of short- and long-chain PFAA, with other prospective precursors originating from the same group.

The Montreal Protocol entered into force in 1987 due to the depletion of stratospheric ozone caused by CFCs. Along with the Kyoto Protocol in 2005, these international policies aim to

protect the global environment through responsible chemical management and regulation of various damaging substances. As a result, many chemical companies have been compelled to develop 'environmentally friendly' alternatives. As indicated by others (Hossaini et al., 2017), the Montreal Protocol has, and will, continue to benefit stratospheric ozone levels and climate long into the future. However, the wider environmental impact of such replacements currently appears to have gone unchecked. Given the high concentrations observed in the remote environment and increasing global demand for heat exchange fluids (MMR, 2020), then levels of PFAA are certain to rise in the future.

In addition, while voluntary actions from some major chemical companies show a measurable short-term effect on global emissions, increasing long-term trends reveal that the manufacture of long-chain PFCA precursors is still ongoing and increasing. While the results in this study are not able to identify the exact geographical regions that are responsible, a reported shift in production sites of long- chain PFCA, fluoropolymers and other PFAS products from developed to emerging economies regions suggest that the proportion of global emissions of PFCA originating from continental Asia has increased. The evidence gathered in this study shows that these new sources may more than offset the reductions obtained by the former major global manufactures for some chemicals. Given the growing demand for fluorotelomer-based in the foreseeable future (Industry_Today, 2020), then greater emissions of long-chain PFAA into the environment are also to be expected.

This study illustrates that snow cores are useful tools that can provide multidecadal records which enable us to better understand the sources and deposition of chemical pollution in the global environment. Our data provides compelling evidence that international legislation and voluntary actions from the chemical industry thus far have been insufficient to reduce the burden of PFOA and other PFCA entering the remote Antarctic environment. We propose that more work is done to identify the exact chemical sources and recommend long-term monitoring of PFAS. We also recommend "green principles" being incorporated into the design of alternative products to ensure chemicals break-down into innocuous degradation products (Anastas and Eghbali, 2010).

ANASTAS, P. & EGHBALI, N. 2010. Green Chemistry: Principles and Practice. *Chem Soc Rev,* 39**,** 301-312.

AWI. 2018. *Kohnen Station* [Online]. Available: https://www.awi.de/en/expedition/stations/kohnen-station.html [Accessed 2020].

BAS. 2020. *Isotopic Constraints on Past Ozone Layer in Polar Ice - ISOL-ICE* [Online]. Available: https://www.bas.ac.uk/project/isolex-isotopic-constraints-on-past-ozone-layer-and-stratosphere-troposphere-exchange-in-polar-ice/#blog [Accessed].

BENGTSON NASH, S., RINTOUL, S. R., KAWAGUCHI, S., STANILAND, I., HOFF, J. V. D., TIERNEY, M. & BOSSI, R. 2010. Perfluorinated compounds in the Antarctic region: Ocean circulation provides prolonged protection from distant sources. *Environmental Pollution,* 158**,** 2985-2991.

BENSKIN, J. P., PHILLIPS, V., ST. LOUIS, V. L. & MARTIN, J. W. 2011. Source Elucidation of Perfluorinated Carboxylic Acids in Remote Alpine Lake Sediment Cores. *Environmental Science & Technology,* 45**,** 7188-7194.

BRAVO, I., DÍAZ-DE-MERA, Y., ARANDA, A., SMITH, K., SHINE, K. P. & MARSTON, G. 2010. Atmospheric chemistry of C4F9OC2H5 (HFE-7200), C4F9OCH3 (HFE-7100), C3F7OCH3 (HFE-7000) and C3F7CH2OH: temperature dependence of the kinetics of their reactions with OH radicals, atmospheric lifetimes and global warming potentials. *Phys Chem Chem Phys,* 12**,** 5115-5125.

BRENDEL, S., FETTER, É., STAUDE, C., VIERKE, L. & BIEGEL-ENGLER, A. 2018. Short-chain perfluoroalkyl acids: environmental concerns and a regulatory strategy under REACH. *Environmental sciences Europe,* 30**,** 9-9.

BUTT, C. M., YOUNG, C. J., MABURY, S. A., HURLEY, M. D. & WALLINGTON, T. J. 2009. Atmospheric chemistry of 4:2 fluorotelomer acrylate [C4F9CH2CH2OC(O)CH=CH2]: kinetics, mechanisms, and products of chlorine-atom- and OH-radical-initiated oxidation. *J Phys Chem A,* 113**,** 3155-61.

CAI, M., ZHAO, Z., YIN, Z., AHRENS, L., HUANG, P., CAI, M., YANG, H., HE, J., STURM, R., EBINGHAUS, R. & XIE, Z. 2012. Occurrence of Perfluoroalkyl Compounds in Surface Waters from the North Pacific to the Arctic Ocean. *Environmental Science & Technology,* 46**,** 661-668.

CASAL, P., CASAS, G., VILA-COSTA, M., CABRERIZO, A., PIZARRO, M., JIMÉNEZ, B. & DACHS, J. 2019. Snow Amplification of Persistent Organic Pollutants at Coastal Antarctica. *Environmental Science & Technology,* 53**,** 8872-8882.

CASAL, P., ZHANG, Y., MARTIN, J. W., PIZARRO, M., JIMÉNEZ, B. & DACHS, J. 2017. Role of Snow Deposition of Perfluoroalkylated Substances at Coastal Livingston Island (Maritime Antarctica). *Environmental science & technology,* 51**,** 8460.

CODLING, G., HALSALL, C., AHRENS, L., DEL VENTO, S., WIBERG, K., BERGKNUT, M., LAUDON, H. & EBINGHAUS, R. 2014. The fate of per- and polyfluoroalkyl substances within a melting snowpack of a boreal forest. *Environmental Pollution,* 191**,** 190-198.

D'EON J, C., HURLEY, M. D., WALLINGTON, T. J. & MABURY, S. A. 2006. Atmospheric chemistry of N-methyl perfluorobutane sulfonamidoethanol, C4F9SO2N(CH3)CH2CH2OH: kinetics and mechanism of reaction with OH. *Environ Sci Technol,* 40**,** 1862-8.

DREYER, A., WEINBERG, I., TEMME, C. & EBINGHAUS, R. 2009a. Polyfluorinated Compounds in the Atmosphere of the Atlantic and Southern Oceans: Evidence for a Global Distribution. *Environmental Science & Technology,* 43**,** 6507-6514.

DREYER, A., WEINBERG, I., TEMME, C. & EBINGHAUS, R. 2009b. Polyfluorinated compounds in the atmosphere of the Atlantic and Southern Oceans: evidence for a global distribution. *Environmental science & technology,* 43**,** 6507.

ELLIS, D. A., MARTIN, J. W., MABURY, S. A., HURLEY, M. D., SULBAEK ANDERSEN, M. P. & WALLINGTON, T. J. 2003. Atmospheric Lifetime of Fluorotelomer Alcohols. *Environmental Science & Technology,* 37**,** 3816-3820.

GPO 2000. Federal Register Volume 65, Issue 243 (December 18, 2000).

GRANNAS, A. M., BOGDAL, C., HAGEMAN, K. J., HALSALL, C., HARNER, T., HUNG, H., KALLENBORN, R., KLÁN, P., KLÁNOVÁ, J., MACDONALD, R. W., MEYER, T. & WANIA, F. 2013. The role of the global cryosphere in the fate of organic contaminants. *Atmos. Chem. Phys.,* 13**,** 3271-3305.

HOSSAINI, R., CHIPPERFIELD, M. P., MONTZKA, S. A., LEESON, A. A., DHOMSE, S. S. & PYLE, J. A. 2017. The increasing threat to stratospheric ozone from dichloromethane. *Nat Commun,* 8**,** 15962.

HU, X. C., ANDREWS, D. Q., LINDSTROM, A. B., BRUTON, T. A., SCHAIDER, L. A., GRANDJEAN, P., LOHMANN, R., CARIGNAN, C. C., BLUM, A., BALAN, S. A., HIGGINS, C. P. & SUNDERLAND, E. M. 2016. Detection of Poly- and Perfluoroalkyl Substances (PFASs) in U.S. Drinking Water Linked to Industrial Sites, Military Fire Training Areas, and Wastewater Treatment Plants. *Environmental Science & Technology Letters,* 3**,** 344-350.

HURLEY, M. D., BALL, J. C., WALLINGTON, T. J., SULBAEK ANDERSEN, M. P., ELLIS, D. A., MARTIN, J. W. & MABURY, S. A. 2004. Atmospheric Chemistry of 4:2 Fluorotelomer Alcohol (CF3(CF2)3CH2CH2OH): Products

and Mechanism of Cl Atom Initiated Oxidation. *J. Phys. Chem. A,* 108**,** 5635-5642.

INDUSTRY_TODAY. 2020. *Fluorotelomer Market to Witness Robust Expansion by 2025* [Online]. Available: https://industrytoday.co.uk/market-research-industry-today/fluorotelomer-market-to-witness-robust-expansion-by-2025 [Accessed].

JOERSS, H., XIE, Z., WAGNER, C. C., VON APPEN, W.-J., SUNDERLAND, E. M. & EBINGHAUS, R. 2020. Transport of Legacy Perfluoroalkyl Substances and the Replacement Compound HFPO-DA through the Atlantic Gateway to the Arctic Ocean—Is the Arctic a Sink or a Source? *Environmental Science & Technology.*

JOHANSSON, J. H., SALTER, M. E., ACOSTA NAVARRO, J. C., LECK, C., NILSSON, E. D. & COUSINS, I. T. 2019. Global transport of perfluoroalkyl acids via sea spray aerosol. *Environmental science. Processes & impacts,* 21**,** 635.

LAEPPLE, T., HÖRHOLD, M., MÜNCH, T., FREITAG, J., WEGNER, A. & KIPFSTUHL, S. 2016. Layering of surface snow and firn at Kohnen Station, Antarctica: Noise or seasonal signal? *Journal of Geophysical Research: Earth Surface,* 121**,** 1849-1860.

LAND, M., DE WIT, C. A., BIGNERT, A., COUSINS, I. T., HERZKE, D., JOHANSSON, J. H. & MARTIN, J. W. 2018. What is the effect of phasing out long-chain per- and polyfluoroalkyl substances on the concentrations of perfluoroalkyl acids and their precursors in the environment? A systematic review. *Environmental Evidence,* 7**,** 4.

LI, J., DEL VENTO, S., SCHUSTER, J., ZHANG, G., CHAKRABORTY, P., KOBARA, Y. & JONES, K. C. 2011. Perfluorinated Compounds in the Asian Atmosphere. *Environ. Sci. Technol,* 45**,** 7241-7248.

MACINNIS, J. J., FRENCH, K., MUIR, D. C. G., SPENCER, C., CRISCITIELLO, A., DE SILVA, A. O. & YOUNG, C. J. 2017. Emerging investigator series: a 14-year depositional ice record of perfluoroalkyl substances in the High Arctic. *Environ. Sci.: Processes Impacts,* 19**,** 22-30.

MARTIN, J. W., ELLIS, D. A., MABURY, S. A., HURLEY, M. D. & WALLINGTON, T. J. 2006. Atmospheric chemistry of perfluoroalkanesulfonamides: kinetic and product studies of the OH radical and Cl atom initiated oxidation of N-ethyl perfluorobutanesulfonamide. *Environ Sci Technol,* 40**,** 864-72.

MEYER, T., LEI, Y., MURADI, I. & WANIA, F. 2009a. Organic Contaminant Release from Melting Snow. 1. Influence of Chemical Partitioning. *Environmental Science & Technology,* 43**,** 657.

MEYER, T., LEI, Y., MURADI, I. & WANIA, F. 2009b. Organic Contaminant Release from Melting Snow. 2. Influence of Snow Pack and Melt Characteristics. *Environmental Science & Technology,* 43**,** 663.

MMR. 2020. *Global Heat Transfer Fluids Market: Industry Analysis and Forecast (2019-2026)* [Online]. Available: https://www.maximizemarketresearch.com/market-report/global-heat-transfer-fluids-market/30456/#details [Accessed].

NAKAYAMA, T., TAKAHASHI, K., MATSUMI, Y., TOFT, A., SULBAEK ANDERSEN, M. P., NIELSEN, O. J., WATERLAND, R. L., BUCK, R. C., HURLEY, M. D. & WALLINGTON, T. J. 2007. Atmospheric chemistry of CF 3 CH=CH 2 and C 4 F 9 CH=CH 2 : Products of the gas-phase reactions with Cl atoms and OH radicals. *Journal of Physical Chemistry A,* 111**,** 909-915.

NICNAS 2006. HFE-7100. *In:* SCHEME, N. I. C. N. A. A. (ed.) *Existing Chemical Secondary Notification Assessment NA/482S.* Sydney, Australia.

OECD 2015. WORKING TOWARDS A GLOBAL EMISSION INVENTORY OF PFASS: FOCUS ON PFCAS - STATUS QUO AND THE WAY FORWARD. *OECD Environment, Health and Safety Publications Series on Risk Management.*

OERTER, H., GRAF, W., WILHELMS, F., MINIKIN, A. & MILLER, H. 1999. Accumulation studies on Amundsenisen, Dronning Maud Land, Antarctica, by means of tritium, dielectric profiling and stable-isotope measurements: first results from the 1995–96 and 1996–97 field seasons. *Annals of Glaciology,* 29**,** 1-9.

PICKARD, H. M., CRISCITIELLO, A. S., PERSAUD, D., SPENCER, C., MUIR, D. C. G., LEHNHERR, I., SHARP, M. J., DE SILVA, A. O. & YOUNG, C. J. 2020. Ice Core Record of Persistent Short-Chain Fluorinated Alkyl Acids: Evidence of the Impact From Global Environmental Regulations. *Geophysical Research Letters,* 47**,** e2020GL087535.

PICKARD, H. M., CRISCITIELLO, A. S., SPENCER, C., SHARP, M. J., MUIR, D. C. G., DE SILVA, A. O. & YOUNG, C. J. 2018. Continuous non-marine inputs of per- and polyfluoroalkyl substances to the High Arctic: a multi-decadal temporal record. *Atmos. Chem. Phys.,* 18**,** 5045-5058.

PINGLOT, J. F., VAIKMÄE, R. A., KAMIYAMA, K., IGARASHI, M., FRITZSCHE, D., WILHELMS, F., KOERNER, R., HENDERSON, L., ISAKSSON, E., WINTHER, J.-G., VAN DE WAL, R. S. W., FOURNIER, M., BOUISSET, P. & MEIJER, H. A. J. 2003. Ice cores from Arctic sub-polar glaciers: chronology and post-depositional processes deduced from radioactivity measurements. *J. Glaciol,* 49**,** 149-158.

POULSEN, P. B. J., ALLAN ASTRUP; WALLSTRÖM; EVA 2005. More environmentally friendly alternatives to PFOS-compounds and PFOA. *In:* JENSEN, F. (ed.). Denmark: The Danish Environmental Protection Agency.

PREVEDOUROS, K., COUSINS, I., BUCK, R. C. & KORZENIOWSKI, S. 2006. Sources, fate and transport of perfluorocarboxylates. *Environ. Sci. Technol.*

STAUFFER, B., FLÜCKIGER, J., WOLFF, E. & BARNES, P. 2004. The EPICA deep ice cores: first results and perspectives. *Annals of Glaciology,* 39**,** 93-100.

SULBAEK ANDERSEN, M. P., NIELSEN, O. J., HURLEY, M. D., BALL, J. C., WALLINGTON, T. J., ELLIS, D. A., MARTIN, J. W. & MABURY, S. A. 2005. Atmospheric chemistry of 4:2 fluorotelomer alcohol (n-C4F9CH2CH2OH): products and mechanism of Cl atom initiated oxidation in the presence of NOx. *J Phys Chem A,* 109**,** 1849-56.

THACKRAY, C. P. & SELIN, N. E. 2017. Uncertainty and variability in atmospheric formation of PFCAs from fluorotelomer precursors. *Atmospheric chemistry and physics,* 17**,** 4585-4597.

TSAI, W.-T. 2005. Environmental risk assessment of hydrofluoroethers (HFEs). *Journal of Hazardous Materials,* 119**,** 69-78.

VENTO, S. D., HALSALL, C., GIOIA, R., JONES, K. & DACHS, J. 2012. Volatile per- and polyfluoroalkyl compounds in the remote atmosphere of the western Antarctic Peninsula: an indirect source of perfluoroalkyl acids to Antarctic waters? *Atmospheric Pollution Research,* 3**,** 450-455.

VIEIRA, V. M., HOFFMAN, K., SHIN, H.-M., WEINBERG, J. M., WEBSTER, T. F. & FLETCHER, T. 2013. Perfluorooctanoic acid exposure and cancer outcomes in a contaminated community: a geographic analysis. *Environmental health perspectives,* 121**,** 318-323.

WALLINGTON, T. J., HURLEY, M. D., XIA, J., WUEBBLES, D. J., SILLMAN, S., ITO, A., PENNER, J. E., ELLIS, D. A., MARTIN, J., MABURY, S. A., NIELSEN, O. J. & SULBAEK ANDERSEN, M. P. 2006. Formation of C7F15COOH (PFOA) and other perfluorocarboxylic acids during the atmospheric oxidation of 8:2 fluorotelomer alcohol. *Environmental science & technology,* 40**,** 924.

WANG, X., HALSALL, C., CODLING, G., XIE, Z., XU, B., ZHAO, Z., XUE, Y., EBINGHAUS, R. & JONES, K. C. 2014a. Accumulation of perfluoroalkyl compounds in tibetan mountain snow: temporal patterns from 1980 to 2010. *Environ Sci Technol,* 48**,** 173-81.

WANG, Z., COUSINS, I. T., SCHERINGER, M., BUCK, R. C. & HUNGERBÜHLER, K. 2014b. Global emission inventories for C4-C14 perfluoroalkyl carboxylic acid (PFCA) homologues from 1951 to 2030, Part I: production and emissions from quantifiable sources. *Environ Int,* 70**,** 62-75.

WANG, Z., COUSINS, I. T., SCHERINGER, M., BUCK, R. C. & HUNGERBÜHLER, K. 2014c. Global emission inventories for C4–C14 perfluoroalkyl carboxylic acid (PFCA) homologues from 1951 to 2030, part II: The remaining pieces of the puzzle. *Environment International,* 69**,** 166-176.

WANG, Z., COUSINS, I. T., SCHERINGER, M. & HUNGERBUEHLER, K. 2015. Hazard assessment of fluorinated alternatives to long-chain perfluoroalkyl acids (PFAAs) and their precursors: Status quo, ongoing challenges and possible solutions. *Environment International,* 75**,** 172-179.

WELLER, R. & WAGENBACH, D. 2007. Year-round chemical aerosol records in continental Antarctica obtained by automatic samplings. *Tellus B: Chemical and Physical Meteorology,* 59**,** 755-765.

WELLER, R. & WAGENBACH, D. 2017. Year-round chemical aerosol records in continental Antarctica obtained by automatic samplings. *Tellus. Series B, Chemical and physical meteorology,* 59**,** 755-765.

WILD, S., MCLAGAN, D., SCHLABACH, M., BOSSI, R., HAWKER, D., CROPP, R., KING, C. K., STARK, J. S., MONDON, J. & NASH, S. B. 2015. An Antarctic research station as a source of brominated and perfluorinated persistent organic pollutants to the local environment. *Environ Sci Technol,* 49**,** 103-12.

XIE, Z., WANG, Z., MAGAND, O., THOLLOT, A., EBINGHAUS, R., MI, W. & DOMMERGUE, A. 2020. Occurrence of legacy and emerging organic contaminants in snow at Dome C in the Antarctic. *The Science of the total environment,* 741.

XIE, Z., WANG, Z., MI, W., MÖLLER, A., WOLSCHKE, H. & EBINGHAUS, R. 2015. Neutral Poly-/perfluoroalkyl Substances in Air and Snow from the Arctic. *Scientific Reports,* 5**,** 8912.

YOUNG, C. J., HURLEY, M. D., WALLINGTON, T. & MABURY, S. A. 2008. Atmospheric Chemistry of 4:2 Fluorotelomer Iodide (n-C4F9CH2CH2I): Kinetics and Products of Photolysis and Reaction with OH Radicals and Cl Atoms. *J. Phys. Chem. A,* 112**,** 13542-13548.

Jack Garnett[1], Crispin Halsall[1*], Robert Mulvaney[2], Anna Jones[2], Holly Winton[2], Hanna Joerss[3], Ralf Ebinghaus[3], Amber Leeson[1], Peter Wynn[1]

1 Lancaster Environment Centre, Lancaster University, Lancaster, LA1 4YQ, UK

2 British Antarctic Survey, Cambridge, High Cross, Madingley Road, Cambridge, CB3 0ET, UK

3 Helmholtz-Zentrum Hereon, Max-Planck-Straße 1, 21502 Geesthacht, Germany

Email: c.halsall@lancaster.ac.uk

Supporting Information to:

Increasing accumulation of perfluorocarboxylate contaminants revealed in an Antarctic snow core (1958-2017).

Table S1: Depth (m) and date (AD) of snow samples measured in this study.

Upper depth (m)	Lower depths (m)	Section upper year (AD)	Section lower year (AD)	Average year (AD)
0	0.88	2017	2013	2015
*0	0.88	2017	2013	2015
*0.88	0.94	2013	2012	2013
0.88	1.67	2013	2009	2011
1.67	2.32	2009	2006	2008
2.32	3.06	2006	2003	2004
3.06	3.66	2003	1999	2001
3.66	4.38	1999	1997	1998
4.38	5.08	1997	1992	1995
5.08	5.75	1992	1990	1991
5.75	6.56	1990	1985	1987
6.56	7.17	1985	1981	1983
7.17	8.02	1981	1972	1977
8.02	8.71	1972	1966	1969
8.71	9.19	1966	1963	1965
9.19	9.68	1963	1958	1960

*To avoid possible PFAS contamination arising from contact with surfaces, and to preserve the maximum amount of snow meltwater needed for PFAS analysis, the age of snow was determined from a shallow snow core that was mechanically drilled at Kohnen Station during the ISOL-Ice campaign in 2017. The time-depth scale was transposed directly on to the snow core analysed for PFAS in this study. * Represents samples obtained from a duplicate snow core (0 – 0.94m).*

Table S2: Snow accumulation (m) and date (AD) of snow samples measured in this study.

Date	Accumulation period (Years)	Section thickness (m)	*Density (kg m^{-3})	Meltwater equiv. accumulation (kg m^{-2})	Average annual snow accumulation rate (kg m^{-2} a^{-1})
2013-2017	4.2	0.88	311	274	65
*2013-2017	4.2	0.88	311	274	65
*2012-2013	0.3	0.06	320	19	64
2009-2013	3.7	0.79	326	256	68
2006-2009	2.7	0.66	339	222	81
2003-2006	3.7	0.74	351	258	70
1999-2003	3.4	0.61	363	220	65
1997-1999	2.5	0.72	374	268	107
1992-1997	4.3	0.70	387	271	64
1990-1992	2.9	0.67	399	267	92
1985-1990	4.1	0.81	412	334	81
1981-1985	3.9	0.61	424	260	66
1972-1981	9.3	0.84	437	369	40
1966-1972	5.8	0.69	451	311	54
1963-1966	3.8	0.49	461	224	60
1958-1963	4.5	0.48	470	228	50
Mean (± 1.s.d.)	4.2 ± 1.7	0.7 ± 0.1	n/a	n/a	68 ± 18

Average values do *not* include those marked with asterisk to avoid numerical duplication.

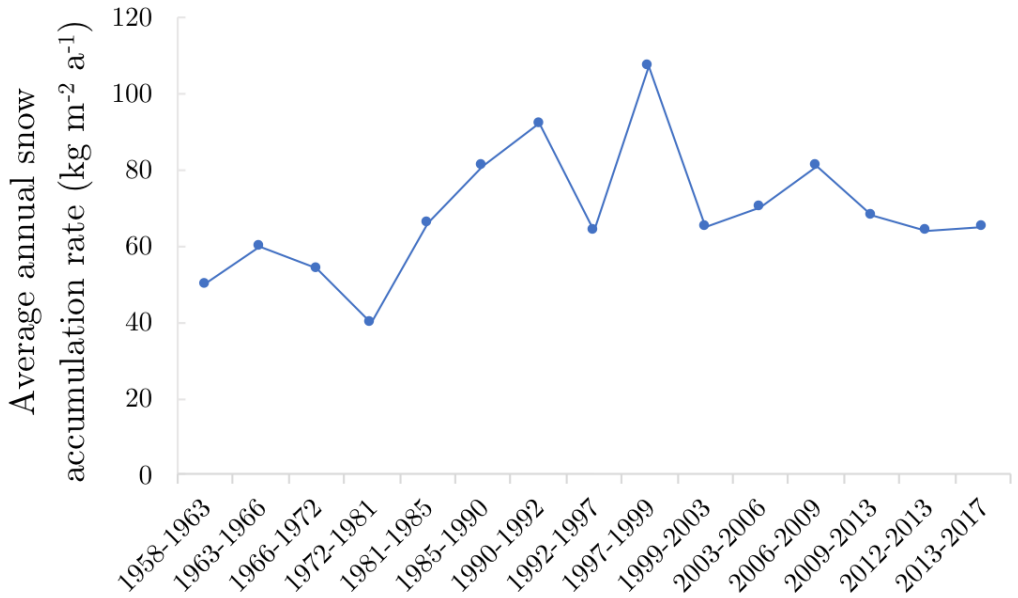

Figure S1: Average annual snow accumulation rate at Kohnen Station, Antarctica

Snow core samples in this study were used to derive a mean annual snow accumulation of 68 ± 18 kg m^{-2} a^{-1}, which corresponds well with other studies at the same site (Oerter et al., 1999)

Table S3: Overview of analytical standards, CAS numbers, the standard suppliers, purity and concentration/amount

Acronym	Analytical standard	CAS number	Supplier, purity and concentration/amount
PFBA	perfluoro-*n*-butanoic acid	375-22-4 (acid)	PFC-MXA (mixture) Wellington Laboratories, > 98 % 2.0 µg/mL ± 5 % of the single compounds
PFPeA	perfluoro-*n*-pentanoic acid	2706-90-3 (acid)	
PFHxA	perfluoro-*n*-hexanoic acid	307-24-4 (acid)	
PFHpA	perfluoro-*n*-heptanoic acid	375-85-9 (acid)	
PFOA	perfluoro-*n*-octanoic acid	335-67-1 (acid)	
PFNA	perfluoro-*n*-nonanoic acid	375-95-1 (acid)	
PFDA	perfluoro-*n*-decanoic acid	335-76-2 (acid)	
PFUnDA	perfluoro-*n*-undecanoic acid	2058-94-8 (acid)	
PFDoDA	perfluoro-*n*-dodecanoic acid	307-55-1 (acid)	
PFTrDA	perfluoro-*n*-tridecanoic acid	72629-94-8 (acid)	
PFTeDA	perfluoro-n-tetradecanoic acid	376-06-7 (acid)	
PFBS	potassium perfluoro-*n*-butanesulfonate	29420-49-3 (K+ salt) 375-73-5 (acid)	PFS-MXA (mixture) Wellington Laboratories, > 98 % 2.0 µg/mL ± 5 % of the single compounds
PFHxS	sodium perfluoro-*n*-hexanesulfonate	82382-12-5 (Na+ salt) 355-46-4 (acid)	
PFHpS	sodium perfluoro-*n*-heptanesulfonate	22767-50-6 (Na+ salt) 375-92-8 (acid)	
PFOS	sodium perfluoro-*n*-octanesulfonate	4021-47-0 (Na+ salt) 1763-23-1 (acid)	
PFDS	sodium perfluoro-*n*-decanesulfonate	2806-15-7 (Na+ salt) 335-77-3 (acid)	
13C4-PFBA	perfluoro-*n*-[13C4]-butanoic acid	-	MPFAC-MXA (mixture) Wellington Laboratories, > 98 %, 2.0 µg/mL ± 5 % of the single compounds
13C2-PFHxA	perfluoro-*n*-[1,2-13C2]-hexanoic acid	-	
13C4-PFOA	perfluoro-*n*-[1,2,3,4-13C4]-octanoic acid	-	
13C5-PFNA	perfluoro-*n*-[1,2,3,4,5-13C5]-nonanoic acid	-	
13C2-PFDA	perfluoro-*n*-[1,2-13C2]-decanoic acid	-	
13C2-PFUnDA	perfluoro-*n*-[1,2-13C2]-undecanoic acid	-	
13C2-PFDoDA	perfluoro-*n*-[1,2-13C2]-dodecanoic acid	-	
18O2-PFHxS	sodium perfluorohexane-*n*-[18O2]-sulfonate	-	
13C4-PFOS	sodium perfluoro-*n*-[1,2,3,4-13C4]-octanesulfonate	-	
13C8-PFOA	perfluoro-[13C8]-octanoic acid (injection standard)	-	Wellington Laboratories, > 98 %, (50 ± 2.5) µg/mL

Target PFAS included 11 PFCA (C_4 to C_{14}), five PFSA (C_4, C_6, C_7, C_8, C_{10}),

Table SX: Overview of the components and the compound-independent parameter settings for the LC-MS/MS analysis of PFAS.

liquid chromatography				
component	**type (manufacturer, country)**			
binary pump	HP 1100 LC binary pump G1312 (Agilent, USA)			
autosampler	HP 1100 LC autosampler G1313 (Agilent, USA)			
analytical column	Synergi Fusion-RP: polar embedded C18 phase with trimethylsilyl endcapping, 150 mm x 2 mm, particle size 4 µm, pore size 80 Å (Phenomenex, USA)			
guard column	SecurityGuard cartridge for Fusion-RP HPLC columns, 4 mm x 2 mm (Phenomenex, USA)			
software	Analyst 1.5 (AB Sciex, USA)			
parameter	**setting**			
injection volume	10 µL (needle rinsed twice with methanol before injection)			
column temperature	30 °C			
flow rate	0.2 mL/min			
mobile phases	A: 2 mM ammonium acetate aqueous solution B: 0.05 % acetic acid in methanol			
sample/standard solvent	methanol:water 80:20 (v/v)			
gradient	time [min]	A [%]	B [%]	note
	–8	70	30	equilibration
	0	70	30	
	3	30	70	
	29	10	90	
	31	0	100	purging
	45	0	100	
tandem mass spectrometry				
component	**type (manufacturer, country)**			
instrument	API 4000 triple quadrupole mass spectrometer (AB Sciex, USA)			
ion source	Turbo V Ion Source (AB Sciex, USA)			
software	Analyst 1.5 (AB Sciex, USA)			
parameter	**settings**			
ionization	electrospray ionization (ESI) in negative mode			
ion spray voltage	–4500 V			
source temperature	400 °C			
gas 1 (nebulizer gas)	N2, 4.2 bar			
gas 2 (heater gas)	N2, 2.8 bar			
curtain gas	N2, 1.0 bar			
collision gas	N2, 0.6 bar			
scan type	Scheduled Multiple Reaction Monitoring (MRM) retention time window: 180 s, target scan time: 2 s			

Table SX: Compound-specific parameter settings for the LC-MS/MS analysis of native PFAS.

acronym analyte	t_R [min][1]	molecular formula precursor ion	mass transition [m/z][2]	transition-specific parameters [V][3]			
				DP	EP	CE	CXP
PFBA	6.1	[C4F7O2]–	213>169*	–30	–5	–13	–9
PFPeA	9.6	[C5F9O2]–	263>219*	–26	–4	–12	–13
PFHxA	10.4	[C6F11O2]–	313>269*	–28	–4	–13	–16
			313>119	–28	–4	–30	–5
PFHpA	11.1	[C7F13O2]–	363>319*	–29	–4	–14	–19
			363>169	–29	–4	–25	–8
PFOA	11.9	[C8F15O2]–	413>369*	–24	–4	–15	–8
			413>169	–24	–4	–28	–8
PFNA	12.9	[C9F17O2]–	463>419*	–34	–4	–15	–9
			463>219	–34	–4	–24	–12
PFDA	14.2	[C10F19O2]–	513>469*	–35	–6	–15	–11
			513>219	–35	–6	–29	–12
PFUnDA	15.9	[C11F21O2]–	563>519*	–35	–5	–17	–13
			563>169	–35	–5	–37	–8
PFDoDA	18.0	[C12F23O2]–	613>569*	–38	–9	–17	–15
			613>169	–38	–9	–38	–8
PFTrDA	20.3	[C13F25O2]–	663>619*	–39	–8	–18	–14
			663>169	–39	–8	–41	–8
PFTeDA	22.7	[C14F27O2]–	713>669*	–36	–9	–22	–15
			713>169	–36	–9	–40	–8
PFBS	9.7	[C4F9O3S]–	299>99*	–66	–12	–42	–16
			299>80	–66	–12	–60	–2
PFHxS	11.1	[C6F13O3S]–	399>99	–70	–14	–50	–15
			399>80*	–70	–14	–66	–2
PFHpS	11.8	[C7F15O3S]–	449>99	–80	–12	–61	–16
			449>80*	–80	–12	–85	–2
PFOS	12.8	[C8F17O3S]–	499>99	–73	–12	–74	–17
			499>80*	–73	–12	–90	–2
PFDS	15.8	[C10F21O3S]–	599>99	–80	–14	–62	–3
			599>80*	–80	–14	–90	–2

[1] The column provides exemplary retention times. They changed in dependence of the age of the column and were determined before each measurement sequence in a non-scheduled MRM run.

[2] Asterisks mark the product ion that was used as quantifier, whereas the second product ion was used as qualifier.

[3] Optimized mass spectrometric parameters include the declustering potential (DP), the entrance potential (EP), the collision energy (CE) and the cell exit potential (CXP).

Table SX: Compound-specific parameter settings for the LC-MS/MS analysis of the internal standards used for PFAS quantification. 13C8-PFOA was added as injection standard.

acronym analyte	tR [min]	molecular formula precursor ion	mass transitions [m/z]	transition-specific parameters [V]			
				DP	EP	CE	CXP
13C4-PFBA	6.1	[13C4F7O2]–	217>172*	–22	–4	–13	–9
13C2-PFHxA	10.4	[13C212C4F11O2]–	315>270*	–23	–6	–12	–16
			315>120	–23	–6	–31	–4
13C4-PFOA	11.9	[13C412C4F15O2]–	417>372*	–32	–4	–13	–8
			417>169	–32	–4	–27	–8
13C8-PFOA	11.9	[13C8F15O2]–	421>376*	–25	–6	–14	–8
			421>172	–25	–6	–26	–8
13C5-PFNA	12.9	[13C512C4F17O2]–	468>423*	–30	–7	–14	–10
			468>223	–30	–7	–24	–12
13C2-PFDA	14.2	[13C212C8F19O2]–	515>470*	–39	–6	–16	–10
			515>220	–39	–6	–26	–12
13C2-PFUnDA	15.9	[13C212C9F21O2]–	565>520*	–33	–6	–16	–13
			565>169	–33	–6	–34	–8
13C2-PFDoDA	18.0	[13C212C10F23O2]–	615>570*	–38	–9	–17	–15
			615>169	–38	–9	–41	–8
18O2-PFHxS	11.1	[C6F1318O216OS]–	403>103	–82	–10	–55	–4
			403>84*	–82	–10	–79	–2
13C4-PFOS	12.8	[13C412C4F17O3S]–	503>99	–65	–12	–64	–4
			503>80*	–65	–12	–92	–2

Table SX: Overview of the components and parameter settings for the LC-QToF-MS analysis to confirm the identity of PFAS, for which only one mass transition was monitored by LC-MS/MS.

liquid chromatography			
component	**type**		
system	1290 Infinity II UHPLC (Agilent, USA)		
analytical column	Zorbax Eclipse Plus C18, 2.1 mm x 100 mm, particle size: 1.8 µm, pore size: 95 Å (Agilent, USA)		
software	Mass Hunter, version 10.0 (Agilent, USA)		
parameter	**setting**		
injection volume	10 µL (needle wash: 20 s flush port, methanol)		
column temperature	30 °C		
flow rate	0.2 mL/min		
mobile phases	A: 2 mM ammonium acetate aqueous solution B: methanol		
gradient	time [min]	A [%]	B [%]
	0	90	10
	10	2	98
	15	2	98
	15.1	90	10
high resolution mass spectrometry			
component	**type (manufacturer, country)**		
instrument	6546 QToF-MS (Agilent, USA)		
software	Mass Hunter, version 10.0 (Agilent, USA)		
instrumental settings			
ionization	electrospray ionization (ESI) in negative mode		
gas temperature	200 °C		
gas flow	12 L/min		
nebulizer gas	45 psig		
sheath gas temperature	350 °C		
sheath gas flow	11 L/min		
mass spectrometric analysis settings			
mode	All Ions (data-independent acquisition mode; all ions are fragmented without a specific isolation of a precursor ion in the first mass analyser)		
mass range	m/z 50–1000		
scan rate	6 spectra/s		
scan segments	#	collision energy [eV]	
	1	0	
	2	10	

	3	40
reference masses	m/z 112.98558700; 980.01637500	

For unequivocal identification, at least two mass transitions by compound have to be monitored by LC-MS/MS. However, for PFBA and PFPeA, only one product ion with high enough intensity was identified when developing the LC-MS/MS method (see table SX). This is consistent with other scientific publications (Gremmel et al., 2017; Munoz et al., 2015) and norms for the analysis of PFAS (e.g. DIN norm 38407-42:2011-03). To confirm the identity of the substances concerned, standards and selected samples were additionally analysed by high resolution mass spectrometry in this study. The following table exemplarily shows the identification points measured by LC-QToF-MS for PFBA in ice core section 2.

	calibration standard	sample (ice core section 2)
precursor ion [C4F7O2]–		
theoretical mass	m/z 213.98648 (neutral mass)	
observed mass	m/z 213.98649	m/z 213.98638
mass error [ppm]	0.08	-0.46
fragment ion [C3F7]-		
theoretical mass	m/z 168.98937	
observed mass	m/z 168.98932	m/z 168.98937
mass error [ppm]	-0.29	-0.03
pattern of additional fragments		

In addition to the retention time and mass transition measured by LC-MS/MS, the exact mass of the precursor ion (mass error << 5 ppm), the exact mass of the selected fragment ion [C3F7]- (mass error << 5 ppm) and the presence of several additional fragment ions with a comparable abundance pattern in the calibration standard and the sample measured by LC-QToF-MS confirm the identity of PFBA in the sample.
It has to be noted that the high resolution of the instrument is "bought" with a lower sensitivity compared to the LC-MS/MS measurement (~ factor 10). Consequently, PFBA was not confirmed in low concentrated standards and samples.

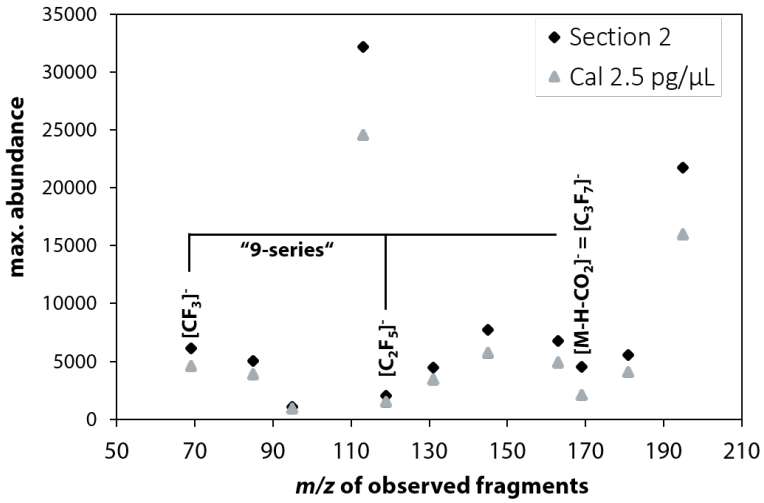

Table S4: Concentrations of PFAAs (pg L^{-1})in a snow core that has been in long-term storage

Sample Name	PFBA	PFPeA	PFHxA	PFHpA	PFOA	PFNA	PFDA	PFUnDA	PFDoDA	PFTrDA	PFTeDA	PFBS	PFHxS	PFHpS	PFOS	PFDS
Interior (Field_blank_1)	<LOD	40.4	18.3	24.5	149.9	9.2	22.1	4.9	11.6	<LOD	2.0	<LOD	<LOD	<LOD	13.9	<LOD
Middle (Field_blank_2)	<LOD	32.9	24.1	28.6	197.2	11.8	32.6	5.8	13.7	1.8	2.8	<LOD	<LOD	<LOD	23.2	<LOD
Exterior (Field_blank_3)	<LOD	113.0	160.1	184.7	2622.8	88.3	351.7	47.4	132.6	8.3	19.8	117.9	13.9	<LOD	181.7	<LOD

We screened a snow core for PFAS that had been acquired from the Antarctic Peninsula and dated to around 1920s (predated the onset of PFAS manufacture in 1950s) to determine whether snow cores that were collected during historical sampling campaigns (now in storage) were viable for temporal PFAS studies. PFAS have now been in-use for several decades within various garments (e.g. gloves) as waterproofing agents and therefore contact with these items during their extraction in the field and/or subsequent handling/storage may serve as a source of contamination thereby compromising their integrity. We cut three samples that consisted of inner, middle and outer edges (see schematic below) and subject each melted sample to PFAS analysis. Concentrations of PFAS in the external samples were significantly higher than inner layers, which suggests that contamination with PFAS at some stage after extraction had occurred with subsequent diffusion to the inner layers. Hence, caution is advised when working with snow cores obtained from historical campaigns, ensuring sufficient outer edge of cores is removed to eliminate possible contamination.

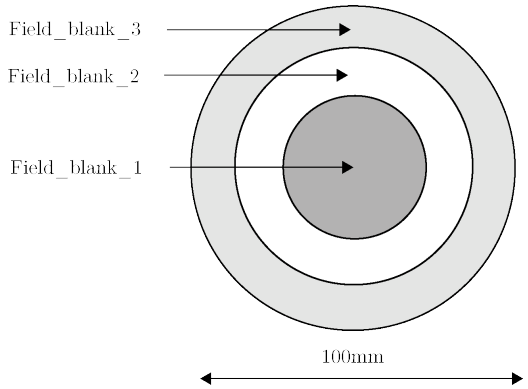

Table S5: Quality control/quality assurance criteria implemented in this study.

Native chemical	PFBA	PFPeA	PFHxA	PFHpA	PFOA	PFNA	PFDA	PFUnDA	PFDoDA	PFTrDA	PFTeDA	PFBS	PFHxS	PFHpS	PFOS	PFDS
$\overline{x}_{\text{lab blank}}$ (n=4) [pg L^{-1}]	27.5	37.4	20.9	14.9	37.0	<LOD	<LOD	<LOD	<LOD	<LOD	<LOD	<LOD	<LOD	<LOD	15.9	<LOD
$SD_{\text{lab blank}}$ (n=4) [pg L^{-1}]	2.6	3.0	2.5	3.3	4.7	<LOD	n/a	n/a	n/a	n/a	n/a	<LOD	<LOD	<LOD	7.9	<LOD
$\overline{x}_{\text{Field blank}}$ (n=2) [pg L^{-1}]	<LOD	36.7	21.2	26.6	173.6	10.5	27.4	5.4	12.7	0.9	2.4	<LOD	<LOD	<LOD	18.6	<LOD
MDL = $\overline{x}_{\text{lab blank}} + 3 \cdot SD_{\text{lab blank}}$ [pg L^{-1}]	35.4	46.5	28.5	24.8	51.2	*10.5	*27.4	*5.4	*12.7	*0.9	*2.4	<LOD	<LOD	<LOD	39.6	<LOD
% of samples >MDL (n=18)	72	39	67	61	78	72	6	22	6	22	6	0	0	0	11	0
Internal standard (IS)	13C4-PFBA	13C2-PFHxA		13C4-PFOA		13C5-PFNA	13C2-PFDA	13C2-PFUnDA	13C2-PFDoDA			18O2-PFHxS			13C4-PFOS	

Various quality control samples were taken throughout this study to meet strict criteria needed for trace chemical analysis. Field blanks consisted of a snow core that had its outer surface removed to avoid possible contamination from handling during extraction/storage (See Table S4). Asterisk (*) denotes those chemicals that have had their MDLs determined using field blank samples as per described in methodology. Higher concentrations of some PFASs (e.g. PFOA) compared with laboratory blanks may have occurred due to differences in PFAS levels in coastal regions.

Table S6: Density measurements made on snow core at Kohnen

Depth (m)	Density (kg m^{-3})
0.80	308
1.60	328
2.40	312
3.24	387
4.03	381
4.85	402
5.66	405
6.46	434
7.26	443
8.06	439
9.83	469
10.66	476

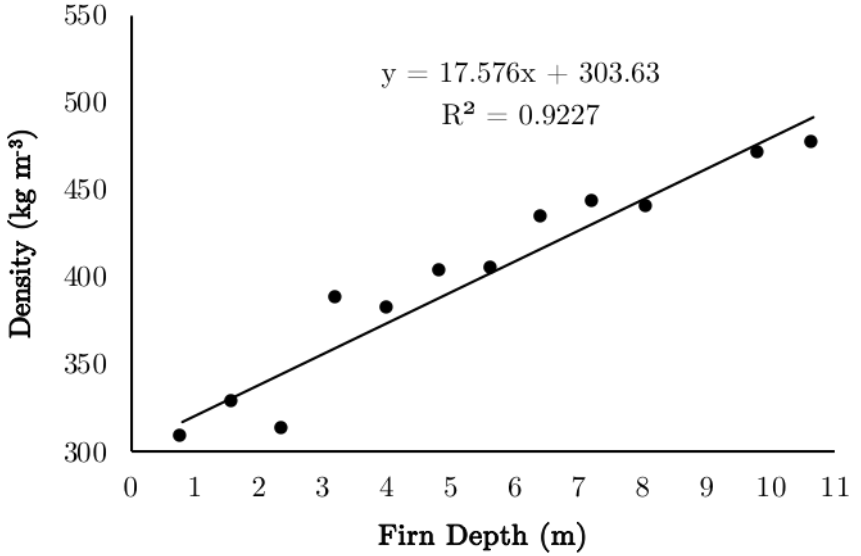

Figure S2: Density-depth profile of snow at Kohnen. Lower snow densities correspond to surface snow and higher densities relate to deeper snow.

To avoid possible PFAS contamination arising from contact with surfaces, and to preserve the maximum amount of snow meltwater needed for PFAS analysis, snow density was derived from a second shallow snow core that was manually drilled at Kohnen Station during the ISOL-Ice campaign in 2017. Density measurements (see Table) were determined gravimetrically and a linear regression (See Figure 1) was subsequently applied to derive a density-depth scale for the snow core in this study.

Table S7: Concentration of PFAS in melted samples (pg L^{-1})

	PFBA	PFPeA	PFHxA	PFHpA	PFOA	PFNA	PFDA	PFUnDA	PFDoDA	PFTrDA	PFTeDA	PFBS	PFHxS	PFHpS	PFOS	PFDS	HFPO-DA
1958-1963	25.5	22.6	12.8	12.7	39.5	4.5	7.3	<LOD	<LOD	<LOD	<LOD	<LOD	<LOD	<LOD	12.3	<LOD	<LOD
1963-1966	26.6	29.1	19.1	13.3	51.7	9.0	7.0	<LOD	<LOD	<LOD	<LOD	<LOD	<LOD	<LOD	14.4	<LOD	<LOD
1966-1972	26.7	13.5	15.7	10.4	30.0	12.1	32.6	10.7	20.7	4.6	10.7	<LOD	<LOD	<LOD	10.2	<LOD	<LOD
1972-1981	32.2	27.8	8.6	12.8	37.8	14.3	2.8	8.5	<LOD	3.5	1.2	<LOD	<LOD	<LOD	9.9	<LOD	<LOD
1972-1981	33.3	35.1	21.6	20.1	57.4	15.2	3.0	4.9	<LOD	2.6	2.4	<LOD	<LOD	<LOD	16.8	<LOD	<LOD
1981-1985	39.3	17.8	10.3	12.2	56.7	7.6	5.9	2.5	4.6	1.7	1.6	<LOD	<LOD	<LOD	12.4	<LOD	<LOD
1985-1990	40.2	47.3	31.9	23.6	52.8	17.6	<LOD	7.7	<LOD	<LOD	<LOD	<LOD	<LOD	<LOD	16.1	<LOD	<LOD
1985-1990	41.9	62.3	40.8	32.9	67.5	14.5	<LOD	<LOD	<LOD	<LOD	<LOD	<LOD	<LOD	<LOD	17.3	<LOD	299.3
1990-1992	48.8	34.4	36.8	38.4	46.7	8.0	3.3	4.0	3.2	<LOD	0.9	<LOD	<LOD	<LOD	12.6	<LOD	<LOD
1992-1997	71.8	74.5	34.9	58.6	64.4	9.9	4.7	3.2	3.6	<LOD	<LOD	<LOD	<LOD	<LOD	13.1	<LOD	<LOD
1997-1999	57.0	49.2	43.0	122.1	117.8	24.7	<LOD	<LOD	<LOD	<LOD	<LOD	<LOD	<LOD	<LOD	16.7	<LOD	46.4
1999-2003	241.2	33.2	56.2	90.9	82.8	14.4	<LOD	3.7	3.4	<LOD	<LOD	<LOD	<LOD	<LOD	17.0	<LOD	<LOD
2003-2006	541.8	45.2	73.6	120.9	86.1	30.9	<LOD	<LOD	<LOD	<LOD	<LOD	<LOD	<LOD	<LOD	<LOD	<LOD	<LOD
2006-2009	1920.3	36.3	61.7	89.5	106.2	35.5	7.7	2.6	<LOD	<LOD	<LOD	<LOD	<LOD	<LOD	14.4	<LOD	<LOD
2009-2013	2607.7	34.3	41.8	65.4	107.0	70.4	9.4	4.0	<LOD	<LOD	1.3	<LOD	<LOD	<LOD	14.1	<LOD	<LOD
2012-2013	3027.4	81.7	89.7	93.5	132.6	54.3	<LOD	<LOD	<LOD	<LOD	<LOD	<LOD	<LOD	<LOD	52.6	<LOD	<LOD
2013-2017	4147.0	73.0	81.8	122.9	96.4	46.0	<LOD	<LOD	<LOD	<LOD	<LOD	<LOD	<LOD	<LOD	30.8	<LOD	<LOD
2013-2017	4321.4	55.6	75.5	123.8	108.0	60.3	19.5	6.8	5.9	<LOD	2.1	<LOD	<LOD	<LOD	11.1	<LOD	9.8

Red values indicate those analytes that were below method detection limits

Table S8: Depositional fluxes of PFAS in Antarctica (ng m^{-2} a^{-1})

	PFBA	PFPeA	PFHxA	PFHpA	PFOA	PFNA	PFDA	PFUnDA	PFDoDA	PFTrDA	PFTeDA	PFBS	PFHxS	PFHpS	PFOS	PFDS
1958-1963	1.3	1.1	0.6	0.6	2.0	0.2	0.4	<LOD	<LOD	<LOD	<LOD	<LOD	<LOD	<LOD	0.6	<LOD
1963-1966	1.6	1.7	1.1	0.8	3.1	0.5	0.4	<LOD	<LOD	<LOD	<LOD	<LOD	<LOD	<LOD	0.9	<LOD
1966-1972	1.4	0.7	0.8	0.6	1.6	0.7	1.8	0.6	1.1	0.2	0.6	<LOD	<LOD	<LOD	0.5	<LOD
1972-1981	1.3	1.1	0.3	0.5	1.5	0.6	0.1	0.3	<LOD	0.1	0.0	<LOD	<LOD	<LOD	0.4	<LOD
1972-1981	1.3	1.4	0.9	0.8	2.3	0.6	0.1	0.2	<LOD	0.1	0.1	<LOD	<LOD	<LOD	0.7	<LOD
1981-1985	2.6	1.2	0.7	0.8	3.8	0.5	0.4	0.2	0.3	0.1	0.1	<LOD	<LOD	<LOD	0.8	<LOD
1985-1990	3.3	3.8	2.6	1.9	4.3	1.4	<LOD	0.6	<LOD	<LOD	<LOD	<LOD	<LOD	<LOD	1.3	<LOD
1985-1990	3.4	5.0	3.3	2.7	5.5	1.2	<LOD	<LOD	<LOD	<LOD	<LOD	<LOD	<LOD	<LOD	1.4	<LOD
1990-1992	4.5	3.1	3.4	3.5	4.3	0.7	0.3	0.4	0.3	<LOD	0.1	<LOD	<LOD	<LOD	1.2	<LOD
1992-1997	4.6	4.7	2.2	3.7	4.1	0.6	0.3	0.2	0.2	<LOD	<LOD	<LOD	<LOD	<LOD	0.8	<LOD
1997-1999	6.1	5.3	4.6	13.1	12.6	2.7	<LOD	<LOD	<LOD	<LOD	<LOD	<LOD	<LOD	<LOD	1.8	<LOD
1999-2003	15.8	2.2	3.7	5.9	5.4	0.9	<LOD	0.2	0.2	<LOD	<LOD	<LOD	<LOD	<LOD	1.1	<LOD
2003-2006	37.8	3.1	5.1	8.4	6.0	2.2	<LOD	<LOD	<LOD	<LOD	<LOD	<LOD	<LOD	<LOD	<LOD	<LOD
2006-2009	155.5	2.9	5.0	7.2	8.6	2.9	0.6	0.2	<LOD	<LOD	<LOD	<LOD	<LOD	<LOD	1.2	<LOD
2009-2013	178.4	2.3	2.9	4.5	7.3	4.8	0.6	0.3	<LOD	<LOD	0.1	<LOD	<LOD	<LOD	1.0	<LOD
2012-2013	193.5	5.2	5.7	5.8	8.5	3.5	<LOD	<LOD	<LOD	<LOD	<LOD	<LOD	<LOD	<LOD	3.4	<LOD
2013-2017	269.2	4.7	5.3	8.0	6.3	3.0	<LOD	<LOD	<LOD	<LOD	<LOD	<LOD	<LOD	<LOD	2.0	<LOD
2013-2017	280.6	3.6	4.9	8.0	7.0	3.9	1.3	0.4	0.4	<LOD	0.1	<LOD	<LOD	<LOD	0.7	<LOD

Red values indicate those analytes that were below method detection limits

Table S9: Chemicals identified as potential precursors of perfluoroalkyl acids and relevant properties.

Chemical Family	Fluorotelomer alcohols (FTOHs)									
Manufacturing process	Telomerization									
Main precursor chemicals	4:2 FTOH		6:2 FTOH		8:2 FTOH		10:2 FTOH		12:2 FTOH	
Atmospheric lifetime (approx. days)	20 (Ellis et al., 2004)		50 (Piekarz et al., 2007)		80 (Piekarz et al., 2007)		70 (Piekarz et al., 2007)		50 – 80 (Piekarz et al., 2007)	
Use	Intermediate/ End-product		Intermediate/ End-product		Intermediate/ End-product		Intermediate/ End-product		Intermediate/ End-product	
Measured in urban atmosphere	(Li et al., 2011)		(Chen et al., 2018) (Li et al., 2011)		(Chen et al., 2018) (Li et al., 2011)		(Chen et al., 2018) (Li et al., 2011)		(Chen et al., 2018) (Li et al., 2011)	
Measured in remote atmosphere	Southern Ocean: (Dreyer et al., 2009)*		Antarctic/ Southern Ocean: (Vento et al., 2012, Dreyer et al., 2009) Arctic: (AMAP, 2016) TP: (Wang et al., Wang et al., 2014) (Wang et al., 2014)		Antarctic: (Vento et al., 2012) Southern Ocean: (Dreyer et al., 2009) Arctic: (AMAP, 2016) TP: (Wang et al., 2014)		Antarctic: (Vento et al., 2012) Southern Ocean: (Dreyer et al., 2009) Arctic: (AMAP, 2016) TP: (Wang et al., 2014)		Antarctic: (Vento et al., 2012) Southern Ocean: (Dreyer et al., 2009) Arctic: (AMAP, 2016) TP: (Wang et al., 2014)	
Products	PFBA (C4)	PFPeA (C5)	PFHxA (C6)	PFHpA (C7)	PFOA (C8)	PFNA (C9)	PFDA (C10)	PFUnDA (C11)	PFDoDA (C12)	PFTrDA (C13)
Current usage trends	Increasing		Increasing		Increasing (AMAP, 2016)		Increasing (AMAP, 2016)		Increasing AP, 2016)	

*FTOHs are a major group of PFASs that are manufactured with carbon chain length up to C_{18}. The degradation of FTOHs proceed via a mechanism that leads to the potential production of a series of shorter chain PFCAs. * indicates those chemicals that were screened for but were <LOD in that study. TP=Tibetan Plateau*

Table S10:: Chemicals identified as potential precursors of perfluoroalkyl acids and relevant properties.

Chemical Family	Hydrofluoroethers (HFEs)	Fluorotelomer Iodides (FTIs)	Fluorotelomer Acrylates (FTAs)		Fluorotelomer Olefins (FTOs)	N-alkyl perfluoroalkane sulfonamidoethanbol (FASE)	N-alkyl perfluoroalkane sulfonamide (FASA)
Manufacturing process	unknown	Telomerization				Electrochemical fluorination (ECF)	
Main precursor chemicals	HFE 7000 HFE 7100 HFE 7200	n:2 FTI	6:2 FTA	8:2 FTA	8:2 FTO	NMeFBSE (C_4) NMeFOSE (C_8)	NMeFBSE (C_4) NMeFOSE (C_8)
Atmospheric lifetime (approx. days)	>157 (Bravo et al., 2010)	5 – 10 (Young et al., 2008)	10 (Butt et al., 2009)		8 (Nakayama et al., 2007)	2 † (D'Eon J et al., 2006)	>20 (D'Eon J et al., 2006)
Use	End-product	Raw material for all FT-based compounds	End-product		Raw material for PFNA	Intermediate/ End-product	Intermediate/ End-product
Measured in urban atmosphere	[not yet assessed]	(Chen et al., 2018) (Ruan et al., 2010)	(Li et al., 2011)	(Li et al., 2011)	(Li et al., 2011)		
Measured in remote atmosphere	[not yet assessed]	[not yet assessed]	Antarctic: (Vento et al., 2012) Southern Ocean: (Dreyer et al., 2009) Arctic: TP: (Wang et al., 2014)*	Antarctic: (Vento et al., 2012)* Southern Ocean: (Dreyer et al., 2009) Arctic: TP: (Wang et al., 2014)*	Antarctic: (Vento et al., 2012)* Arctic: TP: (Wang et al., 2014)	Antarctic: (Vento et al., 2012)* Arctic: Xie TP: (Wang et al., 2014)	Antarctic: (Vento et al., 2012)* Arctic: Xie TP: (Wang et al., 2014)
products	PFCA (C2 – C4)	PFCA (C8 – C11)	PFHxA (C6) / PFHpA (C7)	PFOA (C8) / PFNA (C9)	PFNA (C9)	PFBS (C4) PFOS (C8)	PFBS (C4) PFOS (C8)
Current atmospheric/market trends	Increasing	Increasing	Increasing	Increasing	Increasing	Increasing Decreasing	Increasing Decreasing

*FTIs are produced as chemical intermediates for most FT-based products with carbon chain length up to C_{18}. For many FT-based chemicals, degradation mechanisms often proceed via a perfluoroaldehyde (PFAL) intermediate which can be further oxidised to PFCAs. † Despite FASEs displaying a relatively short atmospheric lifetime (i.e. 2 days) in comparison to other precursors, the main degradation pathway proceeds via FASAs which have an atmospheric lifetime of over 20days. * indicates those chemicals that were screened for but were <LOD in that study. TP=Tibetan Plateau.*

Figure S3. Spearmans rank correlation of PFAAs in snow samples at Kohnen Station (1958 – 2017)

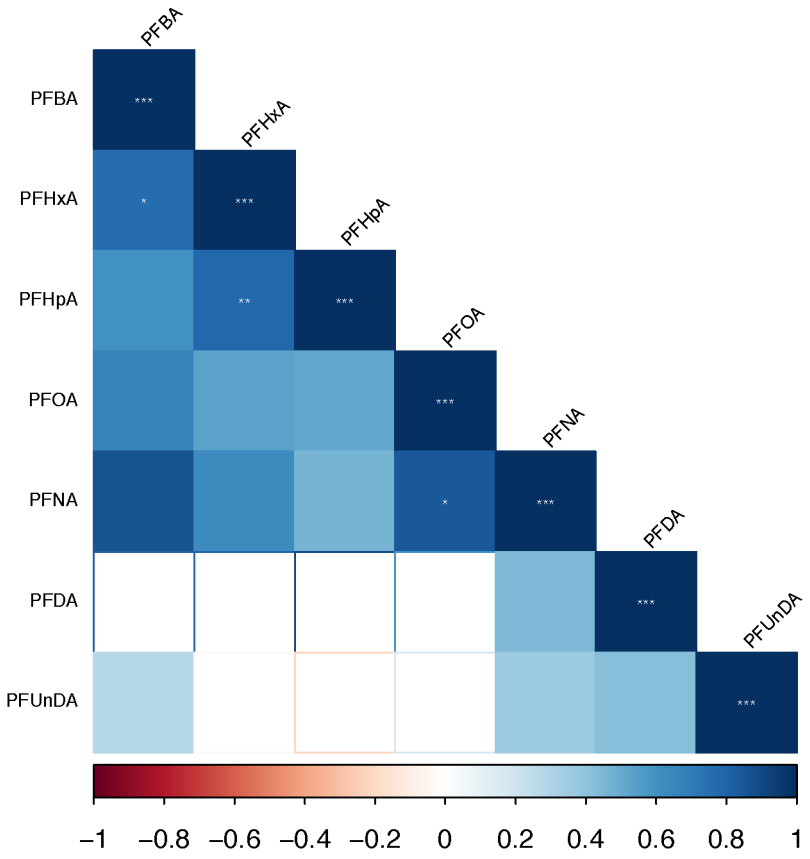

Data analysis was performed on chemical concentration data (pg/L) and only values >MDL were included. Normality was checked using the Shapiro-Wilk test (a = 0.05) and a non-parametric test (Spearmans rank) was applied due to some chemical data not being normal. Only correlations with more than 50% of complete pairwise observations are displayed in correlogram. Asterisk denotes those pairwise observations that are statistically significant (= p<0.05; ** p<0.01; *** p<0.001).*

Table S11: Dispositional flux ratios for PFCAs homologues.

	C4/C5	C6/C7	C8/C9	C10/C11	C12/C13
1958-1963	1.1	1.0	8.7	-	-
1963-1966	0.9	1.4	5.8	-	-
1966-1972	2.0	1.5	2.5	3.1	4.5
1972-1981	1.0	0.9	3.2	0.4	-
1981-1985	2.2	0.8	7.4	2.4	2.7
1985-1990	0.7	1.3	3.7	-	-
1990-1992	1.4	1.0	5.8	0.8	-
1992-1997	1.0	0.6	6.5	1.5	-
1997-1999	1.2	0.4	4.8	-	-
1999-2003	7.3	0.6	5.8	-	-
2003-2006	12.0	0.6	2.8	-	-
2006-2009	52.9	0.7	3.0	3.0	-
2009-2013	76.1	0.6	1.5	2.3	-
2012-2013	37.1	1.0	2.4	-	-
2013-2017	65.9	0.6	1.9	2.9	-
Mean (± 1.s.d.)	18 ± 27	0.9 ± 0.3	4.4 ± 2.2	2.0 ± 1.0	3.6 ± 1.3

Depositional flux ratios for PFCAs were calculated throughout the timeseries. Average values close to one for even/odd (n/n+1) suggest that FTOHs are a significant source. Blank values (-) indicate those samples that had at least one homolog less than detection limits .

Table S12: Estimated total mass of individual perfluoroalkyl acids deposited in Antarctica between 2013 - 2017.

Chemical	Annual deposition flux (kg)
PFBA	8892
PFPeA	135
PFHxA	165
PFHpA	259
PFOA	215
PFNA	112
PFDA	41
PFUnDA	14
PFDoDA	12
PFTrDA	<LOD
PFTeDA	4
PFBS	<LOD
PFHxS	<LOD
PFHpS	<LOD
PFOS	<MDL
PFDS	<LOD

Average concentrations in the most recent snow sample (2013 - 2017) and modelled annual turnover of snow in Antarctica of 2100 Gt (SWE; snow water equivalent) (Rignot et al., 2019) were used to estimate the annual deposition flux (kg) of individual PFAAs deposited across the entire continent of Antarctica in a single year. This provided a basis upon which to determine chemical emissions/production rates and thus propose credible chemical sources. These annual deposition fluxes calculated using this simple method are most likely an underestimate of most PFAAs in Antarctica due to the lower concentrations of PFAAs measured in snow at Kohnen (East Antarctic Plateau) compared with coastal regions (Antarctic Peninsula) (Casal et al., 2019, Casal et al., 2017).

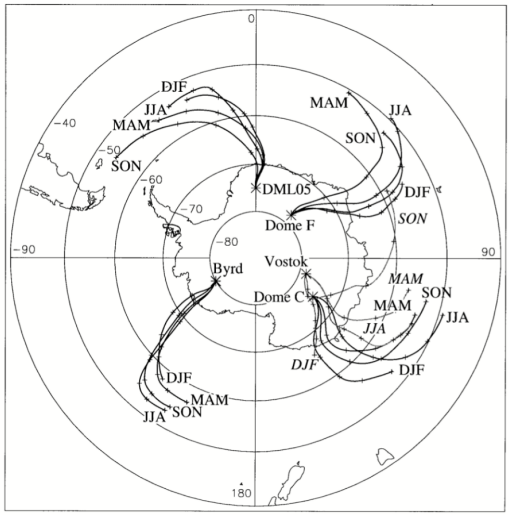

Figure S4: Mean 5-day backward trajectories of air masses arriving in Antarctica. Kohnen Station corresponds to DML05. Different seasons are denoted by DJF (summer), MAM (autumn), JJA (winter), and SON (spring) (Reijmer, Van Den Broeke, & Scheele, 2002)

The direction of wind at Kohnen Station is generally North-Easterly, yet mean 5-day backward trajectories of air masses indicate that Kohnen Station is influenced from all major ocean sectors, predominantly from the South Atlantic Ocean (50 - 60°S) (Reijmer, Van Den Broeke, & Scheele, 2002) (Figure 2). Given that the atmospheric lifetime of many PFAA-precursors significantly exceeds 5 days (τ_{OH} = up to 156 days) and that the annual mean wind speed is approximately 4.6 m s^{-1} (Reijmer C. H., 2001), this provides significant scope for various chemical precursors to be emitted from industrial sources and tranported over 32000km to Kohnen Station, Antarctica.

Table S13: Measured depositional fluxes (ng m^{-2} a^{-1})for PFCAs in remote polar regions in other studies.

Date	Location	Matrix	Range	Reference	PFBA	PFPeA	PFHxA	PFHpA	PFOA	PFNA	PFDA	PFUnDA	PFDoDA	PFTrDA	PFTeDA
1980 - 1999	Mt. Muztagata, Tibet	Snow core	lower	(Wang et al., 2014)	-	20	7	-	15	3	2	2	4	-	-
			upper		-	90	63	-	154	26	32	6	21	-	-
1996 - 2007	Mt. Zuoqiupu, Tibet	Snow core	lower	(Wang et al., 2014)	22	32	6	-	27	18	30	-	-	-	-
			upper		62	46	45	-	188	22	56	-	-	-	-
1996-2008	Colle Gnifetti (Swiss/Italian Alps)	Snow core	lower	(Kirchgeorg et al., 2013)	242	-	-	-	165	86	-	<LOD	-	-	-
			upper		545	-	-	-	218	923	-	223	-	-	-
1990 - 2004	Svalbard	Snow core	lower	(Kwok et al., 2013) rewritten in (Muir et al., 2019)	-	-	50	-	180	100	-	-	-	-	-
			upper		-	-	650	-	1200	600	-	-	-	-	-
1953 - 2008	Lake Oesa, Canada	Sediment core	lower	(Benskin et al., 2011)	-	-	-	-	<1	<1	<1	<1	<1	<1	<1
			upper		-	-	-	-	30	30	<LOD	30	20	30	10
1945 - 2008	Lake Opabin, Canada	Sediment core	lower	(Benskin et al., 2011)	-	-	-	-	<LOD	<LOD	-	-	-	-	-
			upper		-	-	-	-	4	8	-	-	-	-	-
1996-2006	Devon Island ice cap, Canada	Snow core	lower	(Young et al., 2007)	-	-	-	-	21	20	3	3	-	-	-
			upper		-	-	-	-	83	105	9	13	-	-	-
1993 - 2007	Devon Island ice cap, Canada	Snow core	lower	(Macinnis et al., 2017)	15	7	5	10	7	8	2	2	<1	<1	<1
			upper		244	68	60	99	98	220	36	38	4	4	1
1977 - 2015	Devon Island ice cap, Canada	Snow core	lower	(Pickard et al., 2018)	-	<LOD	3	6	6	6	<1	2	< LOD	< LOD	-
			upper		-	37	38	87	81	141	17	29	2	<1	-
1977 - 2015	Devon Island ice cap, Canada	Snow core		(Pickard et al., 2020)		-	-	-	-	-	-	-	-	-	-
						-	-	-	-	-	-	-	-	-	-
1958 - 2017	Kohnen Station, Antarctica (this study)	Snow core	lower	(This study)	2	1	<1	<1	2	<1	<LOD	<LOD	<LOD	<LOD	<LOD
			upper		359	6	7	10	9	5	3	<1	2	<1	<1
2014	Livingston Island, Antarctica	Snow core	mean	(Casal et al., 2017)	-	-	29	67	240	74	102	47	28	6	-
				(Xie et al., 2020)											

Red values were below method detection limits. All values were rounded to nearest whole integer. Some studies did not report fluxes for all PFASs (-) and so were unable to perform an adequate comparison. Some values have been approximated from figures due to missing data from published supplementary information.

Table S14: Measured depositional fluxes (ng m^{-2} a^{-1}) for PFSAs in remote polar regions in other studies.

Date	Location	Matrix	Range	Reference	PFBS	PFHxS	PFHpS	PFOS
1980 - 1999	Mt. Muztagata, Tibet	Snow core	lower	(Wang et al., 2014)	-	-	-	21
			upper		-	-	-	195
1996 - 2007	Mt. Zuoqiupu, Tibet	Snow core	lower	(Wang et al., 2014)	-	-	-	-
			upper		-	-	-	-
1996-2008	Colle Gnifetti (Swiss/Italian Alps)	Snow core	lower	(Kirchgeorg et al., 2013)	-	-	-	-
			upper		-	-	-	-
1990 - 2004	Svalbard	Snow core	lower	(Kwok et al., 2013) rewritten in (Muir et al., 2019)	-	-	-	-
			upper		-	-	-	-
1953 - 2008	Lake Oesa, Canada	Sediment core	lower	(Benskin et al., 2011)	-	-	-	-
			upper		-	-	-	-
1945 - 2008	Lake Opabin, Canada	Sediment core	lower	(Benskin et al., 2011)	-	-	-	-
			upper		-	-	-	-
1996-2006	Devon Island ice cap, Canada	Snow core	lower	(Young et al., 2007)	-	-	-	<1
			upper		-	-	-	<1
1993 - 2007	Devon Island ice cap, Canada	Snow core	lower	(Macinnis et al., 2017)	<1	<1	<1	1
			upper		40	<1	<1	4
1977 - 2015	Devon Island ice cap, Canada	Snow core	lower	(Pickard et al., 2018)	<LOD	-	<LOD	<LOD
			upper		<1	-	2	80
1977 - 2015	Devon Island ice cap, Canada	Snow core		(Pickard et al., 2020)	-	-	-	-
					-	-	-	-
1958 - 2017	Kohnen Station, Antarctica	Snow core	lower	(This study)	<LOD	<LOD	<LOD	<LOD
			upper		<LOD	<LOD	<LOD	3
2014	Livingston Island, Antarctica	Snow core	mean	(Casal et al., 2017)				
				(Xie et al., 2020)				

Equation S1: Average depositional flux of PFASs in snow

$$\text{Average depositional flux (ng m}^{-2}\text{ a}^{-1}) = \left[\frac{\text{Snow density (kg m}^{-3}\text{) x core section length (m) x sample concentration (ng L}^{-1}\text{)}}{\text{accumulation period (a)}}\right] \quad (1)$$

Where 1L = 1kg

Average depositional fluxes were calculated for each PFAA in order to compare to other studies. The snow density was derived from a depth-density profile and used the central cumulative depth of that particular sample.

Equation S2: Error propagation used to assess total uncertainty from laboratory and field sample replicates

$$\text{Total uncertainty (\%)} = \sqrt{\left[\frac{\sigma\ \text{laboratory replicates}}{\bar{x}\ \text{laboratory replicates}}\right]^2 + \left[\frac{\sigma\ \text{Field replicates}}{\bar{x}\ \text{Field replicates}}\right]^2} \quad (2)$$

Where σ = standard deviation

$\overline{x}$ = *mean*

Sample variability in PFASs concentrations originates from laboratory analysis and small-scale variations in snow concentrations in the field. Due to the limited number of laboratory (n=2) and field (n=2) replicates, a conservative approach to assess the total uncertainty associated with each PFAA was adopted using the above formula.

References

AMAP 2016. AMAP Assessment 2015: Temporal Trends in Persistent Organic Pollutants in the Arctic. vi ed. Oslo, Norway.

BENSKIN, J. P., PHILLIPS, V., ST. LOUIS, V. L. & MARTIN, J. W. 2011. Source Elucidation of Perfluorinated Carboxylic Acids in Remote Alpine Lake Sediment Cores. *Environmental Science & Technology,* 45**,** 7188-7194.

BRAVO, I., DÍAZ-DE-MERA, Y., ARANDA, A., SMITH, K., SHINE, K. P. & MARSTON, G. 2010. Atmospheric chemistry of C4F9OC2H5 (HFE-7200), C4F9OCH3 (HFE-7100), C3F7OCH3 (HFE-7000) and C3F7CH2OH: temperature dependence of the kinetics of their reactions with OH radicals, atmospheric lifetimes and global warming potentials. *Phys Chem Chem Phys,* 12**,** 5115-5125.

BUTT, C. M., YOUNG, C. J., MABURY, S. A., HURLEY, M. D. & WALLINGTON, T. 2009. Atmospheric Chemistry of 4:2 Fluorotelomer Acrylate [C4F9CH2CH2OC(O)CH=CH2]: Kinetics, Mechanisms, and Products of Chlorine-Atom- and OH-Radical-Initiated Oxidation. *J. Phys. Chem. A,* 113**,** 3155-3161.

CASAL, P., CASAS, G., VILA-COSTA, M., CABRERIZO, A., PIZARRO, M., JIMÉNEZ, B. & DACHS, J. 2019. Snow Amplification of Persistent Organic Pollutants at Coastal Antarctica. *Environmental Science & Technology,* 53**,** 8872-8882.

CASAL, P., ZHANG, Y., MARTIN, J. W., PIZARRO, M., JIMÉNEZ, B. & DACHS, J. 2017. Role of Snow Deposition of Perfluoroalkylated Substances at Coastal Livingston Island (Maritime Antarctica). *Environmental science & technology,* 51**,** 8460.

CHEN, H., YAO, Y., ZHAO, Z., WANG, Y., WANG, Q., REN, C., WANG, B., SUN, H., ALDER, A. C. & KANNAN, K. 2018. Multimedia Distribution and Transfer of Per- and Polyfluoroalkyl Substances (PFASs) Surrounding Two Fluorochemical Manufacturing Facilities in Fuxin, China. *Environmental Science & Technology,* 52**,** 8263-8271.

D'EON J, C., HURLEY, M. D., WALLINGTON, T. J. & MABURY, S. A. 2006. Atmospheric chemistry of N-methyl perfluorobutane sulfonamidoethanol, C4F9SO2N(CH3)CH2CH2OH: kinetics and mechanism of reaction with OH. *Environ Sci Technol,* 40**,** 1862-8.

DREYER, A., WEINBERG, I., TEMME, C. & EBINGHAUS, R. 2009. Polyfluorinated compounds in the atmosphere of the Atlantic and Southern Oceans: evidence for a global distribution. *Environmental science & technology,* 43**,** 6507.

ELLIS, D., MARTIN, J. W., DE SILVA, A., MABURY, S. A., HURLEY, M. D., ANDERSEN, M. P. S. & WALLINGTON, T. 2004. Degradation of

fluorotelomer alcohols: A likely atmospheric source of perfluorinated carboxylic acids. *Environ. Sci. Technol.,* 38**,** 3316-3321.

KIRCHGEORG, T., DREYER, A., GABRIELI, J., KEHRWALD, N., SIGL, M., SCHWIKOWSKI, M., BOUTRON, C., GAMBARO, A., BARBANTE, C. & EBINGHAUS, R. 2013. Temporal variations of perfluoroalkyl substances and polybrominated diphenyl ethers in alpine snow. *Environ Pollut,* 178**,** 367-374.

KWOK, K. Y., YAMAZAKI, E., YAMASHITA, N., TANIYASU, S., MURPHY, M. B., HORII, Y., PETRICK, G., KALLERBORN, R., KANNAN, K., MURANO, K. & LAM, P. K. 2013. Transport of perfluoroalkyl substances (PFAS) from an arctic glacier to downstream locations: implications for sources. *Sci Total Environ,* 447**,** 46-55.

LI, J., DEL VENTO, S., SCHUSTER, J., ZHANG, G., CHAKRABORTY, P., KOBARA, Y. & JONES, K. C. 2011. Perfluorinated Compounds in the Asian Atmosphere. *Environ. Sci. Technol,* 45**,** 7241-7248.

MACINNIS, J. J., FRENCH, K., MUIR, D. C. G., SPENCER, C., CRISCITIELLO, A., DE SILVA, A. O. & YOUNG, C. J. 2017. Emerging investigator series: a 14-year depositional ice record of perfluoroalkyl substances in the High Arctic. *Environ. Sci.: Processes Impacts,* 19**,** 22-30.

MUIR, D., BOSSI, R., CARLSSON, P., EVANS, M., DE SILVA, A., HALSALL, C., RAUERT, C., HERZKE, D., HUNG, H., LETCHER, R., RIGÉT, F. & ROOS, A. 2019. Levels and trends of poly- and perfluoroalkyl substances in the Arctic environment – An update. *Emerging Contaminants,* 5**,** 240-271.

NAKAYAMA, T., TAKAHASHI, K., MATSUMI, Y., TOFT, A., SULBAEK ANDERSEN, M. P., NIELSEN, O. J., WATERLAND, R. L., BUCK, R. C., HURLEY, M. D. & WALLINGTON, T. J. 2007. Atmospheric chemistry of CF 3 CH=CH 2 and C 4 F 9 CH=CH 2 : Products of the gas-phase reactions with Cl atoms and OH radicals. *Journal of Physical Chemistry A,* 111**,** 909-915.

OERTER, H., GRAF, W., WILHELMS, F., MINIKIN, A. & MILLER, H. 1999. Accumulation studies on Amundsenisen, Dronning Maud Land, Antarctica, by means of tritium, dielectric profiling and stable-isotope measurements: first results from the 1995–96 and 1996–97 field seasons. *Annals of Glaciology,* 29**,** 1-9.

PICKARD, H. M., CRISCITIELLO, A. S., PERSAUD, D., SPENCER, C., MUIR, D. C. G., LEHNHERR, I., SHARP, M. J., DE SILVA, A. O. & YOUNG, C. J. 2020. Ice Core Record of Persistent Short-Chain Fluorinated Alkyl Acids: Evidence of the Impact From Global Environmental Regulations. *Geophysical Research Letters,* 47**,** e2020GL087535.

PICKARD, H. M., CRISCITIELLO, A. S., SPENCER, C., SHARP, M. J., MUIR, D. C. G., DE SILVA, A. O. & YOUNG, C. J. 2018. Continuous non-marine inputs of per- and polyfluoroalkyl substances to the High Arctic: a multi-decadal temporal record. *Atmos. Chem. Phys.,* 18**,** 5045-5058.

PIEKARZ, A. M., PRIMBS, T., FIELD, J. A., BAROFSKY, D. F. & SIMONICH, S. 2007. Semivolatile fluorinated organic compounds in Asian and western U.S. air masses. *Environmental science & technology,* 41**,** 8248.

RIGNOT, E., MOUGINOT, J., SCHEUCHL, B., VAN DEN BROEKE, M., VAN WESSEM, M. J. & MORLIGHEM, M. 2019. Four decades of Antarctic Ice Sheet mass balance from 1979–2017. *Proceedings of the National Academy of Sciences,* 116**,** 1095.

RUAN, T., WANG, Y., WANG, T., ZHANG, Q., DING, L., LIU, J., WANG, C., QU, G. & JIANG, G. 2010. Presence and Partitioning Behavior of Polyfluorinated Iodine Alkanes in Environmental Matrices around a Fluorochemical Manufacturing Plant: Another Possible Source for Perfluorinated Carboxylic Acids? *Environmental Science & Technology,* 44**,** 5755-5761.

VENTO, S. D., HALSALL, C., GIOIA, R., JONES, K. & DACHS, J. 2012. Volatile per- and polyfluoroalkyl compounds in the remote atmosphere of the western Antarctic Peninsula: an indirect source of perfluoroalkyl acids to Antarctic waters? *Atmospheric Pollution Research,* 3**,** 450-455.

WANG, X., HALSALL, C., CODLING, G., XIE, Z., XU, B., ZHAO, Z., XUE, Y., EBINGHAUS, R. & JONES, K. C. 2014. Accumulation of perfluoroalkyl compounds in tibetan mountain snow: temporal patterns from 1980 to 2010. *Environ Sci Technol,* 48**,** 173-81.

WANG, X., SCHUSTER, J., JONES, K. C. & GONG, P.

XIE, Z., WANG, Z., MAGAND, O., THOLLOT, A., EBINGHAUS, R., MI, W. & DOMMERGUE, A. 2020. Occurrence of legacy and emerging organic contaminants in snow at Dome C in the Antarctic. *The Science of the total environment,* 741.

YOUNG, C. J., FURDUI, V. I., FRANKLIN, J., KOERNER, R. M., MUIR, D. C. G. & MABURY, S. A. 2007. Perfluorinated Acids in Arctic Snow: New Evidence for Atmospheric Formation. *Environmental Science & Technology,* 41**,** 3455-3461.

YOUNG, C. J., HURLEY, M. D., WALLINGTON, T. & MABURY, S. A. 2008. Atmospheric Chemistry of 4:2 Fluorotelomer Iodide (n-C4F9CH2CH2I): Kinetics and Products of Photolysis and Reaction with OH Radicals and Cl Atoms. *J. Phys. Chem. A,* 112**,** 13542-13548.

Chapter 3

Mechanistic insight into the uptake and fate of persistent organic pollutants in sea ice

This chapter presents results from a series of laboratory-based experiments that were conducted in a state-of-the-art sea ice facility that was built to understand biogeochemical processes in the polar regions. The data furthers our understanding of the fundamental mechanisms that govern the uptake behaviour of POPs into artificial sea ice during its formation and melt.

This chapter was published in the journal Environmental Science and Technology in 2019 as a research article in volume 53.

The candidate's contribution was designing and conducting the experimental plans; structuring own and co-authors' ideas as a manuscript; writing the manuscript for supervisor review; co-ordinating co-author feedback; submission of manuscript.

Candidate: ..... J.garnett. *.....Date:.....22-Jul-21.....*

Mr Jack R. Garnett

Supervisor: .....

.....Date:...26-Jul-21.....

Prof. Crispin J. Halsall.

Mechanistic insight into the uptake and fate of persistent organic pollutants in sea ice

Jack Garnett[1], Crispin Halsall[1*], Max Thomas[2], James France[2,3,4],
Jan Kaiser[2], Carola Graf[1], Amber Leeson[1], Peter Wynn[1]

1 Lancaster Environment Centre, Lancaster University, Lancaster, LA1 4YQ, UK

2 Centre for Ocean and Atmospheric Sciences, School of Environmental Sciences, University of East Anglia, Norwich Research Park, Norwich, NR4 7TJ, UK

3 British Antarctic Survey, High Cross, Madingley Road, Cambridge, CB3 0ET

4 Department of Earth Sciences, Royal Holloway, University of London, Egham Hill, Egham TW20 0EX, UK

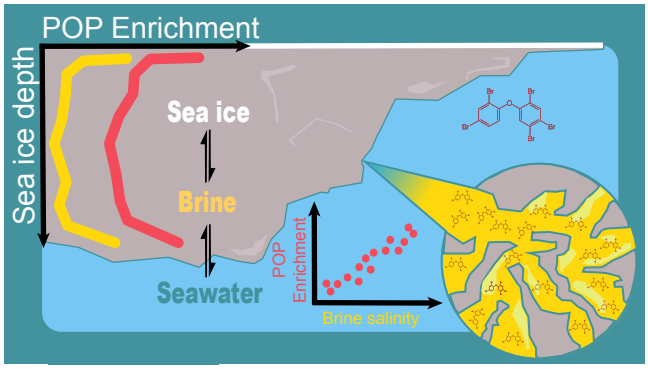

Abstract

The fate of persistent organic pollutants in sea ice is a poorly researched area and yet ice serves as an important habitat for organisms at the base of the marine foodweb. This study presents laboratory-controlled experiments to investigate the mechanisms governing the fate of organic contaminants in sea ice grown from artificial seawater. Sea ice formation was shown to result in the entrainment of chemicals from seawater, and concentration profiles in bulk ice generally showed the highest levels in both the upper (ice-atmosphere interface) and lower (ice-ocean interface) ice layers, suggesting their incorporation and distribution is influenced by brine advection. Results from a 1-D sea ice brine dynamics model supported this, but also indicated that other processes may be needed to accurately model low-polarity compounds in sea ice. This was reinforced by results from a melt experiment, which not only showed chemicals were more enriched in saltier brine, but also revealed that chemicals are released from sea ice at variable rates. We use our results to demonstrate the importance of processes related to the occurrence and movement of brine for controlling chemical fate in sea ice which provides a pathway for exposure to ice-associated biota at the base of the pelagic food web.

1. Introduction

Persistent organic pollutants (POPs) comprise a large group of mainly synthetic, toxic chemicals that have long environmental half-lives and are subject to long-range transport by global atmospheric and oceanic circulation currents [1] . As such, these chemicals are present in the marine environment of polar regions and have been shown to bioaccumulate and biomagnify in Arctic food webs [2, 3] The role of snow and sea ice in the fate and transfer of both older 'legacy' and contemporary 'emerging' chemicals to biological systems has not been well studied despite their occurrence in Arctic seawater. There are now a number of observational studies that have reported relatively high POP concentrations in the remote sea ice snow pack [4-6] and their presence in sea ice itself [7-10].

A warming climate is resulting in substantial changes to the volume and properties of sea ice [11]. There is a strong declining trend in the areal extent of Arctic sea ice cover, which currently ranges between 4 and 16 million km^2 over the annual seasonal cycle [12]. Furthermore, the nature of sea ice is also changing, with the Arctic Ocean now dominated by first-year sea ice (FYI) [13]. As sea ice forms, most of the salts present in the freezing sea water are rejected into the underlying ocean, leaving only small amount entrapped within a network of highly saline brine pockets. As ice continues to grow, more salts are expelled and seasonal meltwater at the surface often 'flushes' the sea ice, reducing its bulk salinity further. Multi-year sea ice (MYI) therefore has a lower bulk salinity and a lower salt flux to the ocean during melt [14] Compared to older MYI, young ice contains more brine per unit volume, and this appears to influence the behaviour and fate of organic micro-pollutants present in the sea ice system [8]. Importantly, many organisms situated at the base of the pelagic food web are abundant in sea ice and inhabit the network of brine inclusions. As the Arctic environment is rapidly changing, there is a rising motivation to understand the biogeochemical cycling of these toxic chemicals in sea ice.

Whilst the presence of POPs such as polychlorinated biphenyls (PCBs) has been established in sea ice [7] most of the recent knowledge on chemical behaviour in sea ice and interactions with seawater and the overlying snowpack has been established through the field observations of Pućko et al., [5, 6, 8, 9, 15, 16] who examined the α- and γ-isomers of hexachlorocyclohexane (HCH) in FYI in the Amundsen Gulf of the Canadian Arctic. The key findings from these studies

showed sea ice to have some of the highest concentrations of HCHs measured anywhere in the Arctic. The majority of the HCHs were present in brine, and brine advection influenced the transfer of HCHs between the sea ice, overlying snowpack and underlying seawater.

The aim of this study was to better understand the basic mechanisms governing the uptake and release of organic pollutants in growing and melting sea ice, repectively. We hypothesize that chemical uptake and distribution is strongly influenced by the formation of brine during sea ice growth and melt. To test this, we performed sea ice growth experiments under controlled laboratory conditions where an artificial 'ocean' was spiked with several persistent organic pollutants. To assess the role of brine in determining their fate, we measured vertical profiles of pollutant concentrations through bulk sea ice samples and made comparisons to predictions from a sea ice brine dynamics model during sea ice formation. We also conducted an experiment to extract brine and assess its composition to examine how organic chemicals are released from sea ice during melt.

2. Materials and methods

2.1. Experimental facility and conditions

The study was conducted in the Roland von Glasow Air-Sea-Ice Chamber (RvG-ASIC) at the University of East Anglia, UK. In essence, the facility consists of a glass-walled tank (approximately 3.5m^3; height: 1.2m; width 1.2m; length 2.5m) located inside an enclosed chamber that can be chilled to –55ºC (see https://www.uea.ac.uk/environmental-sciences/sea-ice-chamber). The tank was filled with artificial sea water (de-ionised water with NaCl – (AksoNobel Sanal-P; purity > 99.5%)). A submerged pump (flow rate: 1000 L h^{-1}) was used to mix the seawater (SW; we refer to it as seawater even though it only contains NaCl). The tank was equipped with an *in-situ* conductivity-temperature sensor (SeaStar DST CTD) along with a series of automated *in-situ* thermistors spanning the depth of the ice profile to measure the ice temperature throughout the experimental periods. Table 1 presents an overview of the experimental conditions for two freeze periods (1 & 2). For the main experiment (Freeze - 1), the air temperature of the chamber was chilled to –35 ºC for 3 days resulting in rapid ice growth and the formation of an ice layer 17±1 cm in depth (uncertainty reflects ice thickness variations across the tank). The ice was subsequently sampled to establish the presence of

chemicals in the ice and their distribution throughout the ice column. After the ice had completely melted, 'Freeze - 2' was undertaken with the air temperature set to -18°C but for a longer duration (7 days) resulting in slower ice growth but with a thicker final ice layer 26±1 cm. The ice sampled during 'Freeze - 2' was also subject to an additional slow-melt experiment to assess chemical behaviour during melt (see Section 2.4.).

Table 5. Experimental conditions and sea ice physical properties for two freeze experiments. Sea ice samples used to assess chemical release in the slow-melt experiment were taken from Freeze - 2 (see section 2.4).

	Freeze - 1	Freeze - 2
Initial NaCl concentration (g L^{-1})	35.4 ± 0.1	35.4 ± 0.1
Air temperature during freezing phase (°C)	-35	-18
Air temperature during melting phase (°C)	5	0
Maximum sea ice depth (cm)	17 ± 1	26 ± 1
Freezing duration (days)	3	7
Coldest recorded temperature in ice (°C)	-13.8	-11.3
Maximum modelled brine salinity (g L^{-1})	178.2*	154.8*
Average ice growth rate (cm d^{-1})	5.7	3.7
Melting phase (days)	6	3

* Derived using the recorded minimum temperature in the sea ice using Equation S1 [17].

An array of chemicals that have been previously observed in the Arctic marine system (see Table 2) and that cover a wide range of physical-chemical properties (Table S1) were spiked into the tank using a stock solution (0.2 to 1.4 μM in 1 L ethanol) to give concentrations between 0.1 and 0.4 nM (Table S2). This was undertaken once the temperature of the seawater had cooled to -1°C to ensure minimal loss of chemicals by volatilisation. The chemical concentrations were up to two orders of magnitude below the estimated aqueous solubilities in seawater (see Table S1), but also up to two orders of magnitude greater than those typically observed in Arctic seawater. The freeze experiments conducted in the facility were performed in darkness to limit the growth of algae and reduce any photochemical loss of the compounds.

2.2. Sampling procedures

Prior to the introduction of chemicals into the chilled seawater, a short period (2 days) of ice growth at –35 ºC permitted samples of seawater (*SW*) (0.2 L; $n = 3$) and bulk ice (*BI*) (3.5 L; $n = 1$) to be collected for the purpose of method blanks. After the ice had melted, the chemical stock spike solution was added and mixed under pumping. A seawater sample (0.2 L, $n = 1$) was taken daily, and triplicate samples (0.2 L; $n = 3$) were obtained on three key days of Freeze - 1 (start: day 1 (before any ice formation); middle: day 4 (once maximum ice had formed);, end: day 11 (after complete ice melt)) to assess analytical precision. Seawater was taken via a pre-installed silicone hose (I.D. 8 mm) with an inlet set at 0.5 m above the base of the tank to avoid interference with any forming ice layer. Bulk ice samples ($n = 2$) were taken once the ice had reached a suitable handling depth using techniques developed by Cottier et al., [18] to limit brine loss and displacement during sampling. Following sampling, ice samples were immediately wrapped in pre-cleaned polyethylene (PE) sheets and transferred to a freezer (–40 ºC) where they were stored prior to further processing. Bulk ice samples were subsequently sectioned into horizontal layers (0.4 to 1.2 L each; $n = 9$) using a grease-free electric band saw in a cold room (–25 ºC), transferred to individual PE bags and melted at room temperature. Frost Flowers (0.2 L; $n = 1$) present on the surface of the ice were carefully collected using a polyethylene spatula and stored in a freezer before melting for analysis.

2.3. Sample processing and analysis

Salinity was measured in melted sea ice samples, 'slow-melt' aliquots, and melted frost flowers using a calibrated conductivity probe (Hach HQd40 logger with CDC401 probe) after 50 L of surrogate standard (^{13}C)PCB-28, (^{13}C)PCB-52, (^{13}C)PCB-180 at 60 pg µL^{-1} in ethanol) was added to each solution. Samples were then subject to solid phase extraction (SPE) using a 12-port vacuum manifold system. Briefly, SPE cartridges (30 mg of 3 cc OASIS HLB) were conditioned using 5 mL of methanol followed by 5 mL of chemical-free purified water (MilliQ; >18 MΩ cm) and then loaded with sample at a rate of 1 to 2 drops per second. Subsequently, the cartridges were centrifuged for 5 minutes at 2000 rpm and later air-dried for a further 40 minutes whilst fitted with an additional cartridge as a precaution against airborne

contamination. Cartridges were then soaked with 3 mL of hexane:dichloromethane (1:1) for 5 minutes and eluted with a further 3 mL of this solvent mix. Each sample extract was then subject to a clean-up procedure involving elution through an alumina/silica column followed by gel permeation chromatography (GPC). Samples were then transferred to amber GC vials containing 50 µL of recovery standard (IS) ([^{13}C]PCB-141 [25 pg µL^{-1}] and BDE-69 [75 pg µL^{-1}]) in *n*-dodecane was then added before being reduced under N_2 to a final volume of 50 µL.

Analysis of extracts was performed using a Thermo GC-MS (Trace GC Ultra - DSQ) (Xcalibur software Version 1.4.x) operating in electron impact mode (70 eV) and equipped with an Agilent CP-Sil 8 CB 50 m x 0.25 mm capillary column with 0.12 µm film thickness. A 10-point mixed calibration standard in *n*-dodecane was used for quantification (10 to 450 pg µL^{-1} for OCPs, 10 to 120 pg µL^{-1} for PCBs and 10 to 1250 pg µL^{-1} for PBDEs, respectively). Chemical concentrations presented in this study were corrected for recovery, but not blank corrected. Method detection limits (MDL) were calculated from method blanks (MDL = $\overline{x}_{\text{method blank}} \pm 3 \cdot SD_{\text{method blank}}$) (see Table S3).

2.4. Slow-melt experiment

Following Freeze 2, a separate experiment was conducted (outside of the glass tank but within the coldroom) to examine the release of chemicals from ice during thaw, and to determine how strongly associated each chemical was with brine. Sea ice cores (n = 8) were sampled from across the ice slab using a pre-cleaned titanium manual corer (75 mm I.D.). These were individually split into top (T) and bottom (B) sections of approximately equal length, with each section placed into a separate pre-cleaned PE bag, which were subsequently kept at 0±1 ºC to induce melt, as described by Pućko, et al., [8] and others [19-22]. Sequential meltwater (MW) fractions (0.1 to 1.2 L; n = 8) were collected from the respective top and bottom sections and analysed separately (Table S4).

2.5. Calculations and data analysis

Enrichment factors (*EF*) were calculated using Equation 1 to assess the accumulation of chemicals in a particular compartment, relative to seawater. The average chemical concentration of all seawater samples over the experimental period was used for the

denominator for each chemical (SW; day 1 to day 11). The brine (BR) assessed in this study was operationally defined using the average of the first meltwater (MW) fraction from both the top and bottom ice sections (MW_{F1T} & MW_{F1B}; $n = 2$) and FF is a frost flower sample (taken in Freeze 1). Hence, EF values >1 and <1 indicate specific enrichment or depletion, relative to seawater, respectively.

$$EF = \frac{[\text{chemical}]_{\,e.g.\ bulk\ ice\ (BI);\ brine(BR);\ frost\ flower(FF);\ meltwater(MW);}}{[\text{chemical}]_{\,seawater\ (SW)}} \quad (1)$$

Sea ice depths were normalised to the total sea ice thickness in that experiment (i.e. in Freeze - 1 & 2) to aid comparison between modelled and measured data. A mass-balance calculation was used to assess chemical loss from the system (e.g. volatilisation and/or chamber-side sorption) and evaluate the fraction of chemical present in the various compartments i.e. seawater, bulk ice and brine (at maximum ice depth). Average sea ice concentrations were used to calculate the mass fraction of chemical in the bulk ice, with respect to the total measured mass in the seawater at day 1. The relative standard deviation (RSD) of triplicate seawater samples were used to calculate conservative estimates of the variability of some samples (e.g. frost flowers) (see Table S3). For more information on calculations and data analysis, refer to Equations S1 - S5).

2.6. Brine dynamics model

A 1-dimensional sea ice growth and desalination model was used to predict brine dynamics in a forming sea-ice layer, using the gravity drainage parameterisation presented by [17]. The model is presented in detail in Thomas, et al., [23, 24] where it is has been shown to have predictive capability for the dynamics of brine in sea ice. The brine dynamics parameterization has also been evaluated previously [17]. The model was initialised by prescribing an initial seawater salinity, concentration of a dissolved solute in seawater (e.g. an organic chemical), sea ice thickness, and ocean mass. For this study, the initial salinity and chemical concentrations were taken from the measured values in the seawater at the beginning of the experiment (i.e. day 1). The model was run with ± 2 s.d. of the initial starting conditions, based on the precision of the measurements of the chemical concentrations in the seawater. The initial sea ice

thickness was set to 1cm, and the bulk sea ice salinity and chemical concentrations were set to initial ocean concentrations for all model sea ice layers. The model was forced using measured sea ice temperature profiles, and sea ice thicknesses calculated by extrapolating those profiles back to the measured seawater temperature. In this case, measurements were used instead of a thermodynamic model to minimise errors. Full details including the key equations governing brine salinity (derived using the ice temperature), and how the model simulates brine dynamics (gravity drainage) are presented in the SI.

3. Results and Discussion

3.1. Quality controls & mass-balance

Average recoveries of the surrogate standards were 42 ± 17 % and did not vary significantly between sample type (Table S3). Some blanks contained low levels of several target analytes (e.g. α-HCH γ-HCH, PCB-28, PCB-52) thereby increasing the method detection limits (MDLs) for these compounds. The relative standard deviation (RSD) of triplicate seawater analyses demonstrated precisions of 8 to 40% between all test compounds (see Table S3). Table 2 shows the relative distribution of chemicals in the various compartments of the experimental system on selected days. By day 11, all of the ice had melted and a comparison of the relative mass in the seawater on the initial (day 1) and final (day 11) days of the experiments showed that there was no significant difference ($p > 0.05$; student t-test) for any of the chemicals, indicating negligible losses during the experimental period. Hence, all of the chemicals in the system can be accounted for and are not subject to an artefact of the experimental set-up.

Table 2. Chemical mass (± 1.s.d) apportionment for the experimental compartments on day 1, day 4 and day 11 of Freeze - 1.

Experimental day	Start (day 1)	Middle (day 4)			End (day 11)
Compartment	Seawater	Seawater	Bulk ice	Frost flowers	Seawater
Volume fraction of compartment	100 ± <1	83 ± <1	17 ± <1	<<1%	100 ± <1
NaCl ($\%_{mass}$)	100 ± <1	93 ± <1	7 ± <1	<<1%	100 ± <1
α-HCH ($\%_{mass}$)	100 ± 15	96 ± 18	4 ± 1	<<1%	97 ± 14
γ-HCH ($\%_{mass}$)	100 ± 22	97 ± 34	3 ± 1	<<1%	83 ± 2
PCB-28 ($\%_{mass}$)	100 ± 18	93 ± 10	7 ± 1	<<1%	116 ± 17
PCB-52 ($\%_{mass}$)	100 ± 12	96 ± 14	4 ± 1	<<1%	108 ± 11
Chlorpyrifos ($\%_{mass}$)	100 ± 29	96 ± 32	4 ± 1	<<1%	156 ± 42
BDE-47 ($\%_{mass}$)	100 ± 16	94 ± 64	6 ± 2	<<1%	114 ± 32
BDE-99 ($\%_{mass}$)	100 ± 17	91 ± 48	9 ± 3	<<1%	80 ± 5

Under natural conditions, the transfer of chemicals and salts (e.g. NaCl) can also occur through other pathways such as snow scavenging of airborne pollution and the deposition of sea salt aerosol which serve as an additional source to the sea ice system [4, 5, 15]. However, in this study, airborne sources were negligible (demonstrated by clean blanks). Hence, chemicals present in our experimental sea ice are shown to have originated from the seawater. The results shown in Table 2 from Freeze -1 also show that only a small fraction (3 to 9 %) of the total initial mass of chemicals present in the seawater was entrapped within sea ice during its formation, akin to salt (7%).

3.2. Entrainment of POPs in sea ice.

A time-series for the concentration of NaCl and chemicals in seawater throughout the experiment (day 1 – day 11) can be seen in Figure S1. During the period of sea ice formation (day 1 – day 4) an increase in sea ice thickness and decrease in seawater volume was accompanied by solute rejection from the sea ice, and an increase in the underlying NaCl concentration (from around 35 to 39 g L^{-1}). Given the experimental precision of the

measurements made for the organic chemicals seawater (8 to 40 %), it was not possible to establish whether they followed a similar trend to the salt. However, the measured concentrations of salt and all chemicals were markedly lower in bulk ice than seawater, as indicated by the Enrichment Factors ($EF_{BI\text{-}SW} < 1$) presented in Table 3. This finding suggests that organic chemicals are rejected from sea ice throughout ice growth. Interestingly, $EF_{BI\text{-}SW\ [NaCl]} > EF_{BI\text{-}SW\ [POPs]}$ which may indicate preferential rejection of organic chemicals during sea-ice growth.

Despite the low chemical concentrations present in bulk ice, results presented in Table 3 show that $EF_{BR\text{-}SW} > EF_{BI\text{-}SW}$ ($p<0.05$; student t-test), indicating that the chemicals are more strongly associated with the brine fraction and are entrained within the complex network of brine inclusions which extends throughout the ice [25]. Pućko et al., [8] quoted the mean depth-averaged salinity of bulk ice to be 11.6g L^{-1} which gave $EF_{BI\text{-}SW} = 0.4$ for NaCl. Similarly, values for $EF_{BI\text{-}SW}$ were obtained for α-HCH and γ-HCH at 0.4 and 0.5, respectively. The resemblance between this calculated index for NaCl and the two HCH isomers suggests that the levels of HCH in FYI are probably governed by processes that function to conservatively distribute brine in sea ice. In our study, $EF_{BI\text{-}SW}$ of NaCl resulted in a value of 0.4, although there is a larger range (0.1 – 0.4) between the index for all of the chemicals presented in our study. Natural sea ice is a highly complex medium with marked heterogeneity in physical features over relatively narrow spatial scales (i.e. cms). The chamber ice is markedly younger and thinner than the mid/late-winter Arctic sea ice measured in the field studies above, but the ice formation processes and physical features such as brine channels and frost flowers etc are similar [23]. Some of the differences between our enrichment factors and previous field studies could be due to different temperature and sea-ice growth regimes. However, the higher brine salinity concentrations observed in the Arctic sea ice could have affected organic chemical occurrence and distribution, and is likely to account for differences between the field studies and the chamber ice of this study.

Table 3: Enrichment factors (±1.s.d) for NaCl and chemical contaminants in the different sea ice system compartments. BI=bulk ice; BR=brine; SW=seawater; FF=frost flower; L1= uppermost sea ice layer sampled.

Enrichment Factor	Bulk ice depth(cm)	NaCl	α-HCH	γ-HCH	PCB-28	PCB-52	Chlorpyrifos	BDE-47	BDE-99	Reference
EF_{BI-SW}	17 ± 1	0.4 ± <0.1	0.1 ± <0.1	0.1 ± 0.1	0.2 ± 0.1	0.2 ± <0.1	0.2 ± 0.1	0.1 ± 0.1	0.4 ± 0.2	Freeze -1
EF_{BI-SW}	26 ± 1	0.3 ± <0.1	0.2 ± 0.1	0.3 ± 0.2	0.2 ± 0.1	0.1 ± <0.1	0.3 ± 0.2	0.2 ± 0.1	0.4 ± 0.2	Freeze - 2
EF_{BI-SW}	30	0.4	0.4	0.5	n/m					[8]
EF_{BI-SW}	90	0.2	0.3	0.3	n/m					[9]
EF_{BI-SW}	5	0.3	0.3	0.4	n/m					[9]
EF_{BR-SW}	26 ± 1	1.4 ± <0.1	0.6 ± 0.2	1.0 ± 0.8	1.3 ± 0.5	1.2 ± 0.3	1.2 ± 0.7	0.7 ± 0.5	0.9 ± 0.6	Freeze - 2
EF_{BR-SW}	90	4.4	3.9	4	n/m					[8]
EF_{FF-SW}	n/a	2.3 ± <0.1	0.2 ± 0.1	0.2 ± 0.2	0.2 ± 0.1	0.4 ± 0.1	0.3 ± 0.2	6.6 ± 4.4	24 ± 15	Freeze - 1
EF_{FF-SW}	n/a	< 2.0	0.7	2.1	0.0 – 38.9 [Δ]					[10]
EF_{FF-L1}	n/a	5.0 ± <0.1	1.5 ± 0.5	2.0 ± 1.5	2.5 ± 0.9	3.0 ± 0.7	2.4 ± 1.4	30 ± 20	50 ± 31	Freeze - 1
EF_{FF-L1}	n/a	< 0.7	1.7 – 68.0 [Δ]							[10]

n/a=not applicable; n/m=not measured; Δ=different organic chemical used other than that analysed in this study. See Table S5 for values that were used in this literature analysis.

Brine salinity is set by the appropriate *liquidus* relationship [26] and is usually at its respective freezing-point. Changes in the local thermal conditions will cause a corresponding phase-change following this temperature-salinity relationship. Brine salinity measured in Pućko et al.,[8] and in this study was 128 g L^{-1} and 58 g L^{-1}, respectively. Hence, the brine collected in our study was much less concentrated and this is likely to be attributed to differences in sea ice properties (given the age and thickness of the chamber ice) as well as the brine sampling techniques which limited our ability to obtain enough brine for analysis with a salinity >58 g L^{-1}. These factors most likely contribute to the slightly lower *EF*s measured in this study compared to those calculated from Arctic sea ice [8, 9]. Furthermore, additional pollution sources such as the transfer of chemicals from the overlying snowpack into sea ice and the incorporation of other seawater constituents such as organic matter (dissolved and particulate) may also affect the quantity and distribution of POPs in natural sea ice.

3.3. Distribution of chemicals within sea ice

Figure 1 shows the vertical distribution of salt and chemicals in our chamber-grown sea ice. Data were plotted on a log-scale to show all chemicals and account for their wide range in concentrations. A 'c-shape' profile for bulk salinity (Panel A) is typical for first-year sea ice, whereby elevated concentrations exist at the ice-atmosphere and ice-ocean interfaces. The processes governing the distribution of NaCl in sea ice have been reviewed by Notz and Worster [14]. Due to the crystal structure and the close-packing arrangement of water molecules in ice, there is limited inclusion of solutes (e.g. dissolved ions, particulates etc) within the ice itself [25], but are retained within liquid inclusions between the ice lamellae. Due to surface cooling, brine at the surface of sea ice is colder, more saline, and denser than that below, driving convection currents and facilitating the downward movement of salt-rich brine. This process is better known as gravity drainage and is believed to be the predominant mechanism controlling the removal of salts from the bulk sea ice [14].

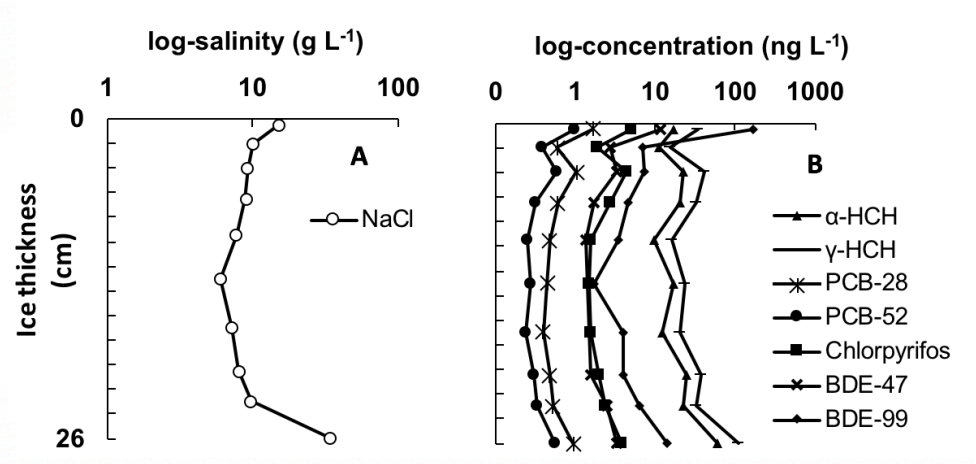

Figure 1: Chemical concentrations in a vertical section of sea ice grown at -18 ºC to a depth of 26cm. Zero on the y-axis represents the upper most surface of the ice in contact with the chamber atmosphere

We are confident that the NaCl profile provided in Figure 1 is driven by brine gravity drainage processes [23]. As the profiles for each organic chemical (Panel B) display a similar shape, we suggest that their distribution in young sea ice is strongly influenced by brine advection during ice growth.

3.4. Accumulation of POPs in frost flowers

Frost flowers (*FF*) are highly saline ice structures that develop on the surface of newly formed sea ice, typically refreezing leads [27]. The salinity of frost flowers sampled in polar environments have been measured up to 110 g L^{-1} (i.e. $EF_{FF\text{-}SW} = 3$) [28] and are typically enriched in other sea-salt ions as well [29, 30]. The leading mechanism proposed for this enrichment suggests that freezing water vapour located at the sea ice surface forms an ice skeleton, causing salts and other solutes to be advected from the surface layer through capillary action [29]. In our study, frost flowers covered around 10% of the surface area of the ice (Freeze - 1) and melted samples measured a salinity of 83 g L^{-1}, representing a significant enrichment of NaCl from the upper layer layer ($EF_{FF\text{-}L1} = 5.0 \pm <0.1$). Results displayed in Table 3 show that $EF_{FF\text{-}L1\ [POPs]} > 1$, indicating they too are advected with brine from the surface layer, but to a lesser degree. However, chemical enrichment factors ($EF_{FF\text{-}L1}$) for BDE-47 and BDE-99 were 30 ± 20 and 50 ± 31, respectively, indicating selective fractionation of organic chemicals in frost flowers. Douglas et al. [10] observed similar enrichments ($EF_{FF\text{-}L1} = 2 - 68$) for a number of analogous chemicals, including higher-chlorinated-PCBs, in frost flowers sampled on coastal sea ice close to Barrow, Alaska.

The relatively large surface area of frost flowers has been suggested as an important feature that enhances the atmospheric scavenging of airborne chemicals [10]. However, atmospheric scavenging is unlikely to be significant in our experiments because the blanks revealed negligible levels of the chemicals in the chamber air (Table S3). A possible mechanism for observing enrichment in frost flowers involves evaporation of chemicals from the relatively warmer surface ice layer, and subsequent condensation to the colder frost flowers [10]. However, we propose that organic solutes may be advected from the ice at different rates and related to factors controlled by their individual physicochemical properties. The high enrichment observed for some of these chemicals suggests that frost flowers may play an important role in the ice-atmosphere exchange of POPs in polar marine environments.

3.5. Simulated chemical behaviour in sea ice

The initial NaCl and chemical concentrations measured in the seawater were used as input parameters for the brine dynamics model. The model predicts the convection of brine, driven by gravity drainage, assuming that: (i) the chemicals are perfectly dissolved and are advected with the moving brine; (ii) the chemicals are well-mixed in the underlying seawater. Figure 2 shows an example of a comparision between the predicted and measured chemical distribution of NaCl (Panel A), α-HCH (Panel B) and BDE-47 (Panel C) (see Figures S3 and S4 for other chemical profiles), normalised by ice thickness. The model produced a predictable 'c-shape' concentration profile for NaCl and organic chemicals, where concentrations were generally highest at the upper and lower sea ice interface.

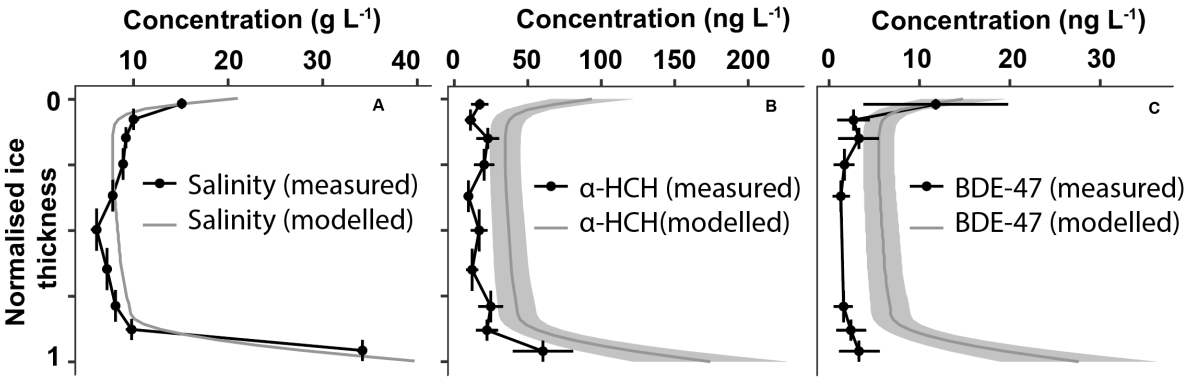

Figure 2: Modelled and measured bulk concentration profile for salinity, α-HCH and BDE-47 in sea ice grown at -18°C to a depth of 26 cm. Vertical bars indicate layer thickness. Horizontal bars represent ± 2 s.d. for modelled (grey shade) and measured data.

Although a qualitative comparison between the measured and modelled chemical profiles in the sea ice was reasonable, the model tended to overestimate the concentrations of the organic chemicals. A ratio of the modelled and measured bulk ice concentrations (integrated vertically over all the sea ice layers) showed a ratio for NaCl of around 1, whereas a ratio of 9 was observed for BDE-47 (see Table S6 for other chemicals). The comparison suggests that low-polarity organic compounds may not be transported conservatively with respect to salt. Rather, additional factors other than gravity drainage may also play a role in the degree of chemical incorporation during sea ice growth.

The extreme environment (i.e. low temperatures and high brine salinity) in sea ice causes large uncertainties regarding the physical-chemical properties of organic solutes in brine inclusions. We derived simple salinity-temperature dependent relationships for each chemical to estimate whether the aqueous solubility was exceeded at the minimum recorded temperature and highest modelled brine salinity within the sea ice (listed in Table 1). Our basic approach indicated that the aqueous solubility was not exceeded for each chemical at these conditions. While we can not state conclusively that this factor did not affect the distribution of chemicals in our experiments, our results suggest that another process(es) currently not described by the physics incorporated within the brine dynamics model may also be at play. Given the dynamic nature of our artificial sea ice, chemical solutes are unlikely to attain equilibrium between the seawater, ice surfaces and ice brine compartments. As sea ice grows thicker (late season Arctic sea ice may be several metres thick), the rate of ice growth generally decreases, allowing more time for exchange of organic chemicals between these compartments and affecting their accumulation in sea ice. We therefore propose that thermodynamic factors such as the partitioning of low polarity organic contaminants between these different ice compartments [31] (processes which do not feature in the model) may account for the descrepancy between the observed and modelled values.

3.6. Brine composition and chemical dynamics

The thermodynamic state controls the fluid dynamics of sea ice and plays a crucial role in the biogeochemical cycling of sea ice constituents [8, 21, 32, 33]. As the brine volume of sea ice approaches around 5%, it is generally accepted that sea ice becomes sufficiently permeable to permit brine to move freely [34] . However, the melting of natural sea ice and hence its desalination during seasonal thaw is a complex process that is governed by the properties of the sea ice and the thermal regime (i.e. basal melt or surface melt). We conducted a slow-melt experiment (see section 2.4.) to investigate the association of organic chemicals with different meltwater fractions of varying NaCl concentrations. This enabled us to observe the composition of brine and therefore infer the temporal behaviour of organic contaminants in sea ice during the transition from FYI to older MYI.

The experiment resulted in brine-rich meltwater being released first (e.g. NaCl; MW_{F1} = 58 g L^{-1}), followed by a supply of fresher meltwater due to the melting of the ice-matrix itself (e.g. NaCl; MW_{F4}= 1.9 g L^{-1}), indicating that brine release is governed by thermodynamically controlled phase-changes within the sea ice pores. Figure S2 shows that the level of chemical enrichment in meltwater (i.e. $EF_{MW\text{-}SW}$) was positively correlated (n=48, r^2=0.507, p<0.01) with the concentration of NaCl in the sea ice meltwater. Therefore, saltier brine can be expected to contain higher concentrations of chemicals. Our results are consistent with field studies investigating inorganic [21, 32] and organic [8, 9] chemical behaviour in sea ice.

Despite earlier meltwater fractions showing a higher degree of chemical enrichment, the volumes of meltwater that were collected varied from 0.2 to 2.4 L (see Table S7). To further investigate the dynamics of chemicals during melt, the percentage mass of chemical in each meltwater fraction was calculated (see Table S8) and shown in Figure 3. The results show that the highest mass of the most hydrophobic chemicals (PCB-28, chlorpyrifos, BDE-47, BDE-99) was present in the final meltwater fraction (MW_{F4}), unlike NaCl which has the lowest mass in MW_{F4}. The results indicate that organic chemicals can be retained within the bulk sea

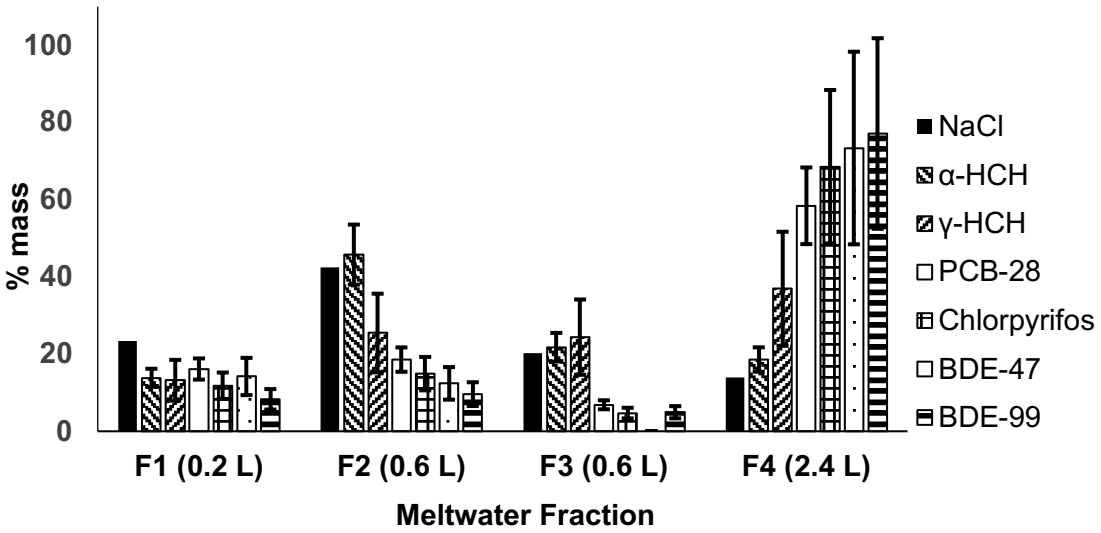

ice even after the brine has drained and implies that more hydrophobic chemicals are preferentially retained within the sea ice.

Figure 3: The percentage mass of individual chemicals in the sequential meltwater fractions. Bracketed values are the actual volumes for each meltwater fraction. PCB-52 was <MDL in several fractions and so was not included in this plot. Error bars calculated from RSD.

The three initial meltwater fractions (MW_{F1-F3}) show that chemical mass loss from the ice is lower than salt, but highest for the more water soluble chemicals (i.e. around 75% of α-HCH and γ-HCH is lost in F1 to F3, compared to only around 20% of BDE-99). The final melt fraction (MW_{F4}) contained >50 % of the mass of (in increasing order) PCB-28, chlorpyrifos, BDE-47 and BDE-99, initially present in the ice prior to the onset of melt. The results suggest that chemicals are released at variable rates, possibly due to thermodynamic factors associated with the aqueous solubility and the rate of dissolution [35], which may affect the phase distribution and rate of transfer between the solid fresh ice matrix to the mobile liquid brine solution. This observation is comparable to studies performed in environmental and laboratory snow, whereby soluble ions are generally released in initial meltwater fractions (i.e. "type I elution" see references [36, 37]), wheareas very hydrophobic organic compounds (possibly associated with particles), are retained in the snow until final meltwater elution associated with complete melting (i.e. "type II elution").

Our results show that brine dynamics play an important role in the distribution of persistent chemicals in young sea ice, supporting our hypothesis that chemical uptake and distribution is strongly influenced by the formation of brine during sea ice growth. However, chemical specific processes may remove these chemicals from the dissolved phase, decoupling them from the NaCl within the sea ice system. Support for this assertion comes from our melting experiments where chemicals were released from the sea ice at varying rates. The most hydrophobic chemicals were preferentially retained within the sea ice relative to the more water soluble chemicals, and to NaCl. Physical-chemical processes such as adsorption to brine inclusion walls or precipitation within brine inclusions are promising explanations for this behaviour. Our results have several important implications for the biogeochemical cycling of persistent organic pollutants in natural sea ice, by: (i) altering the input rate of different contaminants to surface waters from melting sea ice; (ii) affecting the level and retention rates of chemical contaminants in FYI and subsequent MYI, and; (iii) controlling the spatial and temporal exposure of chemicals to ice-associated biota.

Tables S1 – S7 show chemical data along with associated Equations S1 – S5 and Figures S1 – S4 which is available as Supporting Information (SI) to this manuscript.

Acknowledgements

JG's PhD (NE/L002604/1) was funded through NERC's ENVISION Doctoral Training Centre. This work resulted from the EISPAC project (NE/R012857/1), part of the Changing Arctic Ocean programme, jointly funded by the UKRI Natural Environment Research Council (NERC) and the German Federal Ministry of Education and Research (BMBF). The authors are grateful to the British Antarctic Survey for providing funding (British Antarctic Survey Collaboration Voucher) to cover the running costs of the RvG-ASIC facility for the duration of the experimental period. This project/work has received funding from the European Union's Horizon 2020 research and innovation programme through the EUROCHAMP-2020 Infrastructure Activity under grant agreement No 730997. The authors would like to thank Professor Finlo Cottier and two anonymous reviewers.

1. UNEP *Global Report 2003-Regionally Based Assessment of Persistent Toxic Substances*; Geneva, Switzerland, 2003.https://www.researchgate.net/profile/Hindrik_Bouwman/publication/292286858_Regionally_based_assessment_of_persistent_toxic_substances_Global_reprt/links/56ac8fb408ae19a38513e2e7/Regionally-based-assessment-of-persistent-toxic-substances-Global-reprt.pdf
2. de Wit, C. A.; Muir, D., Levels and trends of new contaminants, temporal trends of legacy contaminants and effects of contaminants in the Arctic: Preface. *Science of the Total Environment* **2010,** *408* (15), 2852-2853;10.1016/j.scitotenv.2009.06.011
3. AMAP *AMAP Assessment 2016: Chemicals of Emerging Arctic Concern*; -; -: Oslo, Norway, -, 2017; p 353.https://www.amap.no/documents/doc/AMAP-Assessment-2016-Chemicals-of-Emerging-Arctic-Concern/1624
4. Cai, M.; Yang, H.; Xie, Z.; Zhao, Z.; Wang, F.; Lu, Z.; Sturm, R.; Ebinghaus, R., Per- and polyfluoroalkyl substances in snow, lake, surface runoff water and coastal seawater in Fildes Peninsula, King George Island, Antarctica. *Journal of Hazardous Materials* **2012,** *209-210*, 335-342;10.1016/j.jhazmat.2012.01.030
5. Pućko, M.; Stern, G. A.; Macdonald, R. W.; Rosenberg, B.; Barber, D. G., The influence of the atmosphere-snow-ice-ocean interactions on the levels of hexachlorocyclohexanes in the Arctic cryosphere. *Journal of Geophysical Research: Oceans* **2011,** *116* (C2), n/a-n/a;10.1029/2010JC006614
6. Pućko, M.; Stern, G. A.; Macdonald, R. W.; Jantunen, L. M.; Bidleman, T. F.; Wong, F.; Barber, D. G.; Rysgaard, S., The delivery of organic contaminants to the Arctic food web: Why sea ice matters. *Science of the Total Environment* **2015,** *506-507*, 444-452;10.1016/j.scitotenv.2014.11.040
7. Gustafsson, Ö.; Andersson, P.; Axelman, J.; Bucheli, T. D.; Kömp, P.; McLachlan, M. S.; Sobek, A.; Thörngren, J. O., Observations of the PCB distribution within and in-between ice, snow, ice-rafted debris, ice-interstitial water, and seawater in the Barents Sea marginal ice zone and the North Pole area. *Science of the Total Environment* **2005,** *342* (1), 261-279;10.1016/j.scitotenv.2004.12.044
8. Pućko, M.; Stern, G.; Macdonald, R. W.; Barber, D. G., alpha- and gamma-Hexachlorocyclohexane Measurements in the Brine Fraction of Sea Ice in the Canadian High Arctic Using a Sump-Hole Technique. *Environmental Science & Technology* **2010,** *44* (24), 9258-9264;10.1021/es102275b
9. Pućko, M.; Stern, G. A.; Barber, D. G.; Macdonald, R. W.; Rosenberg, B., The international polar year (IPY) circumpolar flaw lead (CFL) system study: The importance of brine processes for α- and γ-hexachlorocyclohexane (HCH) accumulation or rejection in sea ice. *Atmosphere-Ocean* **2010,** *48* (4), 244-262;10.3137/OC318.2010

10. Douglas, T. A.; Domine, F.; Barret, M.; Anastasio, C.; Beine, H. J.; Bottenheim, J.; Grannas, A.; Houdier, S.; Netcheva, S.; Rowland, G.; Staebler, R.; Steffen, A., Frost flowers growing in the Arctic ocean-atmosphere–sea ice–snow interface: 1. Chemical composition. *Journal of Geophysical Research: Atmospheres* **2012,** *117* (D14), n/a-n/a;10.1029/2011JD016460
11. Vaughan, D. G. C., J.C.; Allison, I.; Carrasco, J.; Kaser, G.; Kwok, R.; Mote, P.; Murray, T.; Paul, F.; Ren, J.; Rignot, E.; Solomina, O.; Steffen, K.; Zhang, T., Observations: Cryosphere. In *Climate Change 2013: The Physical Science Basis. Contribution of Working Group I to the Fifth Assessment Report of the Intergovernmental Panel on Climate Change*, Cambridge University: Cambridge, U.K. & New York, USA., 2013.
12. NSIDC All About Sea Ice: Arctic vs. Antarctic. https://nsidc.org/cryosphere/seaice/characteristics/difference.html
13. Perovich, D. M., W; Tschudi, M; Farrel, S. ; Hendricks, S; Gerland, S; Haas, C; Krumpen, T; Polashenski, C; Ricker, R; Webster, M Sea Ice. In: Arctic Report Card 2015. https://www.arctic.noaa.gov/report-card
14. Notz, D.; Worster, M. G., Desalination processes of sea ice revisited. *Journal of Geophysical Research: Oceans* **2009,** *114* (C5), n/a-n/a;10.1029/2008JC004885
15. Pućko, M.; Stern, G. A.; Barber, D. G.; Macdonald, R. W.; Warner, K. A.; Fuchs, C., Mechanisms and implications of α-HCH enrichment in melt pond water on Arctic sea ice. *Environmental Science & Technology* **2012,** *46* (21), 11862;10.1021/es303039f
16. Pućko, M.; Stern, G. A.; Burt, A. E.; Jantunen, L. M.; Bidleman, T. F.; Macdonald, R. W.; Barber, D. G.; Geilfus, N.-X.; Rysgaard, S., Current use pesticide and legacy organochlorine pesticide dynamics at the ocean-sea ice-atmosphere interface in resolute passage, Canadian Arctic, during winter-summer transition. *Science of the Total Environment* **2017,** *580*, 1460-1469;10.1016/j.scitotenv.2016.12.122
17. Rees Jones, D. W.; Worster, M. G., A physically based parameterization of gravity drainage for sea-ice modeling. *Journal of Geophysical Research: Oceans* **2014,** *119* (9), 5599-5621;10.1002/2013JC009296
18. Cottier, F.; Eicken, H.; Wadhams, P., Linkages between salinity and brine channel distribution in young sea ice. *Journal of Geophysical Research: Oceans* **1999,** *104* (C7), 15859-15871;10.1029/1999JC900128
19. Fripiat, F.; Cardinal, D.; Tison, J. L.; Worby, A.; André, L., Diatom-induced silicon isotopic fractionation in Antarctic sea ice. *Journal of Geophysical Research: Biogeosciences* **2007,** *112* (G2), n/a-n/a;10.1029/2006JG000244
20. Nomura, D.; Takatsuka, T.; Ishikawa, M.; Kawamura, T.; Shirasawa, K.; Yoshikawa-Inoue, H., Transport of chemical components in sea ice and under-ice water during melting in the seasonally ice-covered Saroma-ko Lagoon, Hokkaido, Japan. *Estuarine, Coastal and Shelf Science* **2009,** *81* (2), 201-209;10.1016/j.ecss.2008.10.012
21. Fripiat, F.; Sigman, D. M.; Fawcett, S. E.; Rafter, P. A.; Weigand, M. A.; Tison, J. L., New insights into sea ice nitrogen biogeochemical dynamics from the

nitrogen isotopes. *Global Biogeochemical Cycles* **2014,** *28* (2), 115-130;10.1002/2013GB004729
22. Miller, L. A. F., F; Brent, G. T. Else; Bowman, J S; Brown, K A; Collins, E R; Ewert, M; Fransson, A; Gosselin, M; Lannuzel, D; Meiners, K M; Michel, C; Nishioka, J; Nomura, D; Papadimitriou, S; Russell, L M; Sørensen, L L; Thomas, D N; Tison, J-L; A. van Leeuwe, M; Vancoppenolle, M; Wolff, E W; Zhou, J, Methods for biogeochemical studies of sea ice: The state of the art, caveats, and recommendations. *Elementa: Science of the Anthropocene* **2015,** *3*;10.12952/journal.elementa.000038
23. Thomas, M. Brine and pressure dynamics in growing sea ice: first results from the Roland von Glasow air-sea-ice chamber. Ph.D, University of East Anglia, Norwich, U.K., 2019.
24. Thomas, M. V., M; France, J; Sturges, W. T. ; D. C. E. Bakker, D. C. E. ; Kaiser, J.; von Glasow, R, Tracer measurements in growing sea ice support convective gravity drainage parameterisations (Ph.D Thesis). 2019.
25. Petrich, C. E., Hajo, Overview of sea ice growth and properties. In *Sea ice (Third Edition)*, Third ed.; John Wiley & Sons: Chichester, U.K., 2017; pp 1-41.
26. Assur, A., Composition of sea ice and its tensile strength, in Arctic Sea Ice. Easton, M., Ed. National Research Council, Washington: Easton, Maryland, 1958; pp 106 - 138.
27. Perovich, D. K.; Richter-Menge, J. A., Surface characteristics of lead ice. *Journal of Geophysical Research: Oceans* **1994,** *99* (C8), 16341-16350;10.1029/94JC01194
28. Barber, D. G. E., J K ; Pućko, M ; Rysgaard, S ; Deming, J W ; Bowman, JS ; Papakyriakou, T ; Galley, R J ; Sogaard, D H, Frost flowers on young Arctic sea ice: The climatic, chemical, and microbial significance of an emerging ice type. *Journal Of Geophysical Research-Atmospheres* **2014,** *119* (20), 11593-11612
29. Alvarez-Aviles, L.; Simpson, W. R.; Douglas, T. A.; Sturm, M.; Perovich, D.; Domine, F., Frost flower chemical composition during growth and its implications for aerosol production and bromine activation. *Journal of Geophysical Research: Atmospheres* **2008,** *113* (D21), n/a-n/a;10.1029/2008JD010277
30. Rankin, A. M.; Wolff, E. W.; Martin, S., Frost flowers: Implications for tropospheric chemistry and ice core interpretation. *Journal of Geophysical Research: Atmospheres* **2002,** *107* (D23), AAC 4-1-AAC 4-15;10.1029/2002JD002492
31. Schwarzenbach, R. P. G., Phillip M; Imboden, Dieter M, Sorption of Nonionic organic compounds to Inorganic Surfaces in Water. In *Environmental Organic Chemistry*, John Wiley & Sons: Hoboken, New Jersey, 2003; pp 389 - 417.
32. Lannuzel, D.; Bowie, A. R.; van Der Merwe, P. C.; Townsend, A. T.; Schoemann, V., Distribution of dissolved and particulate metals in Antarctic sea ice. *Marine Chemistry* **2011,** *124* (1), 134-146;10.1016/j.marchem.2011.01.004
33. Zhou, J.; Delille, B.; Kaartokallio, H.; Kattner, G.; Kuosa, H.; Tison, J. L.; Autio, R.; Dieckmann, G. S.; Evers, K. U.; Jørgensen, L.; Kennedy, H.; Kotovitch,

M.; Luhtanen, A. M.; Stedmon, C. A.; Thomas, D. N., Physical and bacterial controls on inorganic nutrients and dissolved organic carbon during a sea ice growth and decay experiment. *Marine Chemistry* **2014,** *166* (C), 59-69;10.1016/j.marchem.2014.09.013
34. Golden; Ackley; Lytle, The percolation phase transition in sea Ice. *Science (New York, N.Y.)* **1998,** *282* (5397), 2238;10.1126/science.282.5397.2238
35. Schwarzenbach, R. P. G., Phillip M; Imboden, Dieter M, Molecular interpretation of the Excess Free Energy of Organic Compounds in Aqueous Solutions. In *Environmental Organic Chemistry*, John Wiley & Sons: Hoboken, New Jersey, 2003; pp 142 - 180.
36. Meyer, T.; Lei, Y.; Muradi, I.; Wania, F., Organic Contaminant Release from Melting Snow. 2. Influence of Snow Pack and Melt Characteristics. *Environmental Science & Technology* **2009,** *43* (3), 663;10.1021/es8020233
37. Meyer, T.; Lei, Y.; Muradi, I.; Wania, F., Organic Contaminant Release from Melting Snow. 1. Influence of Chemical Partitioning. *Environmental Science & Technology* **2009,** *43* (3), 657;10.1021/es8020217

Jack Garnett[1], Crispin Halsall[1*], Max Thomas[2], James France[2,3,4], Jan Kaiser[2], Carola Graf[1], Amber Leeson[1], Peter Wynn[1]

1 Lancaster Environment Centre, Lancaster University, Lancaster, LA1 4YQ, UK

2 Centre for Ocean and Atmospheric Sciences, School of Environmental Sciences, University of East Anglia, Norwich Research Park, Norwich, NR4 7TJ, UK

3 British Antarctic Survey, High Cross, Madingley Road, Cambridge, CB3 0ET

4 Department of Earth Sciences, Royal Holloway, University of London, Egham Hill, Egham TW20 0EX, UK

Email: c.halsall@lancaster.ac.uk

Supporting Information to:

Mechanistic insight into the uptake and fate of persistent organic pollutants in sea ice

Contents include:

Tables

Table S1: Physical-chemical property data for organic chemicals.

Chemical	Molar mass [g/mol]	Aqueous Solubility (nM) [25 °C]	Salinity & Temperature adjusted aqueous solubility [-2 °C] (nM)	Vapour pressure (Pa) [25°C]	Log Kow	References
α - HCH	290.9	3.33×10^{5}	1.68×10^{5}	2.45×10^{-1}	3.9	[1]
γ - HCH	290.9	2.47×10^{5}	9.36×10^{4}	7.59×10^{-2}	3.8	[1]
§Chlorpyrifos	350.6	9.95×10^{3}	2.19×10^{3}	3.10×10^{-3}	5.1	[2]
PCB-28	257.5	6.64×10^{3}	2.26×10^{2}	2.69×10^{-2}	5.7	[3]
PCB-52	292.0	6.50×10^{2}	1.23×10^{2}	1.20×10^{-2}	5.9	[3]
*BDE-47	485.8	3.43×10^{2}	1.02×10^{2}	2.15×10^{-4}	6.4	[4]
*BDE-99	564.7	1.95×10^{2}	3.98×10^{1}	3.63×10^{-5}	6.8	[4]

Aqueous solubility data are reported for 25°C but were adjusted to the freezing temperature of seawater (-2°C) and initial seawater salinity (35.4 g L^{-1}) (see Equation S2) to estimate solubility. Temperature and salinity adjustments were calculated independently using temperature-dependent regression parameters provided in the corresponding references. § denotes those chemicals for which temperature regression parameters were not available. Salinity adjustments were performed using predicted Setchenow constants[5] .

Table S2: Concentrations of chemical spike added into experimental tank

Compound	**Volume (L)**	**Molarity (μM)**	**Volume (L)**	**Molarity (nM)**
	Spike*		Experiment tank	
α-HCH	1	1.43	3500	0.41
γ-HCH		1.43		0.41
PCB-28		1.21		0.35
PCB-52		0.43		0.12
Chlorpyrifos		1.02		0.29
BDE-47		0.21		0.06
BDE-99		0.74		0.21

*The mixed-stock chemical solution was made up with 1 litre of pure ethanol giving a final volume fraction in the experimental tank of approximately 3 x 10^{-4}.

Table S3: QA/QC parameters used throughout experiment

Chemical	α *-HCH*	γ *-HCH*	*PCB-28*	*PCB-52*	*Chlorpyrifos*[*]	*BDE-47*	*BDE-99*
Units	*ng* L^{-1}	*ng* L^{-1}	*ng* L^{-1}	*ng* L^{-1}	*ng* L^{-1}	*ng* L^{-1}	*ng* L^{-1}

**SW Procedural blank (n=3)*	*n/d*	*n/d*	*n/d*	*n/d*	*n/d*	*n/d*	*2 ± 4*
**BI Procedural blank (n=1)*	*<3*	*<3*	*<0.1*	*<0.1*	*n/d*	*n/d*	*n/d*
Method Detection limit (MDL)	*<5*	*<15*	*<0.3*	*<0.3*	*<13*	*<0.3*	*<13*
Recovery Standard	*^{13}C-PCB-28*			*^{13}C-PCB-52*		*^{13}C-PCB-180*	
Internal Standard	*^{13}C-PCB-141*					*BDE-69*	
BI (% recovery)	*38 ± 12*			*42 ± 14*	*42 ± 15*		
SW (% recovery)	*34 ± 11*			*45 ± 12*	*38 ± 19*		
Maximum seawater RSD	17	40	8	13	24	34	32

MDL calculated using SW (n = 3) & BI (n = 1) procedural blanks; n/d=not detected; *Confirmation ions for chlorpyrifos were not always detected in some samples containing low analyte levels. The maximum relative standard deviation in the seawater measurements was used to provide a conservative estimate of the variability for some singlet samples.

Table S4: Values used for calculations for literature analysis

Experimental compartment	NaCl	α -HCH	γ -HCH	PCB-28	PCB-52	Chlorpyrifos	BDE-47	BDE-99	Experiment
	g L^{-1}	ng L^{-1}	ng L^{-1}	ng L^{-1}	ng L^{-1}	ng L^{-1}	ng L^{-1}	ng L^{-1}	
Brine	53.1	107.7	278.1	31.1	10.3	63.5	21.4	60.5	Freeze 2
SW	37.9	185.6	336.3	24.9	8.5	58.0	36.9	73.8	Freeze 1
BI	13.9	25.4	39.8	4.6	1.3	8.5	4.7	23.7	Freeze 1

BI	11.1	31.0	73.6	5.5	0.7	15.6	5.0	25.3	Freeze 2
FF	88.3	35.6	66.6	4.9	3.3	17.9	208.7	1555.7	Freeze 1
L1	17.6	24.1	42.2	2.1	1.1	8.4	8.1	36.1	Freeze 1

Table S5: Modelled and measured integrated concentrations of chemicals in bulk ice.

	NaCl	α-HCH	γ-HCH	PCB-28	PCB-52	Chlorpyrifos	BDE-47	BDE-99	Experiment
Modelled	12.3	54.9	125.8	7.0	2.8	17.7	8.7	21.4	Freeze 1
Measured	13.7	16.0	25.5	1.3	0.8	5.2	1.0	15.1	
Modelled:Measured	0.9	3.4	4.9	5.3	3.5	3.4	8.6	1.4	
Modelled	10.7	47.6	109.2	6.1	2.4	15.3	7.6	18.6	Freeze 2
Measured	13.7	16.0	25.5	1.3	0.8	5.2	1.0	15.1	
Modelled:Measured	0.8	3.0	4.3	4.6	3.1	3.0	7.5	1.2	

Table S6: Concentration of chemicals in meltwater fractions and Enrichment Factor (EF).

MW	H_20	NaCl		α -HCH		γ -HCH		PCB-28		PCB-52		Chlorpyrifos		BDE-47		BDE-99	
	L	g L^{-1}	EF	ng L^{-1}	EF	ng L^{-1}	EF	ng L^{-1}	EF	ng L^{-1}	EF	ng L^{-1}	EF	ng L^{-1}	EF	ng L^{-1}	EF
F1B	0.10	48.3	1.27	109.7	0.59	303.2	0.90	25.2	1.01	10.2	1.21	47.0	0.81	22.7	0.61	53.8	0.73

F1T	0.09	57.9	1.53	105.7	0.57	253.0	0.75	36.9	1.48	10.4	1.23	80.0	1.38	20.2	0.55	67.3	0.91
F2B	0.36	30.1	0.79	122.5	0.66	174.6	0.52	7.9	0.32	<MDL	n/a	11.0	0.19	<MDL	n/a	14.0	0.19
F2T	0.24	31.0	0.82	98.2	0.53	164.3	0.49	16.1	0.65	5.8	0.68	46.2	0.80	14.9	0.40	34.3	0.46
F3B	0.31	12.8	0.34	46.7	0.25	178.4	0.53	2.0	0.08	<MDL	n/a	6.8	0.12	<MDL	n/a	12.9	0.17
F3T	0.28	16.6	0.44	62.2	0.34	148.7	0.44	6.6	0.26	<MDL	n/a	9.3	0.16	<MDL	n/a	9.8	0.13
F4B	1.07	1.9	0.05	13.3	0.07	67.6	0.20	5.3	0.21	<MDL	n/a	20.0	0.34	5.2	0.14	7.1	0.10
F4T	1.30	3.1	0.08	10.2	0.05	58.5	0.17	11.9	0.48	<MDL	n/a	36.8	0.63	11.9	0.32	76.2	1.03

Meltwater was successively collected from the top (T) and bottom (B) sections of the ice samples from Freeze 2 (Fraction 1=F1; Fraction 2=F2; Fraction 3=F3; Fraction 4=F4). <MDL=below method detection limit; n/a=not applicable

Table S7: Percentage mass of chemicals in meltwater fractions.

Fraction Name (Volume (L))	H_20	NaCl	α -HCH	γ -HCH	PCB-28	PCB-52*	Chlorpyrifos	BDE-47	BDE-99
	$\%_{volume}$	$\%_{mass}$	$\%_{mass}$	$\%_{mass}$	$\%_{mass}$	$\%_{mass}$	$\%_{mass}$	$\%_{mass}$	$\%_{mass}$
F1 (0.2 L)	5	23	13.9	13.2	16.1	n/c	11.8	14.2	8.3
F2 (0.6 L)	16	42	45.8	25.5	18.6	n/c	14.9	12.4	9.6
F3 (0.6 L)	16	20	21.8	24.4	6.9	n/c	4.7	0.0	4.9
F4 (2.4 L)	63	14	18.6	36.9	58.4	n/c	68.5	73.4	77.1

The volume of water and the mass of each chemical from the respective meltwater fractions (Fraction 1=F1; Fraction 2=F2; Fraction 3=F3; Fraction 4=F4) obtained from the top (T) and bottom (B) were summed (e.g. F1T + F1B) and the % mass contribution was calculated. *PCB-52 was <MDL in some meltwater fractions and so was excluded from further data analysis; n/c=not calculated

Equations

Equation S1: Brine salinity

$$S_{br} = -17.6T - 0.389^2 - 0.00362T^3 \quad (1)$$

Brine salinity in sea-ice (g kg^{-1}) is a function of temperature because, to an excellent approximation, the salinity of brine remains in thermodynamic equilibrium as water freezes or melts at brine pocket walls (Feltham et al. 2006). Brine salinity is derived from the experimental data [6, 7].

Equation S2: Salinity & Temperature-adjusted aqueous solubility (S^T)

$$\log (S^T / S_0^T) = (-k_{salt}\, C_{salt}) \quad (2)$$

Where k_{salt} is the Setschenow constant derived using k = 0.04Kow + 0.114 [5]; Kow = octanol-water partition coefficient; C_{salt} is the molar concentration of NaCl; S^T and S_0^T are the aqueous solubilities of the organic solute in aqueous salt solution and in water, respectively, at a particular temperature using temperature-dependent regression curves. See references for physical-chemical data. All units of concentration and solubility are Molarity.

Equation S3: Normalised ice depth

$$Normalised\ depth = \frac{ice\ layer\ depth \quad (e.g. 13cm)}{Total\ ice\ thickness\ (e.g. 26cm)} \quad (3)$$

Due to differences in ice thickness between the modelled and measured ice depths, ice thicknesses were normalised to allow comparison of the sea ice datasets.

Equation S4: Bulk ice concentration

$$[chemical]_{bulk\ ice}\ [ng\ L^{-1}] = \frac{\sum(concentration\ x\ depth)}{Total\ ice\ thickness} \quad (4)$$

Chemical concentration in bulk ice was calculated by totalling the amount of chemical at each layer, over the total average ice thickness. Measured concentrations in melted bulk ice samples were previously corrected for ice density using previously determined estimates of 0.95 kg L^{-1}.

Equation S5: Percentage mass

$$Percentage\ mass\ (\%) = \frac{(\ (chemical)_{mass\ e.g.\ F1,\ F2,\ F3,\ F4,})}{Mass\ \Sigma_{(F1-F4)}} x\ 100 \qquad (5)$$

Where (%) is the relative mass of chemical in a particular meltwater fraction compared to the combined mass contained in the meltwater fractions.

Figures

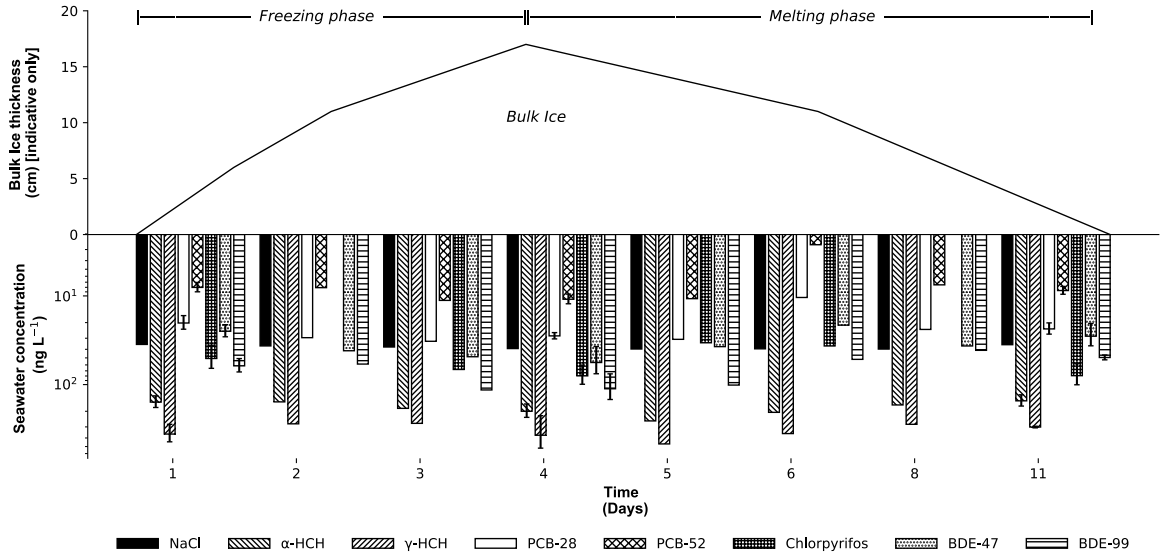

Figure S1: Time-series of NaCl and chemical concentrations in seawater.

Data were plotted on a log-scale to show all chemicals and account for their wide range in concentrations. Error bars indicate the 1.s.d on day 1, day 4 and day 11. The units of NaCl are g L^{-1}.

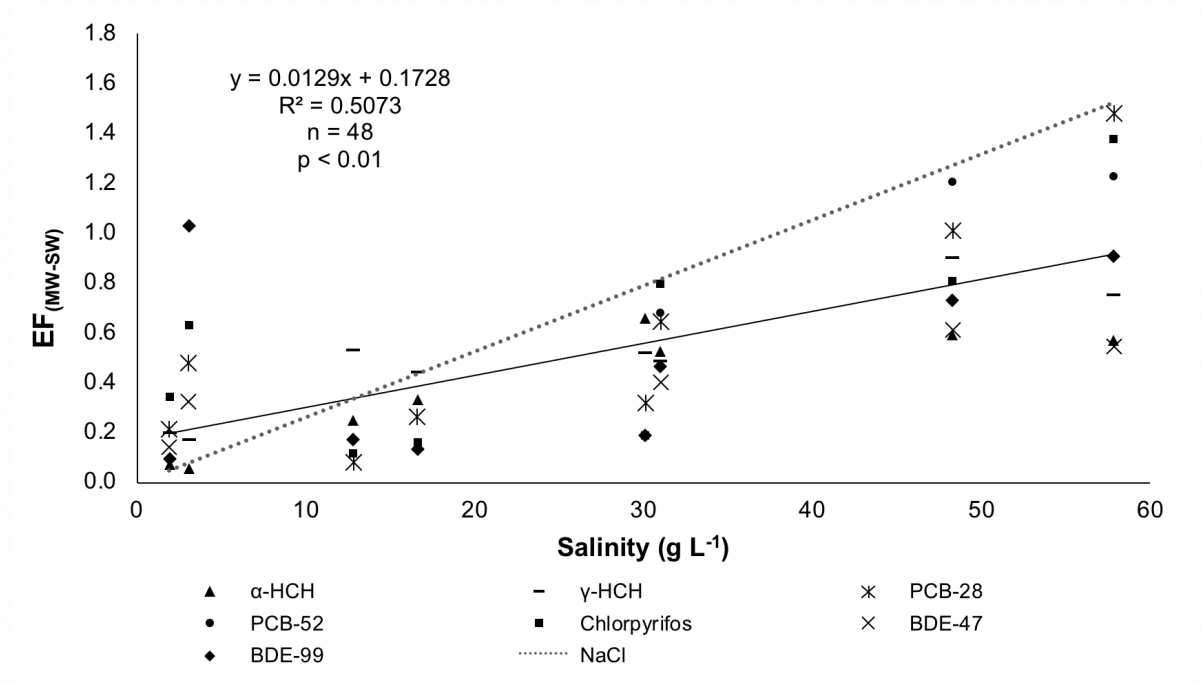

Figure S2: Relationship between the salinity and the level of chemical enrichment.

Symbols represent enrichment (EF_{MW-SW}) individual chemicals in the different meltwater fractions. Hashed line shows the enrichment of NaCl as a reference to compare chemical behaviour.

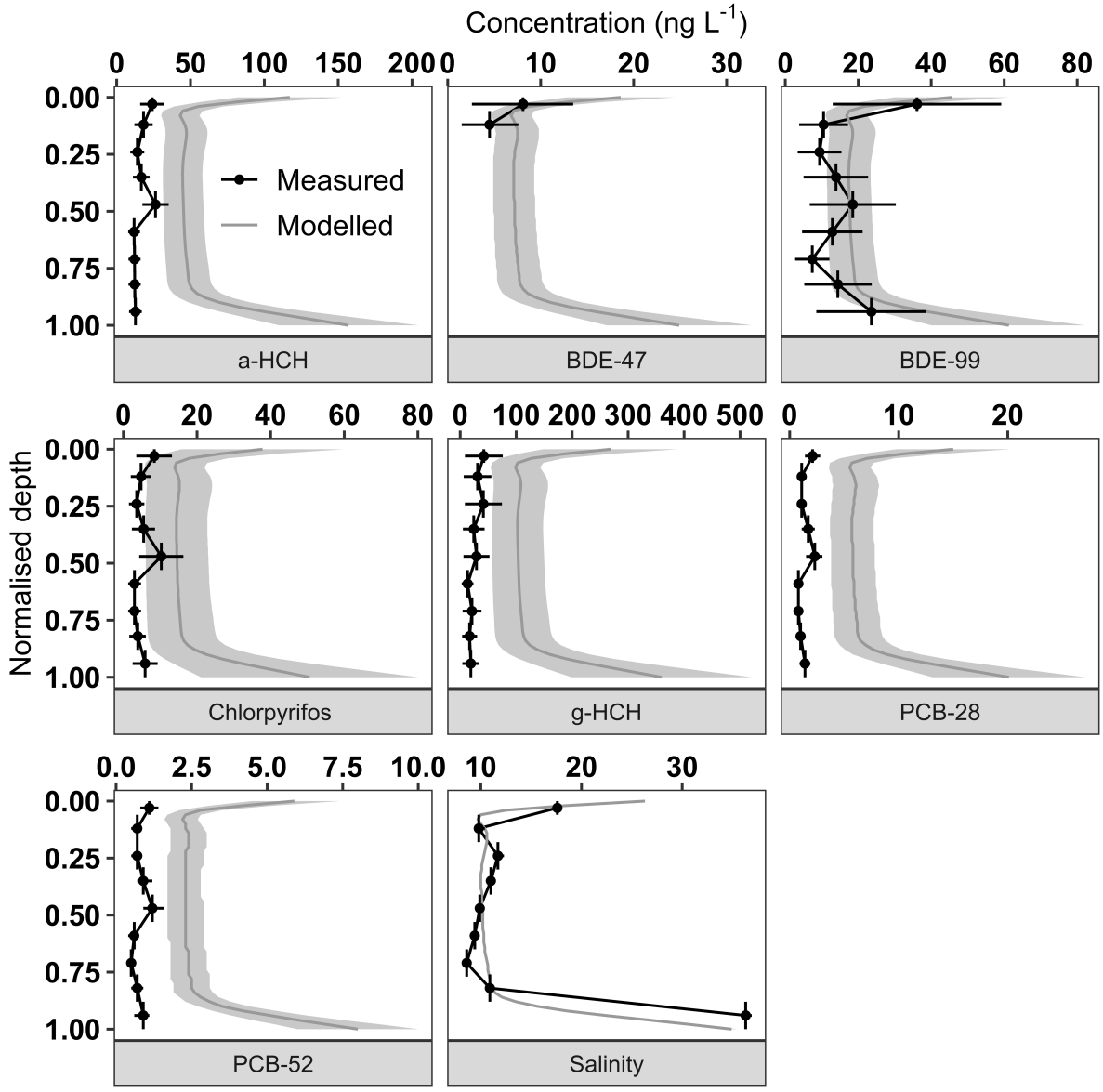

Figure S3: Chemical concentration profiles in sea ice grown during Freeze 1.

The salinity is in g L-1 rather than ng L-1.

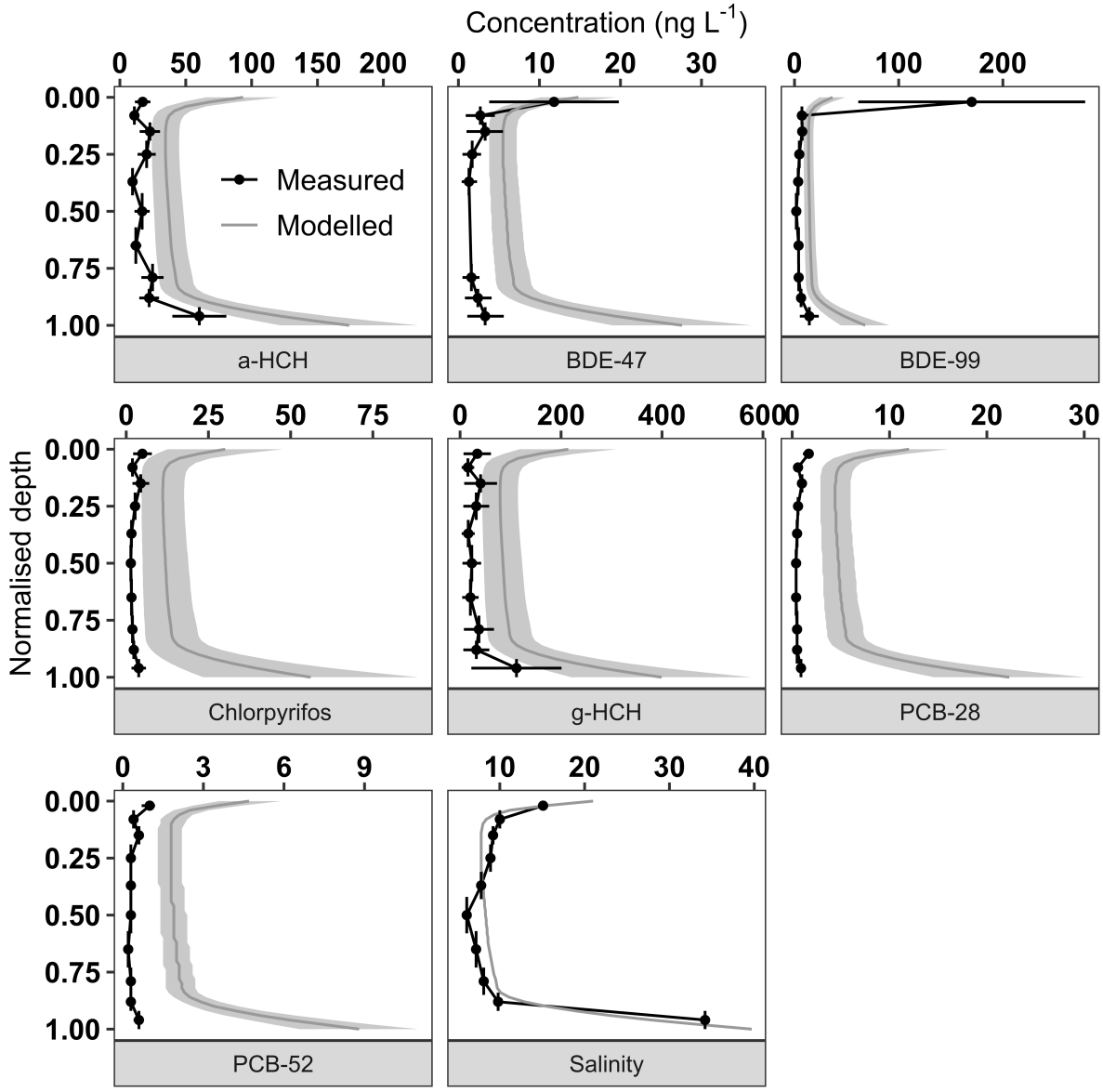

Figure S4: Chemical concentration profiles in sea ice grown during Freeze 2.

Salinity is in g L-1 rather than ng L-1.

Further information

1-dimensional sea ice brine dynamics model

The model used in this work is presented and evaluated in detail [8] Measured vertical sea ice temperature profiles, and sea-ice thicknesses derived from them, were used in lieu of modelled thermodynamics. The only processes affecting the concentrations of chemicals and salt within the model are the growth of new sea ice, which traps all of the dissolved species in the model, and gravity drainage. We parameterise gravity drainage following the well tested scheme [9]. The following describes the key steps in the model, and we re-direct the readers requiring more detail to [8].

During each model timestep, the brine salinity, S_{BR} (g kg^{-1}), is calculated from the local sea-ice temperature, T (°C), using an inversion of the liquidus relationship for freezing NaCl (see Equation S1)

We then use the bulk salinity to calculate ϕ_l for each model layer using Equation S6:

$$\phi_l = \frac{S_b}{S_{br}} \qquad (6)$$

which is a rearrangement of the definition of bulk salinity assuming brine and ice are the only phases. The brine concentration, C_{br}, of any other chemical is calculated using Equation S7:

$$C_{br} = \frac{C_b}{\phi_l} \qquad (7)$$

where C_b is the bulk concentration of a chemical in the sea ice. The concentration of chemicals other than salt does not affect the physical sea-ice properties. From this point in the model there is no difference between the treatment of the transport of salt and any other chemical.

To avoid duplicating equations we use C to represent salt and any other chemical from this point onwards.

Brine dynamics in the model are driven exclusively by gravity drainage [9]. The vertical brine salinity profile is always negative (highest brine salinities near the sea-ice/atmosphere interface) because of the negative temperature profile in growing sea ice (Equation S1). Brine density is proportional to brine salinity [10], so the brine density profile in growing sea ice is also negative. Relatively dense brine overlies less dense brine and ocean. This unstable brine profile can cause convective overturning of brine, a process often referred to as 'gravity drainage'. Brine travels downwards through brine channels to the ocean, and is replaced by upwelling brine travelling through the porous sea-ice matrix. Dissolved chemical species are transported along with this brine, causing a net desalination of the sea ice and a redistribution of other chemicals. Gravity drainage is the dominant process redistributing brine in growing sea ice [6].

We parameterise gravity drainage [9] and note that the parameterisation of Griewank & Notz [11] is basically equivalent and performs equally well [8]. We evolve the concentration profile of salt and tracer using Equation S8:

$$\frac{dC_b}{dt} = -w\frac{dC_{br}}{dz} \tag{8}$$

where t and z represent time and depth, respectively. Rees Jones & Worster [9] parameterise the upward brine velocity, w, as proportional to an effective Rayleigh number, R_e, using Equation S9:

$$w(z) = \begin{cases} -\alpha R_e \frac{k_l}{c_l}\frac{z-z_c}{(h-z_c)^2}, & z \geq z_c \\ 0, & otherwise \end{cases} \tag{9}$$

where α is a free tuning parameter, k_l and c_l are the thermal conductivity and volumetric heat capacity of brine, respectively, and z_c and z are the depth of the convecting layer and the

depth of the model layer, respectively. The depth of the convecting layer is taken to be the shallowest depth where the local Rayleigh number, $R(z)$, is greater that some critical Rayleigh number, R_c, which is a free tuning parameter. We use the formulation of Rees Jones & Worster [9] to calculate $R(z)$ for each model layer, then calculate R_e as a function of the maximum super critical Rayleigh number using Equation S10.

$$R_e = \max\left(R(z) - R_c\right) \tag{10}$$

Rayleigh numbers have been used extensively to diagnose and parameterise sea-ice brine convection [9, 11, 12]. A Rayleigh number represents the ratio of the timescale over which a brine parcel descends to the timescale over which that parcel comes into thermal equilibrium with its surroundings. See Worster & Rees Jones [13] for a detailed discussion of Rayleigh numbers in sea ice.

Sea ice growth (change in thickness, dh) was calculated using Equation S11:

$$dh = h_i - h_{i-1} \tag{11}$$

where i denotes the model timestep. The new thickness of sea ice is taken to have the same concentration as the sea water for each chemical species; consistent with measurements of a continuous salinity profile during Arctic sea ice growth [14], and our current best understanding of brine dynamics. After sea ice growth, the concentration of the chemical species in the sea water (C_o) was determined using a discrete mass balance approach using Equations S12 – S14:

$$mC_{o,i} = mC_{o,i-1} - (mC_{si,i} - mC_{si,i-1}) \tag{12}$$

$$m_{o,i} = m_{o,i-1} - (m_{si,i} - m_{si,i-1}) \tag{13}$$

$$C_{o,i} = \frac{mC_{o,i}}{m_{o,i}} \tag{14}$$

In Equations S12 - S14, the updated mass of some chemical in the seawater , $mC_{o,i}$, is equal to the mass of that chemical in the seawater at the previous timestep, $mC_{o,i-1}$, minus the change in mass of that chemical in the sea ice, mC_{si}, after desalination and sea ice growth. The updated mass of ocean, $m_{o,i}$, is calculated in a similar fashion, using the change in sea ice mass, m_{si}. The updated seawater concentration, $C_{o,i}$, is then the updated mass of chemical in the seawater divided by the mass of ocean. The seawater is assumed to be perfectly mixed. At the end of each timestep, the model predicts the vertically-resolved bulk ice and brine concentrations, and well-mixed concentrations in seawater for any perfectly dissolved chemical species in the ocean/sea ice system.

Supporting References

1. Xiao, H.; Li, N.; Wania, F., Compilation, evaluation, and selection of physical-chemical property data for alpha-, beta-, and gamma-hexachlorocyclohexane. In *Journal of Chemical and Engineering Data*, 2004; Vol. 49, pp 173-185.
2. Muir, D. C. G.; Teixeira, C.; Wania, F., Empirical and modeling evidence of regional atmospheric transport of current-use pesticides. *Environmental Toxicology and Chemistry* **2004,** *23* (10), 2421-2432;10.1897/03-457
3. Li, N.; Wania, F.; Lei, Y. D.; Daly, G. L., A Comprehensive and Critical Compilation, Evaluation, and Selection of Physical–Chemical Property Data for Selected Polychlorinated Biphenyls. *Journal of Physical and Chemical Reference Data* **2003,** *32* (4), 1545-1590;10.1063/1.1562632
4. Wania, F.; Dugani, C., Assessing the long-range transport potential of polybrominated diphenyl ethers: A comparison of four multimedia models. *Environmental Toxicology and Chemistry* **2003,** *22* (6), 1252-1261
5. Ni, N.; Yalkowsky, S. H., Prediction of Setschenow constants. *International Journal of Pharmaceutics* **2003,** *254* (2), 167-172;10.1016/S0378-5173(03)00008-5
6. Notz, D. Thermodynamic and Fluid-Dynamical Processes in Sea Ice (Ph.D Thesis). Ph.D, University of Cambridge, Cambridge, U.K., 2005.
7. Weast, R. C., *CRC handbook of chemistry and physics: a ready-reference book of chemical and physical data*. 52nd ed.; Chemical Rubber Co: Cleveland, Ohio, 1971.
8. Thomas, M. Brine and pressure dynamics in growing sea ice: first results from the Roland von Glasow air-sea-ice chamber. Ph.D, University of East Anglia, Norwich, U.K., 2019.
9. Rees Jones, D. W.; Worster, M. G., A physically based parameterization of gravity drainage for sea-ice modeling. *Journal of Geophysical Research: Oceans* **2014,** *119* (9), 5599-5621;10.1002/2013JC009296
10. Cox, G.; Weeks, W., Numerical simulations of the profile properties of undeformed first-year sea ice during the growth season. *Journal of Geophysical Research: Oceans* **1988,** *93* (C10), 12449-12460;10.1029/JC093iC10p12449
11. Griewank, P. J.; Notz, D., Insights into brine dynamics and sea ice desalination from a 1-D model study of gravity drainage. *Journal of Geophysical Research: Oceans* **2013,** *118* (7), 3370-3386;10.1002/jgrc.20247
12. Vancoppenolle, M.; Goosse, H.; De Montety, A.; Fichefet, T.; Tremblay, B.; Tison, J. L., Modeling brine and nutrient dynamics in Antarctic sea ice: The case of dissolved silica. *Journal of Geophysical Research: Oceans* **2010,** *115* (C2), n/a-n/a;10.1029/2009JC005369
13. Worster, M. G.; Rees Jones, D. W., Sea-ice thermodynamics and brine drainage. *Philosophical transactions. Series A, Mathematical, physical, and engineering sciences* **2015,** *373* (2045);10.1098/rsta.2014.0166

14. Notz, D.; Worster, M. G., In situ measurements of the evolution of young sea ice. *Journal of Geophysical Research: Oceans* **2008,** *113* (C3), n/a-n/a;10.1029/2007JC004333

Chapter 4

Investigating the uptake and fate of poly- and perfluoroalkylated substances (PFAS) in sea ice using an experimental sea ice chamber.

This chapter presents further data from laboratory-based experiments that were conducted in order to understand the behaviour of POPs during sea ice growth and melt. This is the first study which evaluates the vertical and phase distribution of the 'emerging' group of POPs known as PFASs

This chapter was published in the journal Environmental Science and Technology in 2021 as a research article.

The candidate's contribution was designing and conducting the experimental plans; structuring own and co-authors' ideas as a manuscript; writing the manuscript for supervisor review; co-ordinating co-author feedback; submission of manuscript.

Candidate: ..... J.garnett. *.....Date:.....22-Jul-21.....*

Mr Jack R. Garnett

Supervisor: .....

.....Date:...26-Jul-21.....

Prof. Crispin J. Halsall.

Investigating the uptake and fate of poly- and perfluoroalkylated substances (PFAS) in sea ice using an experimental sea ice chamber.

Jack Garnett[1], * Crispin Halsall[1], Max Thomas[2, 3], Odile Crabeck[2], James France[2, 4, 5], Hanna Joerss[6], Ralf Ebinghaus[6], Jan Kaiser[2], Amber Leeson[1], Peter M. Wynn[1]

1 Lancaster Environment Centre, Lancaster University, Lancaster, LA1 4YQ, UK

2 Centre for Ocean and Atmospheric Sciences, School of Environmental Sciences, University of East Anglia, Norwich, NR4 7TJ, UK

3 Department of Physics, University of Otago, Dunedin, New Zealand

4 British Antarctic Survey, High Cross, Madingley Road, Cambridge, CB3 0ET

5 Department of Earth Sciences, Royal Holloway, University of London, Egham Hill, Egham TW20 0EX, UK

6 Helmholtz-Zentrum Geesthacht Centre for Materials and Coastal Research, Max-Planck-Straße 1, 21502 Geesthacht, Germany

Email: c.halsall@lancaster.ac.uk

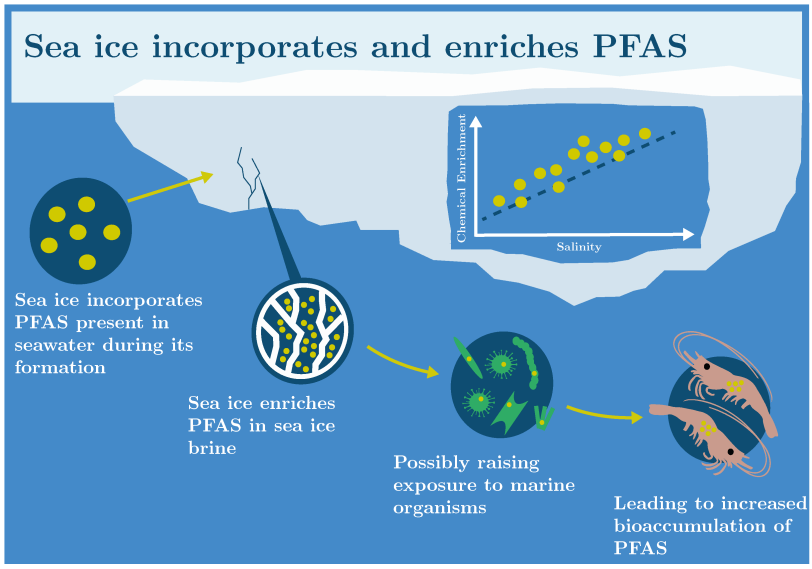

Abstract

Poly- and perfluoroalkyl substances (PFAS) are contaminants of emerging Arctic concern and are present in the marine environments of the polar regions. Their input to and fate within the marine cryosphere are poorly understood. We conducted a series of laboratory experiments to investigate the uptake, distribution and release of ten PFAS of varying carbon chain length ($C_4 - C_{12}$) in young sea ice grown from artificial sea water (NaCl solution). We show that PFAS are incorporated into bulk sea ice during ice formation and regression analyses for individual PFAS concentrations in bulk sea ice were linearly related to salinity ($r^2 = 0.30$ to 0.88, $n = 18$, $p<0.05$). This shows that their distribution is strongly governed by the presence and dynamics of brine (high salinity water) within the sea ice. Furthermore, long-chain PFAS ($C_8 - C_{12}$), were enriched in bulk ice up to 3-fold more than short-chain PFAS ($C_4 - C_7$) and NaCl. This suggests that chemical partitioning of PFAS between the different phases of sea ice also plays a role in their uptake during its formation. During sea ice melt, initial meltwater fractions were highly saline and predominantly contained short-chain PFAS, whereas the later, fresher meltwater fractions predominantly contained long-chain PFAS. Our results demonstrate that in highly saline parts of sea ice (near the upper and lower interfaces and in brine channels) significant chemical enrichment (ε) of PFAS can occur with concentrations in brine channels greatly exceeding those in sea water from which it forms (e.g. for PFOA, $\varepsilon_{\text{Brine}} = 10 \pm 4$).

This observation has implications for biological exposure to PFAS present in brine channels, a common feature of first-year sea ice which is the dominant ice type in a warming Arctic.

Keywords

PFAS; sea ice; chemical enrichment; brine; biological exposure; Arctic

Synopsis

Poly- and perfluoroalkyl substances (PFAS) are contaminants of emerging Arctic concern yet their fate and behaviour in the marine cryosphere is poorly understood. Here, laboratory experiments show that PFAS are incorporated into bulk sea ice during ice formation leading to significant chemical enrichment in brine. This has implications for biological exposure to PFAS in first-year sea ice which is the dominant ice type in a warming Arctic.

Introduction

Poly- and perfluoroalkyl substances (PFAS) are present in the Polar regions due to their long-range environmental transport (via atmosphere and ocean) and are considered "contaminants of emerging Arctic concern" (CEACs) [1-6] The chemical structure of many PFAS consist of a hydrophilic moiety (e.g. COO^-, SO_3^-) along with a hydrophobic perfluorocarbon chain backbone of varying length which complicates the understanding of their environmental behaviour and fate. Perfluoroalkyl acids (PFAA) are one major sub-group of PFAS that have received considerable regulatory attention, with 'long-chain' perfluoroalkyl carboxylic acids ($\geq C_8$, PFCA) and perfluoroalkyl sulfonic acids ($\geq C_7$, PFSA) shown to bioaccumulate more than their 'short-chain' analogues and hence pose a greater risk to higher trophic level organisms and polar marine ecosystems [7, 8].

PFAS have been observed in the sea-ice snowpack and in sea ice in the Arctic [2] indicating deposition from the atmosphere with accumulation in the snowpack, as well as possible entrainment into sea ice from sea water during sea-ice growth in winter. Several studies have also observed some organochlorine persistent organic pollutants (POPs) in young or first-year

sea ice [9-12]. Pućko et al, (2010a) measured the levels of α- and γ-HCH in first year sea ice in the Canadian Arctic and demonstrated significantly higher concentrations of these chemicals in the sea ice brine compared to under-ice seawater. Furthermore, they determined that their distribution and concentration in sea ice appears to be a function of circulating brine (a concentrated salt solution present within young sea ice). Recently, experimental studies in artificial sea ice also showed elevated levels of organic pollutants in brine and demonstrated their distribution in newly-formed bulk sea ice was primarily due to the movement of brine [13]. Furthermore, α-HCH was released at a faster rate from melting sea ice compared to less soluble chemicals (i.e. BDE-47, BDE-99), suggesting that partitioning of chemicals between internal solid ice surfaces and liquid brine was also an important process. Due to their known surface acting properties, we anticipate PFAS to display partitioning within sea ice which could result in their enrichment, presenting a motivation to undertake similar experiments to investigate their behaviour during sea ice formation and subsequent melt.

During sea-ice growth, brine convection causes most salts and other solutes to be rejected into the underlying seawater (e.g. Notz & Worster, 2008; Thomas et al., 2020). This process, referred to as gravity drainage, is the dominant process causing desalination during sea ice formation [14]. The relationship between salinity and other solutes present in sea ice is indicative of the way in which chemicals are entrained and rejected from sea ice. Salinity-normalised concentrations have been used to study the behaviour of nutrients [15], metals [16] and dissolved organic matter (DOM) [17] during sea ice formation and melt processes.

Understanding the behaviour of PFAS in growing and melting sea ice will allow better predictions of contaminant fate during winter (freeze) and spring (thaw) periods in polar marine environments, and hence the timing and extent of PFAS exposure to ice–associated biota. Undertaking process-based studies to resolve contaminant fate in natural sea ice is challenging. Therefore, we used an artificial sea-ice chamber to conduct controlled experiments to quantify chemical transfer between seawater and sea ice. We investigate the behaviour of several PFAS in sea ice during ice formation (freeze) and melt (thaw), testing the hypothesis that the uptake and distribution of PFAS (like like chloro- and bromo-POPs; see Garnett et al., 2019) in sea ice are controlled largely by the movement of brine.

2. Materials and methods

2.1. Experimental facility and conditions

The study was conducted in the Roland von Glasow Air-Sea-Ice Chamber (RvG-ASIC) at the University of East Anglia, UK [18]. The facility consists of an insulated glass-walled tank (dimensions: height: 1.2m; width 1.2m; length 2.5m) located inside a refrigerated chamber (air can be chilled). Artificial seawater was made by dissolving NaCl in deionised water to a concentration of ~35 g L^{-1} (all volume concentrations are reported for 20 °C). A submerged pump was used to continuously mix the seawater throughout each experiment and a series of digital thermometers measured the *in-situ* sea-ice temperature profile and calculate the sea ice depth. Two freeze-thaw experiments, referred to as 'Freeze–1' and 'Freeze–2' hereafter, were performed at air temperatures of –18 ± 1 °C and –35 ± 1 °C, respectively.

A range of perfluoroalkyl carboxylic acids (PFPeA, C_5; PFHxA, C_6; PFHpA, C_7; PFOA, C_8; PFNA, C_9; PFUnDA, C_{11}; and PFDoDA, C_{12}), perfluoroalkyl sulfonic acids (PFBS, C_4; PFOS, C_8), and one n:2 fluorotelomer sulfonic acid (6:2 FTSA, C_8) were utilised in this experimental study (See Table S1 – S2). An ethanolic solution containing a mix of all the PFAS (individual chemical concentrations 0.21 to 0.46 μM) were introduced into the artificial seawater before first sea ice formation to give initial concentrations in seawater of individual PFAS between 0.06 and 0.14 nM.

2.2. Sampling procedures

Prior to the commencement of Freeze–1 and the introduction of the mixed-PFAS 'spike' solution into the chilled seawater, a short period (2 days) of sea ice growth at –35 °C was undertaken to obtain preliminary procedural blanks of seawater (0.2 L; $n = 3$) and bulk ice (3.5 L; $n = 1$) to determinine background PFAS contamination associated with the sea ice chamber. Once this preliminary sea ice had melted, the mixed-PFAS 'spike' was added into the experimental tank seawater. After mixing for 24 hours, initial seawater samples for Freeze–1 (0.2 L, $n = 3$) were collected with further seawater samples taken at the beginning of Freeze–2 (0.2 L, $n = 4$) and end of Freeze–2 (0.2 L, $n = 4$) as illustrated in Figure S1. Collection of

seawater samples was always undertaken when all of the ice had melted. Seawater was sampled via a pre-installed silicone hose (internal diameter: 8 mm) with an inlet set at 0.5 m above the base of the tank to avoid interference with any forming sea ice layer. All sample containers were made of polyethylene and pre-cleaned with methanol.

Bulk sea-ice samples were collected ($n = 4$) in Freeze–1 (depth = 0.26 ± 0.01 m) and Freeze–2 (depth 0.17 ± 0.01 m) from across the tank area using techniques developed by Cottier et al., (1999) to limit brine loss. Samples were subsequently covered in polyethylene sheets and stored in a freezer (–40 °C) until further processing. Sea-ice samples were sectioned into horizontal layers (1 – 4 cm; see Table S3 – S4) using an electric band saw in a cold room (–25 °C) and transferred to individual polyethylene bags. Following melting at room temperature, sea ice samples were combined with adjacent sea ice layer samples ready for PFAS analysis. Frost flowers (0.2 L; $n = 1$) on the sea ice surface of Freeze–2 were carefully collected using a polyethylene spatula and stored in a freezer before melting for analysis.

2.3. Slow-melt experiment

An additional experiment to observe chemical dynamics during sea ice melt was conducted in order to assess chemical interactions with sea ice during thawing. Sea ice cores ($n = 8$) sampled from across the sea ice (Freeze–1) using a titanium corer (Kovacs, 75 mm I.D.) were sectioned to give a top (T) and bottom (B) section of approximate equal length (13 ± 1 cm), placed into separate polyethylene bags and melted at 0 ± 1 °C as described by Garnett et al.[13] and others [11, 19, 20 21, 22]. Meltwater fractions ($n = 8$) were then sequentially collected over a 48 h period in individual containers (0.1 – 2.5 L) and analysed separately to investigate chemical dynamics.

2.4. Chemical analysis and quality assurance

All sea ice samples were melted and the salinity of every sample was measured using a calibrated conductivity probe (Hach HQd40 logger with CDC401 probe). For PFAS, sample analysis followed established methods performed previously [23, 24]. Briefly, samples were loaded onto solid phase extraction cartridges (Oasis WAX, 3 cc, 150 mg sorbent, 30 µm particle size,

Waters, USA) with subsequent instrumental analysis performed by HPLC-MS/MS, using an HP 1100 LC system (Agilent Technologies, USA) coupled to an API 4000 triple quadrupole mass spectrometer (AB Sciex, USA). A more detailed description of the analysis can be found in the supporting information. As part of the quality assurance, we added 100 μL of a solution (20 pg μL^{-1}) containing 6 mass-labelled PFCA ($^{13}C_4$-PFBA, $^{13}C_2$-PFHxA, $^{13}C_4$-PFOA, $^{13}C_5$-PFNA, $^{13}C_2$-PFUnDA, $^{13}C_2$-PFDoDA) and 3 PFSA ($^{13}C_3$-PFBS, $^{18}O_2$-PFHxS, $^{13}C_4$-PFOS) to each sample to assess analytical performance (see Table S5). In cases where mass-labelled analogues were not available, a surrogate standard was used (see Table S5). All PFAS concentrations reported in this study were recovery-corrected. Method detection limits (MDL) were calculated as the mean of the procedural blank ($n = 4$) concentration plus 3 times its standard deviation (MDL: $\overline{c}_{\,procedural\ blank} + 3 \cdot \sigma_{\,procedural\ blank}$). Samples were not blank-corrected as PFAS levels in the blanks were low (see Table S5). Mass-balance calculations were performed as a quality control measure to assess the recovery (e.g. loss of chemical through chamber-side sorption) of individual PFAS at two key points within this study. First, the 'expected' concentrations of PFAS in the experimental tank seawater (i.e. $c_{\,expected\ seawater}$) and the 'measured' seawater concentrations 24 hours after the addition of the 'spike' solution based on the known amount of PFAS added to the experimental seawater (i.e. $c_{0\ seawater}$) were expressed as a fraction (%) to give the recovery during the experimental setup (i.e. r_{setup}). Second, the average 'measured' concentrations of PFAS in the experimental tank seawater before sea ice formation in Freeze–1 and Freeze–2 (i.e. $c_{initial\ seawater}$) were compared to the final seawater samples when all of the ice had completely melted at the end of Freeze–2 (i.e. $c_{final\ seawater}$) and expressed as a fraction (%) to show the recovery throughout the experiments (i.e. $r_{experiment}$). For more information, see Figure S1 and Table S6.

2.5. Data analysis

PFAS concentrations are used for further calculations of enrichment factors (see Table S7 – S16). However, bulk sea ice samples located at the bottom of the core were previously shown to suffer from a sampling artefact and were excluded from further calculations although concentration data are still reported (see Table S7). The method precision was given as the relative standard deviation (RSD) of initial experimental seawater samples ($n = 7$) and was

included in uncertainty analysis for each individual PFAS. Equation 1 was used to calculate enrichment factors (ε) using concentrations (per volume concentrations in melted samples) with mean initial seawater concentrations measured at the start of the experiments as the denominator (unless stated otherwise).

$$\varepsilon_{,\,\textit{(e.g. bulk ice, frost flowers etc)}} = \frac{c_{\textit{(e.g. bulk ice, frost flowers etc)}}(\mathrm{PFAS})}{c_{\textit{initial seawater}}(\mathrm{PFAS})} \qquad (1)$$

The 'conservative mixing line' (i.e. the predicted concentration of PFAS based solely on the movement of NaCl) was calculated by multiplying the $\varepsilon_{,\,\text{bulk ice}}$ for NaCl in different sea ice layer samples by the initial measured subsurface seawater concentrations for each PFAS. We also calculated salinity-normalised enrichment factors, ε_s, for each PFAS using Equation 2 where S is the salinity (g L^{-1}) in a sample. $\varepsilon_s = 1$ represents conservative behavior, with respect to salinity. $\varepsilon_s \neq 1$ denotes non-conservative behavior which corresponds to a specific depletion ($\varepsilon_s < 1$) or enrichment ($\varepsilon_s > 1$), respectively.

$$\varepsilon_{S,\,\textit{(e.g. bulk ice, frost flowers etc)}} = \frac{\varepsilon_{,\textit{(e.g. bulk ice, frost flowers etc)}}}{S_{,\,\textit{(e.g. bulk ice, frost flowers etc)}} / S_{,\,\textit{initial seawater}}} \qquad (2)$$

Statistical analyses were performed on enrichment factor data using a significance level of $\alpha = 0.05$. Normality was tested using the Shapiro-Wilk Test. Regression analyses were used to test for relationships between PFAS concentrations and bulk ice salinity. Significant differences in PFAS enrichment between groups of data were assessed applying the Welch's t-test and student paired t-test. To test for significant differences in PFAS enrichment between sea-ice layers, a one-way ANOVA test was applied followed by a Tukey post-hoc test for multiple pairwise comparisons.

3. Results and Discussion

3.1. Uptake, rejection, and distribution of PFAS in growing sea ice

Low levels of PFAS were detected in procedural blanks ensuring that the method detection limits were well below the concentrations arising from the addition of the PFAS 'spike' to the seawater (see Table S5). Initial concentrations of PFAS in experimental seawater were

comparable to those at the end of the study (see Table S6) demonstrating that PFAS loss from the chamber during the course of the experiments (e.g. vessel-side or glass-wall sorption artefacts [31]) or addition through contamination artefacts were negligible. This ensured that the experimental system and the conditions of the sea ice chamber were suitable for conducting an investigation on the chemical fate of PFAS in sea ice. Low recoveries of some of the long-chain PFAS are discussed later.

Concentrations of PFAS in the different compartments of the experimental ice system are shown in Figure 1. Bulk sea ice were highest at the ice-air and ice-seawater interfaces, giving each chemical a 'C' shape profile. Salinity showed a similar 'C' shape, which is well documented in newly-formed sea ice and develops as salt is rejected from the ice matrix into the surrounding seawater, resulting from convective overturning of brine [25]. This process, known as 'gravity drainage', is the primary mechanism of desalinisation in sea ice and governs the incorporation and distribution of many dissolved metals [26], nutrients [27] and other dissolved constituents in seawater such as dissolved organic matter [28].

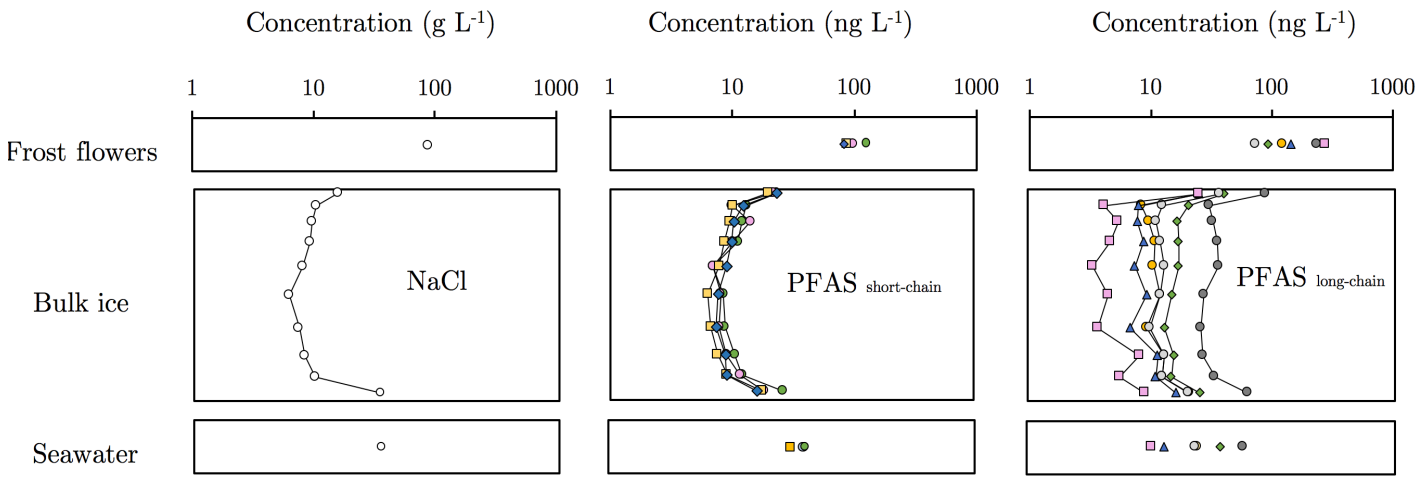

Figure 1: Measured chemical concentrations in different compartments of the experimental ice system during Freeze – 1 (NB: Frost flower data relates to Freeze – 2). A logarithmic scale was used on x-axis to allow the large range of measured concentrations to be illustrated. The y-axis on the bulk ice panel corresponds to ice depth with the upper most points corresponding to the layer of sea ice in contact with chamber air. The left, middle and right panels show NaCl, short-chain PFAS and long-chain PFAS, respectively. Short-chain PFAS include PFBS (C_4, green circle) PFPeA (C_5, pink circle) PFHxA (C_6, yellow square) and PFHpA (C_7, blue diamond). Long-chain PFAS include PFOA (C_8, green diamond), PFOS (C_8, yellow circle), PFNA(C_9, grey circle), PFUnDA (C_{11}, blue diamond) and PFDoDA (C_{12}, pink square) Although 6:2 FTSA (C_8, dark grey circle) is considered a precursor to short-chain PFAS

[29], its behavior in sea ice was more analogous to long-chain PFAS (see below) and so was grouped accordingly.

Figure 2 shows the relationship between measured concentration of PFAS and salinity in bulk ice samples collected from Freeze–1 and Freeze–2. The predicted concentration for each PFAS is also displayed (conservative mixing line). PFAS concentrations in bulk sea ice were positively correlated with salinity and regression analyses also showed that relationships were strong for short-chain PFAS (C_4 – C_7) with the data lying close to the conservative mixing line ($r^2 = 0.68 – 0.94$; $p<0.05$). Relationships for long-chain PFAS (C_8 – C_{12}) were weaker ($r^2 = 0.29 – 0.57$; $p<0.05$), but still significant and concentrations generally fell above the conservative mixing line (See SI for complete data). If the data for the two surface ice layers (uppermost ice) are removed then the correlations for the C_8 – C_{12} compounds are not significant ($p >0.05$).

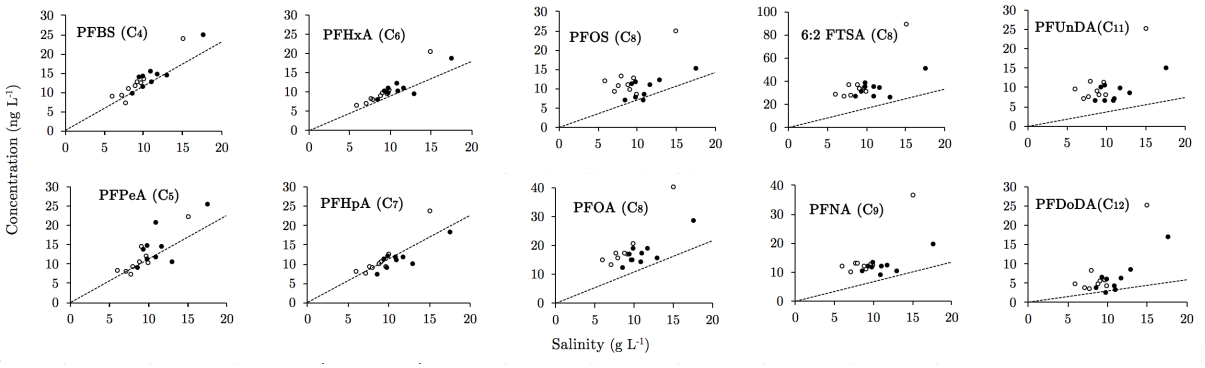

Figure 2: Concentrations of salinity (g L^{-1}) and PFAS (ng L^{-1}) in bulk ice samples. Open and closed symbols represent bulk ice samples collected from Freeze–1 (–18 °C) and Freeze–2 (–35 °C), respectively. Dashed line represents the conservative mixing line. Note that the two data points to the far right in each pane represent the surface ice layers (L1) (0-1 cm depth) in Freeze-1 and -2 experiments.

The qualitative similarities between PFAS and salinity profiles (Figure 1) combined with the quantitative agreement between the measured and conservative mixing lines (Figure 2) are strong evidence that brine dynamics determine PFAS concentrations in sea ice to a leading order. Measured concentrations of long-chain PFAS tend to be above the conservative mixing line which indicates that they are enriched in bulk sea ice by up to 3-fold (see Figure 3, upper left panel) and their chemical behaviour deviates to some extent from the behaviour of salt. This non-conservative behaviour suggests that other processes, such as diffusion within sea ice, heterogeneous ice nucleation or partitioning to solid ice surfaces, play an important role in retaining long-chain PFAS within the ice matrix.

PFAS, like most other dissolved solutes, are not expected to be incorporated within the ice crystal lattice due to their relatively large molecular size. Instead, they are incorporated in bulk sea-ice within interstitial brine channels. While studies have observed non-conservative behaviour of some dissolved organic components in sea ice [16, 28, 30, 31], little is known about the mechanisms of enrichment (i.e. $\varepsilon_s > 1$). The enrichment of dissolved organic matter (DOM) may be related to differences in the diffusion rates of chemicals, which leads to the preferential rejection of small molecules as they diffuse at relatively faster rates in ice than larger DOM molecules [27, 32]. However, rhodamine 6G (a useful dye/tracer with a molecular mass akin to PFAS) did not noticeably deviate from conservative behaviour [33]. The presence of extracellular polymeric substances (EPS) in sea ice (high molecular mass gel-like organic material that is present in brine channels) can act as a sorbent for other chemicals [34]. However, in this study artificial seawater (NaCl dissolved in ultrapure water) was used with no EPS.

Enrichment of long-chain PFAS in sea ice may also be related to elevated concentrations in the sea surface microlayer (top 1000 μm of surface ocean), a phenomenon that has been observed in the environment [35] and in experimental systems exploring enrichment of PFAS in sea spray aerosol [36, 31]. This behaviour of PFAS in the surface microlayer is likely driven by the presence of colloidal organic matter, although this is expected to have been absent in our experimental system but was not measured. Low recoveries for the long-chain PFAS (PFOA, C_8; PFOS, C_8; PFNA, C_9; PFUnDA, C_{11}; PFDoDA, C_{12}) were apparent in the seawater samples taken initially at the start of the experiment (see Table S6). Preferential partitioning of these long-chain compounds to a sea surface microlayer may then have occurred, resulting in elevated concentrations at the seawater surface where ice growth begins and thus leading to chemical enrichment in sea ice. However, the calculated concentrations of PFAS in sea ice based on the initial seawater concentrations that accounted for the unrecovered mass of PFAS using the assumption that they were transported conservatively with salt, were significantly higher (up to 50-fold) than measured concentrations in the sea ice (see Table S17 & S18). This indicates that most of the mass of PFAS that was not recovered in the initial sea water measurements was probably sorbed to the chamber surfaces (mainly glass) and hence was unlikely to play a

role in the observed PFAS enrichment in sea ice. Volatilisation of PFAS to the overlying chamber air was another possible loss process but was considered to be insignificant. Perfluoroalkyl acids have relatively high aqueous solubilities, low volatilities and exist as their anionic form in seawater at pH ~8 with negligible water to air partitioning (dimensionless Henry's Law constants, $c_{gas} \ / \ c_{water} < 0.01$)[37].

PFAS were particularly enriched in the surface layer (L1) of sea ice ($\varepsilon_{s,\,L1} > 1$) with values significantly higher (Tukey-HSD; $p<0.01$) compared to lower bulk ice layers in both Freeze–1 and Freeze–2 (see Figure 3; upper right panel). This was surprising given that solute rejection and accociated processes known to govern chemical distribution in forming sea ice are expected to occur relatively consistently throughout all stages of sea ice growth and suggests that a secondary selective process may be at play within the surface layer, or during the initial onset of sea ice formation. Garnett et al., (2019) observed relatively high concentrations for several hydrophobic POPs in surface sea ice, which were higher than those predicted using a 1D halo-dynamic model. Chemicals such as polybrominated diphenyl ethers (PBDEs) are hydrophobic and are not known, or expected, to partition to the air-water interface although have been shown to interact strongly with ice surfaces. The process of sea-ice growth begins at the surface of seawater with a layer of granular ice, proceeding with columnar ice as it thickens, as expected during both Freeze –1 and –2. Columnar ice also forms more slowly than granular ice, which proceeds through frazil ice accretion and is reported to be less effective at the rejection of impurities [25]. The higher bulk sea-ice salinities in surface sea ice layers formed when granular ice is dominant is in good agreement with these observations and may help to explain higher concentrations of PFAS in the surface bulk ice layer (L1). Alternatively, PFAS may serve play a role in heterogeneous ice nucleation during sea ice growth

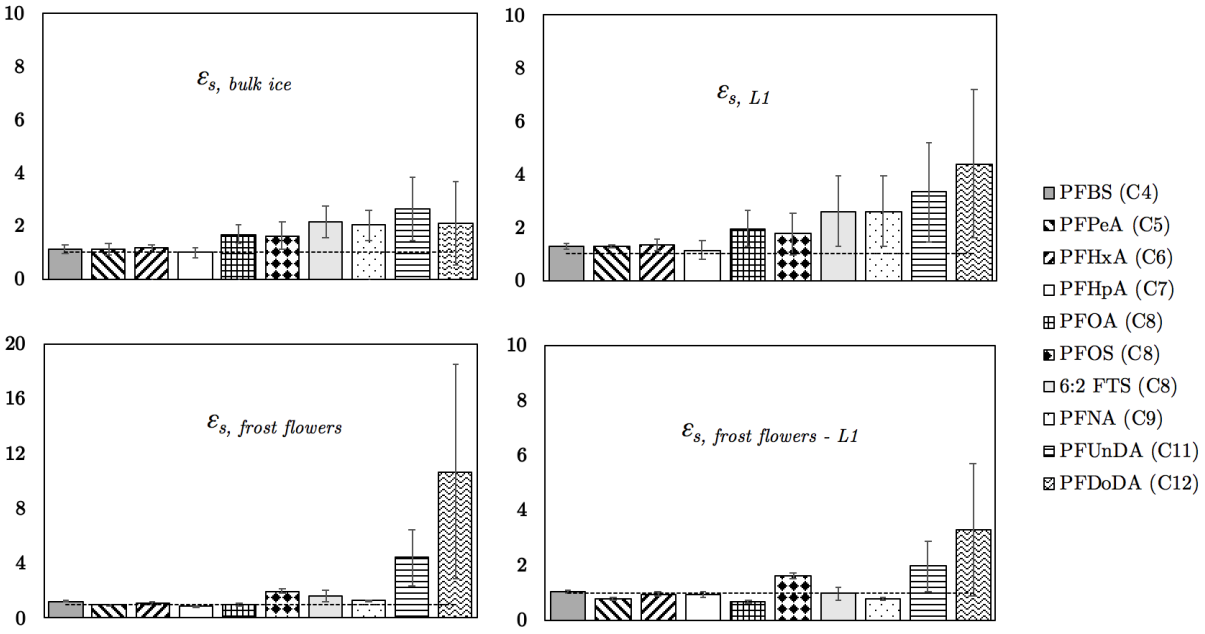

Figure 3: Salinity-normalised enrichment factors, ε_s, or key compartments of the experimental ice system. Mean values (± 1 s.d.) from Freeze–1 and Freeze–2. Calculated enrichment factors for frost flowers with surface sea ice layer (L1) were performed using samples taken during Freeze–2. Horizontal dashed line represents $\varepsilon_s = 1$.

We collected frost flowers during Freeze–2 which showed high concentrations with significant enrichment of PFAS, relative to the initial seawater concentrations ($\varepsilon_{,\ frost\ flowers} = 2 - 27$; see Table S7 – S8). Frost flowers are highly saline ice structures that develop under extreme cold, calm atmospheric conditions [38]. Brine and other solutes are 'wicked' from the surface layer (1 – 2 mm) by capillarity and concentrated on the ice structure. The presence of PFAS in frost flowers suggests they are also transported with brine. However, $\varepsilon_{s,\ frost\ flowers} > 1$ (up to 11) also indicates that other processes may contribute to the enrichment of PFAS in frost flowers (see Figure 3; bottom left panel). Garnett et al. (2019) saw a similar enrichment for a number of hydrophobic semi-volatile organic chemicals and postulated that their enrichment was due to evaporation and subsequent condensation on the frost flower ice crystal structure [39]. This study investigated perfluoroalkyl acids, which in their conjugate base form are effectively non-volatile and therefore evaporation is highly unlikely to play a role in the observed enrichment in frost flowers. Enrichment factors for PFAS in frost flowers were calculated in relation to the surface sea ice layer (L1) which is known to be the source of NaCl (and other solutes) in frost flowers

as sea ice grows [33]. Values of $\varepsilon_{s,\ frost\ flowers\ -\ L1}$ were much closer to 1 (Figure 3, lower right panel) which suggests the absence of a secondary fractionation mechanism that leads to significant enrichment specifically in frost flowers. Nonetheless, this result along with the high concentration of long-chain PFAS in frost flowers signify that PFAS concentrations at the air-ice interface are likely to be much higher than those measured in the surface bulk ice layer sample we collected during Freeze – 2 (L1 sample depth ~10mm). While the sample of frost flowers we collected is preliminary ($n = 1$), we highlight that these covered a large area of the sea ice in Freeze–2 (approximately 0.3 m^2). We therefore believe that high concentrations of long-chain PFAS in frost flowers is evidence that chemical sorption to ice surfaces plays a role in their enrichment (discussed further in Section 3.2). PFAS decoupling from convecting brine in this way could increase bulk sea-ice PFAS concentrations by preventing their rejection through gravity brine drainage. This does, however, demonstrate that our current understanding of the processes controlling chemical uptake during sea ice formation remains incomplete.

3.2. Rejection of PFAS during sea ice melt

The slow-melt experiment was designed to investigate chemical dynamics of PFAS during controlled sea-ice melt [22]. The volumes of collected meltwater fractions varied from 0.2 – 2.5 L and displayed a wide range in salinity (2 – 58 g L^{-1}). Initial meltwater fractions were more saline and contained higher concentrations of short-chain PFAS than later meltwater fractions. In contrast, higher concentrations of long-chain PFAS were associated with the later meltwater fractions that were less saline. The total amount of NaCl and individual PFAS in the combined slow-melt samples were used to derive enrichment factors in each of the meltwater fractions (See Tables S13 – S16). Short- and long-chain PFAS displayed $\varepsilon_{s,\ meltwater}$ values that were ~1 and >1, respectively (Figure 4). This shows that short-chain PFAS (C_4 – C_7) were mainly 'eluted' in the first meltwater fractions and so behaved conservatively with respect to NaCl. Conversely, long-chain PFAS (C_8 – C_{12}) showed non-conservative behaviour and were preferentially retained in the melting ice being released in later meltwater fractions.

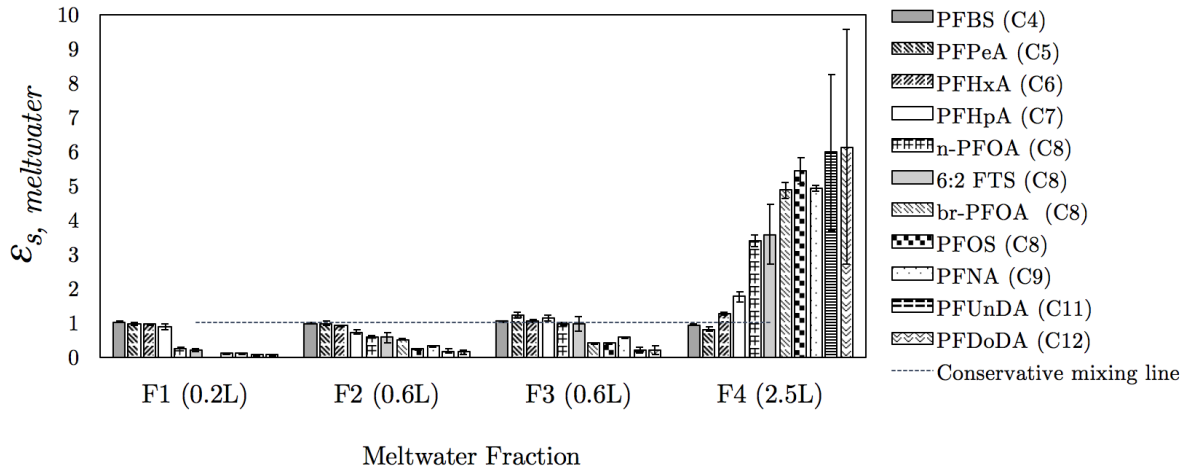

Figure 4: Salinity-normalised enrichment factors for PFAS in meltwater fractions, $\varepsilon_{s,\ meltwater}$, from melting sea ice. Linear (n-PFOA) and branched (br-PFOA) isomers of PFOA were included in this analysis. Dashed line is the conservative mixing line.

Sea ice is composed of a solid (fresh ice matrix) and liquid (brine) phases. The distribution of the PFAS between these two phases at equilibrium is expected to vary according to carbon chain length [40]. Long-chain PFAS have, in general, been found to partition more towards solid phases in sediments [23] and in snow [40, 41]. Our results suggest PFAS behave analogously in sea ice and indicate that long-chain PFAS preferentially partition to solid ice surfaces, relative to short-chain PFAS. These findings are also supported by previous studies in sea ice which display similar findings for hydrophobic POPs of varying molecular mass and aqueous solubility [13]. Partitioning of PFAS to ice surfaces can be linked to hydrophobic interactions, which increase with carbon chain length. Interestingly, differences were also observed between PFAS with the same carbon chain length (e.g. 6:2 FTSA, PFOS and PFOA) which shows that other physico-chemical properties also control the their behaviour in sea ice, such as the number of fluorine atoms and different functional groups. Based on the evidence we provide here, we believe it is reasonable to assume that the non-conservative behaviour of long-chain PFAS, specifically their enrichment, is related to their tendency to interact with and partition to ice surfaces. The similarity in enrichment behaviour of some PFAS (e.g. 6:2 FTSA) with those that have already received global regulatory attention (e.g. PFOS) should caution policy makers to develop better strategies for grouping PFAS to protect human and environmental health [42].

3.3. Environmental implications

Given the propensity of PFAS and other organic chemicals to sorb to ice surfaces, as indicated in the slow-melt experiment, it is possible that chemical partitioning to frazil ice during the onset of ice formation may be an important process controlling the uptake of dissolved chemicals into bulk sea ice. This may help explain why the enrichment of PFAS in the uppermost ice layers was significantly higher compared to the lower ice layers. Moreover, this is also supported by significantly higher enrichment factors (paired student t-test, $p<0.001$) in the surface layer of ice during Freeze–1, which formed at a slower rate due to a warmer ambient temperature (–18 °C), compared to Freeze-2 (–35 °C). This slower ice formation will have increased the contact time between ice cyrstals and PFAS during the initial ice growth stages of the experiment and this 'concentrating effect' has been observed for organic matter [43] and other components in seawater such as algae [44].

The results demonstrate that PFAS are incorporated within sea ice during its formation and long-chain PFAS can be enriched relative to salt (NaCl) as well as short-chain PFAS. However, PFAS are included within the ice-brine network (i.e. distributed between sorbed internal ice walls and dissolved in brine) of sea ice, which represents a much smaller volume fraction of the total bulk sea ice. The salinity of ice-brine is governed by thermodynamic phase-changes, fluctuating in the environment according to diurnal and seasonal temperature changes (e.g. as temperatures decrease in sea ice brine salinity increases). Sea ice is considered to be porous when the brine volume fraction (V_b) reaches 5 % [45]. Above 5 % brine volume, ice-associated (sympagic) organisms can thrive in the brine network commonly observed on the underside of ice floes. Based on this, we performed a simple calculation ($\varepsilon_{,\ bulk\ ice}$ divided by 0.05) to estimate the enrichment of PFAS for the *in-situ* sea ice brine ($\varepsilon_{,\ brine}$) and so assess the likely chemical exposure presented to brine-dwelling organisms. This approach indicates that the sympagic community may be exposed to individual PFAS concentrations that are more than an order of magnitude greater (e.g. for PFOA, $\varepsilon_{,\ \mathrm{Brine}} = 10 \pm 4$) than those present in seawater (see Table S19). This demonstrates that enrichment in sea ice brine is likely to be a significant exposure pathway to an array of organisms situated at the base of the marine food web thereby

exacerbating bioaccumulation of toxic contaminants particularly in brine-rich single season ice.

In the Arctic and other regions where sea ice is prevalent, the total burden of PFAS in sea ice will be a function of the many different PFAS present in surface seawater, but also that which is deposited from the atmosphere through snowfall and other depositional processes. Furthermore, natural sea ice is subject to various freeze-thaw cycles which could transfer organic chemical pollutants between the ice-rafted snowpack and sea ice in winter and during seasonal thaw [11, 12, 46-49]. The very high enrichment of PFAS observed in a frost flower sample (present at the ice-atmosphere interface) is intriguing and also raises implications for ice surfaces serving as an aerosol-driven source of PFAS to the local or regional atmosphere [36]. More controlled experiments, together with careful observational studies in the field, are now required to understand these complex yet potentially important processes, particularly with regard to chemical exposure to organisms at the base of the marine foodweb.

Supporting Information. List of target PFAS and details of analytical methods; quality assurance criteria with concentration data and accociated equations are supplied as Supporting Information (SI).

Acknowledgements

JG's PhD (NE/L002604/1) was funded through NERC's ENVISION Doctoral Training Centre. This work resulted from the EISPAC project (NE/R012857/1), part of the Changing Arctic Ocean programme, jointly funded by the UKRI Natural Environment Research Council (NERC) and the German Federal Ministry of Education and Research (BMBF). The authors are grateful to the British Antarctic Survey for providing funding (British Antarctic Survey Collaboration Voucher) to cover the running costs of the RvG-ASIC facility for the duration of the experimental period. This work has received funding from the European Union's Horizon 2020 research and innovation programme through the EUROCHAMP-2020 Infrastructure Activity under grant agreement No 730997. The authors would also like to thank the two anonymous reviewers whose insightful comments helped improve this manuscript.

4. References

1. AMAP *AMAP Assessment 2016: Chemicals of Emerging Arctic Concern*; -; -: Oslo, Norway, -, 2017; p 353.https://www.amap.no/documents/doc/AMAP-Assessment-2016-Chemicals-of-Emerging-Arctic-Concern/1624

2. Cai, M.; Zhao, Z.; Yin, Z.; Ahrens, L.; Huang, P.; Cai, M.; Yang, H.; He, J.; Sturm, R.; Ebinghaus, R.; Xie, Z., Occurrence of Perfluoroalkyl Compounds in Surface Waters from the North Pacific to the Arctic Ocean. *Environmental Science & Technology* **2012,** *46* (2), 661-668;10.1021/es2026278

3. Casal, P.; Zhang, Y.; Martin, J. W.; Pizarro, M.; Jiménez, B.; Dachs, J., Role of Snow Deposition of Perfluoroalkylated Substances at Coastal Livingston Island (Maritime Antarctica). *Environmental science & technology* **2017,** *51* (15), 8460;10.1021/acs.est.7b02521

4. Pickard, H. M.; Criscitiello, A. S.; Persaud, D.; Spencer, C.; Muir, D. C. G.; Lehnherr, I.; Sharp, M. J.; De Silva, A. O.; Young, C. J., Ice Core Record of Persistent Short-Chain Fluorinated Alkyl Acids: Evidence of the Impact From Global Environmental Regulations. *Geophysical Research Letters* **2020,** *47* (10), e2020GL087535;10.1029/2020GL087535

5. Pickard, H. M.; Criscitiello, A. S.; Spencer, C.; Sharp, M. J.; Muir, D. C. G.; De Silva, A. O.; Young, C. J., Continuous non-marine inputs of per- and polyfluoroalkyl substances to the High Arctic: a multi-decadal temporal record. *Atmos. Chem. Phys.* **2018,** *18* (7), 5045-5058;10.5194/acp-18-5045-2018

6. Muir, D.; Bossi, R.; Carlsson, P.; Evans, M.; De Silva, A.; Halsall, C.; Rauert, C.; Herzke, D.; Hung, H.; Letcher, R.; Rigét, F.; Roos, A., Levels and trends of poly- and perfluoroalkyl substances in the Arctic environment – An update. *Emerging Contaminants* **2019,** *5*, 240-271;https://doi.org/10.1016/j.emcon.2019.06.002

7. Tartu, S.; Gabrielsen, G. W.; Blévin, P.; Ellis, H.; Bustnes, J. O.; Herzke, D.; Chastel, O., Endocrine and Fitness Correlates of Long-Chain Perfluorinated Carboxylates Exposure in Arctic Breeding Black-Legged Kittiwakes. *Environmental Science & Technology* **2014,** *48* (22), 13504-13510;10.1021/es503297n

8. Haukås, M.; Berger, U.; Hop, H.; Gulliksen, B.; Gabrielsen, G. W., Bioaccumulation of per- and polyfluorinated alkyl substances (PFAS) in selected species from the Barents Sea food web. *Environmental Pollution* **2007,** *148* (1), 360-371;https://doi.org/10.1016/j.envpol.2006.09.021

9. Hargrave, B. T.; Vass, W. P.; Erickson, P. E.; Fowler, B. R., Atmospheric transport of organochlorines to the Arctic Ocean. *Tellus B: Chemical and Physical Meteorology* **1988,** *40* (5), 480-493;10.3402/tellusb.v40i5.16015

10. Gustafsson, Ö.; Andersson, P.; Axelman, J.; Bucheli, T. D.; Kömp, P.; McLachlan, M. S.; Sobek, A.; Thörngren, J. O., Observations of the PCB distribution

within and in-between ice, snow, ice-rafted debris, ice-interstitial water, and seawater in the Barents Sea marginal ice zone and the North Pole area. *Science of the Total Environment* **2005,** *342* (1-3), 261-279;10.1016/j.scitotenv.2004.12.044

11. Pućko, M.; Stern, G.; Macdonald, R. W.; Barber, D. G., alpha- and gamma-Hexachlorocyclohexane Measurements in the Brine Fraction of Sea Ice in the Canadian High Arctic Using a Sump-Hole Technique. *Environmental Science & Technology* **2010,** *44* (24), 9258-9264;10.1021/es102275b

12. Pućko, M.; Stern, G. A.; Barber, D. G.; Macdonald, R. W.; Rosenberg, B., The international polar year (IPY) circumpolar flaw lead (CFL) system study: The importance of brine processes for α- and γ-hexachlorocyclohexane (HCH) accumulation or rejection in sea ice. *Atmosphere-Ocean* **2010,** *48* (4), 244-262;10.3137/OC318.2010

13. Garnett, J.; Halsall, C.; Thomas, M.; France, J.; Kaiser, J.; Graf, C.; Leeson, A.; Wynn, P., Mechanistic Insight into the Uptake and Fate of Persistent Organic Pollutants in Sea Ice. *Environmental science & technology* **2019,** *53* (12), 6757;10.1021/acs.est.9b00967

14. Notz, D.; Worster, M. G., Desalination processes of sea ice revisited. *Journal of Geophysical Research: Oceans* **2009,** *114* (C5), n/a-n/a;10.1029/2008JC004885

15. Lannuzel, D.; Chever, F.; van der Merwe, P. C.; Janssens, J.; Roukaerts, A.; Cavagna, A.-J.; Townsend, A. T.; Bowie, A. R.; Meiners, K. M., Iron biogeochemistry in Antarctic pack ice during SIPEX-2. *Deep Sea Research Part II: Topical Studies in Oceanography* **2016,** *131*, 111-122;https://doi.org/10.1016/j.dsr2.2014.12.003

16. Janssens, J.; Meiners, K. M.; Tison, J.-L.; Dieckmann, G.; Delille, B.; Lannuzel, D., Incorporation of iron and organic matter into young Antarctic sea ice during its initial growth stages.(Report). *Elementa: Science of the Anthropocene* **2016,** *4* (3);10.12952/journal.elementa.000123

17. Zhou, J.; Delille, B.; Kaartokallio, H.; Kattner, G.; Kuosa, H.; Tison, J. L.; Autio, R.; Dieckmann, G. S.; Evers, K. U.; Jørgensen, L.; Kennedy, H.; Kotovitch, M.; Luhtanen, A. M.; Stedmon, C. A.; Thomas, D. N., Physical and bacterial controls on inorganic nutrients and dissolved organic carbon during a sea ice growth and decay experiment. *Marine Chemistry* **2014,** *166* (C), 59-69;10.1016/j.marchem.2014.09.013

18. Thomas, M.; France, J.; Crabeck, O.; Hall, B.; Hof, V.; Notz, D.; Rampai, T.; Riemenschneider, L.; Tooth, O. J.; Tranter, M.; Kaiser, J., The Roland von Glasow Air-Sea-Ice Chamber (RvG-ASIC): an experimental facility for studying ocean–sea-ice–atmosphere interactions. *Atmos. Meas. Tech.* **2021,** *14* (3), 1833-1849;10.5194/amt-14-1833-2021

19. Fripiat, F.; Cardinal, D.; Tison, J. L.; Worby, A.; André, L., Diatom-induced silicon isotopic fractionation in Antarctic sea ice. *Journal of Geophysical Research: Biogeosciences* **2007,** *112* (G2), n/a-n/a;10.1029/2006JG000244

20. Nomura, D.; Takatsuka, T.; Ishikawa, M.; Kawamura, T.; Shirasawa, K.; Yoshikawa-Inoue, H., Transport of chemical components in sea ice and under-ice water

during melting in the seasonally ice-covered Saroma-ko Lagoon, Hokkaido, Japan. *Estuarine, Coastal and Shelf Science* **2009,** *81* (2), 201-209;10.1016/j.ecss.2008.10.012
21. Fripiat, F.; Sigman, D. M.; Fawcett, S. E.; Rafter, P. A.; Weigand, M. A.; Tison, J. L., New insights into sea ice nitrogen biogeochemical dynamics from the nitrogen isotopes. *Global Biogeochemical Cycles* **2014,** *28* (2), 115-130;10.1002/2013GB004729
22. Miller, L.; Fripiat, F.; Else, B.; Bowman, J.; Brown, K.; Collins, R.; Ewert, M.; Fransson, A.; Gosselin, M.; Lannuzel, D.; Meiners, K.; Michel, C.; Nishioka, J.; Nomura, D.; Papadimitriou, S.; Russell, L.; Sørensen, L.; Thomas, D.; Tison, J., Methods for biogeochemical studies of sea ice: The state of the art, caveats, and recommendations. **2015**,
23. Joerss, H.; Apel, C.; Ebinghaus, R., Emerging per- and polyfluoroalkyl substances (PFASs) in surface water and sediment of the North and Baltic Seas. *Science of The Total Environment* **2019,** *686*, 360-369;https://doi.org/10.1016/j.scitotenv.2019.05.363
24. Joerss, H.; Xie, Z.; Wagner, C. C.; von Appen, W.-J.; Sunderland, E. M.; Ebinghaus, R., Transport of Legacy Perfluoroalkyl Substances and the Replacement Compound HFPO-DA through the Atlantic Gateway to the Arctic Ocean—Is the Arctic a Sink or a Source? *Environmental Science & Technology* **2020**;10.1021/acs.est.0c00228
25. Petrich, C. E., Hajo, Overview of sea ice growth and properties. In *Sea ice (Third Edition)*, Third ed.; John Wiley & Sons: Chichester, U.K., 2017; pp 1-41.
26. Lannuzel, D.; Bowie, A. R.; van Der Merwe, P. C.; Townsend, A. T.; Schoemann, V., Distribution of dissolved and particulate metals in Antarctic sea ice. *Marine Chemistry* **2011,** *124* (1), 134-146;10.1016/j.marchem.2011.01.004
27. Vancoppenolle, M.; Goosse, H.; de Montety, A.; Fichefet, T.; Tremblay, B.; Tison, J.-L., Modeling brine and nutrient dynamics in Antarctic sea ice: The case of dissolved silica. *Journal of Geophysical Research: Oceans* **2010,** *115* (C2);10.1029/2009JC005369
28. Müller, S.; Vähätalo, A. V.; Stedmon, C. A.; Granskog, M. A.; Norman, L.; Aslam, S. N.; Underwood, G. J. C.; Dieckmann, G. S.; Thomas, D. N., Selective incorporation of dissolved organic matter (DOM) during sea ice formation. *Marine Chemistry* **2013,** *155*, 148-157;https://doi.org/10.1016/j.marchem.2013.06.008
29. Buck, R. C.; Franklin, J.; Berger, U.; Conder, J. M.; Cousins, I. T.; de Voogt, P.; Jensen, A. A.; Kannan, K.; Mabury, S. A.; van Leeuwen, S. P. J., Perfluoroalkyl and polyfluoroalkyl substances in the environment: Terminology, classification, and origins. *Integr Environ Assess Manag* **2011,** *7* (4), 513-541;10.1002/ieam.258
30. Giannelli, V.; Thomas, D. N.; Haas, C.; Kattner, G.; Kennedy, H.; Dieckmann, G. S., Behaviour of dissolved organic matter and inorganic nutrients

during experimental sea-ice formation. *Annals of Glaciology* **2001,** *33*, 317-321;10.3189/172756401781818572
31. Müller, S.; Vähätalo, A. V.; Granskog, M. A.; Autio, R.; Kaartokallio, H., Behaviour of dissolved organic matter during formation of natural and artificially grown Baltic Sea ice. *Annals of Glaciology* **2011,** *52* (57), 233-241;10.3189/172756411795931886
32. Granskog, M. A.; Virkkunen, K.; Thomas, D. N.; Ehn, J.; Kola, H.; Martma, T., Chemical properties of brackish water ice in the Bothnian Bay, the Baltic Sea. *Journal of Glaciology* **2004,** *50* (169), 292-302;10.3189/172756504781830079
33. Thomas, M.; Vancoppenolle, M.; France, J. L.; Sturges, W. T.; Bakker, D. C. E.; Kaiser, J.; von Glasow, R., Tracer Measurements in Growing Sea Ice Support Convective Gravity Drainage Parameterizations. *Journal of Geophysical Research: Oceans* **2020,** *125* (2), e2019JC015791;10.1029/2019JC015791
34. Krembs, C.; Eicken, H.; Deming, J. W., Exopolymer alteration of physical properties of sea ice and implications for ice habitability and biogeochemistry in a warmer Arctic. *Proceedings of the National Academy of Sciences* **2011,** *108* (9), 3653;10.1073/pnas.1100701108
35. Ju, X.; Jin, Y.; Sasaki, K.; Saito, N., Perfluorinated Surfactants in Surface, Subsurface Water and Microlayer from Dalian Coastal Waters in China. *Environmental Science & Technology* **2008,** *42* (10), 3538-3542;10.1021/es703006d
36. Johansson, J. H.; Salter, M. E.; Acosta Navarro, J. C.; Leck, C.; Nilsson, E. D.; Cousins, I. T., Global transport of perfluoroalkyl acids via sea spray aerosol. *Environmental science. Processes & impacts* **2019,** *21* (4), 635;10.1039/c8em00525g
37. Li, H.; Ellis, D.; Mackay, D., Measurement of Low Air—Water Partition Coefficients of Organic Acids by Evaporation from a Water Surface. *Journal of Chemical & Engineering Data* **2007,** *52* (5), 1580-1584;10.1021/je600556d
38. Style, R. W.; Worster, M. G., Frost flower formation on sea ice and lake ice. *Geophysical Research Letters* **2009,** *36* (11);10.1029/2009GL037304
39. Douglas, T. A.; Domine, F.; Barret, M.; Anastasio, C.; Beine, H. J.; Bottenheim, J.; Grannas, A.; Houdier, S.; Netcheva, S.; Rowland, G.; Staebler, R.; Steffen, A., Frost flowers growing in the Arctic ocean-atmosphere–sea ice–snow interface: 1. Chemical composition. *Journal of Geophysical Research: Atmospheres* **2012,** *117* (D14), n/a-n/a;10.1029/2011JD016460
40. Meyer, T.; Lei, Y.; Muradi, I.; Wania, F., Organic Contaminant Release from Melting Snow. 1. Influence of Chemical Partitioning. *Environmental Science & Technology* **2009,** *43* (3), 657;10.1021/es8020217
41. Meyer, T.; Lei, Y.; Muradi, I.; Wania, F., Organic Contaminant Release from Melting Snow. 2. Influence of Snow Pack and Melt Characteristics. *Environmental Science & Technology* **2009,** *43* (3), 663;10.1021/es8020233
42. Cousins, I. T.; DeWitt, J. C.; Glüge, J.; Goldenman, G.; Herzke, D.; Lohmann, R.; Miller, M.; Ng, C. A.; Scheringer, M.; Vierke, L.; Wang, Z., Strategies

for grouping per- and polyfluoroalkyl substances (PFAS) to protect human and environmental health. *Environmental Science: Processes & Impacts* **2020,** *22* (7), 1444-1460;10.1039/D0EM00147C

43. Reimnitz, E.; Clayton, J. R.; Kempema, E. W.; Payne, J. R.; Weber, W. S., Interaction of rising frazil with suspended particles: tank experiments with applications to nature. *Cold Regions Science and Technology* **1993,** *21* (2), 117-135;https://doi.org/10.1016/0165-232X(93)90002-P

44. Garrison, D. L.; Close, A. R.; Reimnitz, E., Algae concentrated by frazil ice: evidence from laboratory experiments and field measurements. *Antarctic Science* **1989,** *1* (4), 313-316;10.1017/S0954102089000477

45. Golden; Ackley; Lytle, The percolation phase transition in sea Ice. *Science (New York, N.Y.)* **1998,** *282* (5397), 2238;10.1126/science.282.5397.2238

46. Pućko, M.; Stern, G. A.; Barber, D. G.; Macdonald, R. W.; Warner, K. A.; Fuchs, C., Mechanisms and implications of α-HCH enrichment in melt pond water on Arctic sea ice. *Environmental Science & Technology* **2012,** *46* (21), 11862;10.1021/es303039f

47. Pućko, M.; Stern, G. A.; Burt, A. E.; Jantunen, L. M.; Bidleman, T. F.; Macdonald, R. W.; Barber, D. G.; Geilfus, N.-X.; Rysgaard, S., Current use pesticide and legacy organochlorine pesticide dynamics at the ocean-sea ice-atmosphere interface in resolute passage, Canadian Arctic, during winter-summer transition. *Science of the Total Environment* **2017,** *580*, 1460-1469;10.1016/j.scitotenv.2016.12.122

48. Pućko, M.; Stern, G. A.; Macdonald, R. W.; Jantunen, L. M.; Bidleman, T. F.; Wong, F.; Barber, D. G.; Rysgaard, S., The delivery of organic contaminants to the Arctic food web: Why sea ice matters. *Science of the Total Environment* **2015,** *506-507*, 444-452;10.1016/j.scitotenv.2014.11.040

49. Pućko, M.; Stern, G. A.; Macdonald, R. W.; Rosenberg, B.; Barber, D. G., The influence of the atmosphere-snow-ice-ocean interactions on the levels of hexachlorocyclohexanes in the Arctic cryosphere. *Journal of Geophysical Research: Oceans* **2011,** *116* (C2), n/a-n/a;10.1029/2010JC006614

Supporting Information to:

Investigating the uptake and fate of poly- and perfluoroalkylated substances (PFAS) in sea ice using an experimental sea ice chamber.

Jack Garnett[1], Crispin Halsall *[1], Max Thomas[2, 3], Odile Crabeck[2], James France[2, 4, 5], Hanna Joerss[6], Ralf Ebinghaus[6], Jan Kaiser[2], Amber Leeson[1], Peter M. Wynn[1]

1 Lancaster Environment Centre, Lancaster University, Lancaster, LA1 4YQ, UK

2 Centre for Ocean and Atmospheric Sciences, School of Environmental Sciences, University of East Anglia, Norwich, NR4 7TJ, UK

3 Department of Physics, University of Otago, Dunedin, NZ 9054, New Zealand

4 British Antarctic Survey, High Cross, Madingley Road, Cambridge, CB3 0ET, UK

5 Department of Earth Sciences, Royal Holloway, University of London, Egham Hill, Egham TW20 0EX, UK

6 Helmholtz-Zentrum Geesthacht Centre for Materials and Coastal Research, Max-Planck-Straße 1, 21502 Geesthacht, Germany

Email: c.halsall@lancaster.ac.uk

Contents include:

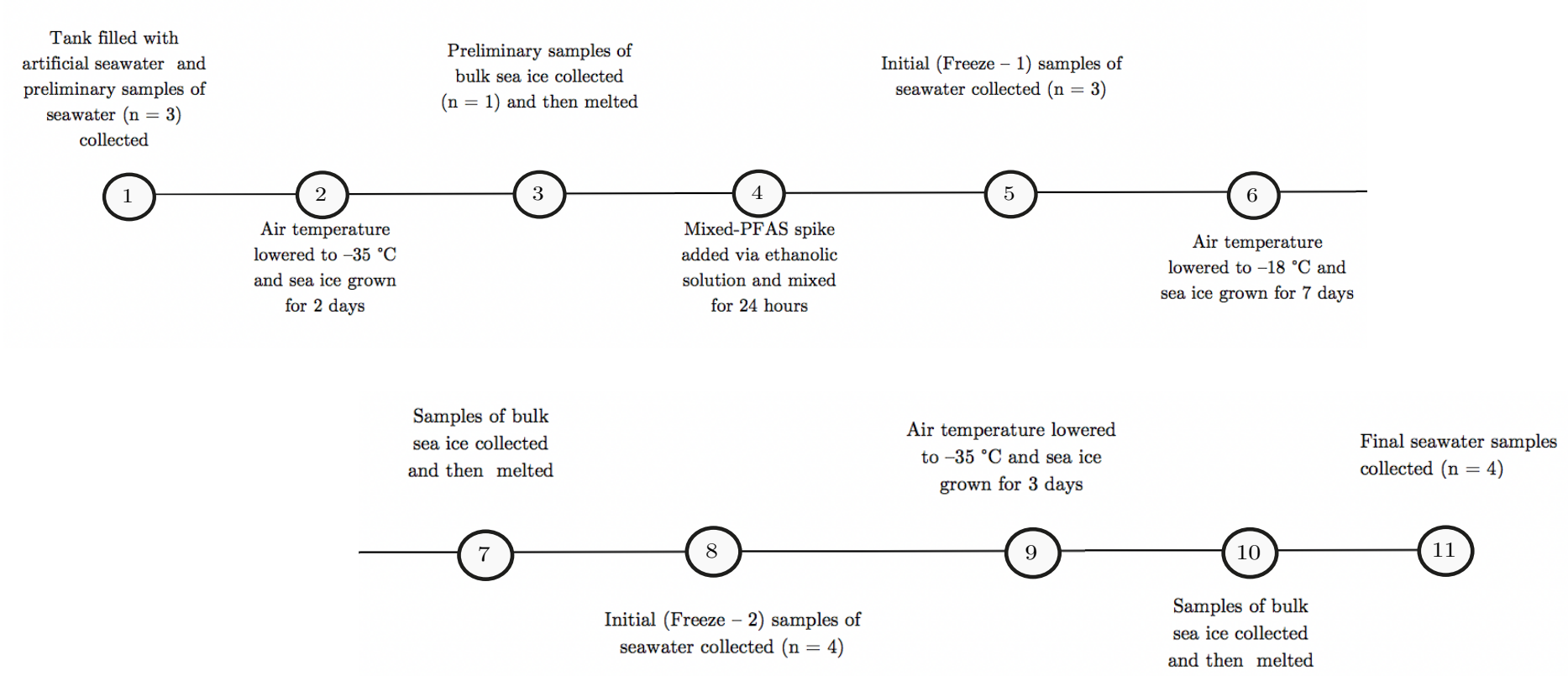

Figure S1: Timeline indicating the key steps (1 – 11) involved in the experiment including the experimental setup and the sampling points. Seawater samples collected at step 5 correspond to $c_{0\ seawater}$. Seawater samples collected at step 5 and step 8 correspond to $c_{initial\ seawater}$ (average concentrations at step 5 and step 8 were statistically indistinguishable; student t-test, $p>0.05$). Seawater samples collected at step 11 correspond to $c_{final\ seawater}$.

Table S1: Poly- and perfluoroalkyated substances (PFAS) used in experimental study and their respective concentrations.

PFAS acronym (Carbon chain length)	PFAS	Relative molecular mass	Spike concentration c_{spike} / μM	Expected initial seawater concentrations in tank $c_{\text{expected seawater}}$ / nM
PFBS (C_4)	perfluoro-*n*-butanesulfonate	300.1	0.5	0.14
PFPeA (C_5)	perfluoro-*n*-pentanoic acid	264.0	0.5	0.13
PFHxA (C_6)	perfluoro-*n*-hexanoic acid	314.1	0.4	0.11
PFHpA (C_7)	perfluoro-*n*-heptanoic acid	364.1	0.3	0.10
PFOA (C_8)	perfluoro-*n*-octanoic acid	414.1	0.4	0.11
PFOS (C_8)	perfluoro-*n*-octanesulfonate	500.1	0.2	0.07
6:2 FTSA (C_8)	6:2 fluorotelomer sulfonate	428.2	0.3	0.08
PFNA (C_9)	perfluoro-*n*-nonanoic acid	464.1	0.3	0.08
PFUnDA (C_{11})	perfluoro-*n*-undecanoic acid	564.1	0.2	0.07
PFDoDA (C_{12})	perfluoro-*n*-dodecanoic acid	614.1	0.2	0.06

PFAS were introduced into the experimental tank via a mixed-chemical ('spike') solution made up in 1 litre of pure ethanol. The spike solution presented a negligible volume fraction in the experimental tank of approximately 3×10^{-4}.

Table S2: Overview of analytical standards, CAS numbers, the standard suppliers, purity and concentration/amount

Acronym	Analytical standard	CAS number	Supplier, purity and concentration
PFPeA	perfluoro-*n*-pentanoic acid	2706-90-3 (acid)	PFC-MXA (mixture) Wellington Laboratories, $>$ 98 % 2.0 µg/mL ± 5 % of the single compounds
PFHxA	perfluoro-*n*-hexanoic acid	307-24-4 (acid)	
PFHpA	perfluoro-*n*-heptanoic acid	375-85-9 (acid)	
PFOA	perfluoro-*n*-octanoic acid	335-67-1 (acid)	
PFNA	perfluoro-*n*-nonanoic acid	375-95-1 (acid)	
PFUnDA	perfluoro-*n*-undecanoic acid	2058-94-8 (acid)	
PFDoDA	perfluoro-*n*-dodecanoic acid	307-55-1 (acid)	
PFBS	potassium perfluoro-*n*-butanesulfonate	29420-49-3 (K+ salt) 375-73-5 (acid)	PFS-MXA (mixture) Wellington Laboratories, $>$ 98 % 2.0 µg/mL ± 5 % of the single compounds
PFOS	sodium perfluoro-*n*-octanesulfonate	4021-47-0 (Na+ salt) 1763-23-1 (acid)	
$^{13}C_4$-PFBA	perfluoro-*n*-[$^{13}C_4$]-butanoic acid	-	MPFAC-MXA (mixture) Wellington Laboratories
$^{13}C_2$-PFHxA	perfluoro-*n*-[1,2-$^{13}C_2$]-hexanoic acid	-	
$^{13}C_4$-PFOA	perfluoro-*n*-[1,2,3,4-$^{13}C_4$]-octanoic acid	-	
$^{13}C_5$-PFNA	perfluoro-*n*-[1,2,3,4,5-$^{13}C_5$]-nonanoic acid	-	
$^{13}C_2$-PFDA	perfluoro-*n*-[1,2-$^{13}C_2$]-decanoic acid	-	
$^{13}C_2$-PFUnDA	perfluoro-*n*-[1,2-$^{13}C_2$]-undecanoic acid	-	
$^{13}C_2$-PFDoDA	perfluoro-*n*-[1,2-$^{13}C_2$]-dodecanoic acid	-	
$^{18}O_2$-PFHxS	sodium perfluorohexane-*n*-[$^{18}O_2$]-sulfonate	-	
$^{13}C_4$-PFOS	sodium perfluoro-*n*-[1,2,3,4-$^{13}C_4$]-octanesulfonate	-	
$^{13}C_8$-PFOA	perfluoro-[$^{13}C_8$]-octanoic acid (injection standard)	-	

Table S3: Depths of bulk ice samples collected during Freeze – 1

Sample Name	Sea ice layer depth, z_{layer} / cm
Freeze – 1_ L1	0 – 1
Freeze – 1_ L2	1 – 3
Freeze – 1_ L3	3 – 5
Freeze – 1_ L4	5 – 8
Freeze – 1_ L5	8 – 11
Freeze – 1_ L6	11 – 14
Freeze – 1_ L7	15 – 19
Freeze – 1_ L8	19 – 22
Freeze – 1_ L9	22 – 24
Freeze – 1_ L10	24 – 26

Table S4: Depths of bulk ice samples collected during Freeze – 2

Sample Name	Sea ice layer depth, z_{layer} / cm
Freeze – 2_ L1	0 – 1
Freeze – 2_ L2	1 – 3
Freeze – 2_ L3	3 – 5
Freeze – 2_ L4	5 – 7
Freeze – 2_ L5	7 – 9
Freeze – 2_ L6	9 – 11
Freeze – 2_ L7	11 – 13
Freeze – 2_ L8	13 – 15
Freeze – 2_ L9	15 – 17
Freeze – 2_ L1 – L9	0 – 17

The ice thickness varied between Freeze – 1 and Freeze – 2 so bulk ice thickness was normalised to allow comparison of the sea ice datasets.

Depth-normalised sea ice is given by: $$z_{norm} = z_{layer} / h_{ice} \quad (3)$$

where z_{layer} is the sea ice layer depth; h_{ice} is the total sea ice height

Table S5: Quality assurance

Compound	PFPeA	PFHxA	PFHpA	PFOA	PFNA	PFUnDA	PFDoDA	PFBS	PFOS	6:2 FTSA
Seawater blank concentration [ng L^{-1}] (n = 3)	2.1 ± 0.2	4.3 ± 0.4	0.3 ± 0.0	0.7 ± 0.1	0.3 ± 0.1	0.1 ± 0.0	0.4 ± 0.0	0.6 ± 0.1	1.4 ± 0.1	2.3 ± 0.7
Sea ice blank concentration [ng L^{-1}] (n = 1)	1.2	1.5	0.6	0.4	0.5	0.3	0.2	0.2	-	1.1
Procedural blank concentration [ng L^{-1}] (n = 4)	1.9 ± 0.5	3.6 ± 1.4	0.3 ± 0.3	0.6 ± 0.2	0.3 ± 0.1	0.2 ± 0.1	0.4 ± 0.1	0.5 ± 0.2	1.0 ± 0.7	2.0 ± 0.8
Method Detection Limit [ng L^{-1}]	3.3	7.9	0.9	1.2	0.8	0.4	0.7	1.1	3.1	4.5
Absolute recovery, r_{abs} / %	41 ± 5		60 ± 10		63 ± 11	33 ± 9	22 ± 6	50 ± 8	34 ± 9	43 ± 9
Internal standard (IS)	$^{13}C_2$-PFHxA		$^{13}C_4$-PFOA		$^{13}C_5$-PFNA	$^{13}C_2$-PFUnDA	$^{13}C_2$-PFDoDA	$^{18}O_2$-PFHxS	$^{13}C_4$-PFOS	$^{18}O_2$-PFHxS/$^{13}C_4$-PFOS
Method precision, p_{method} / % (n = 7)	4	6	8	6	5	33	52	3	5	18

The method detection limit for each PFAS was calculated using the mean of procedural blanks (n = 4) plus 3 times standard deviation (s.d.). A mass-labelled anologue of some PFAS was not available (e.g. 6:2 FTSA) and therefore a structurally similar chemical was utilised. Analytical recovery was consistent for all surrogates and in accordance with previous trace PFAS studies. The method precision (%) was given by the relative standard deviation (RSD) of initial seawater concentrations ($c_{intial\ seawater}$).

Absolute recovery (%) is given by:

$$r_{abs} = m_{measured\ IS,sample} / m_{actual\ IS,sample} \quad (4)$$

where $m_{measured\ IS,sample}$ is the mass of internal standard (pg) measured in each sample; $m_{actual\ IS,sample}$ is the actual mass of internal standard (pg) introduced into each sample

Method precision (%) is given by:

$$p_{method} = \sigma_{initial\ seawater} / \overline{x}_{initial\ seawater} \quad (5)$$

where $\sigma_{initial\ seawater}$ is the standard deviation of initial seawater concentrations; $\overline{x}_{initial\ seawater}$ is the mean of initial seawater concentrations

Table S6: Perfluoroalkylated substances (PFAS) and their recoveries (%) for the experimental setup and throughout the experiment.

PFAS (Carbon chain length)	Recovery at experimental setup r_{setup} / %	Recovery during the experiment $r_{\text{experiment}}$ / %
PFBS (C_4)	99 ± 3	100 ± 3
* PFPeA (C_5)	108 ± 4	96 ± 4
PFHxA (C_6)	84 ± 5	101 ± 6
* PFHpA (C_7)	108 ± 9	101 ± 8
PFOA (C_8)	80 ± 5	101 ± 6
PFOS (C_8)	66 ± 3	97 ± 5
* 6:2 FTSA (C_8)	157 ± 28	102 ± 18
PFNA (C_9)	63 ± 3	99 ± 4
PFUnDA (C_{11})	35 ± 12	108 ± 36
PFDoDA (C_{12})	28 ± 14	113 ± 58

**Mass-labelled analogues were not available for all PFAS and therefore chemical surrogates were used (see Table S6). This is most likely the reason for observing recoveries during the experimental setup > 100%.*

Recovery at experimental setup is given by: $r_{\text{setup}} = c_{0\ \text{seawater}} \ / \ c_{\text{expected seawater}}$ (1)

where; $c_{0\ \text{seawater}}$ is the average concentration of PFAS in seawater sampled 24 hours after the addition of the 'spike' solution; $c_{\text{expected seawater}}$ is the expected seawater concentrations in tank

Recovery at end of the experiment is given by: $r_{\text{experiment}} = c_{\text{final seawater}} \ / \ c_{\text{inital seawater}}$ (2)

where; $c_{\text{final seawater}}$ is the average concentration of PFAS in seawater samples once all of the sea ice had re-melted at the end of Freeze–2; $c_{\text{initial seawater}}$ is the average concentration of PFAS in seawater before ice formation.

Table S7: Concentrations of PFAS (ng L^{-1}) and NaCl (g L^{-1}) measured in different compartments of the experimental sea ice system

Sample Name	NaCl	PFPeA	PFHxA	PFHpA	PFOA	PFNA	PFUnDA	PFDoDA	PFBS	PFOS	6:2 FTSA
Seawater ($c_{0\ seawater}$)	35.3 ± 0.1	40.1 ± 1.1	32.2 ± 1.3	40.3 ± 3.4	38.8 ± 0.7	24.5 ± 0.5	13.3 ± 6.3	10.2 ± 8.0	41.6 ± 1.2	25.7 ± 0.9	53.0. ± 1.2
Seawater ($c_{intial\ seawater}$)	35.3 ± 0.1	40.1 ± 1.7	31.5 ± 1.9	39.8 ± 3.3	38.4 ± 2.2	24.0 ± 1.1	13.2 ± 4.4	10.4 ± 5.4	41.0 ± 1.4	25.1 ± 1.3	58.8. ± 10.3
Freeze - 1 _ L1	15.1	22.0	20.2	23.5	39.9	36.5	25.0	24.9	23.7	24.9	87.8
Freeze - 1 _ L2	10.0	10.1	10.3	12.4	20.5	12.4	8.0	4.2	13.3	8.4	30.2
Freeze - 1 _ L3	9.2	14.2	9.6	10.5	16.6	11.1	7.9	5.4	12.3	9.7	32.4
Freeze - 1 _ L4	8.9	10.2	8.8	10.0	16.9	12.0	8.8	4.7	11.3	11.0	35.3
Freeze - 1 _ L5	7.8	7.1	8.0	9.0	16.9	13.1	7.4	3.4	7.0	10.6	36.0
Freeze - 1 _ L6	6.1	8.1	6.4	7.8	14.9	12.1	9.3	4.5	8.6	12.0	27.2
Freeze - 1 _ L7	7.2	8.0	6.8	7.5	13.2	9.9	6.8	3.7	8.8	9.3	25.8
Freeze - 1 _ L8	8.1	9.0	7.7	8.9	15.5	13.1	11.5	8.2	10.7	13.1	26.9
Freeze - 1 _ L9	9.8	11.8	9.2	9.1	14.8	12.5	11.0	5.6	12.2	12.6	33.6
Freeze - 1 _ L10	n/a	n/a	n/a	n/a	n/a	n/a	n/a	n/a	n/a	n/a	n/a
Freeze - 2 _ L1	17.6	25.5	18.7	18.3	28.4	19.9	14.9	16.9	24.7	15.3	50.6
Freeze - 2 _ L2	9.8	11.2	9.7	9.1	14.8	11.8	6.4	2.4	11.4	7.9	34.2
Freeze - 2 _ L3	11.7	14.5	10.9	11.8	18.7	12.4	9.7	6.1	14.6	11.0	34.1
Freeze - 2 _ L4	11.0	11.8	10.3	10.9	17.2	12.2	6.9	3.3	12.5	8.6	34.5
Freeze - 2 _ L5	9.9	14.8	10.9	12.1	18.9	13.4	10.5	6.0	14.1	11.9	37.5
Freeze - 2 _ L6	9.4	13.6	10.1	11.2	16.8	12.3	10.0	6.5	13.7	11.4	30.1
Freeze - 2 _ L7	8.6	8.9	7.9	7.2	12.2	10.5	6.5	3.7	9.7	7.1	26.4
Freeze - 2 _ L8	10.9	20.8	12.0	11.7	14.1	9.0	6.6	4.2	15.4	7.1	25.8
Freeze - 2 _ L9	n/a	n/a	n/a	n/a	n/a	n/a	n/a	n/a	n/a	n/a	n/a
Freeze - 2 _ L1 – L9	13.0	10.6	9.5	10.0	15.4	10.6	8.6	8.4	14.2	12.3	25.4
Freeze - 2 _ frost flowers	88.3	97.3	86.8	82.3	94.1	74.6	145.5	278.7	126.4	123.2	240.7
Seawater ($c_{final\ seawater}$)	35.5 ± 0.1	38.6 ± 0.6	31.7 ± 0.4	40.4 ± 1.4	38.7 ± 0.6	23.6 ± 0.5	14.3 ± 5.4	11.6 ± 6.6	41.0 ± 0.8	24.3 ± 1.7	60.2 ± 14.7

n/a indicates samples that were excluded for quality control purposes (see Table S11 – S12 for more details). Freeze – 2 also included an additional sample taken of the whole bulk ice (Freeze – 2 _ L1 – L9). Due to the use of a different mass-labelled surrogate during chemical analysis for 6:2 FTSA, the method is considered semi-quantitative.

Table S8: Enrichment Factors (ε) for PFAS and NaCl in different compartments of the experimental sea ice system

Sample Name	NaCl	PFPeA	PFHxA	PFHpA	PFOA	PFNA	PFUnDA	PFDoDA	PFBS	PFOS	6:2 FTSA
Seawater ($c_{intial\ seawater}$)	-	-	-	-	-	-	-	-	-	-	-
Freeze - 1 _ L1	0.4	0.5	0.6	0.6	1.0	1.5	1.9	2.4	0.6	1.0	1.5
Freeze - 1 _ L2	0.3	0.3	0.3	0.3	0.5	0.5	0.6	0.4	0.3	0.3	0.5
Freeze - 1 _ L3	0.3	0.4	0.3	0.3	0.4	0.5	0.6	0.5	0.3	0.4	0.6
Freeze - 1 _ L4	0.3	0.3	0.3	0.3	0.4	0.5	0.7	0.5	0.3	0.4	0.6
Freeze - 1 _ L5	0.2	0.2	0.3	0.2	0.4	0.5	0.6	0.3	0.2	0.4	0.6
Freeze - 1 _ L6	0.2	0.2	0.2	0.2	0.4	0.5	0.7	0.4	0.2	0.5	0.5
Freeze - 1 _ L7	0.2	0.2	0.2	0.2	0.3	0.4	0.5	0.4	0.2	0.4	0.4
Freeze - 1 _ L8	0.2	0.2	0.2	0.2	0.4	0.5	0.9	0.8	0.3	0.5	0.5
Freeze - 1 _ L9	0.3	0.3	0.3	0.2	0.4	0.5	0.8	0.5	0.3	0.5	0.6
Freeze - 1 _ L10	n/a	n/a	n/a	n/a	n/a	n/a	n/a	n/a	n/a	n/a	n/a
Freeze - 2 _ L1	0.5	0.6	0.6	0.5	0.7	0.8	1.1	1.6	0.6	0.6	0.9
Freeze - 2 _ L2	0.3	0.3	0.3	0.2	0.4	0.5	0.5	0.2	0.3	0.3	0.6
Freeze - 2 _ L3	0.3	0.4	0.3	0.3	0.5	0.5	0.7	0.6	0.4	0.4	0.6
Freeze - 2 _ L4	0.3	0.3	0.3	0.3	0.4	0.5	0.5	0.3	0.3	0.3	0.6
Freeze - 2 _ L5	0.3	0.4	0.3	0.3	0.5	0.6	0.8	0.6	0.3	0.5	0.6
Freeze - 2 _ L6	0.3	0.3	0.3	0.3	0.4	0.5	0.8	0.6	0.3	0.5	0.5
Freeze - 2 _ L7	0.2	0.2	0.3	0.2	0.3	0.4	0.5	0.4	0.2	0.3	0.4
Freeze - 2 _ L8	0.3	0.5	0.4	0.3	0.4	0.4	0.5	0.4	0.4	0.3	0.4
Freeze - 2 _ L9	n/a	n/a	n/a	n/a	n/a	n/a	n/a	n/a	n/a	n/a	n/a
Freeze - 2 _ L1 – L9	0.4	0.3	0.3	0.3	0.4	0.4	0.6	0.8	0.3	0.5	0.4
Freeze - 2 _ frost flowers	2.5	2.4	2.8	2.1	2.5	3.1	11.0	26.7	3.1	4.9	4.1

Enrichment Factors were calculated (See Equation 1 in main text) by dividing concentrations in a sample to the initial seawater concentration ($c_{intial\ seawater}$). *n/a indicates samples that were excluded for quality assurance purposes (see Table S11 – S12 for more details).*

Table S9: Predicted concentrations of PFAS based on salinity in bulk sea ice.

Sample Name	NaCl	PFPeA	PFHxA	PFHpA	PFOA	PFNA	PFUnDA	PFDoDA	PFBS	PFOS	6:2 FTSA
Freeze - 1 _ L1	-	17.2	13.5	17.1	16.4	10.3	5.7	4.5	17.6	10.7	25.2
Freeze - 1 _ L2	-	11.4	8.9	11.3	10.9	6.8	3.8	3.0	11.7	7.1	16.7
Freeze - 1 _ L3	-	10.4	8.2	10.4	10.0	6.2	3.4	2.7	10.7	6.5	15.3
Freeze - 1 _ L4	-	10.1	8.0	10.1	9.7	6.1	3.3	2.6	10.4	6.3	14.9
Freeze - 1 _ L5	-	8.8	6.9	8.8	8.5	5.3	2.9	2.3	9.0	5.5	13.0
Freeze - 1 _ L6	-	6.9	5.4	6.8	6.6	4.1	2.3	1.8	7.0	4.3	10.1
Freeze - 1 _ L7	-	8.2	6.4	8.2	7.9	4.9	2.7	2.1	8.4	5.1	12.1
Freeze - 1 _ L8	-	9.1	7.2	9.1	8.8	5.5	3.0	2.4	9.3	5.7	13.4
Freeze - 1 _ L9	-	11.1	8.7	11.0	10.6	6.6	3.7	2.9	11.3	6.9	16.2
Freeze - 1 _ L10	-	n/a	n/a	n/a	n/a	n/a	n/a	n/a	n/a	n/a	n/a
Freeze - 2 _ L1	-	20.0	15.7	19.9	19.2	12.0	6.6	5.2	20.5	12.5	29.4
Freeze - 2 _ L2	-	11.2	8.8	11.1	10.7	6.7	3.7	2.9	11.4	7.0	16.4
Freeze - 2 _ L3	-	13.3	10.5	13.2	12.8	8.0	4.4	3.5	13.6	8.3	19.6
Freeze - 2 _ L4	-	12.5	9.8	12.4	12.0	7.5	4.1	3.3	12.8	7.8	18.3
Freeze - 2 _ L5	-	11.2	8.8	11.2	10.8	6.7	3.7	2.9	11.5	7.0	16.5
Freeze - 2 _ L6	-	10.7	8.4	10.6	10.2	6.4	3.5	2.8	10.9	6.7	15.6
Freeze - 2 _ L7	-	9.7	7.6	9.7	9.3	5.8	3.2	2.5	9.9	6.1	14.3
Freeze - 2 _ L8	-	12.4	9.7	12.3	11.9	7.4	4.1	3.2	12.7	7.7	18.2
Freeze - 2 _ L9	-	n/a	n/a	n/a	n/a	n/a	n/a	n/a	n/a	n/a	n/a
Freeze - 2 _ L1 – L9	-	14.7	11.6	14.6	14.1	8.8	4.9	3.8	15.1	9.2	21.6

Predicted concentrations for PFAS were calculated by multiplying the initial seawater concentration by the $\varepsilon_{bulk\ ice}(NaCl)$. *n/a indicates samples that were excluded for quality assurance purposes (see Table S11 – S12 for more details).*

Table S10: Salinity-normalised enrichment factors, *(ε_s)*, for PFAS in different compartments of the experimental sea ice system.

Sample Name	PFPeA	PFHxA	PFHpA	PFOA	PFNA	PFUnDA	PFDoDA	PFBS	PFOS	6:2 FTSA
Freeze - 1 _ L1	1.3	1.5	1.4	2.4	3.6	4.4	5.6	1.3	2.3	3.5
Freeze - 1 _ L2	0.9	1.1	1.1	1.9	1.8	2.1	1.4	1.1	1.2	1.8
Freeze - 1 _ L3	1.4	1.2	1.0	1.7	1.8	2.3	2.0	1.2	1.5	2.1
Freeze - 1 _ L4	1.0	1.1	1.0	1.7	2.0	2.6	1.8	1.1	1.7	2.4
Freeze - 1 _ L5	0.8	1.1	1.0	2.0	2.5	2.6	1.5	0.8	1.9	2.8
Freeze - 1 _ L6	1.2	1.2	1.1	2.3	2.9	4.1	2.5	1.2	2.8	2.7
Freeze - 1 _ L7	1.0	1.1	0.9	1.7	2.0	2.5	1.7	1.1	1.8	2.1
Freeze - 1 _ L8	1.0	1.1	1.0	1.8	2.4	3.8	3.4	1.1	2.3	2.0
Freeze - 1 _ L9	1.1	1.1	0.8	1.4	1.9	3.0	1.9	1.1	1.8	2.1
Freeze - 1 _ L10	n/a	n/a	n/a	n/a	n/a	n/a	n/a	n/a	n/a	n/a
Freeze - 2 _ L1	1.3	1.2	0.9	1.5	1.7	2.3	3.2	1.2	1.2	1.7
Freeze - 2 _ L2	1.0	1.1	0.8	1.4	1.8	1.8	0.8	1.0	1.1	2.1
Freeze - 2 _ L3	1.1	1.0	0.9	1.5	1.6	2.2	1.8	1.1	1.3	1.7
Freeze - 2 _ L4	0.9	1.0	0.9	1.4	1.6	1.7	1.0	1.0	1.1	1.9
Freeze - 2 _ L5	1.3	1.2	1.1	1.8	2.0	2.8	2.1	1.2	1.7	2.3
Freeze - 2 _ L6	1.3	1.2	1.1	1.6	1.9	2.8	2.3	1.3	1.7	1.9
Freeze - 2 _ L7	0.9	1.0	0.7	1.3	1.8	2.0	1.4	1.0	1.2	1.8
Freeze - 2 _ L8	1.7	1.2	0.9	1.2	1.2	1.6	1.3	1.2	0.9	1.4
Freeze - 2 _ L9	n/a	n/a	n/a	n/a	n/a	n/a	n/a	n/a	n/a	n/a
Freeze - 2 _ L1 – L9	0.7	0.8	0.7	1.1	1.2	1.8	2.2	0.9	1.3	1.2
Freeze - 2 _ frost flowers	1.0	1.1	0.8	1.0	1.2	4.4	10.7	1.2	2.0	1.6

n/a indicates samples that were excluded for quality control purposes (See Table S11 – S12 for more details).

Table S11: Salinity-normalised enrichment factors for PFAS in bulk sea ice ($\varepsilon_{s,\ bulk\ ice}$) during Freeze - 1.

	PFPeA	PFHxA	PFHpA	PFOA	PFNA	PFUnDA	PFDoDA	PFBS	PFOS	6:2 FTSA
Freeze - 1 _ L1	1.3	1.5	1.4	2.4	3.6	4.4	5.6	1.3	2.3	3.5
Freeze - 1 _ L2	0.9	1.1	1.1	1.9	1.8	2.1	1.4	1.1	1.2	1.8
Freeze - 1 _ L3	1.4	1.2	1.0	1.7	1.8	2.3	2.0	1.2	1.5	2.1
Freeze - 1 _ L4	1.0	1.1	1.0	1.7	2.0	2.6	1.8	1.1	1.7	2.4
Freeze - 1 _ L5	0.8	1.1	1.0	2.0	2.5	2.6	1.5	0.8	1.9	2.8
Freeze - 1 _ L6	1.2	1.2	1.1	2.3	2.9	4.1	2.5	1.2	2.8	2.7
Freeze - 1 _ L7	1.0	1.1	0.9	1.7	2.0	2.5	1.7	1.1	1.8	2.1
Freeze - 1 _ L8	1.0	1.1	1.0	1.8	2.4	3.8	3.4	1.1	2.3	2.0
Freeze - 1 _ L9	1.1	1.1	0.8	1.4	1.9	3.0	1.9	1.1	1.8	2.1
Freeze - 1 _ L10	0.5	0.6	0.4	0.7	0.9	1.3	0.9	0.7	0.9	1.1
Median	1.0	1.1	1.0	1.8	2.0	2.6	1.9	1.1	1.8	2.1
Q1	0.9	1.1	0.9	1.7	1.8	2.3	1.5	1.1	1.5	2.0
Q3	1.2	1.2	1.1	2.0	2.5	3.6	2.4	1.1	2.2	2.6
IQR	0.2	0.1	0.1	0.3	0.6	1.3	0.9	0.1	0.6	0.6
1.5 x IQR	0.4	0.2	0.2	0.5	0.9	1.9	1.3	0.1	1.0	0.9
Lower limit	0.5	0.9	0.7	1.2	0.9	0.4	0.2	0.9	0.6	1.1
Upper limit	1.5	1.3	1.3	2.4	3.4	5.5	3.7	1.3	3.2	3.5

The interquartile range rule was used on enrichment factor data to identify outliers (red). Salinity-normalised enrichment factors (ε_s) <1 inidicate irregular brine movement which can occur during sample storage (during freezing). Bulk ice layers which revealed over 50% of PFAS (C_5 – C_{12}; n = 10) as outliers (e.g. Freeze - 1 _ L10*) were excluded from further analysis to avoid bias.*

Table S12: Salinity-normalised enrichment factors for PFAS in bulk sea ice ($\varepsilon_{s,\ bulk\ ice}$) during Freeze - 2

	PFPeA	PFHxA	PFHpA	PFOA	PFNA	PFUnDA	PFDoDA	PFBS	PFOS	6:2 FTSA
Freeze - 2 _ L1	1.3	1.2	0.9	1.5	1.7	2.3	3.2	1.2	1.2	1.7
Freeze - 2 _ L2	1.0	1.1	0.8	1.4	1.8	1.8	0.8	1.0	1.1	2.1
Freeze - 2 _ L3	1.1	1.0	0.9	1.5	1.6	2.2	1.8	1.1	1.3	1.7
Freeze - 2 _ L4	0.9	1.0	0.9	1.4	1.6	1.7	1.0	1.0	1.1	1.9
Freeze - 2 _ L5	1.3	1.2	1.1	1.8	2.0	2.8	2.1	1.2	1.7	2.3
Freeze - 2 _ L6	1.3	1.2	1.1	1.6	1.9	2.8	2.3	1.3	1.7	1.9
Freeze - 2 _ L7	0.9	1.0	0.7	1.3	1.8	2.0	1.4	1.0	1.2	1.8
Freeze - 2 _ L8	1.7	1.2	0.9	1.2	1.2	1.6	1.3	1.2	0.9	1.4
Freeze - 2 _ L9	0.5	0.6	0.4	0.5	0.6	0.5	0.2	0.6	0.4	0.8
Median	1.1	1.1	0.9	1.4	1.7	2.0	1.4	1.1	1.2	1.8
Q1	0.9	1.0	0.8	1.3	1.6	1.7	1.0	1.0	1.1	1.7
Q3	1.3	1.2	0.9	1.5	1.8	2.3	2.1	1.2	1.3	1.9
IQR	0.3	0.2	0.1	0.2	0.3	0.6	1.0	0.2	0.2	0.2
1.5 x IQR	0.5	0.2	0.2	0.3	0.4	0.9	1.5	0.4	0.3	0.3
Lower limit	0.5	0.8	0.6	1.0	1.2	0.8	-0.5	0.6	0.8	1.4
Upper limit	1.8	1.4	1.1	1.7	2.2	3.1	3.6	1.6	1.6	2.2

The interquartile range rule was used on enrichment factor data to identify outliers (red). Salinity-normalised enrichment factors (ε_s) <1 inidicate irregular brine movement which can occur during sample storage (during freezing). Those bulk ice layers which revealed over 50% of PFAS (C_5 – C_{12}; n=10) as outliers (e.g. Freeze - 2 _ L9*) were excluded from further data analysis to avoid possible bias.*

Table S13: Concentrations of PFAS (ng L^{-1}) and NaCl (g L^{-1}) measured in slow-melt aliquots.

Sample Name	Sample volume (L)	NaCl	PFPeA	PFHxA	PFHpA	PFOA	PFNA	PFUnDA	PFDoDA	PFBS	PFOS	6:2 FTSA	PFOA (branched)
F1	0.19	52.8	60.9	47.9	61.3	19.3	3.9	0.8	2.2	63.4	6.8	25.0	<0
F2	0.60	30.6	35.8	26.6	29.1	25.8	5.8	1.2	3.2	35.1	8.3	42.3	0.02
F3	0.60	14.6	21.3	14.9	21.5	20.2	4.9	0.7	2.2	17.7	6.4	34.3	0.01
F4	2.46	2.6	2.5	3.1	5.8	12.1	7.2	3.4	11.6	2.8	15.2	22.2	0.02

Table S14: Mass of PFAS (ng) and NaCl (g) in slow-melt aliquots.

Sample Name	NaCl	PFPeA	PFHxA	PFHpA	PFOA	PFNA	PFUnDA	PFDoDA	PFBS	PFOS	6:2 FTSA	PFOA(branched)
F1	10	12	9	12	4	1	0	0	12	1	5	0.00
F2	18	21	16	17	15	3	1	2	21	5	25	0.01
F3	9	13	9	13	12	3	0	1	11	4	20	0.01
F4	6	6	8	14	30	18	8	28	7	37	55	0.05
Total	43	52	41	56	61	25	10	32	51	48	105	0.06

Mass is given by:

$$m_{\text{meltwater fraction}} = V_{\text{meltwater fraction}}\, c_{\text{meltwater fraction}} \quad (6)$$

where $V_{\text{meltwater fraction}}$ is the volume of the meltwater fraction (L); $c_{\text{meltwater fraction}}$ is the concentration of PFAS (ng L^{-1}) or NaCl (g L^{-1})

Table S15: Mass fraction of PFAS (%) and NaCl (%) in slow-melt aliquots.

Sample Name	NaCl	PFPeA	PFHxA	PFHpA	PFOA	PFNA	PFUnDA	PFDoDA	PFBS	PFOS	6:2 FTSA	PFOA(branched)
F_1	23	22	22	21	6	3	1	1	24	3	5	0
F_2	42	41	38	31	25	14	8	6	42	10	24	21
F_3	20	24	21	23	20	12	4	4	21	8	19	8
F_4	14	12	18	25	49	71	87	89	14	79	52	71

Mass fraction is given by:

$$f_{\text{meltwater fraction}} = m_{\text{meltwater fraction}}(F_i) \,/\, \Sigma\, m_{\text{meltwater fraction}}(F_i) \tag{7}$$

where $m_{\text{meltwater fraction}}$ is the mass of a PFAS (ng) or NaCl (g) in a particular meltwater fraction; $\Sigma\, m_{\text{meltwater fraction}}(F_i)$ is the total mass of a PFAS (ng) or NaCl (g) in the combined meltwater fractions (F_1 – F_4).

Table S16: Salinity-normalised enrichment factors in meltwater fractions, ($\varepsilon_{s,\ meltwater}$), collected from the slow-melt experiment.

Sample Name	Sample volume	NaCl	PFPeA	PFHxA	PFHpA	PFOA	PFNA	PFUnDA	PFDoDA	PFBS	PFOS	6:2 FTSA	PFOA(branched)
F1	-	-	0.97	0.95	0.90	0.26	0.13	0.06	0.06	1.03	0.12	0.20	0.00
F2	-	-	0.98	0.91	0.73	0.60	0.33	0.18	0.14	0.99	0.25	0.57	0.51
F3	-	-	1.22	1.07	1.14	0.98	0.58	0.21	0.21	1.04	0.40	0.97	0.40
F4	-	-	0.82	1.26	1.76	3.38	4.93	5.99	6.12	0.94	5.44	3.58	4.87

Salinity-normalised enrichment factors ($\varepsilon_{s,\ meltwater}$) is given by:

$$\varepsilon_{s,\ meltwater} = f_{\text{PFAS meltwater fraction}}(F_1) \,/\, f_{\text{NaCl meltwater fraction}}(F_1) \tag{8}$$

where $f_{\text{PFAS meltwater fraction}}(F_1)$ is the percentage mass of a PFAS (%) in a particular meltwater fraction; $f_{\text{NaCl meltwater fraction}}(F_1)$ is the percentage mass of a NaCl (%) in a particular meltwater fraction.

Table S17: Measured concentrations of PFAS (ng L^{-1}) in seawater and in surface bulk ice layers

Chemical	Measured concentration in seawater (ng L^{-1})	Measured concentration in surface bulk ice layer (ng L^{-1})	Measured enrichment factor in surface ice layer ($\varepsilon_{,\ LI}$) (Unitless)
NaCl	35 g L^{-1}	15 g L^{-1}	0.4
PFBS	41	24	0.6
PFHxA	31	20	0.6
PFOA	38	40	1.0
PFOS	25	25	1.0
PFNA	24	37	1.5
PFUnDA	13	25	1.9
PFDoDA	10	25	2.4

Table S18: Measured and predicted concentrations of PFAS (ng L^{-1}) in a theoretical seawater microlayer (SML) and in a sea-surface ice layer

Chemical	Unrecovered mass (%)	Unrecovered mass (ng)	* Predicted concentration in SML (ng L^{-1})	Predicted concentration in surface bulk ice layer {based on salinity} (ng L^{-1})	Predicted / Measured concentrations (surface layer)
PFBS	1	981	30	13	1
PFHxA	16	19545	588	254	13
PFOA	20	32250	971	420	11
PFOS	34	43133	1298	562	23
PFNA	37	47159	1419	614	17
PFUnDA	65	83280	2506	1084	43
PFDoDA	72	91976	2768	1197	48

To apportion the loss of PFAS following the addition of the PFAS spike to the sea water (e.g. an unrecovered mass most evident for the longer chain PFAS) we investigated whether PFAS had sorbed to the glass-walls of the tank or had partitioned to a possible sea surface microlayer (SML). The unrecovered mass (ng) of each chemical from initial seawater samples during the experimental setup period was used along with a theoretical SML volume of 33 dm^3 (*Experimental tank area, 3.3 m^2, multiplied by theoretical SML depth of 0.01 m). We selected to peform our calculations using the thickness of our sea surface bulk ice samples (0.01m) in order to derive a conservative estimate of chemical concentrations in a SML (the true thickness of a SML is probably much thinner (e.g. 50 μm) but 0.01m serves as a useful illustration). Theoretical PFAS concentrations in SML were subsequently used with the ice enrichment factor for NaCl ($\varepsilon_{,\ LI}$(NaCl) = 0.4; see Table S17) to predict concentrations in the sea surface ice layer. Comparisons of the predicted concentrations with the measured concentrations in the ice revealed a notable difference. This indicates that a large proportion of the chemical mass that was not recovered from the initial sea water samples is likely to have been lost through sorption to chamber surfaces (e.g. glass) following initial mixing of the seawater, rather than association with a SML.

Table S19: Enrichment Factors for PFAS and NaCl in brine (i.e. $\varepsilon_{,\ brine}$).

NaCl	PFPeA	PFHxA	PFHpA	PFOA	PFNA	PFUnDA	PFDoDA	PFBS	PFOS	6:2 FTSA
6 ± 2	7 ± 3	7 ± 2	6 ± 2	10 ± 4	11 ± 5	15 ± 8	13 ± 13	6 ± 2	9 ± 3	12 ± 5

Enrichment factor in brine is given by: $\varepsilon_{\text{brine}} = \varepsilon_{\text{bulk ice}} \ / \ V_{\text{b}}$ (9)

where $\varepsilon_{\text{bulk ice}}$ is the average (mean ± 1.s.d.) enrichment factor taken from all bulk ice samples collected from Freeze – 1 and Freeze – 2 (see Table S8); V_{b} is the brine volume fraction when brine channels in sea ice are reported to be accessible to sympagic organisms (e.g. 5 % or 0.05).

PFAS extraction and chemical analysis

Samples were extracted for PFAS using a 12-port vacuum manifold system equipped with weak anion exchange cartridges (Oasis WAX, 3 cc, 150 mg sorbent, 30 µm particle size, Waters, USA) that had been preconditioned with 3 mL of 0.1 % (*v/v* , e.g. 1cm^3 dm^{-3}) aqueous ammonium hydroxide in methanol (i.e. 0.1 mL of 29.5% NH_4OH aq solution made up to 100mL with MeOH) 3 mL methanol and then 3 mL MilliQ water. Samples were loaded at a flow rate of 2 - 3 drops per second and a washing step was implemented using 6 mL MilliQ water. Cartridges were dried under vacuum and stored at –20 °C until further analysis. The target analytes were eluted using 5 mL methanol followed by 5 mL of 0.1 % (*v/v*) aq. ammonium hydroxide in methanol. Finally, the eluates were evaporated to 150 µL under nitrogen and then 10 µL of an injection standard solution containing $^{13}C_8$-PFOA (100 pg µL^{-1}) prepared in a methanol/water (volume ratio 4:1) solution and 40 µL of MilliQ water was added.

Instrumental analysis was performed by HPLC-MS/MS, using an HP 1100 LC system (Agilent Technologies, USA) coupled to an API 4000 triple quadrupole mass spectrometer (AB Sciex, USA). It was equipped with a Turbo V Ion Source (AB Sciex, USA) operating in negative electrospray ionization mode. The injection volume was 10 µL for all test solutions. For chromatographic separation, a polar embedded reversed phase C_{18} separation column (Synergi Fusion-RP C18, 150 mm x 2 mm, particle size 4 µm, pore size 80 Å, Phenomenex, USA) was combined with a reversed phase guard column (4 mm x 2 mm, Phenomenex, USA). A flow rate of 0.2 mL min^{-1} was set using a gradient elution using 2 mM ammonium acetate aqueous solution and a 0.05 % *(v/v)* acetic acid in methanol [1, 2].

References

1. Joerss, H.; Apel, C.; Ebinghaus, R., Emerging per- and polyfluoroalkyl substances (PFASs) in surface water and sediment of the North and Baltic Seas. *Science of The Total Environment* **2019,** *686*, 360-369;https://doi.org/10.1016/j.scitotenv.2019.05.363
2. Joerss, H.; Xie, Z.; Wagner, C. C.; von Appen, W.-J.; Sunderland, E. M.; Ebinghaus, R., Transport of Legacy Perfluoroalkyl Substances and the Replacement Compound HFPO-DA through the Atlantic Gateway to the Arctic Ocean—Is the Arctic a Sink or a Source? *Environmental Science & Technology* **2020**;10.1021/acs.est.0c00228

Chapter 5

High concentrations of perfluoroalkyl acids (PFAA) in Arctic seawater driven by early thawing sea ice

This chapter presents field data gathered from two sites in the high European Arctic in late-summer 2019. Chemical concentrations in snow, sea ice and under-ice seawater samples were compared to evaluate major sources and transport pathways. Stable water isotope measurements facilitated a comparison of concentrations between sites to assess the biochemical cycling of chemicals.

This chapter was published in the journal Environmental Science and Technology in 2021 as a research article.

The candidate's contribution was designing and conducting the field sampling campaign; structuring own and co-authors' ideas as a manuscript; writing the manuscript for supervisor review; co-ordinating co-author feedback; submission of manuscript.

Candidate: ..... J.garnett. *.....Date:.....22-Jul-21.....*

Mr Jack R. Garnett

Supervisor: ..... Crispin Halsall *.....Date:...26-Jul-21.....*

Prof. Crispin J. Halsall.

High concentrations of perfluoroalkyl acids (PFAA) in Arctic seawater driven by early thawing sea ice

Jack Garnett[1], * Crispin Halsall[1], Anna Vader[2],

Hanna Joerss[3], Ralf Ebinghaus[3], Amber Leeson[1], Peter M. Wynn[1]

1 Lancaster Environment Centre, Lancaster University, Lancaster, LA1 4YQ, UK

2 Department of Arctic Biology, The University Centre in Svalbard (UNIS), N-9170 Longyearbyen, Norway,

3 Helmholtz-Zentrum Geesthacht Hereon, Max-Planck-Straße 1, 21502 Geesthacht, Germany

* Email: c.halsall@lancaster.ac.uk

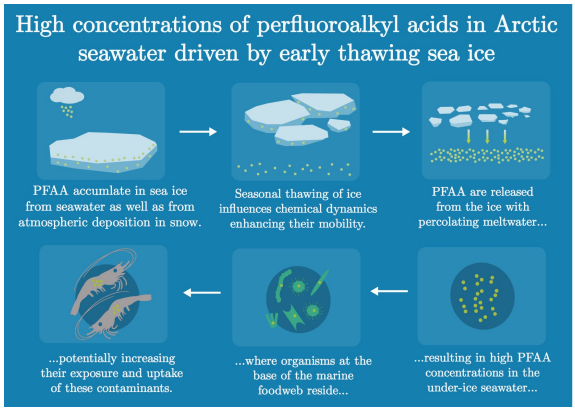

Abstract

Poly- and perfluoroalkyl substances (PFAS) are synthetic chemicals that are widely present in the global environment including the Arctic. However, little is known about how these chemicals (particularly the perfluoroalkyl acids; PFAA) enter the Arctic marine system and cycle between seawater and sea ice compartments. To evaluate this, we analysed sea ice, snow, meltponds and near-surface seawater at two ice-covered stations located north of the Barents Sea (82 °N) with the aim of investigating PFAA dynamics in the late-season ice pack. Sea ice showed high concentrations of PFAA particularly at the surface with snow-ice (the uppermost sea ice layer strongly influenced by snow) comprising 26 – 62 % of the total PFAA burden. Low salinities (<2.5 ppt) and low $\delta^{18}O_{H20}$ values (< 1‰ in snow and upper ice layers) in sea ice revealed the influence of meteoric water to sea ice thus indicating a significant atmospheric source of PFAA with transfer down the sea ice column in meltwater. Importantly, the under-ice seawater (0.5 m depth) displayed some of the highest concentrations notably for the long-chain PFAA (e.g. PFOA 928 ± 617 pg L^{-1}), which were ~3-fold higher than deeper water (5 m depth) and ~2-fold higher than those recently measured in the North Sea. The evidence provided here suggests that meltwater arising early in the melt season from snow and other surface ice floe components drives the higher PFAA concentrations observed in under-ice seawater, which could in turn influence the timing and extent of PFAA exposure for organisms at the base of the marine foodweb.

Keywords: PFAS; Arctic; Sea ice; Seawater; Snow; Meltpond; Chemical Exposure

Synopsis:

Sea ice accumulates perfluoroalkyl acids (PFAA) from seawater as well as from atmospheric deposition in snow. Subsequent melting of surface ice layers through seasonal changes later results in high PFAA concentrations in the under-ice seawater.

2. Introduction

Poly- and perfluoroalkyl substances (PFAS) consist of a large group of synthetic chemicals that are used in a wide variety of industrial and consumer applications [1]. Perfluoroalkyl acids (PFAA), including the perfluoroalkyl carboxylic acids (PFCA) and perfluoroalkyl sulfonic acids (PFSA), are a major group of PFAS which have a ubiquitous presence in the global environment. Moreover, long-chain PFAA (long-chain = PFCA with 8 carbons and greater, and PFSA with 6 carbons and greater [2]) are bioaccumlative and display a range of adverse toxic effects in humans and biota. Understanding the fate and behaviour of PFAA in the environment is therefore important particularly in relation to remote ecosystems such as the Arctic that are reported to be currently experiencing other environmental stressors [3].

PFAA have been observed in the remote Greenland Sea [4] and Chukchi/Beaufort Sea regions of the western Arctic [5] with their presence having been linked to transport through ocean currents originating from industral regions. PFAA are also transported to remote environments like the Arctic indirectly through photochemical oxidation of volatile precursors in the atmosphere followed by deposition, with their occurence in the central Arctic basin snowpack [5] and on the Devon Island ice-cap [6-8] as evidence of atmospheric deposition. However, little is known about the relative importance of these two pathways, and even less about the fate and behaviour of PFAS in sea ice and their subsequent fate during seasonal thaw.

The observation of PFAA in sea ice along with other persistent organic pollutants is limited to a handful of field studies [5, 9-14] but only recent mechanistic investigations have revealed that brine in sea ice plays an important role in distributing these chemicals during sea ice growth [10, 15]. Sea ice brine has also been shown to contain contaminant concentrations at levels significantly greater than those observed in the underlying sea water [10, 15]. In a warming Arctic Ocean dominated by brine-rich single season ice, then this has important implications for contaminant exposure to the many organisms situated at the base of the pelagic foodweb which are abundant in sea ice. Sympagic organisms, such as ice algae and associated heterotrophic

protists and metazoans, inhabit a network of brine inclusions and brine channels at the base of the ice and may be particularly vulnerable to brine which is enriched in contaminants [13].

The late-season ice pack is a dynamic system, whereby organic contaminants that have accumulated in the winter snowpack are re-volatilised to the atmosphere [16] or transferred to other components of the sea ice system [14]. Meltwater originating from snow and sea ice may percolate deeper into sea ice layers or pass directly into seawater transferring contaminants in the process. Meltponds are also common features on late-season ice floes (Fetterer and Untersteiner, 1998) and both snowfall/precipitation and gas-exchange with the overlying atmosphere have been shown to increase some contaminant levels in the ponds [17]. Due to their high water solublities and low volatility, PFAA are likely to be transferred from thawing snow and sea ice to seawater. The aim of this study was to determine the concentrations and distribution of PFAA in the various compartments of the late-season sea ice system and investigate the fate of PFAA during the thawing process. Physical and chemical properties of snow, sea ice and seawater including density, salinity and stable-isotope analysis were measured to evaluate the quantity of entrained meteoric water in ice/meltwater components and the role of melt/fresh water on PFAA fate.

2. Methods

2.1. Sample Collection

Environmental samples were collected in the European High Arctic (See Figure 1) during the 'Nansen Legacy Q3' Summer cruise of the Norwegian research vessel *Kronprins Haakon* on 26-28 August 2019. Samples were taken at two study sites situated on the Barents Sea shelf break (81°16'N, 31°75'E) and Nansen Basin (81°16'N, 29°75'E) which we refer hereafter as P6 and P7, respectively. Both sites were selected on separate large (~1 km^2) undeformed ice floes that were fully covered with a thin layer of snow (~0.05 m) except in areas where melt-ponds were present. Seawater samples (1 L; n=6) were collected at two depths (0.5 m and 5.0 m) using a niskin bottle via an access hole in the sea ice. Sea ice and snow were collected in close proximity (<20 m) to the seawater access hole.

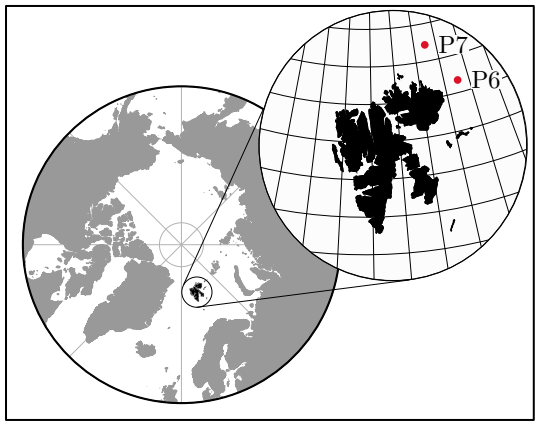

Figure 1: Locations of sampling stations P6 (81°16'N, 31°75'E) and P7 (81°16'N, 29°75'E) during Nansen Legacy Q3 summer cruise in August 2019.

Meltponds were covered by a thin layer of ice which was removed before sampling water (1 L; n=3). Snow was collected above each core site (approximately 0.25 m^2) (2 L; n=4). Sea ice cores (n=4) were drilled (~1 m intervals) and then immediately cut into horizontal sections (n=7 – 10) that were between 0.1 – 0.2 m in length. Ice core sections were bulked with adjacent ice core samples (See Figure S1) to obtain sufficient meltwater for PFAS analysis (~1 L) and placed into polyethylene bags before melting at ambient room temperature (~20 °C). All equipment and sampling bottles (polypropylene) for PFAS analysis were pre-cleaned following set protocols and any clothing worn by samplers that was suspected to contain residues of fluoropolymers were avoided to prevent possible contamination. For more information on sampling protocols, equipment and ancilliary measurements (e.g. bulk density, temperature) see Table S1 – S5 and Figure S2.

2.2. Sample extraction and analysis

Solid phase extraction (SPE) of PFAS took place onboard the ship and several procedural blanks (n=7) were taken to assess possible contamination. Briefly, an internal standard (IS) mix (^{13}C mass-labelled standards) was added to each sample before being loaded onto preconditioned OASIS WAX cartridges (150 mg, 30 μm, 6 mL). Cartridges were then dried under vacuum and stored at –20 °C before further analysis at Helmholtz-Zentrum Geesthacht, Germany. PFAS were analysed by liquid chromatography coupled to tandem mass

spectrometry (LC-MS/MS). Instrumental analysis was performed by HPLC-MS/MS, using an HP 1100 LC system (Agilent Technologies, USA) coupled to an API 4000 triple quadrupole mass spectrometer (AB Sciex, USA). It was equipped with a Turbo V ion source (AB Sciex, USA), operating in negative electrospray ionisation mode. For chromatographic separation, a polar embedded reversed phase C_{18} separation column (Synergi Fusion-RP C_{18}, Phenomenex, USA) was combined with a reversed phase guard column (Phenomenex, USA). As solvents for the gradient elution, 2 mM ammonium acetate aqueous solution (A) and 0.05 % acetic acid in methanol (B) were used. The injection volume was 10 µL for samples and standards, both dissolved in 80:20 (% v/v) methanol/water. Target compounds included 11 perfluoroalkyl carboxylic acids (PFCA; C_4 to C_{14}) and 5 perfluoroalkyl sulfonic acids (PFSA; C_4,C_6 – C_8, C_{10}). See Table S6 for more information on analytical standards

Aliquots of each sample (0.05 L) were also taken for salinity and stable oxygen isotope analysis that were stored at 4 °C in air tight bottles with minimal headspace for <14 days before analysis was undertaken at Lancaster University, UK. Salinity was measured (all volume concentrations reported for 20 °C) using a calibrated conductivity probe (Hach HQd40 logger with CDC401 probe) and reported as parts-per-thousand (ppt or g/L). Sample $^{18}O/^{16}O$ ratios in water were determined by continuous flow isotope ratio mass spectrometry at the University of Lancaster (Elementar pyrocube elemental analyser linked to an Isoprime 100 mass spectrometer). Sample $\delta^{18}O$ analyses were undertaken in pyrolysis mode using sample injection of 0.4 µL over glassy carbon chips at 1450 °C. $\delta^{18}O$ values were corrected against laboratory calibration standards (per mille, ‰) relative to Vienna Standard Mean Ocean Water (V-SMOW; $\delta^{18}O$ = 0 ‰ and Greenland Ice Sheet Precipitation (GISP; $\delta^{18}O$ = -24.78 ‰). Laboratory standards containing NaCl in similar proportion to the field samples were also used to check for any effects of salinity upon the true sample value. Results confirmed no adverse effect of salinity upon analytical precision or accuracy. Within-run standard replication for $\delta^{18}O$ was < 0.2 ‰ (1.s.d.).

2.3. Quality Assurances and Data Analysis

All reported concentrations were recovery-corrected using a mass-labelled analogue unless stated otherwise (see Table S7). Analytical recovery (%) and analytical precision (%) are displayed in Figures S3 and S4, respectively. Method detection limits were determined for each PFAA (MDL: $\overline{x}_{\text{procedural blank}} + 3 \cdot \text{s.d}_{\text{procedural blank}}$) using procedural blanks (n=7) that comprised of laboratory (n=5; SPE filtered milliQ water) and field blanks (n=2; collected washings of field sampling equipment with SPE filtered milliQ water). Concentrations of PFAA in samples that were below method detection limits were considered as non-detects and sample values were then subject to blank-subtraction using an average of all procedural blanks (n=7). All non-detects were taken as zero and all blank-corrected values (see Table S8 – S12) were included in further calculations (See Equations S1 – S13) and statistical testing. Statistical analyses were performed using concentration data (pg L^{-1}) in RStudio (Version 1.1.453; RStudio Team, 2015) using a significance level of $\alpha = 0.05$. Normality was tested using the Shapiro-Wilks test, before further statistical comparisons. Significant differences in PFAA concentrations were determined using the Wilcoxin's signed-rank test. Spearman's correlation analysis was used to investigate relationships between PFAA and other physical properties in sea ice. To fully evaluate the origin of water in sea ice and assess the contribution of meltwater to the surrounding sea ice system, volumetrically-weighted concentrations were calculated (See Equations S4 – S7).

3. Results and Discussion

3.1. Sea ice origin and characteristics

Sea ice is a heterogenous matrix of ice formed from seawater but which over time may have also been influenced by atmospheric inputs (meteoric) through precipitation such as snow. Figure 2 illustrates some of the physical characteristics of sea ice collected at sampling stations P6 (top panels) and P7 (bottom panels). Mean salinities (volumetrically-weighted) in sea ice (<3.0 ppt) at both P6 and P7 were significantly lower than seawater (32 ppt), but higher than snow (<0.1 ppt). As sea ice forms and grows during winter, entrapped seawater is concentrated (due to the freezing-out effect) and is rejected from the sea ice matrix as brine (a super saline

solution present in bulk ice) into the underlying ocean through a process commonly referred to as gravity drainage [18]. A small amount of salt does however become incorporated into the bulk ice [19, 20]. Low salinities are therefore typical in first-year sea ice as well as multi-year ice, particularly during late-summer when additional ice mass may also have been gained through the incorporation of snow. Furthermore, sea ice may have undergone surface 'flushing' of fresh meltwater, a process that occurs frequently during the Arctic summer [21] and also serves to remove salts from sea ice. While the sea ice was thinner at P6 (1.2 ± 0.1 m) compared to P7 (1.4 ± 0.1 m), both showed a vertical "S" -shape salinity profile, where layers at the snow-ice interface were significantly fresher, indicating the influence of snow water on the distribution and likely dilution of salt in the upper ice layers (Figure 2).

The influence of snow was also supported by measurements of $\delta^{18}O_{H20}$ values, which revealed $\delta^{18}O_{H20}$ values in sea ice ($\delta^{18}O_{sea\ ice} = 0.5 \pm 1.2$ ‰) that were significantly more positive than snow ($\delta^{18}O_{snow} = -15.2 \pm 1.1$ ‰) and seawater ($\delta^{18}O_{seawater} = -0.1 \pm 0.4$ ‰). During freezing of ocean water to form sea ice, equilibrium fractionation of oxygen isotopes in water enriches $\delta^{18}O_{sea\ ice}$ by approximately 2.6 ‰.[22] This generates ice core signatures enriched in ^{18}O compared to precursor seawater values. The measurement of $\delta^{18}O_{sea\ ice}$ values which are frequently isotopically lighter than seawater indicates the entrainment of meteoric water which is expected to have occurred during the ageing of sea ice at both sites. One potential other source of meteoric water to sea ice is from glacial run-off entering into fjord environments/coastal fringes of the Barents Sea [23] during the summer season. However, given the sampling locations in this study and the volume of glacial meltwater required to lower the isotopic composition in sea ice by the required amount, then the incorporation of atmospheric snowfall is the most likely source of meteoric water.

Similar to salinity profiles, $\delta^{18}O_{H2O}$ values at the surface of sea ice at both P6 and P7 were lower compared to deeper ice layers which indicate a strong influence of atmospheric precipitation (probably mostly snow) on the composition of sea ice at both sites. However, a comparison of $\delta^{18}O_{\ sea\ ice}$ profiles also revealed some marked differences between sea ice at P6 and P7. A notable feature at P7 were low $\delta^{18}O_{sea\ ice}$ values ($\delta^{18}O_{\ sea\ ice} < -2$ ‰) in the deepest ice situated at the seawater-ice interface. One explanation for this observation is the

percolation and subsequent refreezing of meltwater derived from surface precipitation, forming an ice layer known as superimposed ice. This is also supported by salinity measurements which show that the bottom layers of sea ice were fresher. Superimposed ice forms when the surrounding ice matrix is colder than the freezing temperature of freshwater [24] and is a common feature in Arctic and Antarctic glaciers. Superimposed ice has also been reported in sea ice [25, 26], and its presence suggests that the ice at P7 was second-year ice (SYI) or multi-year ice (MYI).

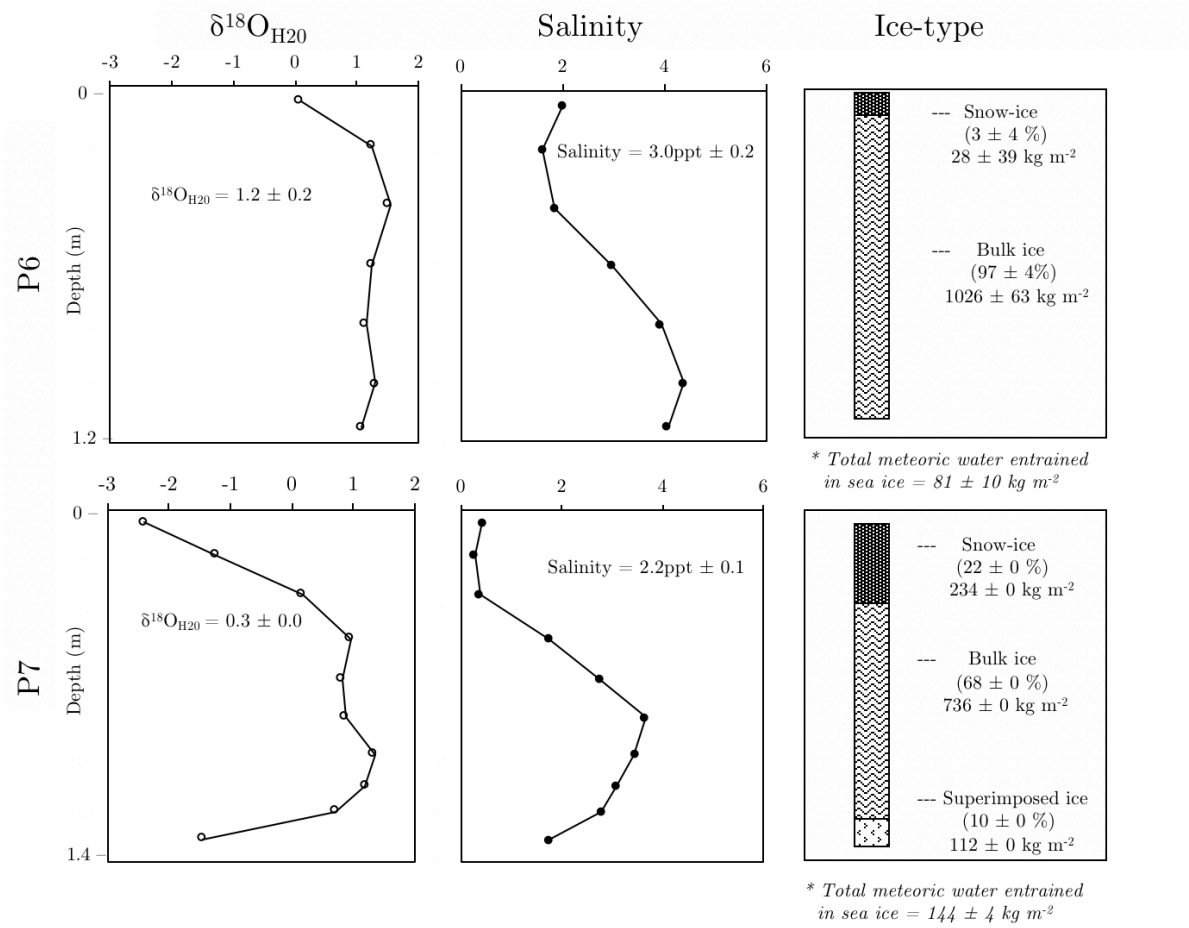

Figure 2: Physical sea ice properties and mass of ice at P6 and P7. Ice type is determined from $\delta^{18}O_{H20}$ values which indicate the origin of meteoric water entrainment. Snow-ice = $\delta^{18}O_{sea\ ice}$ values <1 ‰; Bulk ice = $\delta^{18}O_{sea\ ice}$ values 1–3 ‰; Superimposed ice = $\delta^{18}O_{sea\ ice}$ values <1 ‰ (salinity<2ppt). Snow is not shown in this figure but possessed $\delta^{18}O_{H20}$ values <10 ‰. Amount of different ice types (%) is calculated as a fraction of the total mass of water (kg m^{-2}) in the sea ice system. Points represent ice core samples approximately 0.1 – 0.2 m in length. * Indicates the total amount of meteoric water based on isotopic fractionation in newly-formed sea ice of $\delta^{18}O_{newly\text{-}formed\ sea\ ice}$ = 2.6 ‰ [22].

In order to differentiate between compartments of sea ice that were influenced by differing quantities of water of meteoric origin, sea ice was classified into three broad ice-types based on $\delta^{18}O_{H20}$ values (and salinity): (i) 'Snow-ice' ($\delta^{18}O_{sea\ ice}$ values <1 ‰) that retains a strong meteoric signal; (ii) 'bulk ice' ($\delta^{18}O_{sea\ ice}$ values 1–3 ‰) predominantly influenced by sea water and less by snow meltwater; (iii) 'Superimposed ice' ($\delta^{18}O_{sea\ ice}$ values <1 ‰ and salinity <2 ppt), present at deeper layers and influenced by snow meltwater (or other high latitude atmospherically-derived precipitation). Using the cumulative ice sample length (m) and measured ice densities (kg m^{-3}), then the mass or load of water (kg m^{-2} ice column) was calculated for each of the respective ice types (See Figure 2; right panel). Results showed that while snow-ice was present at both sites, the relative amount (% snow-ice mass/total sea ice mass) varied substantially between P6 (7 ± 2 %) and P7 (22 ± 0 %). Snow-ice is formed when free-floating sea ice receives a substantial snow cover which in turn leads to seawater flooding of the surface sea ice and basal snow layers forming a salty slush layer that can then refreeze [27]. Snow-ice is therefore a mixture of snow and seawater [28]. Such a large difference between the ice floes indicates that the two sites comprised of sea ice of different ages and/or had followed different 'lifecycles'. Increased snow-ice at P7 indicates that the ice floe had retained a greater amount of its snow loading from the previous Winter season. Established methods (Granskog et al., 2017) were used to investigate this further by calculating the relative amount (% meteoric water mass/newly-formed sea ice mass) of meteoric water incorporated within the ice floes at P6 and P7 respectively, based on an intial isotopic fractionation in newly-formed sea ice of $\delta^{18}O_{newly\text{-}formed\ sea\ ice} = 2.6$ ‰ [22]. This indicated that sea ice at P6 and P7 was composed of 8 ± 1 % and 13 ± 0 % meteoric water, respectively. These estimations of entrained meteoric water in the respective ice floes correspond well with those given by Granskog et al., (2017) for first-year sea ice (FYI; 3.3 – 4.4 %) and second-year sea ice (SYI; 12.7 – 16.3 %) sampled in a comparable region (adjacent to the Barents Sea) during Winter. This suggests that sea ice at P6 and P7 is FYI and SYI (or older), repectively and supports the assertion that P7 had received a higher snow load (probably over successive seasons) compared to P6. While our values of meteoric water content for P6 ice are slightly higher than those reported by Granskog et al., our samples of sea ice were collected during late-summer and hence may have entrained

more precipitation (i.e. snow or rain) or been further influenced by freeze-thaw cycles and/or drainage of surface snow-derived meltwater during the Summer.

3.2. Occurrence of PFAA in snow, sea ice and seawater

Table 1 shows a summary of measured concentrations of PFAA in different environmental compartments sampled during the cruise (the complete data set can be found in the SI). Notable differences in concentrations (and environmental behaviours) were observed between the short- and long-chain PFAA and therefore results for each group are reported accordingly. In snow samples, most target PFAA were detected, with the exception of PFBS (C_4) and PFOS (C_8), and showed similar levels across both sites (n=6). Consequently, concentrations in snow (melt water equiv.) were averaged and values hereafter refer to the mean concentrations from both sites. The presence of PFAA in the snowpack implies a meteoric source signifiying atmospheric transport as a major pathway to the Arctic marine environment, although a fraction of PFAA in ice-rafted snow may also have arisen from marine aerosol generated from sea spray [29]. Concentrations of short-chain PFAA in snow in this study were significantly higher (Wilcoxin signed-rank test, $p<0.01$) than long-chain PFAA. Similar findings were reported in snow (see Table 1) sampled from sites located in the Western Arctic [5] and others [6, 7] in the Canadian Arctic Archipelago, suggesting that similar chemical sources influence different Arctic regions. Nevertheless, concentrations of short-chain PFAA in snow were generally much higher in our study driven notably by high levels of perfluorobutanoic acid (PFBA = 2.6 ± 0.7 ng L^{-1}) which probably reflects the higher industrial consumption of chemical precursors resulting in its formation in recent years. Concentrations of long-chain PFAA in snow, however, were similar to those measured in previous studies [5, 7] which shows that atmospheric deposition, presumably through the photooxidation of volatile precursors (e.g. fluorotelomer alcohols), is still ongoing at the same rate over the last 10 years or so.

Table 6: Summary of measured concentrations of short- and long-chain PFAA in relevant compartments reported in key studies throughout the Arctic.

Chemical	$\Sigma PFAA_{short\text{-}chain}$ (ng L^{-1})				$\Sigma PFAA_{long\text{-}chain}$ (ng L^{-1})			
Snow	0.7 ± 0.6	n/a	n/a	2.9 ± 0.8	0.2 ± 0.1	n/a	n/a	0.2 ± 0.1
Sea ice	0.3 ± 0.5	n/a	n/a	1.9 ± 2.8	0.6 ± 0.4	n/a	n/a	0.2 ± 0.2
Seawater	0.3 ± 0.2	0.1 ± 0.0	0.3 ± 0.0	0.6 ± 0.1 (0.5 m) 0.2 ± 0.1 (5.0 m)	0.1 ± 0.0	0.1 ± 0.0	0.4 ± 0.0	1.4 ± 0.9 (0.5 m) 0.4 ± 0.2 (5.0 m)
Location	Western Arctic Ocean (ice-free)	Greenland Sea (ice-free)	North Sea (ice-free)	Barents Sea region	Western Arctic Ocean (ice-free)	Greenland Sea (ice-free)	North Sea (ice-free)	Barents Sea region
Reference	Cai et al., 2012	Joerrs et al., 2020	Joerrs et al., 2020	This study	Cai et al., 2012	Joerrs et al., 2020	Joerrs et al., 2020	This study

Average concentrations (mean ± s.d) use all data from P6 and P7 sampling stations (~81°N). Surface seawater in the North Sea (~58 – 62 °N) and Greenland Sea (~68 – 79 °N) were taken along a latitudinal transect and sampled at a depth of 11 m. Surface seawater (~66 – 70 °N) and sea ice (~77 – 87 °N) samples analysed by Cai et al., (2012) were collected in different areas of the Western Arctic Ocean and the seawater sampling depth was not explicitly stated. Concentrations listed in sea ice in this study are volumetrically-weighted. n/a = no available data. Note: ΣPFAA concentrations listed in this study may differ slightly to those stated in the original reference due to the selection of PFAA to match the same target PFAAas this study.

PFCA and PFSA are formed in the atmosphere from a wide number of precursor chemicals and positive correlations between the various PFAA suggests they share similar sources and/or transport pathways into the Arctic (See Figure S4). While the presence of relatively high levels of PFBA (C_4) is probably linked to chlorofluorocarbon (CFC) replacement compounds [6] other important precursors include perfluoroalkane sulfonyl fluorides (PASF) and fluorotelomer-based compounds (FT-based) [30]. The presence of the long- chain PFCA such as PFDA (C_{10}) and PFUnA (C_{11}) (not primary substances in commercial products) is most likely through the atmospheric photochemical transformation of fluorotelomer chemicals including olefins [31], acrylates [32], and iodides [33] as well as alcohols [34, 35]. Interestingly, PFBS (C_4) and PFOS (C_8) were the only PFSA detected in this study which shows they are still the main perfluoroalkyl sulfonates present in the Arctic environment [36], but they were below detection limits in our snow samples. While low levels of PFOS in snow may be related to industry initiatives aimed to lower the environmental emmisions of PFOS-related compounds, levels of PFBS (C_4) in snow are expected to be higher due to increased global consumption of short-chain precursors

which lead to its formation.[37] This shows that our current understanding of the environmental processes that govern the transport and cycling of some PFAA in the Arctic environment is incomplete and warrants further research. Nevertheless, given that PFOS has recently been detected in most snow samples from the Canadian Arctic [7], the absence of PFSA in our snow samples suggests that concentrations may vary due to seasonal changes in photochemical activity [38] or migration of volatile precursor compounds via the atmosphere [39]. However, it is also likely that PFOS and PFBS (and probably other PFAA) have undergone early elution from the snowpack in meltwater during snow ageing/thawing episodes [40-42] as indicated by high levels of PFBS in sea ice layers directly beneath the snow (See Figure 3).

The mean concentration of both short- and long-chain PFAA in sea ice were comparable to snow, with short-chain PFAA also showing similarly higher levels than long-chain PFAA (Wilcoxin signed-rank test, $p<0.05$). Figure 3 illustrates the vertical concentration profiles of short- (top panels) and long-chain (bottom panels) PFAA in sea ice at P6 (left panels) and P7 (right panels). Concentrations in the surface layers of sea ice tended to be much higher than lower layers. The higher concentrations of PFAA in the surface sea ice layers corresponds well with patterns observed in sea ice located in other regions of the Arctic [5] indicating similar Arctic-wide processes affecting PFAA accumulation in sea ice. Elevated concentrations of PFAA in the uppermost ice layers of sea ice may be a result of entrainment of chemicals present in seawater during initial sea ice formation. [15, 43] However, snowfall deposition is also likely to play an important role in the delivery of PFAA [44] to sea ice with the amount and timing likely to affect accumulation dynamics.

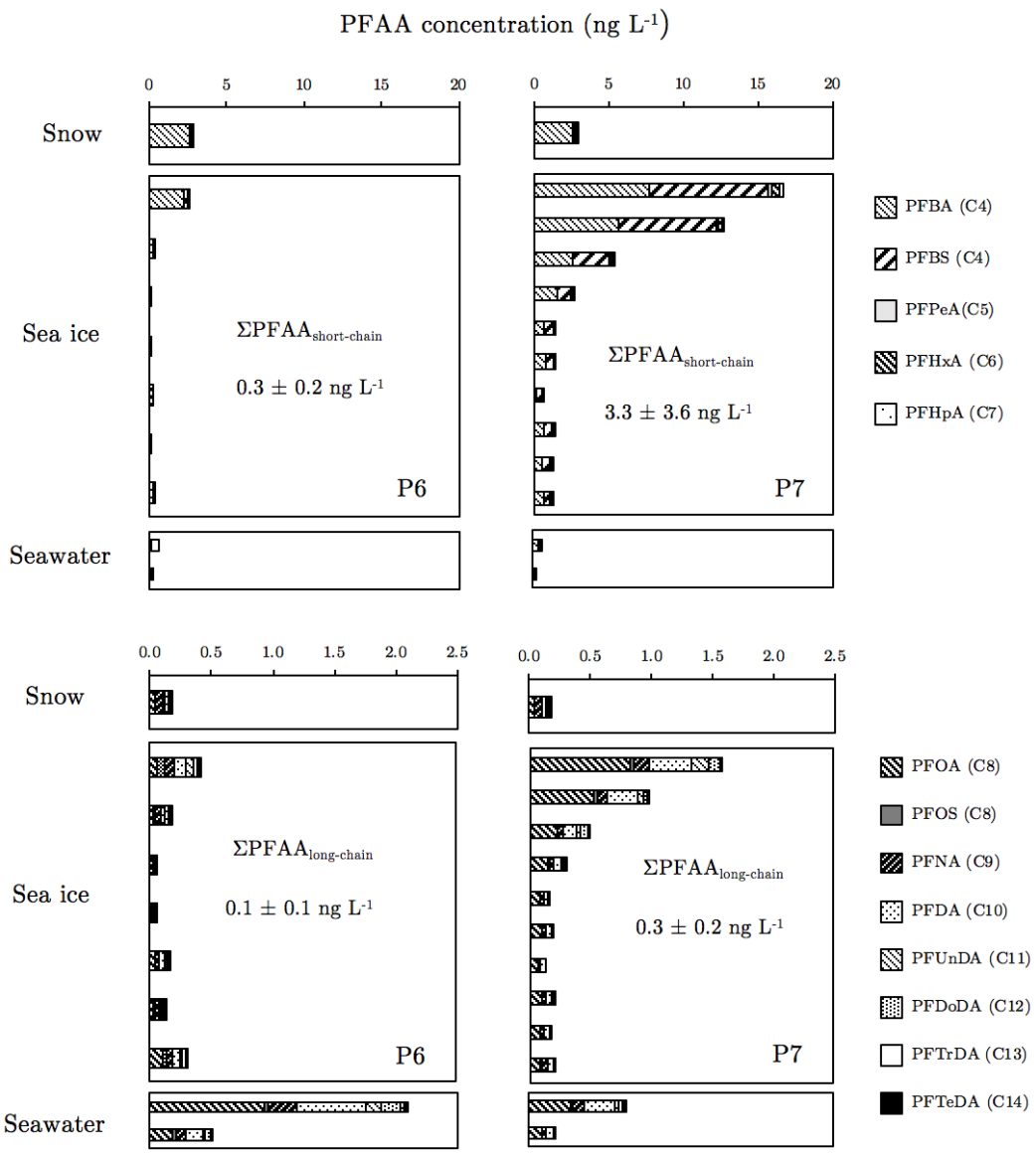

Figure 3: The sum of short- and long-chain PFAA in different environmental compartments. Concentration profiles for short- and long-chain PFAA are shown in the upper and lower panels, respectively. Concentration profiles for P6 and P7 are shown in the left and right panels, respectively. Seawater samples collected at a depth of 0.5 m and 5 m are also represented by the upper and lower bar, respectively. Low concentrations of short-chain PFAA (e.g. PFBA) in seawater are likely to be attributed to analytical issues related to high matrix effects. The sum (mean ± s.d.) of short- and long-chain PFAA in sea ice (volumetrically-weighted) is also included in each panel.

Differences were apparent between the concentrations and distribution of PFAA in sea ice at both sites, notably in the general shape of the concentration profiles. A gradual reduction from high concentrations at the surface towards lower ice layers was seen for short-chain PFAA at P7, but a more marked reduction was observed at P6. Indeed, many short-chain PFAA were

below method detection limits in the deeper ice layers (>70% of sea ice samples) at P6 and this demonstrates the different ice ages and 'weathering' processes (i.e. freeze-thaw activity) between these two sites. The short-chain PFAA are more water soluble than the long-chain PFAA and likely to be more mobile when liquid water is present in the ice system [41-43]. Preferential elution of short-chain PFAA down a snow core has been observed in a temperate Tibetan mountain glacier that experienced summer melt episodes [45] and hence the absence of the short-chain PFAA in the deeper sea ice at P6 most likely indicates loss through elution by meltwater drainage with subsequent replenishment in the surface layers through snow deposition. At P7 this is not apparent and the higher concentrations of short-chain PFAA down the ice core shows that meltwater drainage was more limited compared to P6. While the presence of superimposed ice at the bottom of the sea ice at P7 (see Figure 2; right panel) may affect the downward percolation of PFAA in meltwater [46], it is more likely that less thawing occurred at P7 which in turn preserved the accumulated burden of PFAA. The exact reason for this difference in 'weathering' history (i.e. melt rate) between sites is unknown, but could be due to greater inflow of warmer Atlantic water at P6 compared to P7 [47] and/or related to the amount of snowfall (see Section 3.3) serving as insulation against atmospheric thermal changes [48].

Long-chain PFAA also showed a gradual decrease in concentrations from the surface ice layers of sea ice but with an increase in concentrations in lower layers (notably at P6) to form a concentration profile that resembled a "C" -shape. A c-shape concentration profile in sea ice is typical for salt (NaCl) and other dissolved solutes like PFAS [43] and even hydrophobic organic pollutants [15] during Winter. This feature develops through a process known as gravity drainage whereby chemical constituents present in freezing seawater are excluded from the pure ice crystal matrix and rejected into adjacent brine channels [20]. The stronger resemblance of this c-shape concentration profile for long-chain PFAA at P6 compared to P7 therefore supports the previous assertion that sea ice at P6 and P7 is comprised of FYI and SYI (or older), respectively as discussed in section 3.1. Furthermore, the distinct concentration profiles between the short- and long-chain PFAA illustrates the differences in their physical-chemical

properties and their subsequent behaviour during the transition towards the Summer ice system.

Unlike snow and sea ice which showed higher concentrations of short-chain PFAA, the under-ice seawater revealed greater concentrations of long-chain PFAA compared to short-chain PFAA (See Table 1). This is likely to be a reflection of the longer-term input of PFOA and other long-chain PFAA to Arctic seawater over the last few decades [7, 49, 50]. Concentrations of PFAA in the seawater directly below the ice (0.5 m depth) also supports this by revealing significantly higher (Wilcoxin signed-rank test; $p<0.05$) concentrations than at the greater depth of 5 m at both sites (See Figure 3). A comparision of mean total PFAA concentrations (i.e. short- and long-chain PFAA; ΣPFAA) in seawater samples at 5 m in this study (ΣPFAA = ~0.6 ng L^{-1}) with recent measurements made in ice-free parts of the Greenland Sea (ΣPFAA = ~0.4 ng L^{-1}) showed that our concentrations are comparable to previous observations. In constrast, seawater concentrations at 0.5 m in this study (ΣPFAA = ~2.0 ng L^{-1}) were approximately ~5-fold more and were even higher than those measured in surface seawater in the North Sea closer to source regions (ΣPFAA = ~0.7 ng L^{-1}) .[4] Given the remoteness of the sampling sites in this study, the lack of local sources [51] and low blank values (that rule out potential contamination artefacts) the high concentrations of PFAA in seawater in close proximity to sea ice must be driven by the overlying ice pack through release from meltwater drainage given the time of year when sampling occurred. This is supported by meteorological data (Tables S4 and S5) and measurements made on the sea ice cores (Figure S2) that show temperatures were high enough to cause some melting. Differences in concentrations between the two depths (0.5 m and 5 m) are unlikely to be caused by sampling different stratified water masses as the polar mixed layer (PML) extends from the surface to ~10 m depth in the Barents Sea during summer ice-covered conditions [52], and is characterized by slightly lower salinity compared to deeper waters. These findings are analogous to a fresh water column in a lake located in the Canadian high Arctic whereby elevated concentrations of PFAA were found in surface waters following the onset of melt [53]. Although higher concentrations of short-chain PFAA in under-ice seawater were not as marked relative to long-chain PFAA, this probably reflects the earlier elution of these particular chemicals from the ice pack with subsequent

dispersal. It is also noteworthy that the analytical recovery of some short-chain PFAA in seawater samples was low (e.g. PFBA <10%; see Figure S3, with an analytical precision of 50% RSD for seawater; see Figure S4). Given that PFBA contributed >90% of the sum of short-chain PFAA in snow/sea ice samples (Section 3.2), it is therefore likely that the concentration of PFBA is bias low and thus the concentration of short-chain PFAA in seawater is underestimated. Nonetheless, taking this possible artefact into consideration, PFAA concentrations in under-ice seawater in this study were still higher than those observed in ice-free zones in the North Sea by Joerss et al, (2020) [4] who used the same analytical methodology .

3.3. The thawing ice pack influences PFAA in the underlying seawater

The concentrations of PFAA measured in the under-ice seawater (0.5 m) at P6 were the highest in this study (e.g. $\Sigma PFAA_{P6\_seawater\_0.5m} = 2.7 \pm 1.5$ ng L^{-1}), which suggests that PFAA originate from the overlying melting ice pack. Although the PFAA profile (% $\Sigma PFAA_{long\text{-}chain}$) in seawater was not significantly different between sites (See Figure S6), concentration ratios for individual PFAA (e.g., $c(PFAA)_{P6\_seawater\_0.5m}$ / $c(PFAA)_{P7\_seawater\_0.5m}$) revealed that PFAA concentrations at P6 were on average 4-fold higher than at P7, and this is likely to be related to the different thawing or 'weathering' history of the overlying ice pack at the two study sites.. To investigate this further using a mass-apportionment approach, Figure 4 shows the mass fraction of all PFAA (% ΣPFAA) in the different ice types at P6 (left panel) and P7 (right panel). While large proportions of PFAA were contained within bulk ice (32 – 71 % ΣPFAA) which made up the majority of the total water mass in the ice systems across both sites (see Figure 2), high proportions of PFAA were also present in snow-ice (26 – 62 % ΣPFAA). This ice type, however, made a relatively minor contribution to the total water mass of the ice pack at both sites (3 – 22 %). Similarly the ice-rafted snow layers contained 1 – 3 % ΣPFAA burden at both sites but comprised <1 % of the total water mass of the respective ice systems. Substantial loss of surface layers containing high concentrations of PFAA (see Table S13 – S14), including snow and snow-ice, during periods of thaw will therefore mobilise portions of the sea ice pack. These in turn hold relatively high burdens of PFAA leading to

significant releases of these chemicals particularly when atmospheric temperatures rise resulting in seasonal thaw.

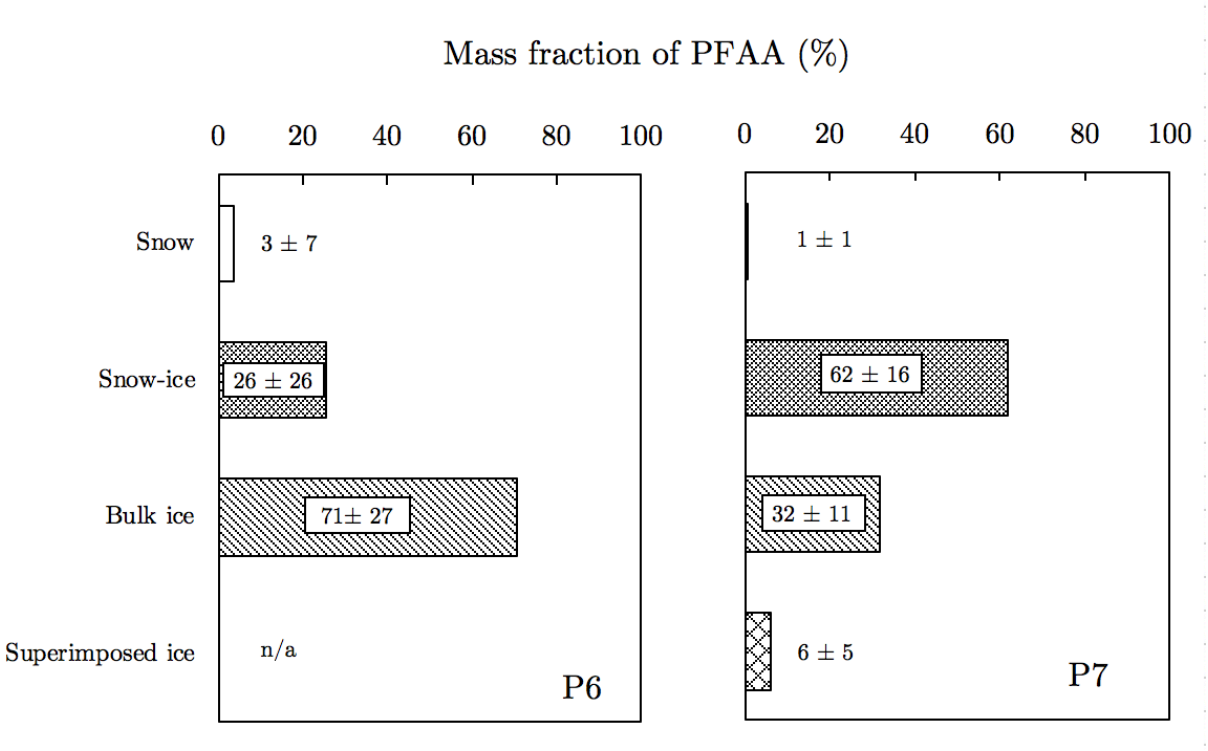

Figure 4. Mass apportionment of ΣPFAA (i.e., short and long-chain PFAA) in different 'ice types' at the sampling stations, P6 and P7. n/a = not applicable.

Using average (mean ± s.d.) snow depth of 0.49 ± 0.13 m and snow density of 363 ± 24 kg m^{-3} for the snowpack across a comparable region (north of Svalbard) during winter [21] gives rise to an estimated annual snow water-equivalent load of 178 ± 49 kg m^{-2}. Mass-apportionment calculations utilising mean $\delta^{18}O_{snow}$ values (assuming constant sea ice mass) show only 81 ± 10 kg m^{-2} of meteoric water at P6, whereas the meteoric water mass at P7 is higher at 144 ± 4 kg m^{-2}, and closer to the annual snow water equivalent value above. This demonstrates that a substantial loss of the annual snowfall occurred over the course of the season at P6 resulting in the lower overall mass of entrained meteoric water. The loss of meteoric water at P6 is likely to have occurred through thawing of snow and other snow-ice layers followed by meltwater percolation through the ice into the under-ice seawater. In turn, this meteorically-influenced meltwater will transfer its relatively high PFAA burden either deeper into the bulk ice or into the under-ice seawater. In contrast, the higher mass of meteoric water at P7, an ice floe likely comprising older ice, demonstrates relatively less thawing during its recent history

and hence lower release of meteorically-derived meltwater compared to P6. As a consequence, high concentrations of PFAA in sea ice are retained in snow-ice and other upper sea ice layers enabling chemicals to accumulate and concentrations to exceed those in sea ice at P6.

The composition (% $\Sigma PFAA_{long\text{-}chain}$) of sea ice and adjacent compartments also indicate that the ice floes at both sites had been influenced by distinct processes leading to different PFAA patterns (Figure S6 – S7) with P6 and P7 being only weakly correlated (r^2 = 0.30, n=8; $p>0.15$) Sea ice composition at P6 was more highly correlated with snow (r^2 = 0.77, n=8; $p<0.01$) than seawater which implies that the ice floe was affected by recent meltwater arising from thawing of moderately fresh snow. Thus the lower entrainment of meteoric water at P6 via snowfall, as indicated by isotopic measurements, illustrate that melting of surface sea ice layers (i.e. snow and snow-ice) probably occurred earlier in the season with later melt originating from fresh snow. Conversely, sea ice at P7 was more highly correlated with seawater (r^2 = 0.98, n=8; $p<0.001$) than snow, which suggests less thawing and greater surface flooding of sea ice with seawater (i.e., snow-ice). The excellent agreement between isotope measurements and PFAA observations made on the same samples in this study provide high confidence that our account of the evolution history of sea ice at both sites is accurate.

3.4. Meltpond significance and environmental implications

This study provides compelling evidence that the melting of the marine ice pack drives high concentrations of PFAA in under-ice seawater and serves as a significant source of these chemicals to the under-ice environment during seasonal thaw. Although PFAA in sea ice may also originate from the uptake of PFAA from seawater during its initial formation, the data presented in this study shows that a high proportion of PFAA is present in snow-ice, and hence probably derived from the atmosphere. This demonstrates that snow plays an important role in both the delivery and storage of PFAA in the sea ice pack, with the timing and amount of snowfall likely to influence the melting and subsequent release of PFAA into the seawater.

We also measured PFAA in water samples collected from meltponds that were present on the ice floes at P6 and P7. Meltponds feature on the surface of predominantly late-season sea ice

in the Arctic and form as snow and sea ice thaw [54]. At more advanced stages, meltponds are influenced by intrusions of seawater and have been shown to play an important ice-mediated annual delivery route of some semi-volatile contaminants (e.g., organochlorine pesticides) to the under-ice seawater [17]. Given the very different physico-chemical properties of PFAA compared with these other previously studied organic contaminants, investigating the significance of meltponds on their environmental cycling is warranted. By comparing meltpond composition (e.g., salinity, $\delta^{18}O$) with the surrounding end-members (i.e., snow, sea ice and seawater) their meteoric/oceanic origin can be established. Using average values of salinity and $\delta^{18}O$ in end-members (Table S15), the mass fraction (%) that each of these three sources contributed to individual meltponds can be calculated [55]. The results shown in Table S16 suggest that snow (35 ± 9 %) and sea ice (64 ± 10 %) were the major contributors to the composition of meltponds, with only a small fraction coming from seawater (0 ± 2 %). The mass fraction (%) and measured PFAA concentration (ng L^{-1}) in each respective end-member were multiplied and then summed to give 'predicted' concentrations of each PFAA in meltpond water (Table S17 – S18). In general, the measured concentrations of PFAA in meltponds were considerably lower than in the under-ice seawater and a comparision between the 'measured' and 'predicted' PFAA concentrations in meltponds revealed no significant difference (Wilcoxin signed-rank test, $p<0.05$). This shows that the meltponds we sampled were not a significant source of PFAA and are unlikely to have played a role in the high PFAA concentrations measured in seawater. These results support the assertion that the meltponds had formed during the later stages of the Arctic summer season after significant thawing had already occurred. Together, this information strongly suggests that the occurrence of high PFAA concentrations in under-ice seawater is more likely attributed to thawing of surface sea ice layers earlier in the season and shows that different contaminant classes (e.g., organochlorine pesticides, PFAA etc) do not nessesarily follow the same environmental cycling patterns in the marine polar environment.

The concentrations of short- and long-chain PFAA in under-ice seawater are comparable to levels observed in coastal seas in temperate latitudes, but the duration of these high concentrations is probably dependent on the presence of different ice types. Following complete ice break-up and thawing, concentrations in surface seawater are likely to decline. Nonetheless,

the presence of PFAA in the under-ice environment at concentrations comparable to temperate coastal seas presents an exposure hazard to ice-associated biota and organisms at the base of the pelagic foodweb. Further efforts are now required to investigate the duration and timing of these periods of elevated concentrations and how they link with biological events such as planktonic blooms. Although more work is needed to ascertain the impact of high concentrations of PFAA on biological communities, the work presented in this study suggests that the thawing of the ice pack may present an efficient pathway for these chemicals to enter the base of the Arctic marine foodweb.

Supporting Information. List of target analytes and quality assurance criteria; concentration, meteorological, density and temperature data with all associated equations are supplied as Supporting Information (SI).

4. Acknowledgements

JG's PhD (NE/L002604/1) was funded through NERC's ENVISION Doctoral Training Centre. This work resulted from the EISPAC project (NE/R012857/1), part of the Changing Arctic Ocean programme, jointly funded by the UKRI Natural Environment Research Council (NERC) and the German Federal Ministry of Education and Research (BMBF). This work is also a contribution to the Nansen Legacy project and would not have been possible without the help and support of participating scientists and staff. The Nansen Legacy is funded by the Research Council of Norway (# 276730). The authors would like to thank all of the scientists and crew members onboard the *Kronprins Haakon* for their assistance in sample collection and hospitality during the cruise. We thank Dave Hughes, Isotope Technician at Lancaster Envrionment Centre, who conducted the isotope analysis. Finally, we would like to thank two anonymous reviewers for their insightful comments.

5. References

1. Buck, R. C.; Franklin, J.; Berger, U.; Conder, J. M.; Cousins, I. T.; de Voogt, P.; Jensen, A. A.; Kannan, K.; Mabury, S. A.; van Leeuwen, S. P. J., Perfluoroalkyl and polyfluoroalkyl substances in the environment: Terminology, classification, and origins. *Integr Environ Assess Manag* **2011,** *7* (4), 513-541;10.1002/ieam.258

2. Buck, R. C.; Franklin, J.; Berger, U.; Conder, J. M.; Cousins, I. T.; de Voogt, P.; Jensen, A. A.; Kannan, K.; Mabury, S. A.; van Leeuwen, S. P. J., Perfluoroalkyl and polyfluoroalkyl substances in the environment: terminology, classification, and origins. *Integrated environmental assessment and management* **2011,** *7* (4), 513-541;10.1002/ieam.258

3. Borgå, K., The Arctic ecosystem: A canary in the coal mine for global multiple stressors. *Environmental Toxicology and Chemistry* **2019,** *38* (3), 487-488;https://doi.org/10.1002/etc.4360

4. Joerss, H.; Xie, Z.; Wagner, C. C.; von Appen, W.-J.; Sunderland, E. M.; Ebinghaus, R., Transport of Legacy Perfluoroalkyl Substances and the Replacement Compound HFPO-DA through the Atlantic Gateway to the Arctic Ocean—Is the Arctic a Sink or a Source? *Environmental Science & Technology* **2020**;10.1021/acs.est.0c00228

5. Cai, M.; Zhao, Z.; Yin, Z.; Ahrens, L.; Huang, P.; Cai, M.; Yang, H.; He, J.; Sturm, R.; Ebinghaus, R.; Xie, Z., Occurrence of Perfluoroalkyl Compounds in Surface Waters from the North Pacific to the Arctic Ocean. *Environmental Science & Technology* **2012,** *46* (2), 661-668;10.1021/es2026278

6. Pickard, H. M.; Criscitiello, A. S.; Persaud, D.; Spencer, C.; Muir, D. C. G.; Lehnherr, I.; Sharp, M. J.; De Silva, A. O.; Young, C. J., Ice Core Record of Persistent Short-Chain Fluorinated Alkyl Acids: Evidence of the Impact From Global Environmental Regulations. *Geophysical Research Letters* **2020,** *47* (10), e2020GL087535;10.1029/2020GL087535

7. Pickard, H. M.; Criscitiello, A. S.; Spencer, C.; Sharp, M. J.; Muir, D. C. G.; De Silva, A. O.; Young, C. J., Continuous non-marine inputs of per- and polyfluoroalkyl substances to the High Arctic: a multi-decadal temporal record. *Atmos. Chem. Phys.* **2018,** *18* (7), 5045-5058;10.5194/acp-18-5045-2018

8. Young, C. J.; Furdui, V. I.; Franklin, J.; Koerner, R. M.; Muir, D. C. G.; Mabury, S. A., Perfluorinated Acids in Arctic Snow: New Evidence for Atmospheric Formation. *Environmental Science & Technology* **2007,** *41* (10), 3455-3461;10.1021/es0626234

9. Gustafsson, Ö.; Andersson, P.; Axelman, J.; Bucheli, T. D.; Kömp, P.; McLachlan, M. S.; Sobek, A.; Thörngren, J. O., Observations of the PCB distribution within and in-between ice, snow, ice-rafted debris, ice-interstitial water, and seawater in the Barents Sea marginal ice zone and the North Pole area. *Science of the Total Environment* **2005,** *342* (1), 261-279;10.1016/j.scitotenv.2004.12.044

10. Pućko, M.; Stern, G.; Macdonald, R. W.; Barber, D. G., alpha- and gamma-Hexachlorocyclohexane Measurements in the Brine Fraction of Sea Ice in the Canadian High Arctic Using a Sump-Hole Technique. *Environmental Science & Technology* **2010,** *44* (24), 9258-9264;10.1021/es102275b

11. Pućko, M.; Stern, G. A.; Barber, D. G.; Macdonald, R. W.; Rosenberg, B., The international polar year (IPY) circumpolar flaw lead (CFL) system study: The

importance of brine processes for α- and γ-hexachlorocyclohexane (HCH) accumulation or rejection in sea ice. *Atmosphere-Ocean* **2010,** *48* (4), 244-262;10.3137/OC318.2010
12. Pućko, M.; Stern, G. A.; Barber, D. G.; Macdonald, R. W.; Warner, K. A.; Fuchs, C., Mechanisms and implications of α-HCH enrichment in melt pond water on Arctic sea ice. *Environmental Science & Technology* **2012,** *46* (21), 11862;10.1021/es303039f
13. Pućko, M.; Stern, G. A.; Macdonald, R. W.; Jantunen, L. M.; Bidleman, T. F.; Wong, F.; Barber, D. G.; Rysgaard, S., The delivery of organic contaminants to the Arctic food web: Why sea ice matters. *Science of the Total Environment* **2015,** *506-507*, 444-452;10.1016/j.scitotenv.2014.11.040
14. Pućko, M.; Stern, G. A.; Macdonald, R. W.; Rosenberg, B.; Barber, D. G., The influence of the atmosphere-snow-ice-ocean interactions on the levels of hexachlorocyclohexanes in the Arctic cryosphere. *Journal of Geophysical Research: Oceans* **2011,** *116* (C2), n/a-n/a;10.1029/2010JC006614
15. Garnett, J.; Halsall, C.; Thomas, M.; France, J.; Kaiser, J.; Graf, C.; Leeson, A.; Wynn, P., Mechanistic Insight into the Uptake and Fate of Persistent Organic Pollutants in Sea Ice. *Environmental science & technology* **2019,** *53* (12), 6757;10.1021/acs.est.9b00967
16. Casal, P.; Casas, G.; Vila-Costa, M.; Cabrerizo, A.; Pizarro, M.; Jiménez, B.; Dachs, J., Snow Amplification of Persistent Organic Pollutants at Coastal Antarctica. *Environmental Science & Technology* **2019,** *53* (15), 8872-8882;10.1021/acs.est.9b03006
17. Pućko, M.; Stern, G. A.; Burt, A. E.; Jantunen, L. M.; Bidleman, T. F.; Macdonald, R. W.; Barber, D. G.; Geilfus, N.-X.; Rysgaard, S., Current use pesticide and legacy organochlorine pesticide dynamics at the ocean-sea ice-atmosphere interface in resolute passage, Canadian Arctic, during winter-summer transition. *Science of the Total Environment* **2017,** *580*, 1460-1469;10.1016/j.scitotenv.2016.12.122
18. Thomas, M.; Vancoppenolle, M.; France, J. L.; Sturges, W. T.; Bakker, D. C. E.; Kaiser, J.; von Glasow, R., Tracer Measurements in Growing Sea Ice Support Convective Gravity Drainage Parameterizations. *Journal of Geophysical Research: Oceans* **2020,** *125* (2), e2019JC015791;10.1029/2019JC015791
19. Griewank, P. J.; Notz, D., Insights into brine dynamics and sea ice desalination from a 1-D model study of gravity drainage. *Journal of Geophysical Research: Oceans* **2013,** *118* (7), 3370-3386;10.1002/jgrc.20247
20. Notz, D.; Worster, M. G., Desalination processes of sea ice revisited. *Journal of Geophysical Research: Oceans* **2009,** *114* (C5), n/a-n/a;10.1029/2008JC004885
21. Granskog, M. A.; Rösel, A.; Dodd, P. A.; Divine, D.; Gerland, S.; Martma, T.; Leng, M. J., Snow contribution to first-year and second-year Arctic sea ice mass balance north of Svalbard. *Journal of Geophysical Research: Oceans* **2017,** *122* (3), 2539-2549;10.1002/2016JC012398

22. Macdonald, R. W.; Paton, D. W.; Carmack, E. C.; Omstedt, A., The freshwater budget and under-ice spreading of Mackenzie River water in the Canadian Beaufort Sea based on salinity and 18O/16O measurements in water and ice. *Journal of Geophysical Research: Oceans* **1995,** *100* (C1), 895-919;10.1029/94JC02700
23. Błaszczyk, M.; Ignatiuk, D.; Uszczyk, A.; Cielecka-Nowak, K.; Grabiec, M.; Jania, J. A.; Moskalik, M.; Walczowski, W., Freshwater input to the Arctic fjord Hornsund (Svalbard). *Polar research* **2019,** *38*, 1-18;10.33265/polar.v38.3506
24. Nicolaus, M.; Haas, C.; Bareiss, J., Observations of superimposed ice formation at melt-onset on fast ice on Kongsfjorden, Svalbard. *Physics and chemistry of the earth. Parts A/B/C* **2003,** *28* (28), 1241-1248;10.1016/j.pce.2003.08.048
25. Eicken, H.; Krouse, H. R.; Kadko, D.; Perovich, D. K., Tracer studies of pathways and rates of meltwater transport through Arctic summer sea ice. *Journal of Geophysical Research: Oceans* **2002,** *107* (C10), SHE 22-1-SHE 22-20;10.1029/2000JC000583
26. Kawamura, T.; Ohshima, K. I.; Takizawa, T.; Ushio, S., Physical, structural, and isotopic characteristics and growth processes of fast sea ice in Lützow-Holm Bay, Antarctica. *Journal of Geophysical Research: Oceans* **1997,** *102* (C2), 3345-3355;10.1029/96JC03206
27. Wang, C.; Cheng, B.; Wang, K.; Gerland, S.; Pavlova, O., Modelling snow ice and superimposed ice on landfast sea ice in Kongsfjorden, Svalbard. *Polar Research* **2015,** *34* (1), 20828;10.3402/polar.v34.20828
28. Merkouriadi, I.; Liston, G. E.; Graham, R. M.; Granskog, M. A., Quantifying the Potential for Snow-Ice Formation in the Arctic Ocean. *Geophysical Research Letters* **2020,** *47* (4), e2019GL085020;https://doi.org/10.1029/2019GL085020
29. Johansson, J. H.; Salter, M. E.; Acosta Navarro, J. C.; Leck, C.; Nilsson, E. D.; Cousins, I. T., Global transport of perfluoroalkyl acids via sea spray aerosol. *Environmental science. Processes & impacts* **2019,** *21* (4), 635;10.1039/c8em00525g
30. Wang, Z.; Cousins, I. T.; Scheringer, M.; Buck, R. C.; Hungerbühler, K., Global emission inventories for C4-C14 perfluoroalkyl carboxylic acid (PFCA) homologues from 1951 to 2030, Part I: production and emissions from quantifiable sources. *Environment international* **2014,** *70*, 62-75;10.1016/j.envint.2014.04.013
31. Vésine, E.; Bossoutrot, V.; Mellouki, A.; Le Bras, G.; Wenger, J.; Sidebottom, H., Kinetic and Mechanistic Study of OH- and Cl-Initiated Oxidation of Two Unsaturated HFCs: C4F9CHCH2 and C6F13CHCH2. *The Journal of Physical Chemistry A* **2000,** *104* (37), 8512-8520;10.1021/jp0013199
32. Butt, C. M.; Young, C. J.; Mabury, S. A.; Hurley, M. D.; Wallington, T., Atmospheric Chemistry of 4:2 Fluorotelomer Acrylate [C4F9CH2CH2OC(O)CH=CH2]: Kinetics, Mechanisms, and Products of Chlorine-Atom- and OH-Radical-Initiated Oxidation. *J. Phys. Chem. A* **2009,** *113* (13), 3155-3161;10.1021/jp810358k

33. Young, C. J.; Hurley, M. D.; Wallington, T.; Mabury, S. A., Atmospheric Chemistry of 4:2 Fluorotelomer Iodide (n-C4F9CH2CH2I): Kinetics and Products of Photolysis and Reaction with OH Radicals and Cl Atoms. *J. Phys. Chem. A* **2008,** *112* (51), 13542-13548;10.1021/jp807322x
34. Ellis, D.; Martin, J.; de Silva, A.; Mabury, S., Degradation of fluorotelomer alcohols: A likely atmospheric source of perfluorinated carboxylic acids. *Environmental Science & Technology* **2004,** *38* (12), 3316-3321;10.1021/es049860w
35. Sulbaek Andersen, M. P.; Nielsen, O. J.; Hurley, M. D.; Ball, J. C.; Wallington, T. J.; Ellis, D. A.; Martin, J. W.; Mabury, S. A., Atmospheric chemistry of 4:2 fluorotelomer alcohol (n-C4F9CH2CH2OH): products and mechanism of Cl atom initiated oxidation in the presence of NOx. *The journal of physical chemistry. A* **2005,** *109* (9), 1849-56;10.1021/jp045672g
36. Benskin, J. P.; Muir, D. C. G.; Scott, B. F.; Spencer, C.; De Silva, A. O.; Kylin, H.; Martin, J. W.; Morris, A.; Lohmann, R.; Tomy, G.; Rosenberg, B.; Taniyasu, S.; Yamashita, N., Perfluoroalkyl Acids in the Atlantic and Canadian Arctic Oceans. *Environmental Science & Technology* **2012,** *46* (11), 5815-5823;10.1021/es300578x
37. Glynn, A.; Berger, U.; Bignert, A.; Ullah, S.; Aune, M.; Lignell, S.; Darnerud, P. O., Perfluorinated Alkyl Acids in Blood Serum from Primiparous Women in Sweden: Serial Sampling during Pregnancy and Nursing, And Temporal Trends 1996–2010. *Environmental Science & Technology* **2012,** *46* (16), 9071-9079;10.1021/es301168c
38. Freeling, F.; Behringer, D.; Heydel, F.; Scheurer, M.; Ternes, T. A.; Nödler, K., Trifluoroacetate in Precipitation: Deriving a Benchmark Data Set. *Environmental Science & Technology* **2020,** *54* (18), 11210-11219;10.1021/acs.est.0c02910
39. Wong, F.; Shoeib, M.; Katsoyiannis, A.; Eckhardt, S.; Stohl, A.; Bohlin-Nizzetto, P.; Li, H.; Fellin, P.; Su, Y.; Hung, H., Assessing temporal trends and source regions of per- and polyfluoroalkyl substances (PFASs) in air under the Arctic Monitoring and Assessment Programme (AMAP). *Atmospheric Environment* **2018,** *172*, 65-73;https://doi.org/10.1016/j.atmosenv.2017.10.028
40. Codling, G.; Halsall, C.; Ahrens, L.; Del Vento, S.; Wiberg, K.; Bergknut, M.; Laudon, H.; Ebinghaus, R., The fate of per- and polyfluoroalkyl substances within a melting snowpack of a boreal forest. *Environmental Pollution* **2014,** *191*, 190-198;10.1016/j.envpol.2014.04.032
41. Meyer, T.; Lei, Y.; Muradi, I.; Wania, F., Organic Contaminant Release from Melting Snow. 2. Influence of Snow Pack and Melt Characteristics. *Environmental Science & Technology* **2009,** *43* (3), 663;10.1021/es8020233
42. Meyer, T.; Lei, Y.; Muradi, I.; Wania, F., Organic Contaminant Release from Melting Snow. 1. Influence of Chemical Partitioning. *Environmental Science & Technology* **2009,** *43* (3), 657;10.1021/es8020217

43. Garnett, J.; Halsall, C.; Thomas, M.; Crabeck, O.; France, J.; Joerss, H.; Ebinghaus, R.; Kaiser, J.; Leeson, A.; Wynn, P. M., Investigating the Uptake and Fate of Poly- and Perfluoroalkylated Substances (PFAS) in Sea Ice Using an Experimental Sea Ice Chamber. *Environmental Science & Technology* **2021**;10.1021/acs.est.1c01645
44. Casal, P.; Zhang, Y.; Martin, J. W.; Pizarro, M.; Jiménez, B.; Dachs, J., Role of Snow Deposition of Perfluoroalkylated Substances at Coastal Livingston Island (Maritime Antarctica). *Environ Sci Technol* **2017,** *51* (15), 8460-8470;10.1021/acs.est.7b02521
45. Wang, X.; Halsall, C.; Codling, G.; Xie, Z.; Xu, B.; Zhao, Z.; Xue, Y.; Ebinghaus, R.; Jones, K. C., Accumulation of perfluoroalkyl compounds in tibetan mountain snow: temporal patterns from 1980 to 2010. *Environ Sci Technol* **2014,** *48* (1), 173-81;10.1021/es4044775
46. Polashenski, C.; Golden, K. M.; Perovich, D. K.; Skyllingstad, E.; Arnsten, A.; Stwertka, C.; Wright, N., Percolation blockage: A process that enables melt pond formation on first year Arctic sea ice. *Journal of Geophysical Research: Oceans* **2017,** *122* (1), 413-440;https://doi.org/10.1002/2016JC011994
47. Renner, A. H. H.; Sundfjord, A.; Janout, M. A.; Ingvaldsen, R. B.; Beszczynska-Möller, A.; Pickart, R. S.; Pérez-Hernández, M. D., Variability and Redistribution of Heat in the Atlantic Water Boundary Current North of Svalbard. *Journal of Geophysical Research: Oceans* **2018,** *123* (9), 6373-6391;https://doi.org/10.1029/2018JC013814
48. Merkouriadi, I.; Gallet, J.-C.; Graham, R. M.; Liston, G. E.; Polashenski, C.; Rösel, A.; Gerland, S., Winter snow conditions on Arctic sea ice north of Svalbard during the Norwegian young sea ICE (N-ICE2015) expedition. *Journal of Geophysical Research: Atmospheres* **2017,** *122* (20), 10,837-10,854;https://doi.org/10.1002/2017JD026753
49. Stemmler, I.; Lammel, G., Pathways of PFOA to the Arctic: variabilities and contributions of oceanic currents and atmospheric transport and chemistry sources. *Atmos. Chem. Phys.* **2010,** *10* (20), 9965-9980;10.5194/acp-10-9965-2010
50. Yeung, L. W. Y.; Dassuncao, C.; Mabury, S.; Sunderland, E. M.; Zhang, X.; Lohmann, R., Vertical Profiles, Sources, and Transport of PFASs in the Arctic Ocean. *Environmental Science & Technology* **2017,** *51* (12), 6735-6744;10.1021/acs.est.7b00788
51. Skaar, J. S.; Ræder, E. M.; Lyche, J. L.; Ahrens, L.; Kallenborn, R., Elucidation of contamination sources for poly- and perfluoroalkyl substances (PFASs) on Svalbard (Norwegian Arctic). *Environmental Science and Pollution Research* **2019,** *26* (8), 7356-7363;10.1007/s11356-018-2162-4
52. Peralta-Ferriz, C.; Woodgate, R. A., Seasonal and interannual variability of pan-Arctic surface mixed layer properties from 1979 to 2012 from hydrographic data,

and the dominance of stratification for multiyear mixed layer depth shoaling. *Progress in Oceanography* **2015,** *134*, 19-53;https://doi.org/10.1016/j.pocean.2014.12.005

53. MacInnis, J. J.; Lehnherr, I.; Muir, D. C.; St. Pierre, K. A.; St. Louis, V. L.; Spencer, C.; De Silva, A. O., Fate and transport of perfluoroalkyl substances from snowpacks into a lake in the High Arctic of Canada. *Environmental science & technology* **2019,** *53* (18), 10753-10762

54. Polashenski, C.; Perovich, D.; Courville, Z., The mechanisms of sea ice melt pond formation and evolution. *Journal of Geophysical Research: Oceans* **2012,** *117* (C1);https://doi.org/10.1029/2011JC007231

55. Marsay, C. M.; Aguilar-Islas, A.; Fitzsimmons, J. N.; Hatta, M.; Jensen, L. T.; John, S. G.; Kadko, D.; Landing, W. M.; Lanning, N. T.; Morton, P. L.; Pasqualini, A.; Rauschenberg, S.; Sherrell, R. M.; Shiller, A. M.; Twining, B. S.; Whitmore, L. M.; Zhang, R.; Buck, C. S., Dissolved and particulate trace elements in late summer Arctic melt ponds. *Marine Chemistry* **2018,** *204*, 70-85;https://doi.org/10.1016/j.marchem.2018.06.002

Supporting Information to:

High concentrations of perfluoroalkyl acids (PFAA) in Arctic seawater driven by early thawing sea ice.

Jack Garnett[1], Crispin Halsall[1*], Anna Vader[2],
Hanna Joerss[3], Ralf Ebinghaus[3], Amber Leeson[1], Peter M. Wynn[1]

1 Lancaster Environment Centre, Lancaster University, Lancaster, LA1 4YQ, UK
2 Department of Arctic Biology, The University Centre in Svalbard (UNIS), N-9170 Longyearbyen, Norway
3 Helmholtz-Zentrum Hereon, Max-Planck-Straße 1, 21502 Geesthacht, Germany

Email: c.halsall@lancaster.c.uk

Contents include:

21 pages
Tables (S1-S18)
Figures (S1-S7)
Equations (S1- S13)

Table S1: Sea ice sampling depths at P6 and P7

Site	Sample section length (m) (n=4)	Mean cumulative depth (m) (n=4)
P6	0.10 ± 0.00	0.00 – 0.10
	0.20 ± 0.00	0.10 – 0.30
	0.20 ± 0.00	0.30 – 0.50
	0.20 ± 0.00	0.50 – 0.70
	0.20 ± 0.00	0.70 – 0.90
	0.20 ± 0.00	0.90 – 1.10
	0.10 ± 0.00	1.10 – 1.20
		Total = 1.20 ± 0.0
Site	Sample section length (m) (n=4)	Mean cumulative depth (m) (n=4)
P7	0.10 ± 0.00	0.00 – 0.10
	0.15 ± 0.00	0.10 – 0.25
	0.18 ± 0.03	0.25 – 0.43
	0.18 ± 0.05	0.43 – 0.60
	0.15 ± 0.00	0.60 – 0.75
	0.15 ± 0.00	0.75 – 0.90
	0.15 ± 0.00	0.90 – 1.05
	0.10 ± 0.00	1.05 – 1.15
	0.10 ± 0.00	1.15 – 1.25
	0.13 ± 0.03	1.25 – 1.38
		Total = 1.38 ± 0.11

Table S2: Sampling equipment used for different samples during the cruise

Matrix	Sampling tool
Snow	Aluminium shovel
Sea ice	Kovac ice corer (90 mm internal diameter)
Melt-pond	HDPE Bucket
Under-ice seawater (0.5m)	Niskin bottle
Under-ice seawater (5.0m)	Niskin bottle

Table S3: Density measurements (mean ±1.s.d.) of different ice type gathered in this study

Compartment	Snow ($n = 7$)	Snow-ice ($n = 7$)	Bulk ice ($n = 17$)
Density (kg m^{-3})	180 ± 14	551 ± 84	892 ± 210

The density (kg m^{-3}) of snow is given by:

$$\rho_{snow} = m / V \quad (1)$$

Where m is the measured mass using gravimetric analysis of a snow sample (kg); V is the volume (m^{-3}) of the snow sample taken using a sampling apparatus. In this case, the reference sampling volume was 0.25 dm^3

The density (kg m^{-3}) of sea ice (snow-ice/bulk ice) is given by:

$$\rho_{sea\ ice} = m / \pi \times r^2 \times h \quad (2)$$

Where m is the gravimetrically measured mass (kg) of a sea ice sample shown to follow characteristics representative of a particular ice type (e.g. snow-ice; see Figure 2 in main text); π is 3.142; r is the radius of sea ice corer (0.045 m); h is the sea ice sample length. Due to the method being implemented the measurement precision on sea ice samples (snow-ice and bulk ice) is expected to be slightly less. The density of superimposed ice was not assessed but assumed to fall within the range of bulk ice.

Table S4: Information obtained from the data logger onboard the *Kronprins Haakon* at P6

Latitude	Longitude	Depth (m)	Heading (Degree)	Speed (knots)	Water temperature (°C)	Wind Speed (Knots)	Wind direction (Degrees)	Air temperature (°C)	Air pressure (hPa)	Humidity (%)
8118.708741 N	03121.021065 E	188.46	344.61	0.4	-1.7	5	128	-0.7	999.7	99
8118.780273 N	03119.421987 E	204.34	344.85	0.4	-1.7	4.8	132	-0.8	999.8	100
8122.935053 N	03117.393097 E	0	313.97	1.6	-1.7	4.1	133	0	1000.1	99
8123.085928 N	03116.334402 E	187.3	351.66	0.6	-1.7	4	135	-0.7	1000.1	101
8124.662287 N	03114.735885 E	205.56	319.14	1.6	-1.7	4.6	133	-0.3	1000.3	99
8124.862982 N	03114.295916 E	209.53	321.56	0.5	-1.5	4.5	137	-0.7	1000.2	101
8125.865978 N	03108.691454 E	256.17	274.09	0.5	-1.7	4.4	147	1	1000.4	99
8126.101201 N	03108.976667 E	285.32	268.58	0.5	-1.6	4.7	167	2.3	1000.6	86
8127.560866 N	03104.672063 E	496.41	28.16	0.8	-1.7	4.8	164	-0.5	1000.8	98
8127.832758 N	03105.628658 E	509.32	33.12	0.5	-1.6	4.2	149	-0.8	1001	101
8127.969840 N	03106.359671 E	514.06	33.4	0.5	-1.6	4.2	152	-0.5	1001.1	100
8130.150125 N	03057.533836 E	693.98	17.05	0.6	-1.7	4.6	153	-0.5	1001.2	94
8130.242814 N	03059.397176 E	693.37	20.71	0.4	-1.6	4.7	156	-0.6	1001.5	100
8131.784129 N	03057.330501 E	789.23	349.72	0.1	-1.6	4.6	217	1.6	1003.2	82
8132.487706 N	03056.853998 E	826.2	356.32	0.3	-1.6	5.6	185	0.5	1004.4	82
8132.990799 N	03057.532873 E	865.44	358.28	0.4	-1.7	5.5	172	-2	1004.8	95

Seawater and air temperature measurements were also made hourly via the on-board data logger at sampling station P6

Table S5: Information obtained from the data logger onboard the *Kronprins Haakon* at P7

Latitude	Longitude	Depth (m)	Heading (Degree)	Speed (knots)	Water temperature (°C)	Wind Speed (Knots)	Wind direction (Degrees)	Air temperature (°C)	Air pressure (hPa)	Humidity (%)
8141.135236 N	03033.760504 E	2830.02	298.16	0.1	-1.6	5.4	56	-4	1012.5	99
8159.093220 N	02959.223986 E	3272.97	164.57	0.2	-1.7	6.4	50	-1.1	1012.1	84
8159.047348 N	02958.664982 E	3272.59	164.48	0.3	-1.7	6.1	51	-1.2	1012	83
8159.016541 N	02958.171317 E	3269.47	164.37	0.3	-1.7	7.4	44	-0.8	1011.5	78
8159.003577 N	02957.936389 E	3270.56	164.35	0.3	-1.7	5.9	53	-0.9	1011.7	81
8158.963006 N	02956.623841 E	3274.07	163.83	0.3	-1.7	6.9	36	-0.5	1011.5	83
8158.929513 N	02953.517375 E	3282	162.92	0.4	-1.7	8.9	47	-0.7	1010.7	86
8158.913733 N	02948.027357 E	3290.5	161.88	0.3	-1.7	8	42	-0.4	1009.9	92
8158.918212 N	02947.652112 E	3290.87	161.82	0.3	-1.7	8.5	39	0.2	1009.7	89
8158.879795 N	02944.011224 E	3294.78	160.97	0.2	-1.7	10.3	44	0.6	1008.4	93
8158.867516 N	02943.724824 E	0	160.84	0.3	-1.7	10.4	43	0.8	1008.2	92
8158.175689 N	02937.467284 E	3293.38	160.71	0.5	-1.7	13.7	42	0.2	1005.8	93
8158.160667 N	02937.305832 E	3293.25	160.76	0.5	-1.7	13.2	40	0.1	1005.8	93
8157.071563 N	02918.895781 E	3306.91	162.92	0.5	-1.7	12.8	29	0.7	1002.3	92
8157.054958 N	02918.444469 E	3306.9	162.85	0.5	-1.7	14.7	24	0.6	1002.4	92
8157.024527 N	02917.667809 E	3309.49	162.85	0.5	-1.7	14.3	23	0.8	1002.3	92
8157.002660 N	02917.150975 E	3313.34	162.83	0.5	-1.7	11.8	22	0.6	1002.2	92
8156.980721 N	02916.671655 E	3313.25	162.88	0.5	-1.7	14.5	23	0.7	1002.1	93
8156.965258 N	02916.377383 E	3315.21	162.89	0.5	-1.7	12.9	21	0.7	1002	92

Seawater and air temperature measurements were also made hourly via the on-board data logger at sampling station.

Table S6: Overview of analytical standards, CAS numbers, the standard suppliers, purity and concentration/amount

Acronym	Analytical standard	CAS number	Supplier, purity and concentration/amount
PFBA	perfluoro-*n*-butanoic acid	375-22-4 (acid)	PFC-MXA (mixture) Wellington Laboratories, > 98 % 2.0 µg/mL ± 5 % of the single compounds
PFPeA	perfluoro-*n*-pentanoic acid	2706-90-3 (acid)	
PFHxA	perfluoro-*n*-hexanoic acid	307-24-4 (acid)	
PFHpA	perfluoro-*n*-heptanoic acid	375-85-9 (acid)	
PFOA	perfluoro-*n*-octanoic acid	335-67-1 (acid)	
PFNA	perfluoro-*n*-nonanoic acid	375-95-1 (acid)	
PFDA	perfluoro-*n*-decanoic acid	335-76-2 (acid)	
PFUnDA	perfluoro-*n*-undecanoic acid	2058-94-8 (acid)	
PFDoDA	perfluoro-*n*-dodecanoic acid	307-55-1 (acid)	
PFTrDA	perfluoro-*n*-tridecanoic acid	72629-94-8 (acid)	
PFTeDA	perfluoro-n-tetradecanoic acid	376-06-7 (acid)	
PFBS	potassium perfluoro-*n*-butanesulfonate	29420-49-3 (K+ salt) 375-73-5 (acid)	PFS-MXA (mixture) Wellington Laboratories, > 98 % 2.0 µg/mL ± 5 % of the single compounds
PFHxS	sodium perfluoro-*n*-hexanesulfonate	82382-12-5 (Na+ salt) 355-46-4 (acid)	
PFHpS	sodium perfluoro-*n*-heptanesulfonate	22767-50-6 (Na+ salt) 375-92-8 (acid)	
PFOS	sodium perfluoro-*n*-octanesulfonate	4021-47-0 (Na+ salt) 1763-23-1 (acid)	
PFDS	sodium perfluoro-*n*-decanesulfonate	2806-15-7 (Na+ salt) 335-77-3 (acid)	
13C4-PFBA	perfluoro-*n*-[13C4]-butanoic acid	-	MPFAC-MXA (mixture) Wellington Laboratories, > 98 %, 2.0 µg/mL ± 5 % of the single compounds
13C2-PFHxA	perfluoro-*n*-[1,2-13C2]-hexanoic acid	-	
13C4-PFOA	perfluoro-*n*-[1,2,3,4-13C4]-octanoic acid	-	
13C5-PFNA	perfluoro-*n*-[1,2,3,4,5-13C5]-nonanoic acid	-	
13C2-PFDA	perfluoro-*n*-[1,2-13C2]-decanoic acid	-	
13C2-PFUnDA	perfluoro-*n*-[1,2-13C2]-undecanoic acid	-	
13C2-PFDoDA	perfluoro-*n*-[1,2-13C2]-dodecanoic acid	-	
18O2-PFHxS	sodium perfluorohexane-*n*-[18O2]-sulfonate	-	
13C4-PFOS	sodium perfluoro-*n*-[1,2,3,4-13C4]-octanesulfonate	-	
13C8-PFOA	perfluoro-[13C8]-octanoic acid (injection standard)	-	Wellington Laboratories, > 98 %, (50 ± 2.5) µg/mL

Target PFAS include 11 PFCA (C_4 to C_{14}) and five PFSA ($C_{4,}$ $C_{6,}$ $C_{7,}$ $C_{8,}$ C_{10})

Table S7: Quality assurance and quality control

Parameter	PFBA	PFPeA	PFHxA	PFHpA	PFOA	PFNA	PFDA	PFUnDA	PFDoDA	PFTrDA	PFTeDA	PFBS	PFHxS	PFHpS	PFOS	PFDS
Laboratory blanks (n=5) (pg L^{-1})	331 ± 108	1 ± 3	41 ± 11	11 ± 4	34 ± 3	1 ± 3	1 ± 3	1 ± 2	1 ± 2	<LOD	<LOD	123 ± 47	<LOD	<LOD	<LOD	<LOD
Field blanks (n=2) (pg L^{-1})	277 ± 74	4 ± 6	38 ± 14	15 ± 6	32 ± 2	3 ± 4	3 ± 4	4 ± 1	<LOD	<LOD	<LOD	67 ± 44	<LOD	<LOD	<LOD	<LOD
*Procedural blanks (n=7) (pg L^{-1})	309 ± 90	2 ± 4	40 ± 11	12 ± 4	33 ± 2	2 ± 3	2 ± 3	1 ± 2	1 ± 2	<LOD	<LOD	107 ± 50	<LOD	<LOD	<LOD	<LOD
Method detection limit (pg L^{-1})	579	13	72	25	41	12	11	7	6	1†	4†	257	1†	1†	5†	1†
Internal Standard (IS)	$^{13}C_4$-PFBA		$^{13}C_2$-PFHxA	$^{13}C_4$-PFOA		$^{13}C_5$-PFNA	$^{13}C_2$-PFDA	$^{13}C_2$-PFUnDA	$^{13}C_2$-PFDoDA			$^{18}O_2$-PFHxS			$^{13}C_4$-PFOS	

*Procedural blanks (n=7) include laboratory (n=5) and field blanks (n=2) and were all used to calculate method detection limits for each PFAA. A mass-labelled analogue of some PFAS was not available (e.g. PFHpA) and therefore a structurally similar chemical was utilised. †Some analytes were not detected in procedural blanks and therefore method detection limits were determined from the signal obtained from the lowest detectable calibration standard with the mean laboratory blank volume (0.8 L).

The method detection limit (pg L^{-1}) is given by:

$$p_{\text{method}} = \overline{x}_{\text{procedural blanks}} + 3.\sigma_{\text{procedural blanks}} \quad (3)$$

where $\overline{x}_{\text{procedural blanks}}$ is the mean of the laboratory and field blanks; $\sigma_{\text{procedural blanks}}$ is the standard deviation of the laboratory and field blanks.

Water mass equivalent of ice per unit area of sea ice (kg m^{-2}) is given by:

$$w_n = L_n \times \rho_n \quad (4)$$

where L is the depth (m) of a particular ice sample type; ρ_n is the mean sample density (kg m^{-3}) of a particular type of ice (see Equations S1 – S2).

Mass of PFAA per unit area (pg m^{-2}) of ice is given by:

$$q_n = c_{PFAA} \times w_n \quad (5)$$

where c_{PFAA} is the concentration (pg L^{-1}; where 1 L = 1 kg) of an individual PFAA in a particular sample; w_n is the water mass equivalent per unit area of ice (kg m^{-2}).

Volumetrically-weighted concentration of PFAA (pg kg^{-1}) in ice is given by:

$$k_n = \Sigma\, q_n \;/\; \Sigma\, w_n \quad (6)$$

where $\Sigma\, q_n$ is the total mass of an individual PFAA per unit area (pg m^{-2}) in all samples containing the same ice type (e.g. snow-ice, bulk ice, etc); $\Sigma\, w_n$ is the total water mass equivalent per unit area (kg m^{-2}) for the same corresponding sample ice type (e.g. snow-ice, bulk ice etc). The volumetrically-weighted concentration of PFAA (pg kg^{-1}) for the entire sea ice system is given by summing the vertical mass of PFAA in the different samples (i.e. snow-ice + bulk ice + superimposed ice) divided by the total sea ice water mass equivalent (i.e. snow-ice + bulk ice + superimposed ice). Volumetrically-weighted $\delta^{18}O$ values in sea ice are also calculated in this manner by exchanging PFAA concentrations (e.g. c_{PFAA}) for $\delta^{18}O$ values (e.g. permil ‰).

PFAA mass fraction (% mass/total mass) in sea ice is given by:

$$f_n = q_n \;/\; \Sigma\, q_n \quad (7)$$

where q_n is the total mass of an individual PFAA within a specific ice type (e.g. snow-ice) per unit area (pg m^{-2}); $\Sigma\, q_n$, is the total mass of an individual PFAA within the combined types of ice (e.g. snow + snow-ice + bulk ice + superimposed ice) per unit area (pg m^{-2}).

Table S8: Concentrations of PFAA (pg L^{-1}) in sea ice at P6

Sea ice depth (m)	PFBA	PFPeA	PFHxA	PFHpA	PFOA	PFNA	PFDA	PFUnDA	PFDoDA	PFTrDA	PFTeDA	PFBS	PFOS	$\Sigma PFAA_{short\text{-}chain}$	$\Sigma PFAA_{long\text{-}chain}$
0.00 – 0.10	2259 ± 1184	12 ± 16	29 ± 41	119 ± 79	60 ± 27	86 ± 40	90 ± 52	68 ± 47	28 ± 21	18 ± 16	4 ± 5	186 ± 263	66 ± 13	2604 ± 1577	419 ± 220
0.10 – 0.30	231 ± 326	<MDL	<MDL	88 ± 53	42 ± 25	38 ± 14	39 ± 25	17 ± 8	11 ± 8	7 ± 7	3 ± 5	<MDL	16 ± 23	318 ± 379	174 ± 114
0.30 – 0.50	<MDL	<MDL	<MDL	94 ± 44	8 ± 12	22 ± 12	9 ± 13	6 ± 8	3 ± 5	7 ± 5	<MDL	<MDL	<MDL	94 ± 44	56 ± 55
0.50 – 0.70	<MDL	11 ± 19	<MDL	40 ± 37	8 ± 7	15 ± 1	12 ± 12	8 ± 3	5 ± 8	4 ± 4	<MDL	<MDL	11 ± 10	51 ± 56	61 ± 45
*0.70 – 0.90	<MDL	<MDL	<MDL	256	44	34	54	14	19	7	<MDL	<MDL	<MDL	256	171
0.90 – 1.10	<MDL	<MDL	14 ± 25	112 ± 20	39 ± 34	32 ± 23	22 ± 16	18 ± 13	11 ± 12	1 ± 2	<MDL	<MDL	5 ± 9	126 ± 45	128 ± 109
1.10 – 1.20	232 ± 328	<MDL	62 ± 88	34 ± 48	107 ± 21	51 ± 1	59 ± 15	22 ± 3	24 ± 9	3 ± 4	3 ± 5	<MDL	30 ± 13	328 ± 464	300 ± 70

* sample replicate was not analysed due to technical issue with sample preparation

Table S9: Concentrations of PFAA (pg L^{-1}) in sea ice at P7

Sea ice depth (m)	PFBA	PFPeA	PFHxA	PFHpA	PFOA	PFNA	PFDA	PFUnDA	PFDoDA	PFTrDA	PFTeDA	PFBS	PFOS	$\Sigma PFAA_{short\text{-}chain}$	$\Sigma PFAA_{long\text{-}chain}$
0.00 – 0.10	7763 ± 9867	161 ± 173	513 ± 594	316 ± 230	815 ± 990	134 ± 37	347 ± 318	132 ± 28	95 ± 83	7 ± 0	6 ± 8	7970 ± 10791	32 ± 12	16723 ± 21654	1568 ± 1476
0.10 – 0.25	5660 ± 7278	93 ± 97	296 ± 418	95 ± 41	527 ± 626	79 ± 3	251 ± 203	53 ± 28	30 ± 11	2 ± 3	<MDL	6578 ± 8770	19 ± 3	12741 ± 16603	960 ± 877
0.25 – 0.43	2548 ± 2711	52 ± 46	137 ± 148	63 ± 14	212 ± 14	48 ± 21	114 ± 101	33 ± 35	54 ± 61	1 ± 1	<MDL	2479 ± 2995	4 ± 5	5280 ± 5914	466 ± 429
0.43 – 0.60	1492 ± 1055	37 ± 17	94 ± 64	51 ±11	144 ± 95	39 ± 7	64 ± 42	11 ± 12	14 ± 17	1 ± 2	<MDL	988 ± 837	8 ± 11	2662 ± 1984	281 ± 185
0.60 – 0.75	593 ± 699	16 ± 14	22 ± 38	62 ± 32	76 ± 40	21 ± 4	34 ± 23	2 ± 4	6 ± 5	<MDL	<MDL	639 ± 434	7 ± 6	1332 ± 1218	146 ± 83
0.75 – 0.90	707 ± 249	20 ± 4	40 ± 7	38 ± 12	93 ± 23	21 ± 0	49 ± 7	<MDL	7 ± 0	<MDL	<MDL	537 ± 323	5 ± 7	1342 ± 595	173 ± 38
0.90 – 1.05	157 ± 223	<MDL	<MDL	23 ± 7	64 ± 5	16 ± 1	37 ± 0	<MDL	<MDL	<MDL	<MDL	323 ± 10	4 ± 6	504 ± 239	121 ± 12
1.05 – 1.15	578 ± 38	41 ± 34	42 ± 59	56 ± 34	87 ± 19	33 ± 12	49 ± 10	8 ± 12	17 ± 15	1 ± 1	0 ± 1	563 ± 187	<MDL	1279 ± 352	196 ± 69
1.15 – 1.25	521 ± 270	25 ± 3	54 ± 22	59 ± 18	79 ± 49	24 ± 2	43 ± 24	<MDL	4 ± 6	<MDL	<MDL	541 ± 470	6 ± 8	1199 ± 782	157 ± 89
1.25 – 1.38	590 ± 438	29 ± 22	38 ± 53	67 ± 10	80 ± 48	53 ± 12	43 ± 18	3 ± 5	14 ± 19	<MDL	<MDL	482 ± 682	15 ± 6	1196 ± 1205	208 ± 108

Table S70: Concentrations of PFAA (pg L^{-1}) in different compartments at P6

Compartment	PFBA	PFBS	PFPeA	PFHxA	PFHpA	PFOA	PFOS	PFNA	PFDA	PFUnDA	PFDoDA	PFTrDA	PFTeDA	$\Sigma PFAA_{short\text{-}chain}$	$\Sigma PFAA_{long\text{-}chain}$
Snow ($n = 3$)	2903 ± 927	<MDL	113 ± 18	110 ± 23	178 ± 100	55 ± 9	<MDL	81 ± 7	28 ± 7	25 ± 11	21 ± 26	<MDL	<MDL	3304 ± 1069	210 ± 61
Sea ice ($n = 14$)	389 ± 874	27 ± 99	4 ± 10	16 ± 36	89 ± 69	42 ± 38	18 ± 24	38 ± 29	38 ± 34	22 ± 25	14 ± 12	6 ± 8	1 ± 3	525 ± 1089	180 ± 174
Seawater (0.5m) ($n = 3$)	<MDL	<MDL	<MDL	128 ± 39	491 ± 214	928 ± 617	42 ± 73	224 ± 118	563 ± 296	128 ± 62	151 ± 100	26 ± 17	37 ± 29	619 ± 254	2099 ± 1313
Seawater (5.0m) ($n = 3$)	<MDL	139 ± 242	<MDL	14 ± 25	144 ± 34	194 ± 39	17 ± 29	80 ± 19	138 ± 17	29 ± 4	37 ± 11	1 ± 2	5 ± 4	298 ± 300	500 ± 127
Melt-pond ($n = 3$)	747 ± 171	<MDL	60 ± 13	61 ± 11	109 ± 34	45 ± 14	<MDL	47 ± 17	3 ± 6	7 ± 7	11 ± 10	<MDL	<MDL	977 ± 228	114 ± 54

Table S81: Concentrations of PFAA (pg L^{-1}) in different compartments at P7

Compartment	PFBA	PFBS	PFPeA	PFHxA	PFHpA	PFOA	PFOS	PFNA	PFDA	PFUnDA	PFDoDA	PFTrDA	PFTeDA	$\Sigma PFAA_{short\text{-}chain}$	$\Sigma PFAA_{long\text{-}chain}$
Snow ($n = 3$)	2356 ± 400	<MDL	63 ± 9	30 ± 26	72 ± 15	27 ± 6	<MDL	47 ± 5	17 ± 8	16 ± 11	10 ± 18	<MDL	<MDL	2520 ± 449	117 ± 47
Sea ice ($n = 20$)	2081 ± 3841	2122 ± 4266	48 ± 66	125 ± 233	82 ± 99	219 ± 368	10 ± 10	47 ± 37	104 ± 139	24 ± 43	24 ± 38	1 ± 2	1 ± 3	4458 ± 8504	430 ± 639
Seawater (0.5m) ($n = 2$)	314 ± 445	<MDL	98 ± 18	16 ± 23	103 ± 49	339 ± 230	15 ± 21	95 ± 30	265 ± 222	25 ± 11	37 ± 16	3 ± 1	4 ± 6	531 ± 535	782 ± 536
Seawater (5.0m) ($n = 2$)	<MDL	<MDL	41 ± 58	<MDL	68 ± 12	107 ± 30	<MDL	41 ± 8	56 ± 24	4 ± 6	7 ± 10	<MDL	<MDL	108 ± 69	214 ± 79
Melt-pond ($n = 3$)	924 ± 151	<MDL	59 ± 21	55 ± 16	131 ± 5	39 ± 7	7 ± 12	44 ± 28	6 ± 6	5 ± 5	10 ± 9	<MDL	<MDL	1169 ± 193	112 ± 66

Table S92: Concentrations of PFAA (pg L^{-1}) in different compartments at P6 and P7

Compartment	PFBA	PFBS	PFPeA	PFHxA	PFHpA	PFOA	PFOS	PFNA	PFDA	PFUnDA	PFDoDA	PFTrDA	PFTeDA	$\Sigma PFAA_{short\text{-}chain}$	$\Sigma PFAA_{long\text{-}chain}$
Snow ($n = 6$)	2629 ± 705	<MDL	88 ± 30	70 ± 49	125 ± 86	41 ± 17	<MDL	64 ± 20	22 ± 9	21 ± 11	15 ± 21	<MDL	<MDL	2912 ± 872	163 ± 78
Sea ice ($n = 34$)	1384 ± 3083	1259 ± 3403	30 ± 55	80 ± 186	85 ± 87	146 ± 294	13 ± 18	43 ± 33	77 ± 112	23 ± 36	20 ± 30	3 ± 6	1 ± 3	2839 ± 6814	327 ± 532
Seawater (0.5m) ($n = 5$)	126 ± 281	<MDL	39 ± 54	83 ± 68	336 ± 262	692 ± 555	31 ± 55	173 ± 111	444 ± 288	87 ± 72	105 ± 95	17 ± 18	24 ± 27	584 ± 666	1573 ± 1220
Seawater (5.0m) ($n = 5$)	<MDL	84 ± 187	16 ± 36	9 ± 19	114 ± 49	159 ± 57	10 ± 23	64 ± 25	105 ± 48	19 ± 14	25 ± 19	1 ± 2	3 ± 4	222 ± 291	386 ± 192
Melt-pond ($n = 6$)	835 ± 174	<MDL	60 ± 15	58 ± 13	120 ± 25	42 ± 10	4 ± 9	46 ± 21	5 ± 5	6 ± 6	10 ± 9	<MDL	<MDL	1073 ± 227	113 ± 59

Concentration data represents mean ± s.d

Table S103: Average sum of PFAA (ng L^{-1}) in different ice types at P6

Ice Type	$\Sigma PFAA_{short\text{-}chain}$	$\Sigma PFAA_{long\text{-}chain}$
Snow	3.3 ± 1.1	0.2 ± 0.0
Snow-ice	5.1 ± 3.1	0.8 ± 0.4
Bulk ice	0.1 ± 0.2	0.1 ± 0.1
Superimposed ice	n.d	n.d

n.d = not detected

Table S114: Average sum of PFAA (ng L^{-1}) in different ice types at P7

Ice Type	$\Sigma PFAA_{short\text{-}chain}$	$\Sigma PFAA_{long\text{-}chain}$
Snow	2.5 ± 0.4	0.1 ± 0.0
Snow-ice	10.6 ± 13.3	0.3 ± 0.3
Bulk ice	1.5 ± 0.9	0.2 ± 0.1
Superimposed ice	1.2 ± 1.2	0.2 ± 0.1

Average data represents mean ± s.d

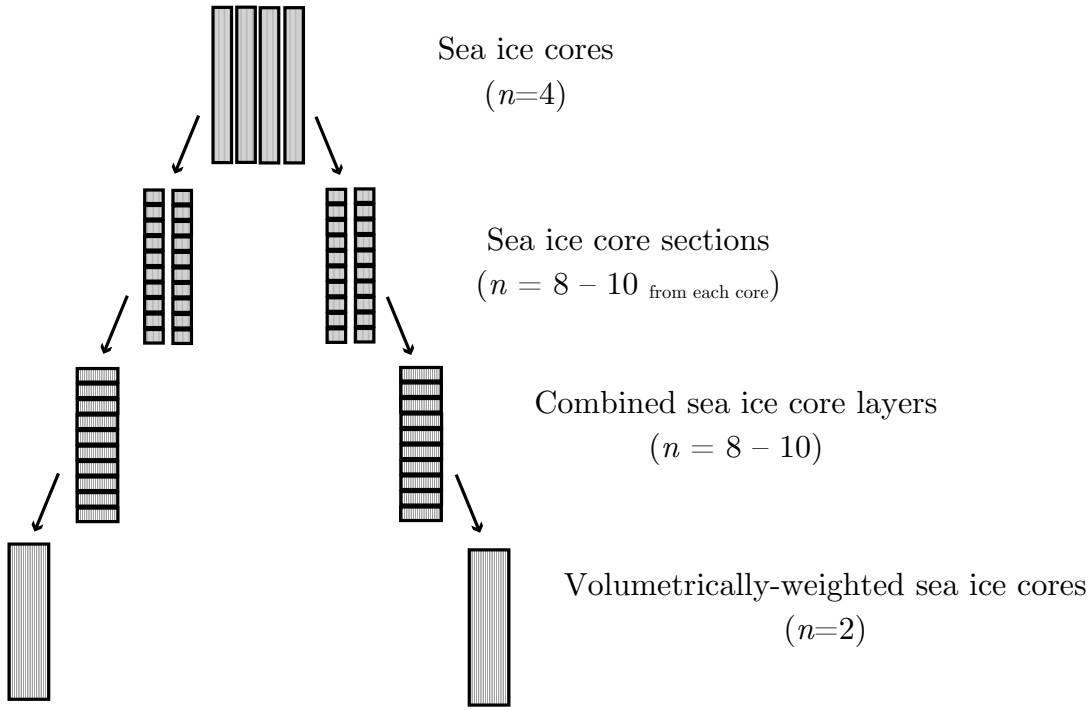

Step 1:

Four sea ice cores were taken at each site

Step 2:

At each site, sea ice cores were then sectioned in the field into equal number of layers

Step 3:

Samples of sea ice were then combined with adjacent layers from another sea ice core to obtain sufficient meltwater for PFAS analysis.

Step 4:

After PFAS analysis in the lab, the concentration data in each of the sea ice core layers could then be integrated during data analysis to achieve a volumetrically-weighted concentration in the entire sea ice core

Figure S1: Schematic indicating the sea ice sampling and handling procedures at each site.

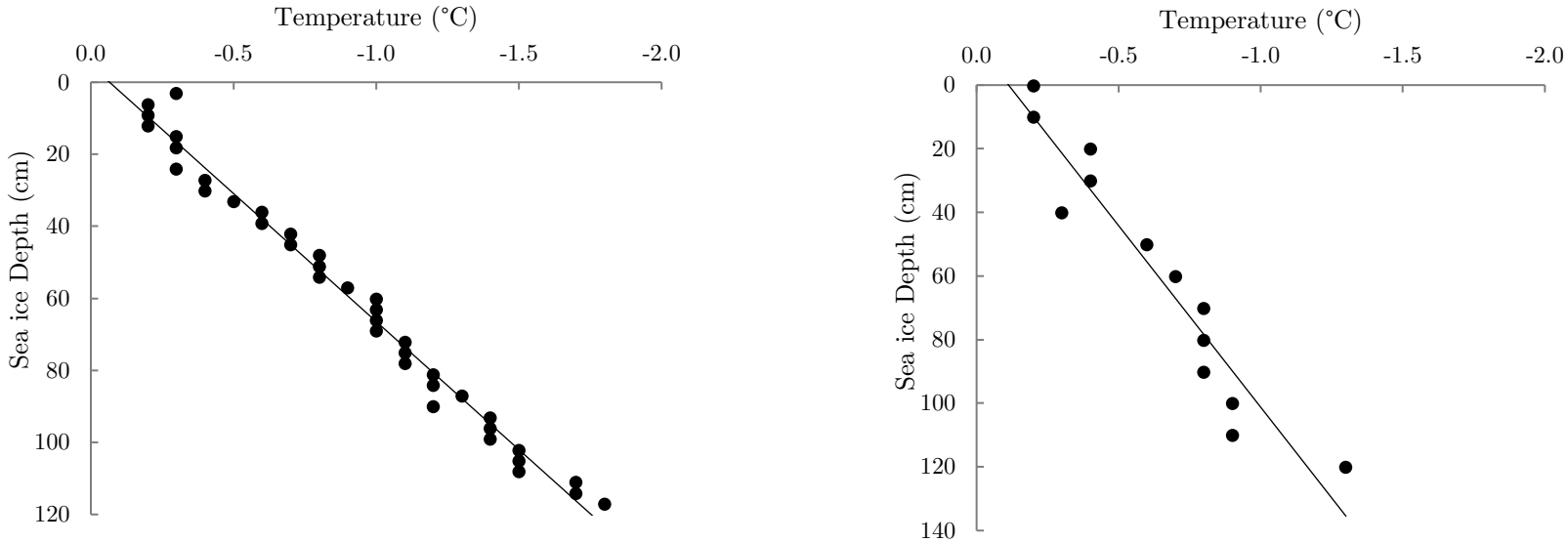

Figure S2: Temperature of sea ice at P6 (left) and P7 (right).

The temperature of sea ice was measured on sea ice cores immediately after extraction. Holes (3 mm diameter) were drilled between 3 cm (P6) and 10 cm (P7) intervals along the length of the core and a probe was inserted and the temperature logged. Temperature profiles showed a negative gradient with depth at both sites, meaning that sea ice growth was unlikely and temperatures were high enough to cause some melting.

.

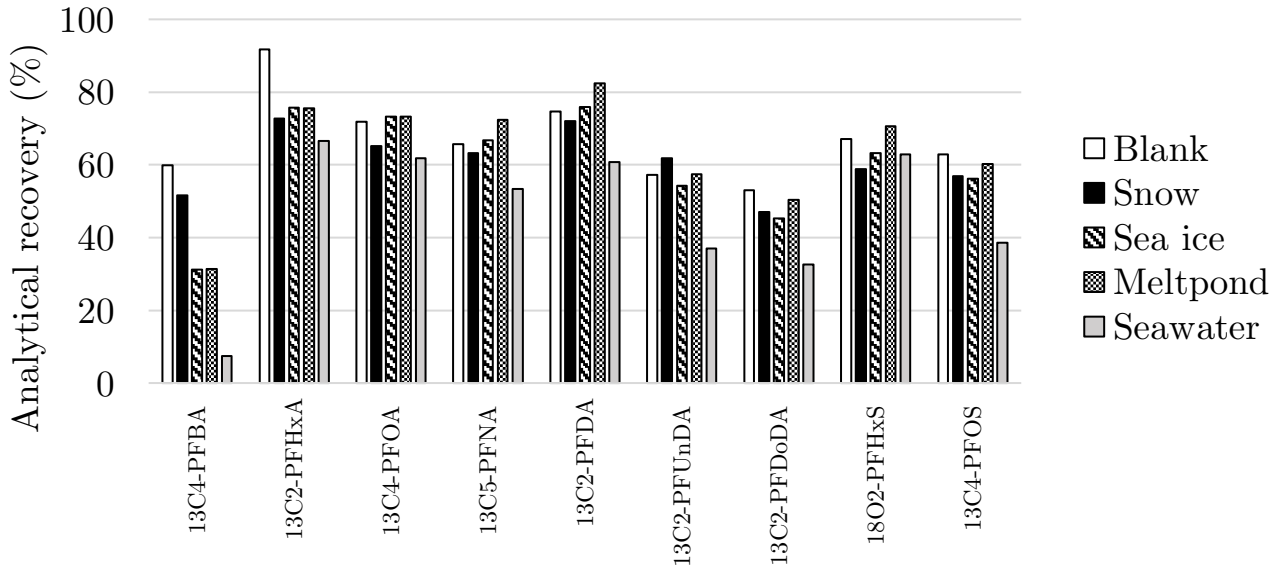

Figure S3 Analytical recovery of surrogate standards in different matrices

Analytical recovery (%) is given by: $$r_{abs} = m_{measured\ IS,sample} / m_{actual\ IS,sample} \quad (9)$$

where $m_{measured\ IS,sample}$ is the mass of internal standard (pg) measured in each sample; $m_{actual\ IS,sample}$ is the actual mass of internal standard (pg) introduced into each sample

The absolute analytical recovery (%) of mass-labelled standards was used to monitor the performance of laboratory analytical procedures. In general, recoveries of individual surrogate standards were above 50% which indicated good laboratory methods/procedures. Although, PFBA revealed poor recoveries (<10%) in seawater and was probably linked to matrix effects associated with high levels of salt.

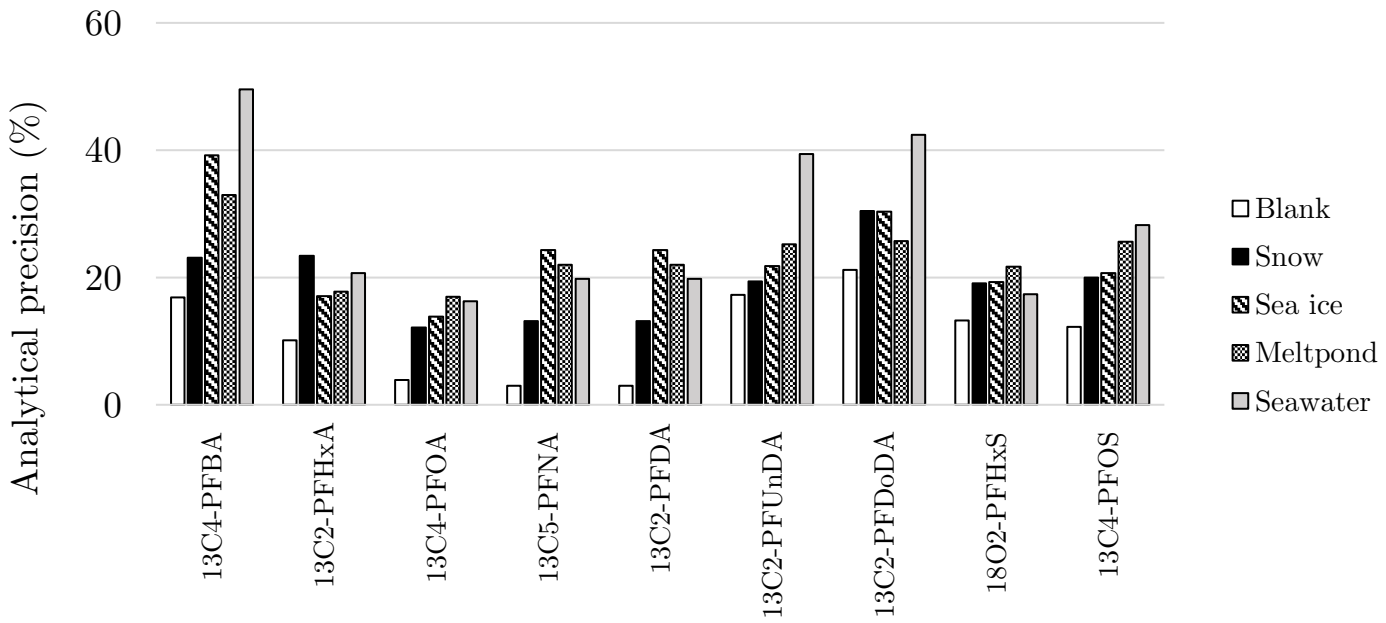

Figure S4: Analytical precision of surrogate standards in different matrices

Analytical precision (%) is given by:

$$p_{\text{analytical}} = \sigma_{\text{abs}} \,/\, \bar{r}_{\text{abs}} \tag{8}$$

where σ_{abs} is the standard deviation of the absolute recovery for a particular surrogate standard (see Equation S3); $\bar{r}_{\text{abs}}$ is the mean of the absolute recovery for a particular surrogate standard

Replicates of field samples were not obtained due to the relatively large sample volume required for PFAS analysis (~1 litre) and therefore the relative standard deviation (RSD) of the absolute recovery was used as an indicator of analytical precision. In general, analytical precision was good (<20%) for individual PFAA, although was higher for some compounds (e.g. $^{13}C_4$-PFBA) particularly in seawater samples. This was probably related to matrix effects.

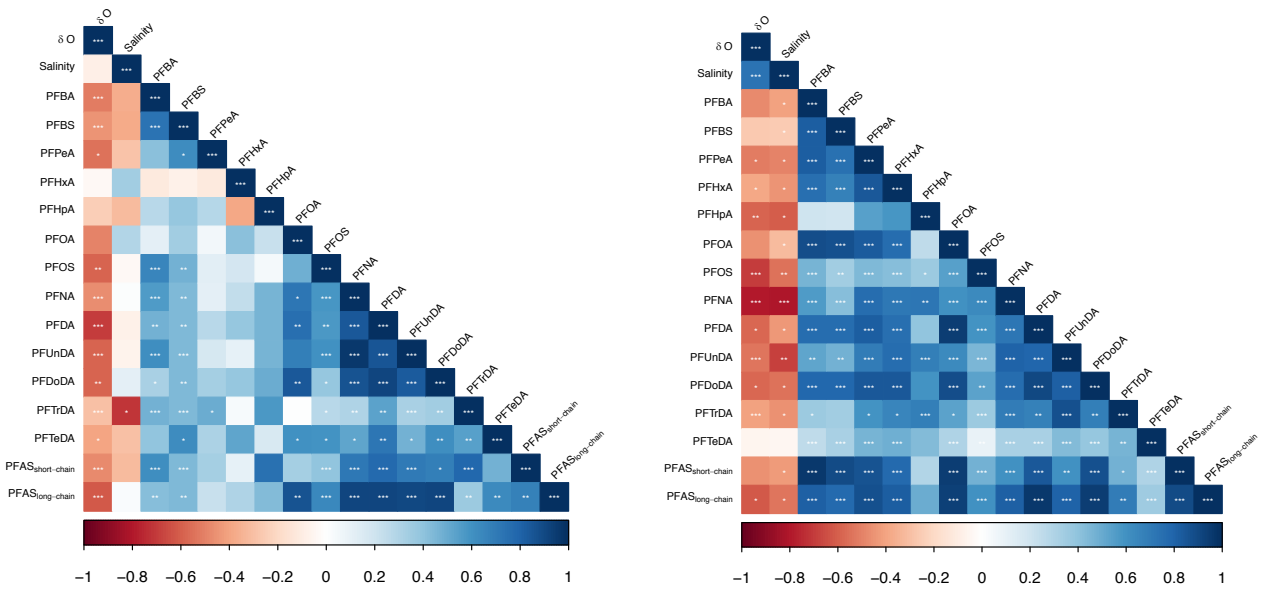

Figure S5: Correlogram of relationships for PFAA, salinity and $\delta^{18}O$ values in sea ice at P6 (left) and P7 (right).

We assessed individual pairwise relationships (Spearmans rank) for PFAA and other physical parameters in sea ice samples at each sampling site. Results showed that most PFAA were positively correlated and were highly significant ($p<0.001$). This indicated that many PFAA share similar sources and behaviour in the Arctic environment. However, short-chain PFAA at P6 showed weak to moderate relationships suggesting they had been strongly influenced by melt processes.

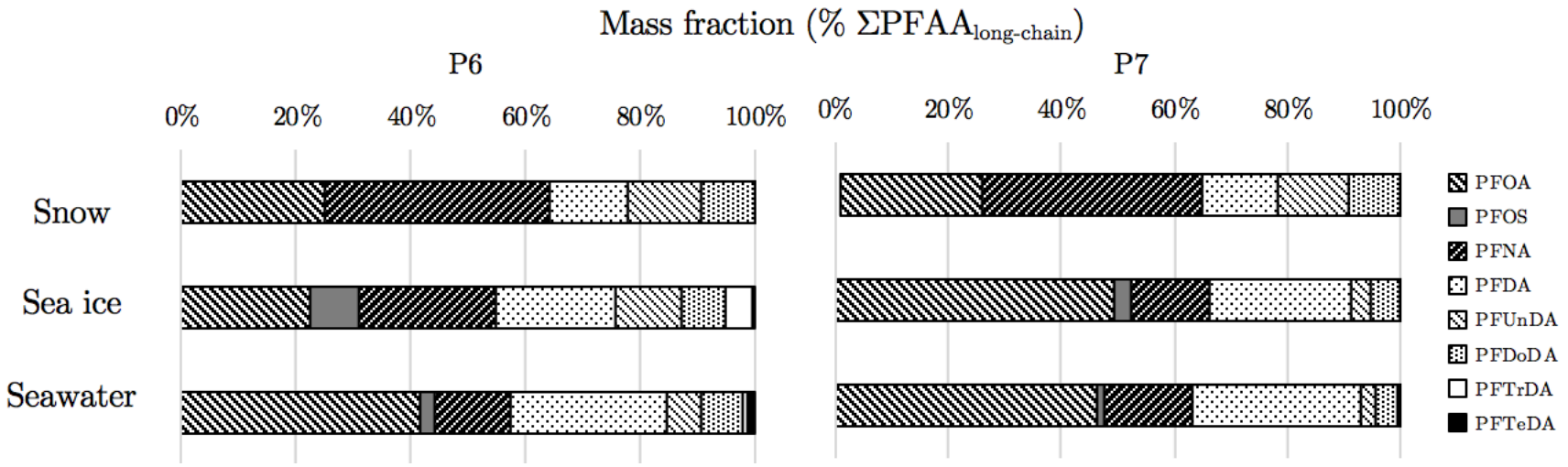

Figure S6: Mass fraction of long-chain PFAA (% $\Sigma PFAA_{long\text{-}chain}$) in different environmental compartments at P6 (left) and P7 (right).

Mass fraction (% $\Sigma PFAA_{long\text{-}chain}$) is given by:

$$f_{PFAA} = c_{PFAA} \quad / \quad c_{\Sigma PFAA} \tag{10}$$

where c_{PFAA} is the concentration of an individual long-chain PFAA (pg L^{-1}) in a particular sample; $c_{\Sigma PFAA}$ is the sum of long-chain PFAA (pg L^{-1}) in a particular sample.

Mass fraction profiles of long-chain PFAA in sea ice was more comparable to snow than seawater at P6. This indicates that snow had a strong influence on the composition probably through surface melting with subsequent transfer of its PFAA signature into sea ice. In contrast, the mass fraction profile of long-chain PFAA in sea ice at P7 was more comparable to seawater than snow. This suggests that seawater had a dominant effect on the composition, probably via processes related to the initial PFAA uptake from seawater during its formation and through surface flooding of seawater during sea ice ageing.

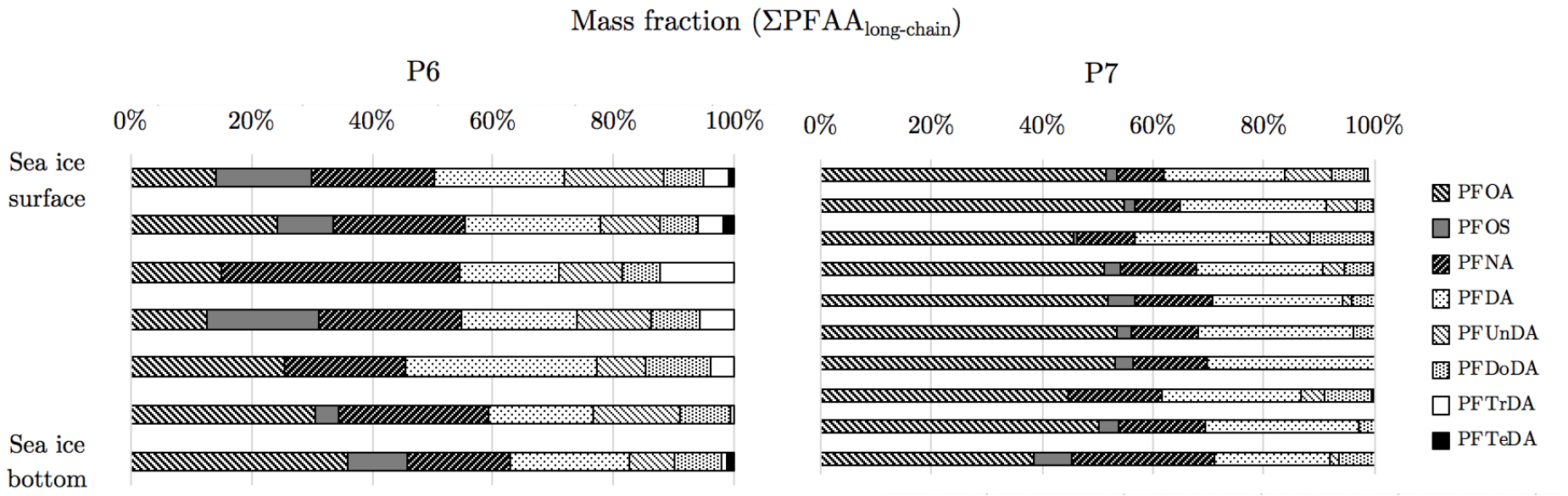

Figure S7: Mass fraction of long-chain PFAA ($\Sigma PFAA_{long\text{-}chain}$) in sea ice at P6 (left) and P7 (right).

Mass fraction profiles of long-chain PFAA in sea ice was significantly different between P6 and P7, although revealed relatively consistent profiles in the different layers at each site. This suggests that sea ice at P6 and P7 were influenced by separate processes (i.e., snowmelt or surface flooding of sea ice with seawater) resulting in different PFAA compositions.

Table S15: Measured salinity and $\delta^{18}O$ values (mean ±1.s.d) in different end-members

Sample type	$\delta^{18}O$ (‰)	Salinity
Snow	-15.2 ± 1.1	0.0 ± 0.0
Seawater	-0.1 ± 0.4	31.1 ± 0.7
* Sea ice	0.8 ± 0.5	2.6 ± 0.5

Values displayed represent averages of all respective sample types taken at P6 and P7. *Volumetrically-weighted values in sea ice were used to avoid sample bias.

The measured values for the different end-members were then used as constants in the following equations in order to determine the mass fraction in each of the millponds sampled in this study (Marsay, et al., 2018).

$$F_{snow} + F_{sea\ ice} + F_{seawater} = 1 \quad (11)$$

Where F_n is the mass fraction of end-member (i.e., snow, sea ice ice or seawater) in the meltpond

$$\delta^{18}O_{meltpond} = (F_{snow}\ \delta^{18}O_{snow}) + (F_{sea\ ice}\ \delta^{18}O_{sea\ ice}) + (F_{\ seawater}\ \delta^{18}O_{\ seawater}) \quad (12)$$

Where F_n is the mass fraction of end-member (i.e., snow, sea ice ice or seawater) in the meltpond; $\delta^{18}O_{meltpond}$ is measured $\delta^{18}O$ values (‰) of end-member (i.e., snow, sea ice ice or seawater) in the meltpond.

$$S_{meltpond} = (F_{snow}\ S_{snow}) + (F_{sea\ ice}\ S_{sea\ ice}) + (F_{seawater}\ S_{seawater}) \quad (13)$$

Where F_n is the mass fraction of end-member (i.e., snow, sea ice ice or seawater) in the meltpond; $S_{meltpond}$ is the measured salinity values of end-member (i.e., snow, sea ice or seawater) in the meltpond.

Equations S11 – S13 were solved simultaneously using the systems of equations calculator (https://www.symbolab.com/solver/system-of-equations-calculator) along with measured salinity/$\delta^{18}O$ values (See Table S16) in each individual meltpond.

Table S16: Measured salinity and $\delta^{18}OH_2O$ values in meltponds at P6 and P7 and their estimated mass fraction contribution of end-members.

Meltpond	Sampling station	Approx. dimensions (Depth x Width x Length)	$\delta^{18}O$ (‰)	Salinity (ppt)	F_{snow}	$F_{seawater}$	$F_{sea\ ice}$
Meltpond 1	P6	0.26 x 3.5 x 1.7	-5.9	2.7	0.42	0.04	0.54
Meltpond 2	P6	0.50 x 3.0 x 7.0	-4.7	1.4	0.34	-0.01	0.67
Meltpond 3	P6	0.18 x 1.0 x 8.0	-3.8	2.0	0.29	0.00	0.71
Meltpond 1	P7	0.30 x 2.0 x 8.0	-2.5	2.1	0.21	0.00	0.79
Meltpond 2	P7	0.34 x 2.0 x 6.0	-6.5	1.3	0.46	0.00	0.55
Meltpond 3	P7	0.38 x 7.0 x 30.0	-5.7	1.0	0.41	-0.02	0.61
					mean (± s.d.) = 0.35 ± 0.09	mean (± s.d.) = 0.00 ± 0.02	mean (± s.d.) = 0.64 ± 0.10

Table S17: Measured PFAA concentrations (mean ± s.d.) in the different end-members.

Measured concentrations (pg L^{-1})	PFBA	PFBS	PFPeA	PFHxA	PFHpA	PFOA	PFOS	PFNA	PFDA	PFUnDA	PFDoDA	PFTrDA	PFTeDA
Snow	2629 ± 705	<MDL	88 ± 30	70 ± 49	125 ± 86	41 ± 17	<MDL	64 ± 20	22 ± 9	21 ± 11	15 ± 21	<MDL	<MDL
Sea ice*	903 ± 1268	812 ± 1404	21 ± 25	52 ± 75	75 ± 41	100 ± 121	9 ± 3	33 ± 11	55 ± 48	15 ± 5	14 ± 11	3 ± 4	1 ± 1
Seawater	63 ± 199	42 ± 132	28 ± 45	46 ± 61	225 ± 213	426 ± 466	21 ± 41	118 ± 95	274 ± 264	53 ± 61	65 ± 77	9 ± 15	13 ± 22
Meltpond	835 ± 174	<MDL	60 ± 15	58 ± 13	120 ± 25	42 ± 10	4 ± 9	46 ± 21	5 ± 5	6 ± 5	10 ± 9	<MDL	<MDL

* Mean volumetrically-weighted values in sea ice were used to avoid possible sample bias originating from differences in the number of sea ice layers taken at either site. Seawater PFAA concentrations include samples acquired at 0.5 m and 5 m depths.

Table S18: Predicted PFAA concentrations (mean ± s.d.) in meltponds based on measured concentrations in end-members and their mass fraction (%) contribution.

Predicted concentration (pg L^{-1})	PFBA	PFBS	PFPeA	PFHxA	PFHpA	PFOA	PFOS	PFNA	PFDA	PFUnDA	PFDoDA	PFTrDA	PFTeDA
Meltpond	1507 ± 1172	523 ± 1179	44 ± 30	58 ± 67	93 ± 60	80 ± 86	6 ± 2	44 ± 17	44 ± 35	17 ± 8	15 ± 15	2 ± 3	0 ± 1

Chapter 6

Conclusions and further research

This chapter presents a synopsis of the results gathered from the previous chapters. It also discusses key areas of research on the occurrence and accumulation of perfluoroalkylated substances and other persistent organic pollutants in snow and ice of the Earth's Polar regions.

6.1. Synopsis of results and conclusions

Whilst the Arctic is widely acknowledged to be undergoing unprecedented changes, very little is known about the effects of climate change on the biogeochemical cycling of synthetic chemicals in the polar marine environment. Sea ice in particular is showing rapid seasonal retreat in the Arctic and shifting to a predominantly first-year sea ice pack, which is very likely to have consequences for the fate and behaviour of POPs. The work presented in this thesis significantly advances our understanding of the processes by which POPs become entrained in ice and their subsequent dynamics as ice grows as well as their eventual release during ice thaw. A key factor controlling chemical fate in sea ice (both for hydrophobic POPs and ionisable PFASs) is brine. Brine is an important feature of fresh sea ice (not aged multi-year ice) and therefore this will determine contaminant fate in the sea ice system in a warmer Arctic dominated by single season ice only. Chemical enrichment in brine (relative to the underlying seawater) is clearly observed in ice brine leading to relatively high concentrations and subsequent exposure risk to ice-associated marine organisms.

The results in Chapter 2 (**paper I**) successfully provided the first ever multidecadal depositional timeseries of PFASs in Antarctica, allowing us to infer with a high degree of certainty the global trends in historical emissions of several PFASs . Importantly, the results demonstrate that this non-coastal snow coring site to be predominantly affected by fluorotelomer-based compounds and, to a lesser known degree, chemicals that are associated with CFC-replacement compounds. Both of these groups of precursor compounds arise through long-range atmospheric transport with subsequent photochemical oxidation to corresponding PFCAs and deposition with snowfall. On the other hand, the PFSAs were below detection limits in the snow samples despite the very sensitive analytical methodology employed in this study. This supports current evidence in the literature that propose long-range atmospheric transport of the perfluoroalkyl sulphonic acids (or more likely their precursors with subsequent photochemical oxidation) is not as efficient (i.e. lower long-range transport potential) and/or is largely controlled by oceanic transport relative to the PFCAs. As this snow coring site was not located near the coast, then the influence of marine sources (such as sea spray aerosol)

was greatly diminished and long-range atmospheric transport is considered the primary influence on this site. The snow core timeseries provides compelling evidence that global industrial emissions of C6-C9 PFCAs or their specific precursor compounds have increased steadily from the 1980s onwards, whereas PFBA (C_4) emissions (or precursors) show a marked increase in deposition from the early 2000s onward. In particular, the increase in deposition of PFOA and other long-chain PFCAs to the end of the time series (2017) appears to suggest ongoing global use/sources of these chemicals (or their precursors) despite declarations in the year 2000 made by the fluorochemical industry to reduce the production and use. Interestingly the marked increase in the shorter chain PFBA from 2000 onwards coincides with increased industrial production of the shorter-chain length chemicals as safer substitutes for the longer-chain analogues. The snow core provides a very good proxy for historical and contemporary trends in atmospheric levels and allows insight into the influences of changing industrial practices on a global scale and the effects of legislation.

In chapter 3 (**paper II**) and 4 (**paper III),** data was gathered from several laboratory-based experiments that use, for the first time, a state-of-the-art sea ice facility to obtain empirical evidence of the dynamics of a number of persistent organic pollutants during sea ice growth and melt in a controlled setting. This data provided enabled a mechanistic explanation of organic chemical incorporation in sea ice during ice growth and highlights the physical role of brine (e.g. gravity drainage) in determining the distribution of POPs throughout sea ice growth and subsequent melt. The data illustrate that sea ice growth acts as a 'solvent depleting' process, and brine rejection leads to an increase in concentrations of POPs in brine channels/pockets with the ice The results from these experiments also revealed other chemical factors that may also be at play during ice formation and melt, decoupling their behaviour from salinity and also contributing to their enrichment. The extent of this enrichment in brine is strongly associated with the temperature of sea ice, with implications for the spatiotemporal distribution and biogeochemical cycling of these chemicals in surface waters. Importantly the predicted concentrations that ice-associated biota could be exposed to may be over one-order of magnitude higher than concentrations observed in underlying seawater. These sea ice brine concentrations are currently not used in BCF/BAF contaminant modelling in polar marine

ecosystems, yet they are likely to be relevant for the lower marine food web, particularly in late winter/spring when brine is mobile.

Finally, the results provided in Chapter 5 (**Paper IV**) presents the first empirical evidence of PFASs in late-summer Arctic sea ice and the surrounding marine environment. Moreover, the analysis of the isotopic signature of ice enabled the determination of the origin of different water masses which qualifies this study to be the most comprehensive study to date investigating the chemical pathways of PFASs into the marine food web. This data successfully evaluates the levels of PFASs in the late-summer Arctic sea ice and the under-ice seawater at two sites. High levels of PFASs were observed in snow and surface layers of sea ice, but also in the under-ice seawater. The results from this study highlight the sea ice system as being a source of high concentrations of PFASs to the under-ice sea water. Ultimately, this data identified 'snow-ice' as a key ice-type with a large capacity for PFASs (possibly other toxic pollutants as well), and suggests that due to its fresher composition and position on the surface is susceptible to atmospheric temperature fluctuations and therefore play a key role in the early release of high contaminant loads the under-ice seawater following the onset of melt . Thus, the atmospheric delivery of PFASs to sea ice is important for the biogeochemical cycling of contaminants into the Arctic marine food web.

In summary, past and current emissions of persistent organic pollutants in industrial regions are transported to remote polar regions where they cycle throughout the environment for several decades. Sea ice covers a vast area in the polar regions, and it accumulates persistent organic pollutants from seawater during its formation and from snow deposited on its surface. During summer melt, these chemicals are released back into the surrounding marine environment and are available to biological organisms at significantly higher concentrations, threatening to increase bioaccumulation in the marine food web.

6.2. Future research

As illustrated in Figure 3, there are a multitude of processes and factors that are expected to influence the spatiotemporal distribution of POPs in snow and ice of the Earths Polar regions. This PhD focusses primarily on PFASs and places and emphasis on the physical and chemical interactions associated with abiotic compartments in sea ice. In response to the findings acquired in Chapter 2 (**paper I**), a proposal to expand temporal studies and arrange permanent monitoring stations in other remote polar sites is recommended. Polar regions serve as a barometer for global emissions of POPs, and a greater understanding from a global context is necessary to improve regulatory policies and abatement strategies in the future. Furthermore, an appeal for chemical companies to work together with academics to highlight potential problematic chemical candidates during the development phase of new substances could help to streamline the chemical industry's path to a greener and more sustainable future.

With regards to Chapter 2 and 3 (**paper II and III**), many questions do still remain in terms of the cycling of biogeochemical of POPs in sea ice. One key area for further research should focus on identifying the mechanisms that are responsible for the enrichment of some chemicals and their importance at different stages of ice development. Further laboratory-based experiments using other 'emerging' groups of pollutants may facilitate this. The experiments that were conducted in this thesis were relatively simple by design and one logical step is to examine the role of other seawater constituents that are present in the natural environment. For example, exopolymeric substances (EPS), dissolved organic matter (DOM) and particulate organic matter may all act as sorbent materials for some pollutants in the environment, which could enhance chemical uptake into sea ice. The latter may yield particularly useful insights into chemical cycling in coastal regions of the Arctic, where riverine inputs and terrestrial runoff have recently been shown to have increased due to melting permafrost. Finally, an assessment of the physical and textural properties of sea ice grown under different conditions i.e. quiescent/turbulent.

Chapter 4 (**paper IV**) provided a snapshot of conditions in the Arctic at two sites during summer, which revealed high levels of PFASs in snow-ice and the under-ice water column. Yet

further research is needed in order to clarify the mechanisms (see previous comments on further experimental research) and various spatiotemporal scales on which these processes occur in order to understanding their wider environmental impact. In addition, there are currently no studies that have investigated the levels of PFASs in the Antarctic sea ice system, which given the contrasting sea ice properties there (e.g. thinner, granular ice, relatively more snow), may yield useful information concerning the biogeochemistry of POPs in polar regions.

6.3. Concluding remarks

This PhD focusses on the levels of PFASs in abiotic compartments together with physical and chemical factors involved in their cycling in sea ice and surrounding polar marine environment. However, understanding how these processes are influenced by climate change and ultimately how these processes translate into effect on biological populations (i.e. bioaccumulation) is currently uncertain and warrants further enquiry. Studying the behaviour of POPs in Polar regions is challenging due to unpredictable environmental conditions and often prohibitive costs associated with obtaining access to remote locations. The results offered in this thesis demonstrate the advantages and potential of utilising state-of-the-art laboratory facilities to better our understanding of polar processes in the future. Importantly, these facilities are designed in order to overcome many of the logistical challenges presented to researchers and permits environmental conditions to be closely controlled. In addition to laboratory studies, this thesis also features a number of samples that were collected from various successful field campaigns in the Antarctic and Arctic regions. In essence, scientific research depends on international collaboration between a global network of experts within different sectors. It requires investment into key infrastructure that facilitate high quality science to be conducted and, critically, it requires the development of schemes that promote sharing and opportunities within a diverse community of people.